

UNIVERSITY OF LONDON THESIS

Degree *PhD*

Year *2005*

Name of Author *HU, Y.*

**COPYRIGHT**

This is a thesis accepted for a Higher Degree of the University of London. It is an unpublished typescript and the copyright is held by the author. All persons consulting the thesis must read and abide by the Copyright Declaration below.

**COPYRIGHT DECLARATION**

I recognise that the copyright of the above-described thesis rests with the author and that no quotation from it or information derived from it may be published without the prior written consent of the author.

**LOAN**

Theses may not be lent to individuals, but the University Library may lend a copy to approved libraries within the United Kingdom, for consultation solely on the premises of those libraries. Application should be made to: The Theses Section, University of London Library, Senate House, Malet Street, London WC1E 7HU.

**REPRODUCTION**

University of London theses may not be reproduced without explicit written permission from the University of London Library. Enquiries should be addressed to the Theses Section of the Library. Regulations concerning reproduction vary according to the date of acceptance of the thesis and are listed below as guidelines.

- A. Before 1962. Permission granted only upon the prior written consent of the author. (The University Library will provide addresses where possible).
- B. 1962 - 1974. In many cases the author has agreed to permit copying upon completion of a Copyright Declaration.
- C. 1975 - 1988. Most theses may be copied upon completion of a Copyright Declaration.
- D. 1989 onwards. Most theses may be copied.

***This thesis comes within category D.***

This copy has been deposited in the Library of *UCL*

This copy has been deposited in the University of London Library, Senate House, Malet Street, London WC1E 7HU.





**Functional and structural studies of anosmin-1, the  
protein implicated in X-linked Kallmann's syndrome**

**Youli Hu**

**A thesis submitted to the University of London in fulfilment of the requirement for  
the degree of Doctor of Philosophy**

**Centre of Neuroendocrinology  
Department of Medicine  
Royal Free and University College Medical School  
University College London  
Rowland Hill Street  
London NW3 2PF**

**January 2005**

UMI Number: U592968

All rights reserved

INFORMATION TO ALL USERS

The quality of this reproduction is dependent upon the quality of the copy submitted.

In the unlikely event that the author did not send a complete manuscript and there are missing pages, these will be noted. Also, if material had to be removed, a note will indicate the deletion.



UMI U592968

Published by ProQuest LLC 2013. Copyright in the Dissertation held by the Author.  
Microform Edition © ProQuest LLC.

All rights reserved. This work is protected against  
unauthorized copying under Title 17, United States Code.



ProQuest LLC  
789 East Eisenhower Parkway  
P.O. Box 1346  
Ann Arbor, MI 48106-1346



## **Abstract**

Kallmann's syndrome (KS) is characterised by the association of anosmia (a loss of sense of smell) and hypogonadotrophic hypogonadism. Defects of anosmin-1, a protein encoded by *KAL-1*, underlie the X-linked inherited form of KS. Anosmin-1 comprises an N-terminal cysteine rich domain and a whey acidic protein like (WAP) domain, followed by four consecutive fibronectin type III (FnIII) like repeats. *In vivo* and *in vitro* studies revealed that anosmin-1 functions as an adherent extracellular matrix protein involved in cell adhesion and neurite outgrowth, actions dependent on an interaction of FnIII domains with heparan sulphate (HS). However, the binding characteristics and kinetics between C-terminal FnIII domains of anosmin-1 and HS have not hitherto been systematically investigated. Although anosmin-1's N-terminal WAP domain shares homology with serine protease inhibitors, its putative protease ligand is still unknown. In this thesis:

1. A *Drosophila* S2 cell expression system was used to express full length and truncated domain specific versions of anosmin-1. The full-length (PIWF4), truncated (PIWF1, with single FnIII-1 domain) protein, and their C172R WAP domain mutants were purified using Ni-NTA affinity chromatography. The high yield of PIWF1 protein enables the generation of an anti-anosmin-1 antibody.
2. A HS competitive assay showed that anosmin-1 was S2 cell surface associated through a FnIII domain-HS interaction. A solid phase ELISA assay indicated purified anosmin-1 bound to HS in a dose-dependent manner. Surface plasmon resonance (SPR) revealed real-time kinetic interactions with  $K_d = 2$  nM.
3. Urokinase-type plasminogen activator (uPA) was identified as a putative anosmin-1 interactant. Anosmin-1 significantly enhanced uPA amidolytic activity *in vitro*; anosmin-1/HS/uPA cooperation induced cell proliferation in a PC-3 prostate carcinoma cell line. Both the HS interaction and an intact WAP domain are required for anosmin-1's mitogenic activity. These effects appear to be mediated by a direct protein interaction between anosmin-1 and uPA since anosmin-1/uPA complex can be co-immunoprecipitated from PC-3 cell lysates as well as their higher binding affinity ( $K_d = 6.91$  nM) is demonstrated by SPR. I thus propose that anosmin-1 may modulate

uPA's catalytic activity and its signalling pathway, whereas HS determines cell surface localization of the anosmin-1/uPA complex.

4. The structure of anosmin-1 was investigated by analytical ultracentrifugation and X-ray scattering experiments, followed by homology modelling. PIWF4 was shown to

uPA's catalytic activity and its signalling pathway, whereas HS determines cell surface localization of the anosmin-1/uPA complex.

4. The structure of anosmin-1 was investigated by analytical ultracentrifugation and X-ray scattering experiments, followed by homology modelling. PIWF4 was shown to exhibit an extended conformation, whereas PIWF1 was supposed to possess a relative compacted structure.

## **Acknowledgements**

The work presented in this thesis resulted from a lot of help and collaborations with several groups in the Royal Free and University College Medical School. I would like to express my gratitude to many colleagues. Firstly, I thank my principal supervisor, Dr. Pierre Bouloux for giving me the opportunity to investigate in the molecular pathogenesis of a human developmental neuroendocrine disease, and for his support throughout my studies. I am also grateful to Dr. Gavin MacColl and Dr. Tim Harrison; Dr. Gavin MacColl in particular provided invaluable help and direction for this project and help with the molecular biological techniques. I am grateful for the help given by my fellow workers in the Centre for Neuroendocrinology; Dr. David González-Martínez assisted me greatly with image design and thesis preparation. We have enjoyed a fruitful collaboration over the past 3 years. Dr. Soo-Hyun Kim, the senior post-doctoral fellow also gave me helpful advice on papers.

I would like to thank the Protein Structure Group in the Department of Biochemistry and Molecular Biology for their help with the structural studies: Prof. Steve Perkins helped with supervision on the structural work and with the correction of the structural chapter in this thesis. Dr. Julian Eaton also helped with the homology modelling, and Dr. Zhe Sun helped with structural data analysis.

I thank Prof. Paul Travers and Anthony Nolan Research Institute for allowing me to use their facilities for the SPR experiments. I am also indebted to Dr. David Perry and Dr. Anne Riddle of the Department of Haemophilia for their help with the design of the thrombin amidolytic activity assay. I thank in addition Action Research and the Hobson Charity for helping to fund this work, the Centre for Hepatology and Gastroenterology laboratory for providing experimental facilities.

## **CONTENTS**

<b>Title page</b>	1
<b>Abstract</b>	2
<b>Dedication</b>	4
<b>Acknowledgements</b>	5
<b>Contents</b>	6
<b>List of figures and tables</b>	12
<b>Abbreviations</b>	16
<b>CHAPTER 1 General Introduction</b>	19
1.1 Introduction to Kallmann's syndrome	19
1.2 Pathophysiology of KS olfactory system	21
1.3 Genetics of KS	25
1.4 Characteristics of anosmin-1, the KAL-1 gene encoded protein	28
1.5 Suggested anosmin-1 functions based on in vivo and in vitro studies	31
1.5.1 Spatio-temporal expression of anosmin-1	31
1.5.2 Anosmin-1, neurite outgrowth and axon branching	31
1.5.3 Anosmin-1 as an adherent extracellular matrix (ECM) molecule	32
1.5.4 WAP and FnIII domain function in anosmin-1	33
1.6 Molecular modelling of anosmin-1	36
1.7 Molecules involved in the olfactory system development	37
1.7.1 Transcription factors and growth factors	38
1.7.2 Molecules involved in neuronal migration	39
1.8 HS – molecular cross talk with anosmin-1	43
1.8.1 Synthesis and modification of the HS	43
1.8.2 HS structure diversity and functional specificity	44
1.8.3 HS-ligand interaction	49
1.8.4 HSPG in cell events	52
1.8.4.1 Focal cell adhesion and cytoskeletal reorganization	52
1.8.4.2 Synapse formation, axon guidance and neurite outgrowth	53
1.8.4.3 Cell proliferation	54
1.8.4.4 Tumour growth and metastasis	56

1.9	Candidate molecules interacting with anosmin-1	57
1.9.1	Serine proteases	57
1.9.1.1	Thrombin	61
1.9.1.2	Plasminogen activator system	62
1.9.1.3	Trypsin	63
1.9.2	FGF2/FGFR1	63
1.10	Hypothesis	65
1.11	Aims of this thesis	65
<b>CHAPTER 2 Characterisation of anosmin-1 expressed in <i>Drosophila</i> S2 cells</b>		<b>68</b>
2.1	Introduction	68
2.2	Aims	69
2.3	Materials and methods	70
2.3.1	Construction of expression plasmid	70
2.3.1.1	PCR amplification	70
2.3.1.2	Purification of DNA from agarose gel	72
2.3.1.3	Restriction digest of DNA	72
2.3.1.4	DNA ligation	72
2.3.1.5	Transformation of recombinant DNA into DH5 $\alpha$ competent cells	72
2.3.1.6	Recombinant DNA mini preparation	73
2.3.1.7	Screening and sequencing of recombinant DNA	73
2.3.1.8	Recombinant DNA maxi preparation	73
2.3.2	Transient transfection of S2 cells by calcium phosphate precipitation	74
2.3.2.1	Expression in DESTM expression medium supplemented with 10% heat-inactivated foetal bovine serum	74
2.3.2.2	Expression of protein in serum-free medium	75
2.3.2.3	HS competition assay	75
2.3.3	Western Blotting	75
2.4	Results	76
2.5	Discussion	79

2.6	Conclusions	82
<b>CHAPTER 3 Expression and Purification of anosmin-1 from stable <i>Drosophila</i> S2 cells</b>		83
3.1	Introduction	83
3.2	Aims	84
3.3	Materials and Methods	86
3.3.1	Hygromycin-B killing curve for S2 cells	86
3.3.2	Selection of stable PIWF1 transformants by 300, 700µg/ml hygromycin-B	87
3.3.3	Scale-up of PIWF1 using stationary flask and spinner flask	89
3.3.4	Protein purification by Ni-NTA agarose chromatography	89
3.3.5	Silver staining	90
3.3.6	Quantitative Protein Assay	90
3.3.7	Mutagenesis of mPIWF1 <sup>172</sup> and mPIWF4 <sup>172</sup> incorporating C172R WAP domain mutation	91
3.3.8	Optimization of expression and purification of recombinant proteins	92
3.3.9	Protein dialysis into PBS	93
3.3.10	Protein storage	93
3.3.11	HS competitive assay using stable S2 cell lines	94
3.3.12	Generation of polyclonal antibody against PIWF1 (AIWF1)	94
3.3.12.1	Dot-Blot	94
3.3.12.2	ELISA assay	95
3.3.12.3	AIWF1 purification	95
3.3.12.4	Western blot	96
3.4	Results	96
3.5	Discussion	111
3.6	Conclusions	113
<b>CHAPTER 4 The binding affinity of anosmin-1 to heparan sulphate</b>		115
4.1	Introduction	115
4.2	Aims	116

4.3	<b>Materials and Methods</b>	116
4.3.1	<b>Solid phase enzyme-linked immunosorbant assay</b>	116
4.3.1.1	<b>Biotinylation of HS</b>	116
4.3.1.2	<b>Effects of varying the concentration of biotinylated HS on binding to a fixed concentration of protein</b>	117
4.3.1.3	<b>Effects of varying protein concentration on binding to a fixed biotinylated HS</b>	117
4.3.1.4	<b><i>In vitro</i> HS competitive assay</b>	117
4.3.2	<b>SPR assay</b>	117
4.3.2.1	<b>The principle of SPR</b>	117
4.3.2.2	<b>The SPR sensor surface and analytic application</b>	118
4.3.2.3	<b>Immobilising biotinylated heparin onto streptavidin sensor chip</b>	120
4.3.2.4	<b>SPR kinetic measurement of the heparin interaction with anosmin-1</b>	120
4.4	<b>Results</b>	122
4.5	<b>Discussion</b>	128
4.6	<b>Conclusions</b>	131
	<b>CHAPTER 5 Interaction between anosmin-1, HS and urokinase-type plasminogen activator in prostate carcinoma PC-3 cell proliferation</b>	132
5.1	<b>Introduction</b>	132
5.2	<b>Aims</b>	135
5.3	<b>Materials and Methods</b>	135
5.3.1	<b>uPA and thrombin amidolytic activity assay</b>	135
5.3.2	<b>Proliferation assays</b>	136
5.3.2.1	<b>Anosmin-1 on PC-3 cell proliferation</b>	136
5.3.2.2	<b>Function-blocking experiment</b>	137
5.3.2.3	<b>Effect of HS on anosmin-1 function using exogenous HS and heparinase III</b>	137
5.3.3	<b>Immunocytochemistry</b>	137
5.3.3.1	<b>Fluorescence labelling of cell surface associated</b>	



anosmin-1	137
5.3.3.2 Fluorescence labelling of intracellular anosmin-1	138
5.3.4 Immunoprecipitation	138
5.3.5 SPR kinetic measurement of the uPA interaction with anosmin-1	139
5.4 Results	139
5.4.1 Anosmin-1 increases uPA amidolytic activity, but does not alter thrombin activity	139
5.4.2 Effects of anosmin-1 on promoting PC-3 cell proliferation	143
5.4.3 Soluble exogenous HS triggers anosmin-1 inhibitory activity on PC-3 cell growth	145
5.4.4 Recombinant anosmin-1 is associated with PC-3 cell surface via HS binding	146
5.4.5 WAP mutated anosmin-1 blocks cell proliferative activity	148
5.4.6 Anosmin-1 induces PC-3 cell proliferation through interaction with uPA	148
5.5 Discussion	151
5.6 Conclusions	159
<b>CHAPTER 6 Structure analysis of anosmin-1 by analytical ultracentrifuge and X-ray scattering</b>	160
6.1 Introduction	160
6.2 The methods for protein structure analysis	161
6.3 X-ray solution scattering	163
6.3.1 X-ray scattering theory	163
6.3.1.1 The Debye equation	165
6.3.1.2 Two-phase model of solution scattering	167
6.3.2 Experimental X-ray solution scattering	168
6.3.2.1 Sample preparation	168
6.3.2.2 X-ray scattering at ESRF Grenoble	168
6.3.2.3 Reduction of ESRF scattering data	170
6.3.3 Analysis of reduced scattering curves $I(Q)$	170
6.3.3.1 Guinier analyses	170

6.3.3.2	Cross-sectional radius of gyration	173
6.3.3.3	Estimation of macromolecular dimensions	174
6.3.3.4	Real space distance distribution function	174
6.4	Analytic ultracentrifugation	175
6.4.1	Sedimentation velocity experiments	175
6.4.2	Sedimentation equilibrium experiments	178
6.5	Materials and methods	180
6.5.1	Purification of PWF1 and PIWF4	180
6.5.2	X-ray scattering data acquisition at ESRF	180
6.5.3	Analysis of reduced X-ray data	182
6.5.4	Analytical ultracentrifugation data acquisition and analysis	182
6.6	Experimental results and discussion	183
6.7	Homology modelling of anosmin-1 domains	191
6.8	Construction of the full models for PIWF1 and PIWF4	196
6.8.1	Debye scattering curve modelling of PIWF1 and PIWF4	198
6.8.2	PIWF1 and PIWF4 models	199
<b>CHAPTER 7 Conclusions and future studies</b>		204
7.1	The questions raised from this study	204
7.2	Future studies	207
<b>Publications</b>		209
<b>References</b>		210

## **List of figures and tables**

<b>Figure 1.1 Schematic diagram showing olfactory system development during embryogenesis</b>	<b>22</b>
<b>Figure 1.2 Diagram depicting the layered structure formation in mature olfactory bulb</b>	<b>24</b>
<b>Figure 1.3 Diagram depicting the disruption of olfactory neuron pathway in a 19-week <i>KAL-1</i> deleted foetus</b>	<b>26</b>
<b>Figure 1.4 Schematic structure of human anosmin-1 protein and five missense Mutations</b>	<b>29</b>
<b>Figure 1.5 (a) Sequence comparison of WAP domain of anosmin-1 within vertebrate and invertebrate. (b) Multiple sequence alignment of human WAP domain sequences in homologous proteins</b>	<b>34</b>
<b>Figure 1.6 Structure of the olfactory system and molecules known to mediate olfactory neuron migration, trajectory and convergence within olfactory bulb region during embryogenesis</b>	<b>40</b>
<b>Figure 1.7 Scheme of HS chain biosynthesis</b>	<b>45</b>
<b>Figure 1.8 Multifunction of HSPG in regulating protein activity</b>	<b>50</b>
<b>Figure 1.9 Mechanism of catalysis of serine proteases</b>	<b>58</b>
<b>Figure 1.10 Structure of human trypsin-like serine proteases</b>	<b>60</b>
<b>Figure 1.11 The hypothesis of molecular mechanism of anosmin-1</b>	<b>66</b>
<b>Figure 2.1 Structure of five variants of recombinant anosmin-1</b>	<b>71</b>
<b>Figure 2.2 Western blot analysis of recombinant anosmin-1 in <i>Drosophila</i> S2 cells</b>	<b>77</b>
<b>Figure 3.1 Structures of PIWF4, PIWF1 and their C172R mutants</b>	<b>85</b>
<b>Figure 3.2 Hygromycin-B induced S2 cell kill curve</b>	<b>88</b>
<b>Figure 3.3 Purification of salt extracted PIWF1 generated from 300 µg/ml hygromycin-B selected S2 cells</b>	<b>97</b>
<b>Figure 3.4 Purification of salt extracted PIWF1 generated from 700 µg/ml</b>	

hygromycin-B selected S2 cells	98
Figure 3.5 Purification of PIWF1 protein from serum-free conditioned medium	100
Figure 3.6 Purification of salt extracted PIWF4	101
Figure 3.7 Purification of salt extracted mPIWF1 <sup>172</sup>	102
Figure 3.8 Purification of salt extracted mPIWF4 <sup>172</sup>	103
Figure 3.9 Initial investigations on the generation and purification of salt extracted PIWF1 protein using suspension culture	104
Figure 3.10 Generation and purification of salt extracted PIWF1, PIWF4 protein and GFP using suspension culture to validate the modified protocol	105
Figure 3.11 Dot blot analysis was performed using the recombinant PIWF1 protein (0.01-1 µg) as antigen on the nitrocellulose membrane	107
Figure 3.12 AIWF1 antibody analysis by ELISA assay	108
Figure 3.13 AIWF1 antibody analysis by Western blot	109
Figure 3.14 Western blot analysis of recombinant anosmin-1, the C172R mutants, empty vector protein and GFP generated by stable S2 cell lines in serum free medium	110
Figure 4.1 The schematic mechanism of SPR	119
Figure 4.2 Typical SPR-plot of the specific interaction of biomolecules to a single spot of the biochip surface	121
Figure 4.3 Investigation of immunosorbant method for protein-HS binding affinity assay	123
Figure 4.4 Immunosorbant assay analysis of anosmin-1-HS binding	125
Figure 4.5 BIAcore analysis of anosmin-1 interaction with heparin	126
Figure 5.1 Effect of anosmin-1 on thrombin amidolytic activity	141
Figure 5.2 Effect of anosmin-1 on uPA amidolytic activity	142
Figure 5.3 Effect of anosmin-1 on PC-3 cell proliferation	144
Figure 5.4 Immunofluoresence analysis of PIWF1 dissociation from PC-3 cell	

and internalisatin following addition of exogenous HS	147
Figure 5.5 Growth suppression effect of anosmin-1 in PC-3 cells	149
Figure 5.6 Involvement of uPA in anosmin-1 induced PC-3 cell proliferation	150
Figure 5.7 BIAcore analysis of anosmin-1 interaction with uPA	152
Figure 5.8 Hypothesis of molecular mechanism of anosmin-1 action	158
Figure 6.1 General features of a solution scattering curve $I(Q)$ measured over a $Q$ range	164
Figure 6.2 Schematic representation of X-ray scattering from two points in a protein molecule	166
Figure 6.3 Flow diagram of the reduction procedure for ESRF X-ray scattering data	171
Figure 6.4 The X-ray diffraction pattern of silver behenate	172
Figure 6.5 Sedimentation velocity cell design and data collection	177
Figure 6.6 Schematic representation of sedimentation equilibrium	179
Figure 6.7 Domain structure of recombinant anosmin-1	181
Figure 6.8 Guinier $R_G$ and $R_{XS}$ analyses of PIWF1 and PIWF4	184
Figure 6.9 Distance distribution functions $P(r)$ for PIWF1 (a) and PIWF4 (b)	186
Figure 6.10 Sedimentation velocity fit of the $g(s^*)$ distribution for PIWF1 and PIWF4	188
Figure 6.11 Sedimentation equilibrium fit for PIWF1 and PIWF4	189
Figure 6.12 The amino acid sequence and residue numbering of the individual domains of recombinant anosmin-1	192-193
Figure 6.13 Sequence alignments of anosmin-1 CR with epidermal growth factor receptor (EGFR) and insulin-like growth factor receptor (IGFR)	194
Figure 6.14 Structural comparison of the CR of anosmin-1 and IGFR	197
Figure 6.15 Representations of extended and compact forms of the PIWF1 and	

PIWF4 construct	202
Figure 6.16 $\ln I(Q) \text{ v } Q$ curve fits for the compact model of PIWF1 (top) and PIWF4 (bottom)	203
<hr/>	
Table 1.1 Mutation of <i>KAL-2</i> gene associated with Kallmann's syndrome	30
Table 1.2 HS-protein interaction	46-47
Table 4.1 BIAcore kinetic data for binding of anosmin-1 to heparin	127
Table 6.1 Summary of the results of modelling PIWF1 and PIWF4 in compact and extended conformations	201

## Abbreviations

BSA	bovine serum albumin
cm	centimetre
cDNA	complementary DNA
CO <sub>2</sub>	carbon dioxide
Cu	copper
°C	degrees Celsius
DES	<i>Drosophila</i> expression system
DNA	deoxyribonucleic acid
ECM	extracellular matrix
ELISA	enzyme-linked immunosorbent assay
FGF	fibroblast growth factor
FGFR	fibroblast growth factor receptor
FnIII	fibronectin-like type III domain
g	gram
GlcA	glucuronic acid
GlcN	glucosamine
GlcNAc	N-acetylglucosamine
GnRH	gonadotrophin releasing hormone
HH	hypogonadotrophic hypogonadism
hour	h
HS	heparan sulphate
HSPG	heparan sulphate proteoglycan
IdoA	iduronic acid
IMAC	immobilized-metal affinity chromatography
kb	kilobase pairs
kDa	kilodalton
K <sub>d</sub>	dissociation constant
KS	Kallmann's syndrome
LOT	lateral olfactory tract
l	litre
LB	Luria broth
LBamp	Luria broth with 50 µg/ml ampicillin
M	molar concentration
µM	micro molar
mA	milliamperes
mAb	monoclonal antibody
min	minute
ml	millilitre
mm	millimetre
mM	millimolar
MMP	matrix metalloproteinases
Ni	nickle
NDST	N-deacetylase/ N-sulfotransferase
nm	nanometre
NMR	nuclear magnetic resonance



<b>OB</b>	olfactory bulb
<b>OD</b>	optic density
<b>OST</b>	O-sulfotransferase
<b>pAb</b>	polyclonal antibody
<b>PAGE</b>	polyacrylamide gel electrophoresis
<b>PCR</b>	polymerase chain reaction
<b>RNA</b>	ribonucleic acid
<b>R<sub>G</sub></b>	radius of gyration
<b>rpm</b>	revolutions per minute
<b>SDS</b>	sodium dodecyl sulphate
<b>SLPI</b>	secretory leucocyte proteinase inhibitor
<b>SPR</b>	Surface Plasmon Resonance
<b>tPA</b>	tissue-type plasminogen activator
<b>U.V.</b>	ultra violet
<b>uPA</b>	urokinase-type plasminogen activator
<b>uPAR</b>	urokinase-type plasminogen activator receptor
<b>WAP</b>	whely acidic protein-like domain
<b>X-KS</b>	X-linked Kallmann's syndrome

#### **Nucleoside bases**

<b>A</b>	adenine
<b>C</b>	cytosine
<b>G</b>	guanine
<b>T</b>	thymine
<b>U</b>	uracil

#### **Amino Acids**

<b>A</b>	alanine
<b>C</b>	cysteine
<b>D</b>	aspartic acid
<b>E</b>	glutamic acid
<b>F</b>	phenylalanine
<b>G</b>	glycine
<b>H</b>	histidine
<b>I</b>	isoleucine
<b>K</b>	lysine
<b>L</b>	leucine
<b>M</b>	methionine
<b>N</b>	asparagine
<b>P</b>	proline
<b>Q</b>	glutamine
<b>R</b>	arginine
<b>S</b>	serine
<b>T</b>	threonine
<b>V</b>	valine
<b>W</b>	tryptophan

## Chapter 1

### General Introduction

#### 1.1 Introduction to Kallmann's syndrome

Kallmann's syndrome (KS) is the association of hypogonadotrophic hypogonadism (HH) and anosmia (a loss of sense of smell), first described in 1856 by the Spanish pathologist Maestre de San Juan (Maestre de San Juan, 1856). It was subsequently recognised as an inherited entity by the American medical geneticist, Kallmann (Kallmann, 1944). While most presentations are sporadic, a significant proportion of KS cases are inherited, with pedigrees demonstrating autosomal dominant, recessive or X-linked modes of inheritance (X-KS). Although HH and anosmia represent the *sine qua non* diagnostic features of KS, depending on the mode of inheritance, KS may occur together with a variety of apparently discordant abnormalities (Oliveira et al., 2001). Signs specifically associated with the X-linked form of the disease include upper body mirror movements, affecting about 80% of cases, and unilateral renal agenesis occurring in approximately 30% of cases. Until recently, the phenotypes associated with the autosomal forms of KS were thought to be less consistent, with a heterogeneous collection of associated defects present in a minority of cases including midline/craniofacial abnormalities (harelip and cleft plate), mental retardation, sensorineural deafness, colour blindness and spastic paraplegia, eye movement disorders and cerebellar signs (Wegenke et al., 1975; Conrad et al., 1978; Oliveira et al., 2001; Quinton et al., 2001). About 1 in 10,000 males suffer from this disease, with a frequency five to seven times lower in females (Jones and Kemmann, 1976).

In KS, anosmia is caused by olfactory bulb dysgenesis; although first documented as a post mortem finding, it is now diagnosable in life using high resolution MRI scanning of the brain. This characteristically shows defective olfactory bulb and sulcus formation. Postnatal nasal biopsies also show abnormal morphological features in the olfactory epithelium, consequent upon lack of central connectivity (Quinton et al., 1996; MacColl et al., 2002a). The hypogonadotrophic hypogonadism

is secondary to hypothalamic GnRH (gonadotrophin releasing hormone) neuronal deficiency leading to failed release of luteinising hormone (LH) and follicle stimulating hormone (FSH) from the pituitary gonadotrophs (Oliveira et al., 2001; Pitteloud et al., 2002; MacColl et al., 2002b). Although micropenis/cryptorchidism may represent the earliest clinical manifestation of the condition, most KS patients present in adolescence with failed or, more rarely, arrested puberty. The successful administration of exogenous pulsatile subcutaneous injection (sc) or intravenous injection (iv) GnRH in invariably producing phasic release of LH and FSH in KS patients (used therapeutically to induce puberty and fertility), has confirmed the hypothalamic origin of the HH (ie hypothalamic GnRH neuronal deficiency), and has proved that gonadotrophs retain their functional secretory capability (Oliveira et al., 2001; Pitteloud et al., 2002).

Bimanual synkinesis, a defining feature of X-KS, has been attributed to misrouting of descending corticospinal tract axons. Cross correlation analysis of surface electromyograms and electromagnetic stimulation of the motor cortex hand areas have revealed fast bilateral conducting projections from each motor cortex in X-KS patients, implicating the presence of a novel ipsilateral corticospinal tract (Krams et al., 1997; Mayston et al., 1997; Krams et al., 1999). Statistical analysis of pooled white matter data from structure T1 weighed MR images has also demonstrated a hypertrophied corticospinal tract in the X-KS patients compared with autosomal KS and normal controls (Krams et al., 1999).

Non-neurological associations of X-KS include urogenital defects such as unilateral renal agenesis and possible renal dysplasia leading to premature renal failure (Duke et al., 1998). It has been proposed that defects in the initial branching of the mesonephros at the stage of uretic bud formation may be present in X-KS. However, defective condensation of the metanephrogenic blastema that forms the metanephros, possibly due to loss of growth signaling or abnormal reciprocal mesenchymal-epithelial cell interactions necessary for organogenesis (Duke et al., 1998; Hardelin et al., 1999; Woolf, 2001), could also be implicated.

## **1.2 Pathophysiology of KS olfactory system**

The joint origin and migration pathway of olfactory and GnRH1 neurons provide important clues as to the pathogenesis of the defining diagnostic features of anosmia and hypogonadotrophic hypogonadism in KS. To understand the effects of disrupted morphogenesis, the normal development of olfactory system is first described.

The olfactory, vomeronasal, terminal neurons (cranial nerve 1 complex) and GnRH1 neurons derive from precursor neuron cells in the olfactory placode. In the human, axons of the cranial nerve 1 have begun to migrate towards the telencephalon, reaching the olfactory bulb (OB) anlage as early as embryonic week four, prior to the appearance of GnRH immunoreactivity in the medial olfactory placodes (about 6 weeks). GnRH1 neurons migrate along the medial portion of the olfactory nerve fibres and at 6.5 weeks enter the medial forebrain at a location slightly caudal to the junction with the olfactory nerve (Schwanzel-Fukuda et al., 1996) (Figure 1.1).

Upon reaching the anterior telencephalon, pioneer axons of olfactory neuron penetrate deeply into the forebrain to induce OB development proper; subsequently later olfactory fibres anchor at the surface of the telencephalon to form the olfactory nerve layer of the outmost OB. Several days prior to the arrival of the first olfactory neuron into the telencephalic vesicle/OB primordium, mitral and tufted cells are born in this region and subsequently proliferate. In the human, at 8 weeks the olfactory bulbs form a distinct structure by protruding from the forebrain in a caudo-lateral direction. At 15 weeks, after the appearance of an obvious OB outgrowth from the forebrain, specific synaptic structures called “glomeruli” start to be formed by the output dendrites of mitral cells with input axons of olfactory sensor neurons, combined with later generation of interneurons, giving rise to the bulk of the glomerular layer. The axons of mitral/tufted cells proceed caudally and move ventrolaterally to form the lateral olfactory tract (LOT) and finally innervate their telencephalic destinations including the anterior olfactory nucleus, the pyriform cortex, the olfactory tubercle and the amygdaloid nuclei (Brunjes and Frazier, 1986). By contrast, neuroblasts from the

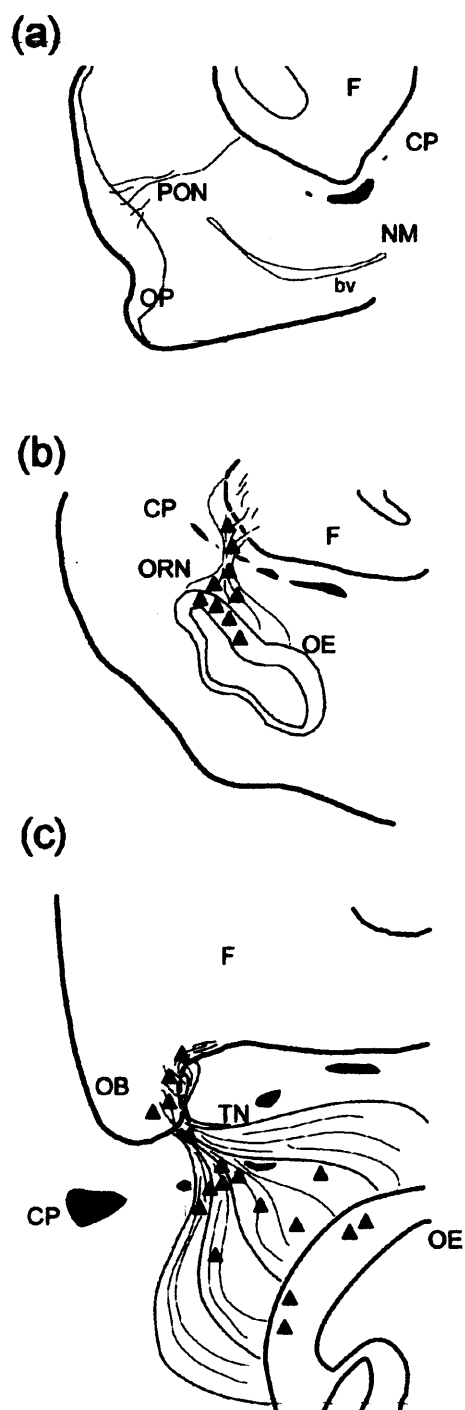


Figure 1.1 Schematic diagram showing olfactory system development during human embryogenesis. (a) 4 weeks (CS 13), 8/9 mm. (b) 5.5 weeks (CS 17), 11/12 mm. (c) 6 weeks (CS 18), 13/15 mm. OP, olfactory placode; PON, primary olfactory neurons; bv, blood vessel; NM, nasal mesenchyme; CP, cribriform plate; F, forebrain; ORN, olfactory receptor neurons; OE, olfactory epithelium; OB, olfactory bulb; TN, terminal nerve; ▲, GnRH immunoreactivity. (Taken from González-Martínez *et al*, 2004)

ventral telencephalon and anterior subventricular zone (SVZ) migrate towards OB as part of the rostral migratory stream (RMS), differentiating into GABAergic interneurons upon reaching the OB. The major type of these interneurons, the periglomerular cells and granule cells, develop the connective network with mitral/tufted cells as a negative regulator and complete the layering of the OB which comprises external and internal plexiform and granule cell layers (Goldman and Luskin, 1998) (Figure 1.2).

GnRH1 neurons enter the ventromedial forebrain, caudal to the anlage of the olfactory bulb, and course along the medial surface of the cerebral hemispheres to enter the septal and preoptic areas of the brain and importantly, the supraoptic hypothalamus. From these areas, GnRH1 neuron subsequently extend axons to the median eminence capillary system, where neurosecretion occurs (Ronnekleiv and Resko, 1990; Norgren and Brackenbury, 1993). GnRH peptide secreted in a pulsatile manner passes to the anterior lobe of the pituitary where it stimulates the pulsatile release of LH and FSH, leading to stimulating germ cell development in testes and ovaries, testosterone and oestrogen synthesis and secretion respectively, together with the ensuing development of secondary sexual characteristics (Schally et al., 1971).

The important permissive role of the olfactory nerve and indeed the cranial nerve 1 complex in guiding GnRH1 neurons into the telencephalon has been clearly established in olfactory transection studies which effectively disabled GnRH1 neuronal migration into its forebrain target (Murakami et al., 1998). In X-KS patients, initial development of olfactory and GnRH1 neurons occur normally, although immunohistochemical analysis of nasal epithelial biopsies from affected subjects do demonstrate immature olfactory epithelial neuronal bodies and persistent existence of GnRH1-immunoreactive neurons in olfactory epithelium (Quinton et al., 1997). These observations implicate a developmental disorder within the anterior tip of telencephalon during morphogenesis, rather than abnormal ontogeny of the early precursor neurons within olfactory placodes in X-KS. Immunohistochemical study of

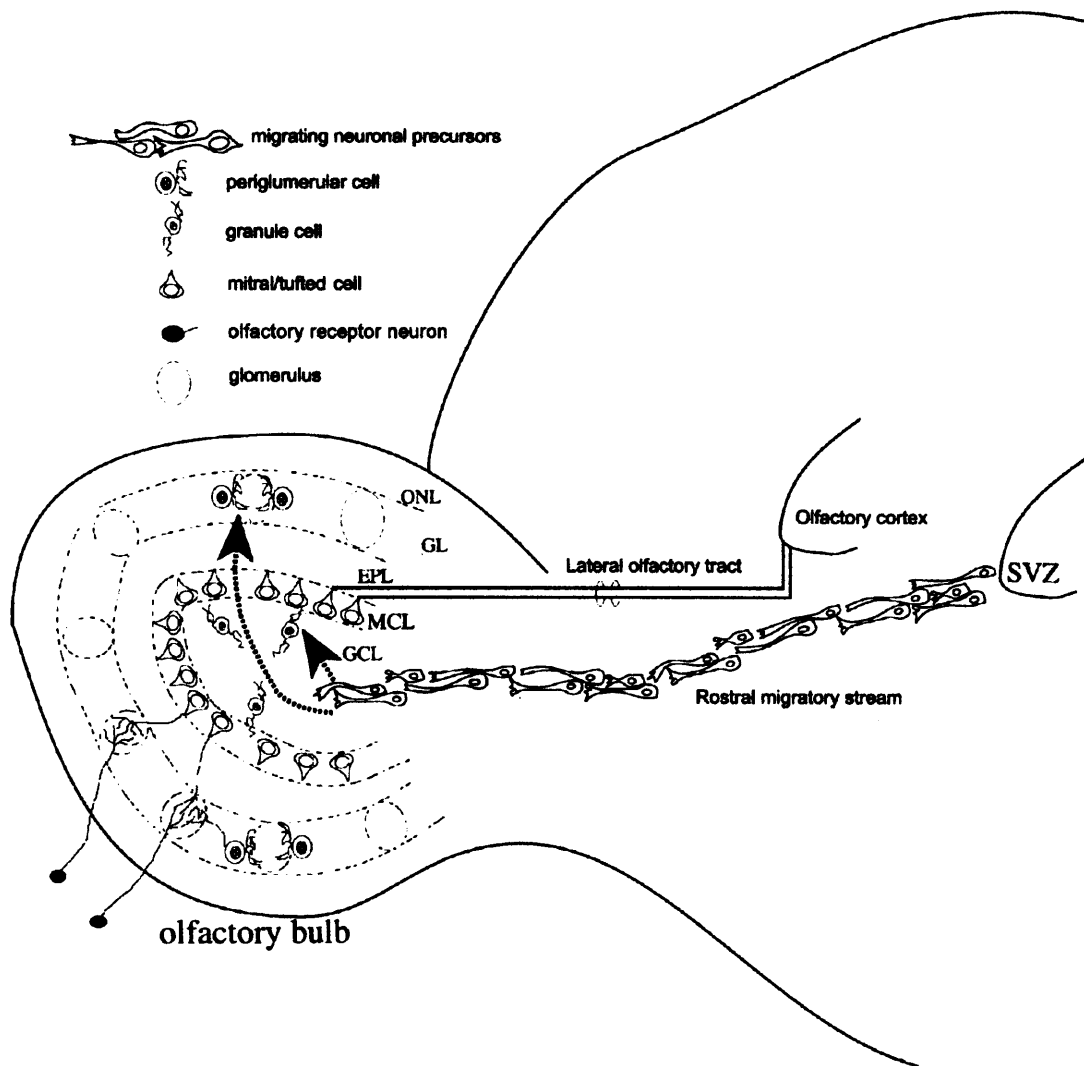


Figure 1.2 Diagram depicting the layered structure formation in mature human olfactory bulb. The olfactory receptor neurons enter the forebrain and form the outer olfactory nerve layer. Their axons synapse with output neurons of the mitral/tufted cells in the specialised sites called glomerulus. With the further connection of periglomerular cells to glomerulus, the glomerular layer is formed. Beneath the glomerulus is the external plexiform layer, mitral cell layer and internal granule cell layer. Axons of the mitral/tufted cells proceed caudally and move ventrolaterally to form the lateral olfactory tract before terminating at the olfactory cortex. Neural precursors from the subventricular zone (SVZ) migrate along the rostral migratory stream towards the centre of the olfactory bulb where they differentiate into interneurons including granule and periglomerular cells. The *short arrow* indicates the differentiation of neural precursors to granule cells; the *long arrow* marks the periglomerular cells. *EPL*, External plexiform layer; *GCL*, granule cell layer; *GL*, glomerular layer; *MCL*, mitral cell layer; *ONL*, olfactory nerve layer. (Taken from Murase and Horwitz, 2002).



a 19-week *KAL-1* deleted foetus has also shown an initial preserved rostral trajectory of olfactory axons but subsequent migratory arrest of both these axons and GnRH1 neurons at the upper nasal sub-cribriform area (Schwanzel-Fukuda and Pfaff, 1989) (Figure 1.3).

Clinical observations, including nasal epithelial biopsies and magnetic resonance imaging (MRI) studies in KS patients have demonstrated dysplastic OB or conspicuous absence of the olfactory bulbs/sulci and reduced volume of the olfactory cortex (Quinton et al., 2001; Vermeulen et al., 2002). Very low or absent gonadotrophin secretion in KS patients with preserved pituitary responsiveness to exogenous GnRH1, confirms the hypothalamic origin of GnRH1 deficiency. Thus, the failed formation of OB and the disruption of the intracerebral common migratory pathway of olfactory and GnRH1 neurons comprise the main pathological defects in KS patients. To date, the molecular mechanisms for this abnormal neuronal development are still far from being completely elucidated. Such mechanisms would be predicted to involve cell-cell interactions as well as axonal guidance, and will be discussed fully later in the introduction.

### **1.3 Genetics of KS**

Although most cases are sporadic, three modes of familial KS inheritance have been identified: X-linked (X-KS), autosomal dominant and autosomal recessive. The gene causing X-KS, *KAL-1*, has been cloned and localised to the Xp22.3 region by classical pedigree analysis and positional cloning; cloning and validation of this locus was the result of work from two independent laboratories in 1991 (Legouis et al., 1991; Franco et al., 1991). The genomic structure of *KAL-1* gene comprises fourteen exons encompassing 220 kb, and this generates a cDNA with a 2043 bp open reading frame. The 2 kb region upstream of the coding sequence shows high GC rich content and contains a CCAAT box, a common transcription factor binding site to a number of house keeping genes and tissue specific genes such as nerve growth factor (Sehgal et al., 1988). The promoter and enhancer sequences have not been fully elucidated; however, a 12 nucleotide sequence upstream of the coding sequence of *KAL-1*,

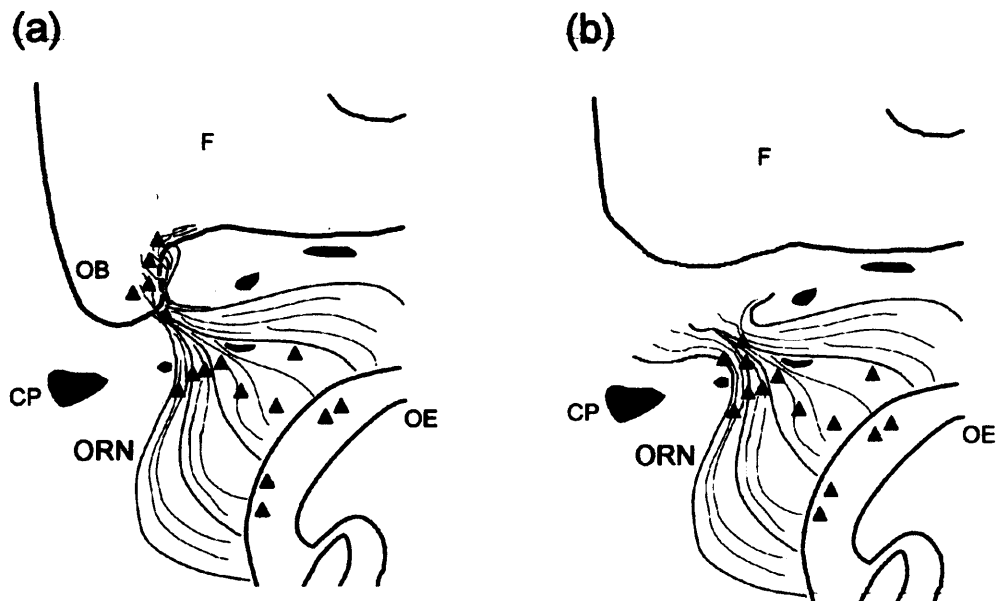


Figure 1.3 Diagram depicting the disruption of olfactory neuron pathway in a 19-week *KAL-1* deleted foetus. (a) Normal development of olfactory neuron pathway. Olfactory receptor neuron (ORN) and GnRH neuron (▲) migrate from their originals of olfactory epithelium (OE), through the cribriform plate (CP), and penetrate into developing forebrain. (b) The disrupted olfactory pathway in a 19-week X-KS foetus was identified by immunohistochemistry. The initial ontogenesis of olfactory neurons appears normal. However, there is arrest of GnRH neuron beneath the dura at the level of the cribriform plate.

proposed to be the candidate promoter site seen in certain CNS expressed genes (Thompson and Ziff, 1989), may be relevant in this regard.

The genetic analysis of X-KS pedigrees has demonstrated a predominant loss of function mutations (deletion and nonsense mutations) within *KAL-1* (Maya-Nunez et al., 1998a; Soderlund et al., 2002). Of relevance, five missense mutations have so far been identified; they are: 1) two nucleotide substitutions in exon 4 (TGT to TAT at codon 163, TGT to CGT at codon 172); 2) exon 6 (AAT to AAA at codon 267); 3) two nucleotide substitutions in exon 11 (GAA to AAA at codon 514, TTC to TTG at codon 517) respectively. These cause C163Y, C172R, N267K, E514K and F517L alterations at the amino acid level (Hardelin et al., 1993; Georgopoulos et al., 1997; Maya-Nunez et al., 1998b; Oliveira et al., 2001; Sato et al., 2004). The absence of mutations in a majority of patients suggests the possibility of the existence of mutations within the *KAL-1* promoter or enhancer region.

Homologues of *Kal-1* genes have been identified in a wide number of species from vertebrates (chicken P33005, zebrafish AF163310 and AF163311) to invertebrates (*Drosophila* AF342988, *Caenorhabditis elegans* AF342986). However, the corresponding *Kal-1* gene has not been cloned in the rodent, possibly due to the gene being located in the mouse pseudoautosomal region. Significantly, the human and *C.elegans* anosmins have the same conserved domain structure (WAP, followed by 4 FnIII domains), and in an *in vivo* transgenic experiment, the human *KAL-1* sequences rescued the abnormal phenotype caused by loss of the *C.elegans Kal-1* gene (Bulow et al., 2002; MacColl et al., 2002a), indicating functional conservation of this gene product during evolution.

Recently, using genetic analysis of polymorphic markers combined with fluorescence *in situ* hybridisation (FISH) analysis, an autosomal dominant gene (*KAL-2*) has been identified on chromosome 8p11-p12, bearing a microdeletion in two individuals with Kallmann's syndrome (Dode et al., 2003). *FGFR1* has been proposed as a dominant autosomal locus for KS based on the demonstration of potential loss-of-

function mutations of *FGFR1* in individuals from pedigrees where the mode of inheritance was most likely autosomal dominant. The high prevalence of cleft palate defects in these patients with *FGFR1* mutations is striking, together with rarer associations such as multiple dental agenesis, hearing loss, agenesis of the corpus callosum, and bimanual synkinesis in one case. No renal aplasia was reported in any affected individual. Recently reported loss of function mutations of *FGFR1* and their associated clinical phenotypes are summarised in Table 1.1. Thus mutations involving *FGFR1*, appear to account for one autosomal dominant form of KS, representing a further important gene involved in olfactory bulb morphogenesis. The autosomal recessive gene (*KAL-3*) has not hitherto been identified.

#### **1.4 Characteristics of anosmin-1, the *KAL-1* gene encoded protein**

The open reading frame of *KAL-1* cDNA encodes a 680 amino acids conceptual modular protein, named anosmin-1, which consists of an N-terminal signal peptide, a cysteine-rich region, a whey acidic protein-like four-disulfide core motif (WAP) and four contiguous fibronectin-like type III domains (FnIII), followed by a histidine rich C terminus (Legouis et al., 1991; Franco et al., 1991) (Figure 1.4). The sequence characteristics with a 23 N-terminal residue signal peptide, together with the absence of a hydrophobic transmembrane region and glycosyl phosphatidyl inositol (GPI) anchorage site, suggest anosmin-1 is a secreted protein. Six potential N-glycosylation sites are predicted within the cysteine-rich region and the 4 consecutive FnIII domains, giving rise to an augmentation of molecular weight from the conceptual 74 kDa protein to the mature size of approximately 100 kDa observed in *in vivo* and *in vitro* analyses and confirmed by experiments using the N-glycosylation inhibitor tunicamycin C (Soussi-Yanicostas et al., 1996; Soussi-Yanicostas et al., 1998; Soussi-Yanicostas et al., 2002). Post-translational modification of newly synthesised proteins, such as glycosylation, has an important role in protein folding and secretion, as well as binding of ligand to receptors and in cellular recognition events (Lis and Sharon, 1993). Hitherto, there has been no conclusive proof of which sites are glycosylated within anosmin-1.

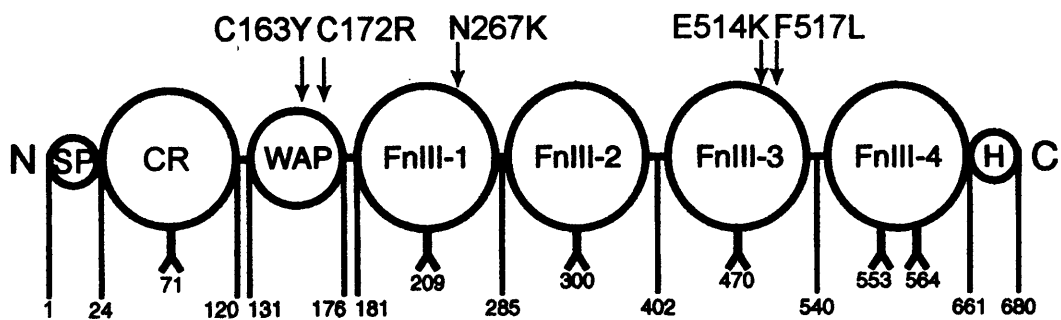


**Figure 1.4 Schematic structure of human anosmin-1 protein and five missense mutations. Each domain is represented by a circle and residue numbering indicates the size of each domain. The positions of the five known missense mutations are indicated by arrows. The predicted six N-linked glycosylation site are also marked by numbered Y symbols. SP, signal peptide; CR, cysteine rich region; WAP, whey acidic protein-like domain; FnIII, fibronectin type III domain; H, histidine rich region.**

**Table 1.1 Mutation of *KAL-2* gene associated with Kallmann's syndrome**

Mutation	Exon/Intron	Kallmann's syndrome associated symptoms	Reference
G97D	exon 3		A
Y99C	exon 3		A
S107X	exon 3		B
303-304 ins CC	exon 3		A
A167S	exon 5	cleft palate, corpus callosum agenesis, unilateral hearing loss	A
C277Y	exon 7		A
936 G to A	exon 7 (donor splice site)	multiple dental agenesis	A
V607M	exon 13	bimanual synkinesis	A
R622X	exon 14	cleft lip or palate	A
1970-1971 delCA	exon 14		A
W666R	exon 15	cleft palate	A
IVS15+ 1G to A	intron 15 (donor splice site)		A
M719R	exon 16		A
P745S	exon 17		B
P772S	exon 18	cleft palate, unilateral absence of nasal cartilage, iris coloboma	A

A-- Dode, et al. Loss-of-function mutations in *FGFR1* cause autosomal dominant Kallmann syndrome. *Nat Genet.* 2003;33:463-5.

B-- Sato, et al. Clinical assessment and mutation analysis of Kallmann syndrome 1 (*KALI*) and fibroblast growth factor receptor 1 (*FGFR1*, or *KAL2*) in five families and 18 sporadic patients. *J Clin Endocrinol Metab.* 2004;89:1079-88

In previous experiments using both *KAL-1* cDNA transfected COS-7 cells and *Drosophila* S2 cells (Rugarli et al., 1996; Robertson et al., 2001), expressed anosmin-1 appeared to be cleaved, generating 55 kDa N-terminal and 45 kDa C-terminal fragments. However, in these studies, protein expression occurred in serum-containing medium; in contrast, only the full-length anosmin-1 has been detected in tissue-extract samples, suggesting that the cleavage is an experimental artefact, possibly caused by the supplemented serum during cell culture.

## **1.5 Suggested anosmin-1 functions based on *in vivo* and *in vitro* studies**

### **1.5.1 Spatio-temporal expression of anosmin-1**

Anosmin-1 was detected from the 5<sup>th</sup> human embryonic week in mitral cells and within the extracellular matrix of the presumptive olfactory bulb, prior to the time when olfactory receptor neurons first make contact with the dendrites of basal telencephalic mitral/tufted cells. Anosmin-1 was also detected in the medial wall of the primitive cerebral hemispheres through which GnRH1 neurons migrate to their final destination and disengaged from their guidance fibres (Hardelin et al., 1999). Furthermore, anosmin-1 was also expressed along the lateral olfactory tract (LOT) formed by afferent axons of mitral cells and in the olfactory cortex from E14 in the rat (Soussi-Yanicostas et al., 2002). In addition to expression in the olfactory system, anosmin-1 immunoreactivity was widely detected in the basement membranes and/or interstitial matrices of various structures including mesonephric tubules and duct, branches of the ureteric bud, bronchial tubes, muscular walls of the digestive tract and larger blood vessels, precartilaginous models of skeletal pieces, muscle tendons, head mesenchyme, inner ear, and forebrain subregions (Hardelin et al., 1999). While expression in the developing kidney suggests a key role of anosmin-1 in nephrogenesis (based on the X-KS phenotype), there are no other clinical correlates of expression in other tissues.

### **1.5.2 Anosmin-1, neurite outgrowth and axon branching**

Dual properties of anosmin-1 on neurite outgrowth have been observed *in vitro*. Cerebellar neurons obtained from 5-day old (P5) mice developed longer neurites when



cultured on 3 µg/ml anosmin-1 coated wells, whereas their neurite outgrowth was reduced when co-cultured with anosmin-1-producing CHO cells. The opposite effects of anosmin-1 on neurite outgrowth observed in these experiments may be caused by difference of anosmin-1 concentrations used, one at constant levels as compared to the other with continuous secretion of anosmin-1 from co-cultured cells. These activities were also cell-type specific since anosmin-1 induced no phenotypic changes in E18 hippocampal and P1 dorsal root ganglion neurons under the same experimental conditions (Soussi-Yanicostas et al., 1998), suggesting that for functional responses the putative receptors or co-ligands are expressed in specific neuronal cells.

Recently, in a systematic study of rat OB explants, dissociation of OB neurons and organotypic cultures showed that recombinant human anosmin-1 either stimulated LOT neurite branching and outgrowth or attracted axons of LOT growing preferentially from OB explants towards the pyriform cortex (Soussi-Yanicostas et al., 2002). Thus, absence and mis-guidance of LOT axon branches would be expected to lead to loss of innervation to the olfactory cortex, with a reciprocal involution of the OB. The transgenic invertebrate studies carried out in *C.elegans* have yielded results similar to that obtained in rat explants with respect to axon branching and neurite outgrowth (Bulow et al., 2002; Rugarli et al., 2002). The alteration in neuronal phenotype induced by the nematode *Kal-1* orthologue (CeKal1) is dosage and time-dependent, both in loss of function mutants and when CeKal is overexpressed in a number of neuronal subtypes. These findings suggest that anosmin-1 is involved in at least two processes in the developing olfactory system: OB development and convergence of LOT neurons towards their olfactory cortical destination, partially accounting for the pathogenesis of the olfactory deficit in KS patients.

### **1.5.3 Anosmin-1 as an adherent extracellular matrix (ECM) molecule**

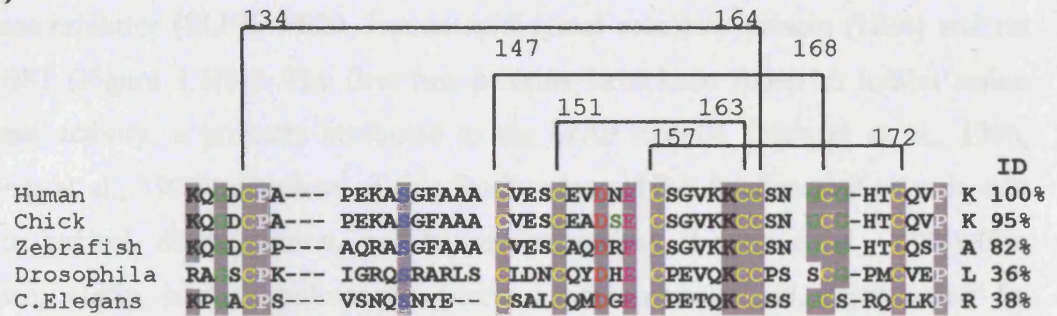
Although the dominant phenotype in X-KS relates to aberrant development of the nervous system, a heterogeneous collection of non-neurological focal disorders are also observed including renal aplasia (Oliveira et al., 2001). Indeed, anosmin-1 has been identified as an adhesion ECM molecule for a variety of neuronal and

nonneuronal cell types, including rat olfactory epithelia cells, GT1-1 (mouse GnRH neuron-derived cell line), cerebellar neurons and canine MDCK1 kidney epithelia cells (Soussi-Yanicostas et al., 1998; Robertson et al., 2001). In keeping with this observation, the loss of function and over-expression of *KAL-1* mutants in the transgenic *C.elegans* also caused at least two distinct morphogenetic abnormalities: defective ventral enclosure and male tail formation defects (Rugarli et al., 2002). In addition to disrupted development, in certain instances, variably penetrant embryonic lethality was also observed. Visualisation of epithelial cell boundaries and tail epithelial cells indicated that, during gastrulation and tail morphogenesis, epidermal cells differentiated correctly and migrated along the neuroblast cell surface, but exhibited abnormal contacts, positioning and shape. Taken together, anosmin-1 appears to play a determining role in providing an active signal and/or a permissive substrate in modulating the formation or stabilisation of epithelial cell contacts in a strictly dose-dependent manner.

#### **1.5.4 WAP and FnIII domain function in anosmin-1**

The high conservation of WAP domain evident in a wide number of species from vertebrates (chicken, zebrafish, human) to invertebrates (*Drosophila*, *Caenorhabditis elegans*) suggests a crucial role of this motif in the integral protein (Figure 1.5(a)). Clinical evidence for this prediction is provided by the presence of a missense mutation generated by a C172R (cysteine into arginine at codon 172) substitution shared by three X-KS brothers (Oliveira et al., 2001). In addition to anosmia and HH, synkinesia was observed in all of them, with bilateral cryptochidism in two and unilateral renal aplasia in one. Another missense mutation of C163Y has recently been described in an X-KS family accompanied by mirror movements. These single amino acid substitutions are predicted to disrupt the conserved C151-C163, C157-C172 disulphide bonds within the WAP domain. These findings emphasize the functional importance of the WAP domain for olfactory system, corticospinal tract and renal development.

(a)



(b)

Anosmin-1	130	KQGD	CPAPEKASGFA-AA	CVES--	CEVDNE	CSGVK	CCSNG	CG-HT	CQVPK		
ps20	62	RADR	PPPPRTLPPG--	ACQAAR	CQADSE	CPRHRR	CCYNGCA	YAC	LEAV		
HE4	77	KEGS	CPQVNINFPQLG-L	CRDQ--	CQVDSQ	CPGOMK	CCRNG	CGKVS	CVTPNF		
Elafin	72	KPGS	CPILIR	CAML--	NPPNR--	CLKD	TD	CPGIKK	CCEGS	CG-MA	CFVPQ
SLPI	85	KPGK	CPVTYGO	CLML--	NPPNF--	CEMDGO	CKRDLK	CCMGM	CG-KS	CVSPVKA	

Figure 1.5 (a) Sequence comparison of anosmin-1's WAP domain within vertebrate/invertebrate. The positions of the four-disulphide bridges and the identity of amino acid sequence to anosmin-1 are indicated. The highly conserved residues are indicated with grey background. (b) Multiple sequence alignment of human WAP domain sequences in homologous proteins. Databases accession numbers corresponding to SWISS-PROT or TrEMBL are P23352 (anosmin-1), Q9HC57 (ps20), Q14508 (HE4), P19957 (Elafin) and P03973 (SLPI). Residue numbers correspond to the beginning of each domain. The conserved cysteine residues are shown in yellow type with a grey background.

Indeed, homologous four-disulfide core motif (4-DSC) proteins have been identified in other members of the WAP family, namely elafin, secretory leukocyte protease inhibitor (SLPI), PS20, human epididymal secretory protein (HE4) and rat WDNM1 (Figure 1.5(b)). The first two proteins have been found to inhibit serine protease activity, a property attributed to the WAP domain (Heinzel et al., 1986; Wiedow et al., 1990); members of this family also exhibit fundamental roles in cell growth control, differentiation, and tissue remodelling (Larsen et al., 1998). For instance, elafin inhibits pulmonary artery smooth muscle cell proliferation by inhibition of elastase-mediated proteolytic release of mitogenic active FGF-2 from ECM (Thompson and Rabinovitch, 1996). WDNM1 gene downregulation has been linked with tumorigenesis in metastatic rat mammary adenocarcinomas (Dear and Kefford, 1991). PS20 is a novel WAP protein family member that shares about 30% amino acid similarity with anosmin-1 WAP domain. Its expression has been identified in rat prostate smooth muscle and vascular smooth muscle. It can inhibit the proliferation of prostate carcinoma (PC-3) and COS-7 cells, acting possibly *via* reduction of active insulin-like growth factor II availability secondary to decreased serine protease activity (Larsen et al., 1998). Based on these models, it was hypothesised that an important function of the anosmin-1 WAP domain might be to regulate cell proliferation and possibly differentiation, by an interaction with a relevant serine protease, and that such an activity might be altered in the C172R or C163Y missense mutations.

By contrast, the FnIII domain was predicted to demonstrate heparan sulphate (HS)-binding activity, there being high homology within these motifs with a number of NCAM superfamily members, such as NrCAM, NgCAM, L1 and neurofascin (Lander, 1989). These CAMs have roles in neuronal interaction, migration and axonal elongation (Dodd and Jessell, 1988; Lander, 1989). While the homologies with these CAM molecules suggest direct FnIII domain involvement in neuronal development, it could not be excluded that these domains possess other functional characteristics. For example, part of the FnIII domains in the insulin and IGF receptors determine the affinity and specificity of ligand binding (Kristensen et al., 1999; Molina et al., 2000),

possibly through regulating the structure/function of N-terminal binding motifs. Thus, upon attachment to HS, the FnIII domain might modify the WAP domain configuration, exposing the active site for ligand binding. Furthermore, it might be expected that the FnIII domains of anosmin-1, and indeed its tertiary structure, determine its adherent properties as well as conferring the binding specificity of anosmin-1.

Recent transgenic studies using *KAL-1* over-expression mutants in *C.elegans* are consistent with the multifunctional roles of these two domains (Bulow et al., 2002). Axonal branching and the misrouting activity of sensory neurons appear to depend on the different domains of the *C.elegans* anosmin; thus the WAP domain induces the misrouting phenotype whilst the FnIII domains control neurite outgrowth and branching, both dependent on HS interactions. Moreover, with respect to the protein domain alignment, the highly conserved regions of anosmins in various species from invertebrates to vertebrates are localised to the N-terminal WAP and the first FnIII domains, implicating these fragments in the molecule biological activity (MacColl et al., 2002a).

### **1.6 Molecular modelling of anosmin-1**

Difficulties in generating milligram quantities of purified anosmin-1 have curtailed structural studies of the three-dimensional structure of anosmin-1, necessary for the understanding of structure-function relationships. Computer generated protein homology modelling has partially overcome this problem. In previous work from this laboratory (Robertson et al., 2001), theoretical model structures for the WAP domain and FnIII domains of anosmin-1 were generated based on protein homologies with the established elafin protease inhibitor structure and 23 structures from 12 crystal and NMR structures of FnIII domains respectively.

Based on the crystal and NMR structures for elafin, a WAP domain model of anosmin-1 was successfully generated. Elafin has four-disulphide bridges: three disulphide bridges are clustered together in a plane (“base” disulphide bridges) linking

the  $\beta$ -sheet core of the protein to the external strands and a single disulphide bridge linking the inner core to the external loop interacting with the protease. In the homology molecular model for anosmin-1, the cluster of disulphide bonds of C134-C164, C151-C163 and C157-C172 serve as the base disulphide bridges for the structural scaffold, and a single disulphide bridge of C147-C168 links the active site to the core. Notably, the cysteine-147 of anosmin-1 had to be relocated to the opposite side of the surface loop in relation to cysteine-83 of elafin. Thus, the equivalent position of the predicted scissile peptide bond of anosmin-1 was shifted to glycine-142-phenylalanine-143 in front of the second cysteine residue, but was still located on the outside of the bottom of the model. Although it is unknown whether this structural arrangement might result in an inhibitory activity similar to the serine protease inhibitory activity of elafin, this site is highly likely to represent a potential WAP-binding motif for protease or receptor.

The four anosmin-1 FnIII domains could be defined in terms of seven conserved  $\beta$ -strands (denoted A, B, C, C', E, F and G). The GFCC' sheet of the FnIII domain is functionally important for intermolecular interactions. A large basic surface electrostatically mapped onto the individual FnIII domain is predicted to represent a HS-binding site, and contains the HS binding-sequence, S<sup>278</sup>KHFRK<sup>283</sup> on the  $\beta$ -strand G of FnIII-1 domain, V<sup>325</sup>HHYKV<sup>330</sup> on the  $\beta$ -strand C of FnIII-2 domain and the Q<sup>421</sup>RRRPTRP<sup>428</sup> at the beginning of FnIII-3 domain, all of which are highly conserved in the human, chicken and quail. Two other predicted HS-binding sites are located immediately following the four FnIII domains in anosmin-1 at residues 660±665 and residues 670±675. All three other FnIII missense residue substitutions (N267K, E514K, F517L) observed in patients with X-KS could be mapped to the GFCC'  $\beta$ -sheet of FnIII-1 and Fn-III-3 domains, in close proximity to the large basic surface; these might be predicted to alter the basic surface charge thereby potentially interfering with adherent binding to HS (Robertson et al., 2001).

## **1.7 Molecules involved in the olfactory system development**

Since anosmia and HH are invariable concomitants of X-KS, anosmin-1 would therefore appear to play an essential role in olfactory and GnRH neuronal ontogeny. However, anosmin-1 is only one of a large number of molecules involved in the ontogeny of this system. Indeed, a variety of transcription factors and growth factors mediate neuronal cell differentiation and proliferation, whereas other soluble and insoluble molecules regulate their migration, destination finding and synaptogenesis.

### 1.7.1 Transcription factors and growth factors

During early embryogenesis, the progenitor neuron cells throughout the CNS express a series of transcriptional factors of the homeodomain class and extracellular growth factors including the Hedgehog (HH), wingless (Wg/Wnt) and fibroblast growth factor (FGF) to continuously generate neurons, subdivide each CNS region into compartments and regulate their size (McMahon and Bradley, 1990; Hynes et al., 1995; Meyers et al., 1998). The deficiency of *Pax6* in the mouse, a homeodomain gene expressed as early as E10.5 (Walther and Gruss, 1991), has been shown to disturb the developmental formation of olfactory bulb, nasal cavities, olfactory epithelia and lead to the absence of GnRH-immunoreactive neurons (Walther and Gruss, 1991; MacColl et al., 2002b). Mutation of other homeodomain genes, including *Emx*, *Xt*, *Tbr1*, have also been shown to lead to failed generation and disrupted connections of mitral/tufted and OB interneuron cells. *Emx2* is expressed as early as E12.5 (Gulisano et al., 1996) and its mutants have been shown to cause the disorganization of mitral/tufted cells in olfactory bulb (Yoshida et al., 1997). In addition, in *Tbr1*<sup>-/-</sup> mice, mitral cells are lacking, but morphogenesis of the bulb still occurs (Bulfone et al., 1998), indicating that mitral cell differentiation and bulb morphogenesis can occur independently of one another.

There are more than 20 members of the FGF family; *Fgf8* is specifically expressed in the anterior forebrain from E9 to at least E12.5 (Crossley and Martin, 1995) and the partial loss of function of *Fgf8* in E18.5 can result in a small telencephalon that lacks olfactory bulbs and a normal midline (Meyers et al., 1998). *Fgf2* has also been implicated in cortical neurogenesis and promoting neuronal

progenitor cell proliferation rather than in telencephalic patterning (Dono et al., 1998). Importantly, *Fgfr1*, one of four known genes encoding for the FGF receptor (FGFR), has been identified with morphological specificity in OB development. In the *Fgfr1*-deficient telencephalon (Hebert et al., 2003), the OB do not form and evaginate normally, while other anterior telencephalic structures and anteroposterior (AP) axis patterning are largely normal, implicating specific FGFR1 signaling-dependent pathways in OB morphogenesis.

### **1.7.2 Molecules involved in neuronal migration**

At the onset of neurogenesis, neurons begin to move and migrate towards their final destinations and then subsequently establish the correct synaptic network. Several classes of molecules have been extensively studied for their potential influences on these pathfinding processes, including those related to local contact (membrane receptors and adhesion extracellular molecules) and those related to communication across distances (chemoattractant or repellent molecules, neurotransmitters) (Figure 1.6).

Several molecules are incriminated in local contact-mediated communication. These include: (1) Olfactory receptor (OR). OR has been demonstrated as a crucial molecule for accurate destination finding in OB glomerulae. Olfactory sensory neurons with deleted or mutated receptor expression do not converge to their original glomerular destination, but divert their projection to different regions (Wang et al., 1998). (2) Cadherin-related neuronal receptor (CNRs). In the olfactory bulb, two different CNRs have been shown to be expressed in a single olfactory neuron while a small proportion of neurons expressed one or the other CNRs. Different CNR combinations in olfactory neurons could impart connection specificity (Serafini, 1999). (3) Nasal embryonic LHRH factor (NELF). NELF has been identified on the surface of olfactory and GnRH neurons (Wray, 2002), and plays a role in guidance of these both neurons to the rostral telencephalon (Kramer and Wray, 2000). Interestingly, down-regulation of NELF is demonstrable when these cells enter the telencephalon and arrive at the outer nerve layers of the OB, suggesting that this



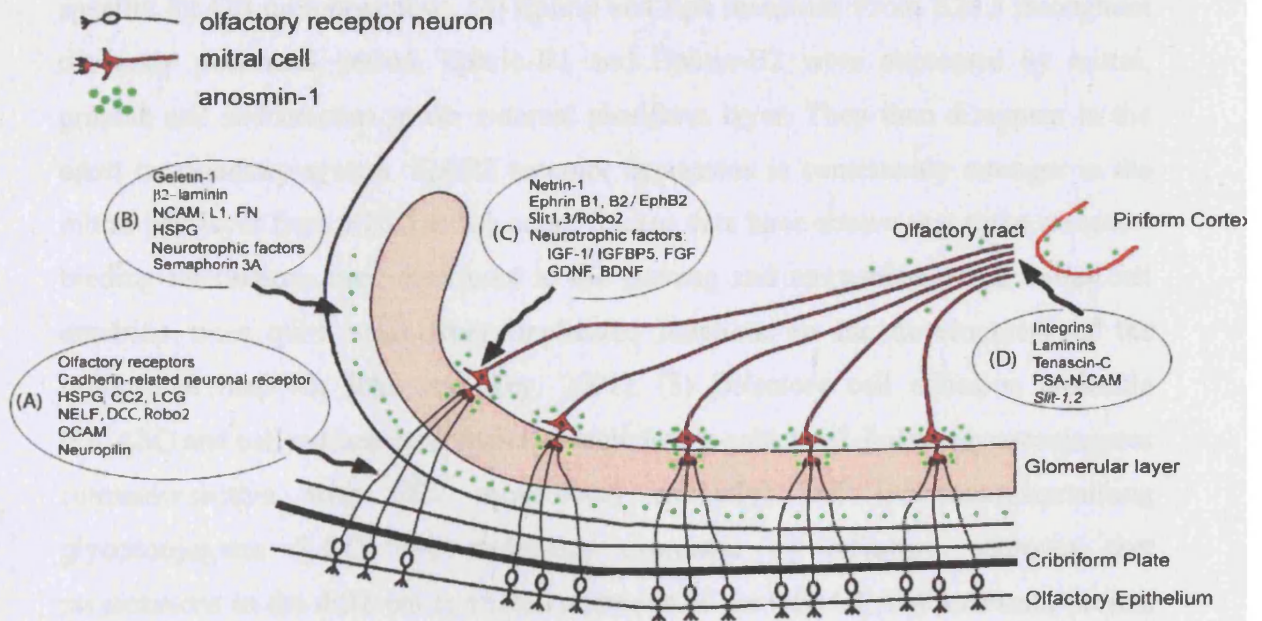


**Figure 1.6** Structure of the olfactory system and molecules known to mediate olfactory neuron migration, trajectory and convergence within olfactory bulb region during embryogenesis. Anosmin-1 is denoted as green dots. Group A: molecules expressed by olfactory neurons guide the migration and topographic projection of olfactory axons to the presumptive olfactory bulb. Group B: molecules within olfactory nerve layer are involved in specifying the olfactory axons projection to correspond glomeruli. Group C: molecules are expressed by mitral cells. Group D: molecules expressed along the olfactory tract direct projection of afferent mitral cell axons to the olfactory cortex. BDNF: Brain-derived neurotrophic factor; CC2: Cell surface glycoprotein; DCC: Deleted in colorectal cancer--netrin receptor; Eph: Ephrin receptor; FGF: Fibroblast growth factor; FN: Fibronectin; GDNF: Glial cell line-derived neurotrophic factor; IGF: Insulin-like growth factor; IGFBP: Insulin-like growth factor binding protein; LCG: Lactosamine-containing glycan; L1: Neural cell adhesion molecule; NCAM: Neural cell adhesion molecule; NELF: Nasal embryonic luteinizing hormone-releasing hormone factor; OCAM: Olfactory cell adhesion molecule; PSA-N-CAM: Polysialylated form of neural cell adhesion molecule; Robo: Roundabout--slit receptor

molecule is location dependent and possibly induces the expression of relay cues specific for OB morphogenesis. (4) Ephrin and Eph receptors. From E20.5 throughout the early post-natal period, Ephrin-B1 and Ephrin-B2 were expressed by mitral, granule cell and neurons in the external plexiform layer. They then disappear in the adult rat olfactory system. EphB2 receptor expression is consistently stronger in the mitral cell layer from E20.5 to the adult. Recent data have shown that these receptor-binding interactions may contribute to the pruning and reorganisation of mitral cell dendritic trees quite apart from implicated functions in the development of the retinotectal map (St John and Key, 2001). (5) Olfactory cell adhesion molecule (OCAM) and cell surface carbohydrates including  $\alpha$ -galactosyl-linked glycoconjugates (immunoreactive with CC2 monoclonal antibody) and lactosamin-containing glycoconjugates (LCG) are molecules expressed by olfactory neurones that project axons to the different restricted segments of the OB. OCAM<sup>+</sup> neurones project axons to the OB excluding the dorsomedial quadrant, which is targeted by CC2<sup>+</sup> axons (Schwartz and Crandall, 1991; Yoshihara et al., 1997). In contrast, LCG (+) axons specifically project to the ventral nerve layer of the OB (Crandall et al., 2000). Interestingly, only migratory GnRH neuron cells but not hypothalamic GnRH cells express immunoreactive LCG, implicating the involvement of this molecule in GnRH migration. (6) Cell adhesion and ECM molecules including laminin, fibronectin, neural cell adhesion molecule (NCAM), tenascin, galectin and proteoglycans are known to play significant roles in development of the nervous system. The expression pattern of laminin, fibronectin and NCAM along the primary olfactory neuron migratory pathway delineate and guide olfactory neuron axons to correctly project towards telencephalon through cell-ECM attachment (Calof and Lander, 1991; Whitesides, III and LaMantia, 1996). Laminin-induced migration of embryonic olfactory neurons can be mediated and enhanced by an endogenous lectin, galectin-1 (Mahanthappa et al., 1994; Gong and Shipley, 1996). Despite providing the adhesion highway for olfactory neuron movement, these molecules might directly stimulate the neurite outgrowth as they do on neurogenesis (Moos et al., 1988; Gong and Shipley, 1996). The importance of the polysialylated form of NCAM (PSA-NCAM) has also been shown on progenitor neuron cell migration from the subventricular zone (SVZ)

to their OB target. GnRH1 cells migrate along the route delineated by immunoreactive PSA-NCAM (Murakami et al., 2000). Furthermore, there have been several studies of proteoglycans in the ECM of the developing olfactory system. The heparan sulphate proteoglycans (HSPG) have been proposed to provide conductive cues for axon growth from olfactory epithelium to forebrain whilst chondroitin sulphate proteoglycans (CSPG) in surrounding mesenchyme restrict this migration (Treloar et al., 1996). Additionally, HSPG acts as activity-regulators on a wide range of insoluble or soluble molecules, which are further discussed in the next section.

Soluble molecules for distance-mediated communication: (1) Semaphorin (Sema)/neuropilin. Semaphorin 3A has been shown to repel the olfactory neuron expressing its receptor neuropilin-1 to project medially and laterally into the OB nerve layer, avoiding projection to OB ventral region with abundant semaphorin 3A expression (Crandall et al., 2000; Schwarting et al., 2000). Interestingly, different functions were observed within the secreted Sema family. Sema 3F repels LOT axons, preventing them penetrating the cortical plate and ganglionic eminence, while Sema 3B attracts LOT axons retaining them to the surface of the telencephalon (de Castro et al., 1999). (2) Slit/ roundabout (Robo). Slit proteins are putatively secreted by the septum and act as a long-range diffusible factor through their functional receptor Robo, a member of the immunoglobulin superfamily. The dominant effect of these ligands and their receptor- notably Slit2 and Robo-1 is to repel the LOT axons migration within the certain restricted pathway along lateral olfactory tract (Li et al., 1999; Hu, 1999; Nguyen Ba-Charvet et al., 1999). The Slit2-Robo-1 interaction is enhanced by cell-surface associated HS; the affinity of Slit for Robo is reduced some threefold in the absence of HS (Hu, 2001). (3) Netrin/deleted in colorectal cancer (DCC). The functional receptor for secreted molecules of the Netrin family, DCC is strongly expressed in developing mitral cells of the OB (Shu et al., 2000). However, neither secreted Netrin-1 nor a secreted form of the Netrin-G1 shows any effect on OB axonal outgrowth (de Castro et al., 1999; Li et al., 1999; Nakashiba et al., 2000). In contrast, Netrin and DCC interaction has been implicated in GnRH neuron guidance

and migration, more specifically in axon targeting to the median eminence (Deiner and Sretavan, 1999).

### **1.8 HS – molecular cross talk with anosmin-1**

Recently, Bulow et al performed a genetic modifier screen in *C.elegans* to identify loci that selectively interact with the *KALI-1* expression induced phenotype. Modifier loci encoding heparan-6-O-sulphotransferase and C5 epimerase (Bulow et al., 2002), which are crucial for normal HS synthesis, were identified; these findings concur with the demonstration of *in vitro* binding of anosmin-1 to heparin (Soussi-Yanicostas et al., 1996). Furthermore, in this experiment, there were little or no demonstrable effects of mutants of netrin/DCC, Ephrin/Eph-receptor, slit/robo, semaphorin,  $\alpha$ -integrin and ECM molecules such as perlecan on the *KALI*-induced phenotype (Bulow et al., 2002). From these studies it is evident that a necessary prerequisite of anosmin-1 function is the presence of HS with specific sulphation patterns. Indeed, HS is known to be involved in the binding of a wide range of ligands in both physiological and pathophysiological processes.

#### **1.8.1 Synthesis and modification of the HS**

HS, a unique class of the macromolecular polysaccharides known as glycosaminoglycans, is composed of disaccharide repeat units of alternating uronic acid (D-glucuronic acid [GlcA] or L-iduronic acid [IdoA]) and D-glucosamine (GlcN) residues with variable sulphation patterns. These sugar chains are anchored onto the specific “core” proteins through covalent complex formation, giving specific HS proteoglycans such as membrane-associated syndecan1-4, glypican1-6, epican, betaglycan, and secreted forms of perlecan, agrin and collagen XVIII. (Kjellen and Lindahl, 1991; Iozzo, 1998; Halfter et al., 1998; Esko and Lindahl, 2001). The biosynthesis of HS comprises three steps: chain initiation, polymerisation and modification (Turnbull et al., 2001; Esko and Lindahl, 2001).

HS synthesis is initiated by attachment of tetrasaccharides (glucuronic acid-galactose-galactose-xylose) onto selected serine residues in the core protein.

Tetrasaccharide linker is synthesized in a step-wise manner by the action of glycosyltransferases. The transfer of the next sugar residue for HS chain elongation is completed by specific transferases (HS co-polymerases) that add alternating [1-4] linked GlcA and N-acetylglucosamine (GlcNAc) residues. As synthesis proceeds, some regions are modified by a series of interdependent enzymatic reactions. First, N-acetylglucosamine GlcNAc is deacetylated and N-sulphated by N-deacetylase/ N-sulfotransferase (NDST). Second, GlcA residues are then epimerised to IdoA units by glucuronyl C-5 epimerase. Finally, these modified disaccharides will receive the bulk of the subsequent O-sulphation. An iduronosyl 2-O-sulphotransferase (2-OST) adds an O-sulphate group to IdoA at C2, followed by the O-sulphation at C6 of glucosamine by a glucosaminyl 6-O-sulphotransferase (6-OST). The modification reactions are completed with modification of a few residues by glucosaminyl 3-O-sulphotransferase (3-OST). In terms of the relative distribution of the major N-substituents of the GlcN residue, HS can be characterized as: contiguous N-acetylated disaccharide units (NA domain), N-sulphated sequences of variable length (NS domain), and alternating N-acetylated and N-sulphated units (NA/NS domain) (Figure 1.7).

### **1.8.2 HS structure diversity and functional specificity**

HS ligand-binding was once thought to be a relatively nonspecific charged ionic interaction between negatively charged HS and positively charged protein. However, many HS ligands require HS sequences of well-defined length and structure (Table 1.2). Van der Waals, hydrogen bond and hydrophobic interactions may also be involved (Thompson et al., 1994). In turn, HS binding proteins often contain consensus sequences consisting of clusters of basic residues. Lysine, arginine or glutamine are frequently involved in contacts with the HS sulphate and carboxyl groups, and their spacing, sometimes determined by secondary structure, may control binding specificity (Hileman et al., 1998).

Specific sets of variably modified disaccharides usually within the NS or NA/NS domains preferentially determine specific ligand binding (Jackson et al., 1991). The best-studied example is the interaction between HS/heparin and antithrombin, which



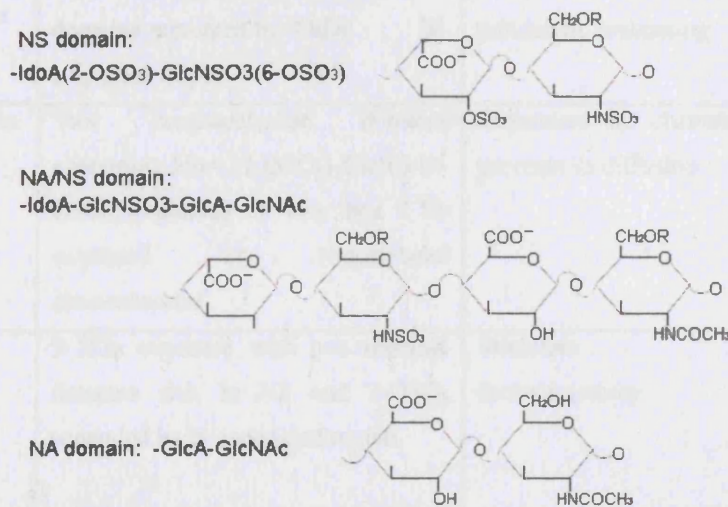
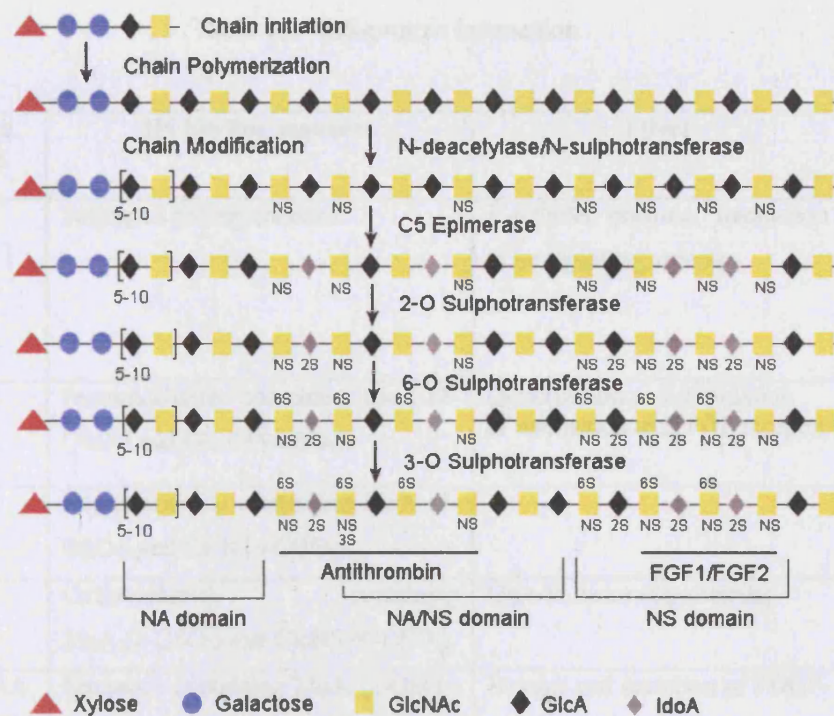


Figure 1.7 Scheme of HS chain biosynthesis. HS biosynthesis begins with the tetrasaccharides linkage region that composed of xylose (Xyl), two galactose (Gal) and a glucuronic acid (GlcA). The HS chain is then polymerised by the alternate addition of N-acetylglucosamine (GlcNAc, yellow square) and glucuronic acid (GlcA, black diamond). These simply unmodified GlcNAc-GlcA disaccharide repeats are then modified by a series of modification enzymes: converting GlcNAc to N-sulphated glucosamine (GlcNS), GlcA to IdoA (gray diamond), and finally adding 2-O sulphate to IdoA, 6-O sulphate to GlcNAc and GlcNS, and 3-O sulphate to GlcNS residues. The modification of the monosaccharides is indicated by NS, 2S, 6S and 3S. The regions implicated in binding of FGF1/FGF2 and antithrombins are also shown. Structural domains (NS, NA/NS, NA) in HS are defined with regard to the distribution of GlcN N-substituents as indicated. (Taken from Esko and Lindahl, 2001).

Table 1.2 HS-protein interaction

	Protein ligand	HS binding sequence	Effect	Reference
GF, C	BMP-2	Sulphated polysaccharides	$K_d=20\text{nM}$ , enhance, interaction to its signalling receptor	(Takada et al., 2003) (Ruppert et al., 1996)
	FGF-2	Pentasaccharide containing IdoA (2-OSO <sub>3</sub> ) and GlcN (6-OSO <sub>3</sub> )	Dimerization and stimulation of interaction with FGF receptor	(Guimond et al., 1993)
	FGF-1	Hexasaccharide containing IdoA (2-OSO <sub>3</sub> ) and GlcN (6-OSO <sub>3</sub> )		(Guimond et al., 1993)
	HGF	Octasaccharide containing IdoA (2-OSO <sub>3</sub> ) and GlcNS (6-OSO <sub>3</sub> )	Growth factor sequestering	(Ashikari et al., 1995)
	PDGF-AA	Sequence containing IdoA (2-OSO <sub>3</sub> ) and GlcNS (6-OSO <sub>3</sub> )	Storage and secretion of PDGF-AA, affecting receptor binding	(Feyzi et al., 1997b)
	$\gamma$ -interferon	Two N-sulphated hexasaccharide domains separated by 7 kDa N-sulphated region	Dimerization and modulation of proteolytic processing	(Lortat-Jacob et al., 1995)
	Interleukin -8	Two hexasaccharide domains containing IdoA (2-OSO <sub>3</sub> )-GlcNS (6-OSO <sub>3</sub> ) separated by less than 7 N-sulphated or N-acetylated disaccharides	Sequesters the chemokine and prevents its diffusion	(Spillmann et al., 1998)
GFBP	Platelet factor 4	9 kDa sequence with two terminal domains rich in NS and 2-OSO <sub>3</sub> separated by N-acetylated region	Stimulate platelet factor 4 activity	(Stringer and Gallagher, 1997)
	IGFBP 5	Sequence containing IdoA (2-OSO <sub>3</sub> )	Decrease IGF/IGFBP binding affinity, and release IGF to bind its receptor	(Arai et al., 1994)
P, PI	uPA	5 disaccharide repeats containing GlcNS (6-OSO <sub>3</sub> )-IdoA (2-OSO <sub>3</sub> )	Confer specificity of uPA/uPA receptor interaction	(Pucci et al., 2001)
	Antithrom bin III	GlcN (S/COCH <sub>3</sub> )-GlcA-GlcNS (3-OSO <sub>3</sub> )-IdoA (2-OSO <sub>3</sub> )-GlcNS (6-OSO <sub>3</sub> )	Conformational change of the protease inhibitor, increasing its antithrombin activity	(Lindahl et al., 1984)

	<b>Protein ligand</b>	<b>HS binding sequence</b>	<b>Effect</b>	<b>Reference</b>
<b>Lipid metabolism</b>	ApoE	Octasaccharide containing. IdoA (2-OSO <sub>3</sub> ), GlcNS(6-OSO <sub>3</sub> ) and limited 3-OSO <sub>3</sub>	Inhibit ApoE related, neurotoxicity	(Bazin et al., 2002)
	lipoprotein lipase	containing stabilization of dimeric LPL, IdoA (2-OSO <sub>3</sub> )-GlcNS(6-OSO <sub>3</sub> )	immobilization, internalization	(Parthasarathy et al., 1994)
<b>ECM molecules</b>	laminin	Dodecasaccharide composed of repeating IdoA(2-OSO <sub>3</sub> )-GlcNS(6-OSO <sub>3</sub> )	Adhesion to ECM	(Parthasarathy et al., 1998)
	fibronectin	7-8 N-sulphated disaccharides containing IdoA ± (2-OSO <sub>3</sub> )	adhesion, focal adhesion formation	(Walker and Gallagher, 1996)

GF, C: Growth factors and cytokines; GFBP: Growth factor binding protein; P, PI: Proteases and proteases inhibitors.



leads to inactivation of thrombin, factor Xa, and other serine proteases of the coagulation cascade. This interaction depends on a very specific structure of a pentasaccharide that contains a central 3-O-sulphated GlcN residue (GlcN(6S)-GlcA-GlcNS(3S)-IdoA(2S)-GlcNS(6S)) (Bourin and Lindahl, 1993). Another example is FGF1 and FGF2 both of which exert their mitogenic activity by interaction with the N-sulphated pentasaccharide HS sequence containing IdoA2S and GlcN6S unites in distinct combination. 2-O-sulphate is required for high affinity binding of FGF to receptor whilst an additional 6-O-sulphation is required for receptor activation (Ornitz et al., 1996). Other factors such as spacing between the protein-binding sites also play a role: HS chains with two binding sequences separated by a 7 kDa region with low sulphation is required for  $\gamma$ -interferon dimerization, thereby modulating cytokine processing and biological activity (Lortat-Jacob et al., 1995). Involvement of discontinuous HS chain domains in protein binding has also been reported for other ligands including platelet factor 4 and IL-8 (Table 1.2).

The *in vivo* role of HS structural specificity has been demonstrated using genetic approaches that involve the disruption of genes for specific enzymes of HS synthesis and modification. In *Drosophila*, mutants lacking N-deacetylase/N-sulfotransferase (NDST) or an HS copolymerase resulted in disrupted signalling by the morphogens Hedgehog (HH), Wingless (Wg) and Decapentaplegic (DPP) and FGF (Perrimon and Bernfield, 2000; Selleck, 2000). The genetic screen of *C.elegans* orthologues of HS-modifying enzymes revealed that C5-epimerization, 2-O-sulphation and 6-O sulphation can affect axonal development. Two specific signalling pathways, the *C.elegans* SLT-1/Slit and *KAL-1/anosmin-1* are disrupted in a 6-O- sulfatransferase or C5-epimerase deficient background (Bulow and Hobert, 2004). The same experimental approach also suggested that sulphation at C6 and C2 site might be important for ephrin and integrin signalling. Studies in the mouse have provided similar evidence. An IdoA 2-O-sulfotransferase gene mutation causes renal agenesis and perinatal lethality (Bullock et al., 1998). NDST1 mutants exhibit neonatal lethality, whereas NDST2 defects have a restricted phenotype in which only heparin

formation in connective tissue mast cells is affected (Forsberg et al., 1999; Ringvall et al., 2000).

### 1.8.3 HS-ligand interaction

HS interacts with a wide spectrum of insoluble and soluble ligands to exert a variety of functions from organization of cell-cell and cell-ECM adhesion to regulation of cell proliferation and differentiation. In these physiological processes, HS can act as a dominant controller to concentrate its ligand either in the ECM or onto cell surface, as a co-receptor to modulate ligand-receptor interaction or as a docking platform for protease-substrate complex formation (Wight et al., 1992; Bernfield et al., 1992; Rapraeger, 1993) (Figure 1.8).

In ECM, HS serves as a storage reservoir from which the growth factors and cytokines can be released in active forms to interact with high-affinity receptor. Specifically, the binding of these molecules to HS protects them from proteolytic degradation. Thus, upon introduction of the stimulus, these molecules can be released rapidly, avoiding *de novo* protein synthesis (Vlodavsky et al., 1996).

HS regulates distribution of potent morphogens, growth factors and even antagonists of these signaling molecules by controlling the diffusion, gradient formation and degradation from the cell surface. In the *Drosophila* wing imaginal discs, Hedgehog (HH) was observed to travel about 8-10 cell diameters from the site of its production to induce the expression of its target gene *patched* and *decapentaplegic (dpp)*, the orthologue of vertebrate BMP (bone morphogenetic protein), along the anteroposterior boundary. This movement has been proposed to be dependent on a specific type II transmembrane HS polymerase encoded by the *tout-velu (ttv)* gene. The properly constituted HS allows Hedgehog detached from cells diffuse through tissues (Strigini and Cohen, 1997; Bellaiche et al., 1998). HS is also required for wingless (Wg/Wnt) signaling in a manner that is not directly involved in activation of its signaling receptors (*Frizzles*), but through limiting extracellular Wg diffusion (Baeg et al., 2001). In addition, scattering of Noggin, a BMP antagonist, appears to be

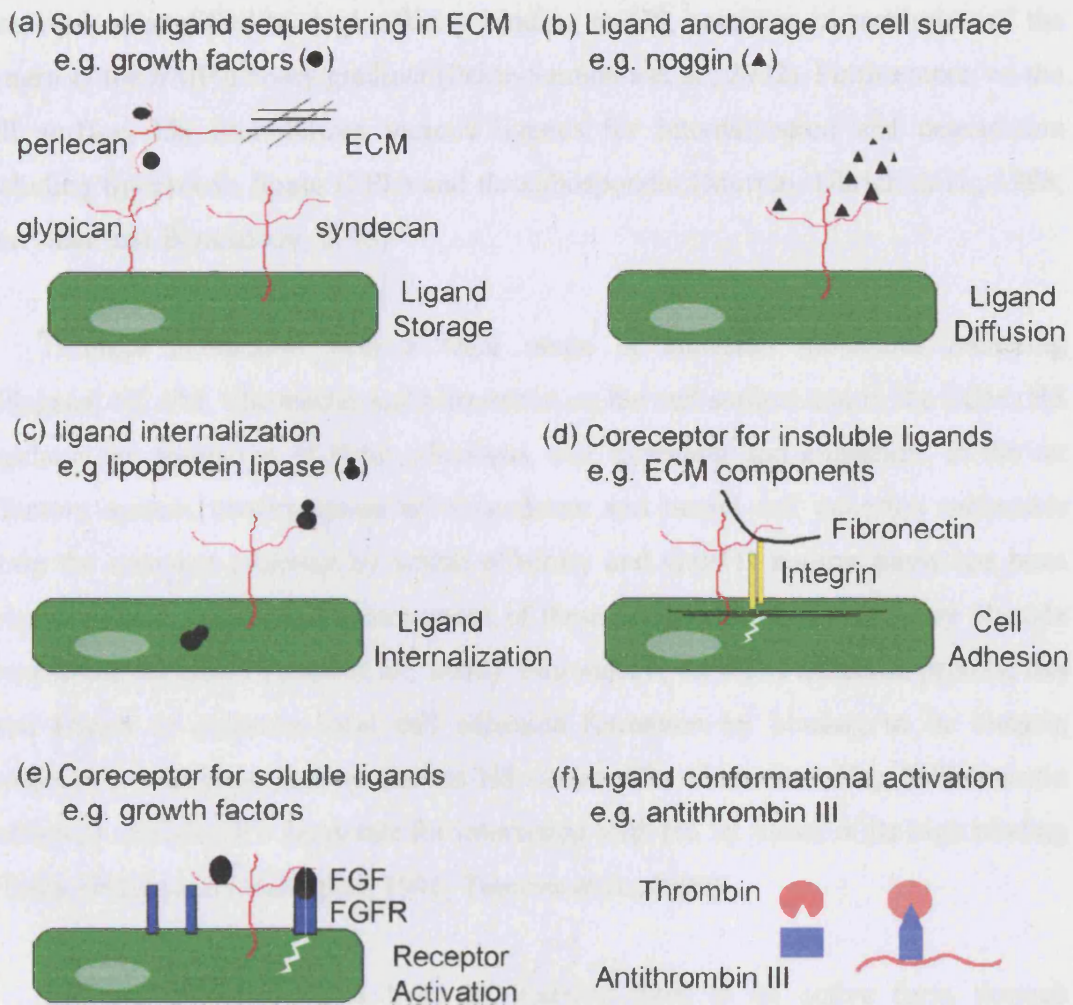


Figure 1.8 Multifunction of HSPG in regulating protein activity. (a) HS chain covalently attaches onto core protein to form typical three types of HSPG. Syndecan contains a conserved transmembrane domain; glypican is tethered to the cell membrane by a GPI anchor, and perlecan is a soluble form of HSPG. In extracellular matrix (ECM), perlecan serves as storage reservoir from which bound ligand (growth factors) can be released when required. (b) HSPG can concentrate ligand (Noggin, Wg/Wnt) onto cell surface and determine its distribution and diffusion. (c) HSPG binds some soluble ligands (lipoprotein lipase and serpin) onto the cell surface and takes ligands into cells for degradation or recycling. (d) Through binding to the ECM component, HSPG immobilizes the receptor complex to the adhesion conjunction site and induce the reorganization of cytoskeleton. (e) As coreceptor for soluble ligand (growth factors, chemokines, cytokines), HSPG promotes dimerization of the ligand and receptor to induce signalling phosphorylation and/or stabilizing an active ligand-receptor complex through the formation of a ternary complex, a model best seen in FGF/FGFR. (f) A specific pentasaccharide sequence containing a specific 3-O-sulphated glucosamine residue can induce a conformational change in antithrombin III that dramatically accelerates its binding and inhibition of the protease thrombin. (Adapted from Bernfield, et al, 1999).

restricted or modified by high affinity binding to HS, resulting in restriction of the pattern of the BMP activity gradient (Paine-Saunders et al., 2002). Furthermore, on the cell surface, HS immobilizes various ligands for internalization and degradation including lipoprotein lipase (LPL) and thrombospondin (Murphy-Ullrich et al., 1988; Berryman and Bensadoun, 1995).

Through interaction with a wide range of adhesion molecules including collagens, NCAM, fibronectin and vitronectin on the cell surface and in the ECM, HS regulates the formation of focal adhesions, cell spreading and migration. In the rat olfactory system, co-expression of N-syndecan and neural cell adhesion molecules along the common pathway by which olfactory and GnRH1 neuron travel has been proposed to contribute to the movement of these neurons from the olfactory placode towards the forebrain (Toba et al., 2002). Fibronectin, an ECM adhesion protein, has been shown to promote local cell adhesion formation by binding to its integrin receptors and glypican and syndecans HS chains. The C-terminal Hep II fibronectin domain is considered a candidate for interacting with HS by virtue of its high binding affinity (Walker and Gallagher, 1996; Tumova et al., 2000).

HS can convert ligands from an inactive form to an active form through conformational changes. A specific example is the action of HS in regulating the anticoagulant activity of antithrombin III (AT III). A specific pentasaccharide sequence containing a specific 3-O-sulphated glucosamine residue can induce a conformational change in antithrombin III (AT III) that accelerates 1000-fold its binding and inhibition of the protease factor Xa (Shriver et al., 2000a).

Finally, HS acts as a receptor or co-receptor to regulate the signalling of HS binding proteins in a number of diverse ways: promoting dimerization of the ligand and receptor to induce signalling phosphorylation and/or stabilizing an active ligand-receptor complex through the formation of a ternary complex. The best studied model for this phenomenon is the interaction between HS and the fibroblast growth factor system. Crystallographic studies show that an FGF2/FGFR1 crystal is formed in the

absence of heparin at an initial low affinity 1:1 complex, which may allow transient receptor dimerization enabling signalling only at high ligand concentrations (Wiesmann and de Vos, 1999; Ornitz, 2000). However, in the presence of appropriate HS molecules, HS bridges FGF2 and the FGFR1 by binding to a groove formed by the heparin-binding sites of both the ligand and the receptor, leading to a much more stable 2:2 FGF/FGFR signalling conformation and higher activation of the intracellular signalling cascade (Yan et al., 1993). So HS enables the formation of a high-affinity complex that potentiates receptor signalling at low growth factor concentrations. The critical effect of HS in this interaction is mediated by a specific pentasaccharide sequence in HS containing essential IdoA2S and GlcN6S residues.

#### **1.8.4 HSPG in cell events**

Physiological and pathophysiological processes are dependent on cell responses to a variety of different ECM cues, and the presence of relevant molecules immobilized on the cell surface. HS is one molecule mediating cellular talk from an extracellular signal to the intracellular response, either by its ligand-binding property, or by virtue of its proteoglycan (HSPG) structure.

##### **1.8.4.1 Focal cell adhesion and cytoskeletal reorganization**

A specific example is the role of HSPG in physiological processes including focal cell adhesion, spreading and cytoskeletal reorganization. Focal adhesions are specialised zones of tight cell-matrix interaction located at the termini of actin stress fibres present at the sites where the ECM is physically connected to a complex of signalling and cytoskeletal proteins *via* transmembrane receptors. Integrin has long been considered as the prototype of a signalling pathway enabling focal cell adhesion and full spreading (Schwartz et al., 1995; Schlaepfer and Hunter, 1998). Tyrosine kinases are activated following integrin (receptor) clustering after attachment to fibronectin, leading to phosphorylation of several focal adhesion components. Indeed, inhibition of tyrosine kinase prevents full spreading of cells and focal adhesion formation (Burrige et al., 1992; Akiyama, 1996). However, HSPG, together with integrin, can now be considered a dual receptor system active in cell-matrix adhesion.

Upon binding of fibronectin to the integrin receptor, cells attach and spread, but do not form stress fibres terminating in focal adhesion. The cytoskeletal reorganization requires the activation of protein kinase C (PKC) that is augmented by oligomerization of syndecan-4 (Oh et al., 1998; Saoncella et al., 1999). In addition, involvement of small Rho family GTPases in signalling through syndecan-4 enabling focal adhesion and stress fibre formation has been suggested (Saoncella et al., 1999). Further evidence for a direct interaction of HSPG to cytoskeletal molecules has come from the recent finding that the conserved cytoplasmic domain of all mammalian syndecans are capable of binding to PDZ domain proteins including syntenin, CASK, synbindin and synectin (Gao et al., 2000; Ethell et al., 2000; Bass and Humphries, 2002). The PDZ proteins are thought to be components of the submembrane molecular scaffold implicated in organising signalling complexes at defined membrane locations, such as cell junctions. These molecular interactions are triggered by extracellular ligands causing clustering of syndecans and inducing their multimerization.

#### **1.8.4.2 Synapse formation, axon guidance and neurite outgrowth**

In nervous system development, HSPG also acts as an essential component in the molecular orchestra in the processes of synapse formation, axon guidance and neurite outgrowth. Synapses can be regarded as highly specialised cell-cell contacts. Ethell et al demonstrated that the syndecan-2 cytoplasmic domain is tyrosine phosphorylated by EphB2 in neurons and phosphorylation promotes syndecan-2 clustering on the surface of dendrites (Ethell et al., 2001). They found that syndecan-2 phosphorylation by EphB receptors is a prerequisite for syndecan-2 induced dendritic spine formation. Thus, the cooperation of a cell surface HS proteoglycan and a receptor tyrosine kinase is a critical downstream event in spine formation triggered by cell surface recognition, most likely the receptor-ligand interactions between B-ephrins on presynaptic neurons and EphB receptor on postsynaptic neurons. Furthermore, the topological regulation of axonal extension, or axonal guidance, is one of the most crucial steps in forming the correct neuronal network. The involvement of HS in these processes has also been demonstrated using the developing *Xenopus* retinotectal pathway. Retinal axon elongation in the optic tract and penetration into the tectum was retarded by addition



of exogenous HS or enzymatic removal of endogenous HS (Walz et al., 1997). A similar observation was made in the cockroach embryo system where a pathfinding error occurred in heparitinase-treated embryos (Nyhus and Denburg, 1998). Interestingly, both experiments showed similar phenotypic alterations in the presence of a dominant negative FGF receptor or FGF2 antibody, suggesting that HS is involved in axon guidance through modulation of FGF signaling. In agreement with these observations, *in vitro* studies have provided insights that HSPG can support neurite outgrowth by activating growth-enhancing molecules, such as laminin, NCAM and FGF (Dow et al., 1988; Aoyagi et al., 1994; Jung et al., 2003).

#### **1.8.4.3 Cell proliferation**

Well defined biological functions of HS include modulation of cell proliferation through interaction with a wide range of growth factors and cytokines, including the family of FGFs (Rahmoune et al., 1998), transforming growth factor- $\beta$  (TGF $\beta$ ) (Lyon et al., 1997), platelet-derived growth factor (PDGF) (Feyzi et al., 1997a), hepatocyte growth factor/scattering factor (HGF/SF) (Lyon and Gallagher, 1994) and IL-2 (Najjam et al., 1998). Among these, modulation of HS in FGF/FGFRs actions on cell proliferation has been extensively studied, leading to the recognition of a number of mechanisms whereby HS acts as a co-receptor facilitating ligand-induced receptor oligodimerization and signal transduction. It has been suggested that HS induce conformational alterations of FGF2 leading to FGFR1 binding. However, this prediction has not been supported by structural analysis of co-crystals of FGF2 and heparin-derived oligosaccharides.

Systematic experiments using a set of size-defined HS saccharides from porcine mucosal HS and distinct FGFR transfected BaF3 cells have confirmed the specific modulating action of HS on FGF/FGFR signalling in both receptor and ligand-specific manner. First, some HS saccharides activated FGF2 signalling mediated by FGFR1c but not FGFR2c, whereas only larger HS fractions (>18 monosaccharide units) were able to strongly activate FGF2 signalling through FGFR3c. Second, these HS saccharides showed differential activation on FGF1 and FGF2 signalling through

FGFR1c (Guimond and Turnbull, 1999). These results highlight the importance of HS size and sequence on FGF/FGFR-specific signalling in cell proliferation. Finally, specific HS fractions of distinct structural composition have been identified, with differences in the primary structure of the constituent saccharides. Kinetic analysis has further confirmed differences in HS/FGFR binding affinity with 10-fold reduction in association constant seen with FGFR1c as compared with FGFR2c (Powell et al., 2002). Furthermore, neural tube derived HS from mouse embryonic forebrain and midbrain differentially regulates FGF signalling in a stage-specific manner (Ford-Perriss et al., 2002). Only HS from embryonic day 10 (E10) stage showed preferential activation for FGF8 *via* FGFR3c, whereas HS from both E10 and E13 activate FGF2 signalling through FGFR1c with greater potency than through other receptors. These stage-specific HS developmental actions are thought to be closely related to expression patterns of HS sulphotransferase isozymes responsible for creating diverse sulphation motifs in HS chain.

In addition, HS plays a role in determination of cellular fate either to proliferation or migration by specifically regulating signalling pathways associated with FGF/FGFR interaction. FGF binding to the cell surface induces FGFR dimerisation, and subsequent activation of receptor tyrosine kinase and autophosphorylation of the cytoplasmic domains of cognate receptors. Tyrosine autophosphorylation sites are then recognised by target enzymes such as PLC $\gamma$  and Src themselves becoming phosphorylated. The autophosphorylation site also serves as binding sites for Grb2-Sos complex formation thereby activating the Ras. Ras activation triggers a signalling cascade involving the Ser/thr kinase Raf, the dual specificity MAP kinase kinase (MEK), and MAP kinase (ERK1/2 isoforms), which are crucial for FGF-induced proliferation of many cell types (Klint and Claesson-Welsh, 1999). FGF-induced cell migration also involves this MAP kinase pathway *via* ERK, accompanied by Src and p38 MAP kinase pathways (Rodier et al., 1995; Jaakkola et al., 1998). It has been reported that in breast cancer cells the defined HS chain could enhance FGF2/FGFR1 interaction leading to proliferation by up-regulating MAPK pathway, whereas other defined HS specifically up-regulate MAPK, Src and its downstream FAK pathway



leading to an increase in the initial rate of cell migration (Nurcombe et al., 2000). HS may thus regulate the duration of FGF/FGFR activation or extent of downstream signalling induced by ternary complex formation.

#### **1.8.4.4 Tumour growth and metastasis**

Tumorogenesis represents a complex process involving selected genotypic and phenotypic changes in cells leading to unregulated cell growth, invasion and metastasis. These pathological processes require sequential steps involving proper coordination of cell proliferation, adhesion and migration, in which, as stated earlier, HSPG is also widely involved during physiological processes. Indeed, growing evidence has shown that HSPGs plays a crucial role as modulators at each step of tumorogenesis.

HS is involved in initial oncogenic transformation of cells. Changes in both expression level and structural characteristics of cell surface HS have been shown to correlate with transformation in certain cell types. For example, syndecan-1 expression is downregulated in various malignant tumours, including uterine carcinoma and multiple myeloma (Sanderson, 2001). Specific structural changes of HS have been noted during malignant transformation of colon cancer cells from adenoma to carcinoma (Jayson et al., 1998). Similarly, glypican-1 is believed to act as a negative regulator of cell proliferation for certain tumour types (Filmus, 2001). In addition to a role in initial cell transformation, HS bind growth factors, cytokines and structural proteins that are involved in modulating autocrine and paracrine signalling loops important for tumour growth and angiogenesis. The diverse structural characteristics of HS allow them to act either as inhibitors or potentiators of these signalling loops, depending on the sequence context (Liu et al., 2002a). Sets of HS fragments released from the cell surface of B16 melanoma cells by heparinase III or heparinase I treatment potentially exhibit opposite effects on primary tumour cell proliferation, neovascularization and secondary metastasis to the lung. Heparinase-III-derived HS fragments showed inhibitory effects on tumour, whereas the opposite changes were observed for heparinase I-treated tumours (Liu et al., 2002b). Furthermore, malignant

tumour cells can detach from the primary site and migrate into neighbouring tissues and remote locations, processes required degradation of cell-cell and cell-ECM adhesion. HS makes this situation more complex: on the one hand, HS along with structural proteins, such as collagen and laminin, form a physical barrier to prevent tumour metastasis; on the other hand, HS could concentrate and activate the tumour cell secreted proteases (plasminogen activator system, matrix metalloproteinases) for degradation of the basement-membrane barrier. It has been reported that HS/heparin could significantly enhance tumour cell invasion *in vitro* through stimulating plasminogen activation by cell-surface uPA; a 70-fold increase of HS induced plasminogen activation was observed (Brunner et al., 1998).

## **1.9 Candidate molecules interacting with anosmin-1**

### **1.9.1 Serine proteases**

As stated earlier, amino acid alignment of the WAP domain of anosmin-1 has shown the presence of eight highly conserved cysteine residues necessary for four-disulphide bridge formation seen in WAP protein family members, some members of which demonstrate inhibitory activity on serine proteases. Although considerable sequence diversity exists between members of this family, it seems plausible that serine proteases might constitute an interacting candidate with anosmin-1.

The serine protease family comprises a group of enzymes that catalyses hydrolysis of peptide bonds *via* a nucleophilic attack triggered by their active site containing serine, histidine and an aspartic acid residue (Figure 1.9). They are usually synthesized and secreted as inactive proenzymes (called zymogens) further activated by proteolysis. Members of this family play a role in intestinal digestion, blood coagulation and fibrinolysis, functions well characterized in the blood coagulation cascade including trypsin-like serine protease (thrombin, urokinase-type plasminogen activator (uPA) and tissue-type plasminogen activator (tPA)). In addition, several lines of evidence have pointed out the role of these serine proteases within the central nervous system. During neural development, serine proteases contribute to cell migration, axon outgrowth and synaptogenesis. In the adult, they play a role in

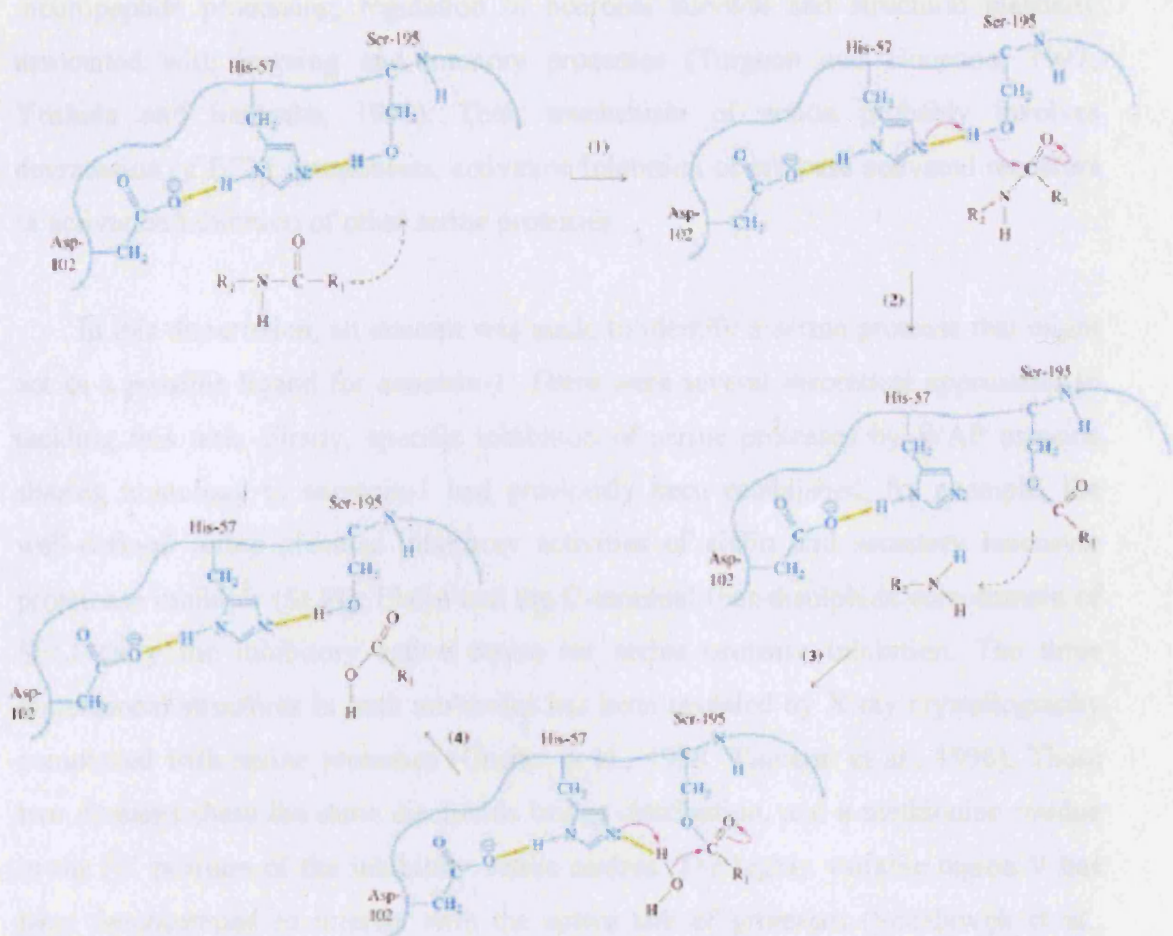


Figure 1.9 Mechanism of serine proteases catalysis. The mechanism by which chymotrypsin cleaves protein chain is shown here as a typical example that is applied to all of the serine proteases. The catalytic work of the proteases is done by the so-called catalytic triad, Asp102, His57, and Ser195. The first step appears to be His57 removing a proton from the Ser195 OH, while the O does a nucleophilic attack on the peptide carbonyl. The next step is the stage at which the protein chain actually is cleaved. The acyl part of the peptide that was cleaved, bound as an ester to Ser195 and the amine group of the peptide was released. A molecule of water was then required to hydrolysis of an ester to release the other end of the original protein and restore the catalytic triad to its beginning state. The yellow dot lines represent the hydrogen bond.

neuropeptide processing, regulation of neuronal survival and structural plasticity associated with learning and memory processes (Turgeon and Houenou, 1997; Yoshida and Shiosaka, 1999). Their mechanism of action probably involves degradation of ECM components, activation/inhibition of protease activated receptors or activation/inhibition of other serine proteases.

In this dissertation, an attempt was made to identify a serine protease that might act as a possible ligand for anosmin-1. There were several theoretical approaches to tackling this task. Firstly, specific inhibition of serine proteases by WAP proteins sharing homology to anosmin-1 had previously been established; for example, the well-defined serine protease inhibitory activities of elafin and secretory leucocyte proteinase inhibitor (SLPI). Elafin and the C-terminal four-disulphide core domain of SPLI carry the inhibitory active centre for serine protease inhibition. The three dimensional structures in both molecules has been revealed by X-ray crystallography complexed with serine proteases (Grutter et al., 1988; Tsunemi et al., 1996). These two domains share the same disulphide bridge distribution, and a methionine residue in the P<sub>1</sub>' position of the inhibitory active centres. The highly variable region V has been demonstrated to interact with the active site of proteases (Schalkwijk et al., 1999), suggesting that the corresponding regions of other WAP proteins might also serve as a specific determinant for serine protease binding. However, the inhibitory specificity is different between these two molecules. It is clear that elafin potentially and specifically inhibits the elastin-degrading serine proteases (human leucocyte elastase, protease 3) with a low equilibrium dissociation constant ( $K_i$ ) of 0.17 nM, while no inhibitory activity on chymotrypsin and trypsin was observed (Ying and Simon, 1993). In contrast, a wide range serine proteases including elastase, chymotrypsin and trypsin can be dramatically inhibited by SLPI (Smith and Johnson, 1985; Ying et al., 1994). These observations suggest that even though they all have a highly conserved 4-disulphide bridge, the various WAP domain proteins can exert distinct and even opposing activities on serine proteases. However, it still provides useful evidence that one member of trypsin-like serine protease (plasminogen activator system, thrombin and trypsin) might be a good candidate for anosmin-1 interaction.



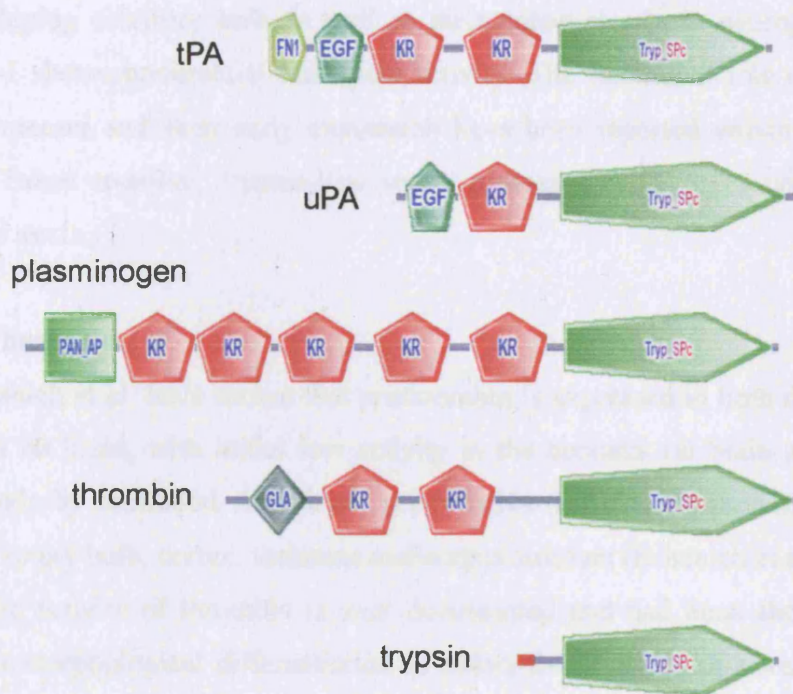


Figure 1.10 Structure of human trypsin-like serine proteases. SMART analysis is used for the comparison of domain alignment (<http://smart.embl-heidelberg.de>). PAN\_AP: divergent subfamily of APPLE domains; GLA: Domain containing Gla (gamma-carboxyglutamate) residues; EGF: epidermal growth factor domain; FN1: fibronectin type 1 domain; KR: kringle domain; Tryp\_SPC: trypsin-like serine protease domain.

The domain comparisons of the members in this serine protease family are shown in Figure 1.10.

A second approach to identifying an interacting candidate serine protease might come from investigating the spatio-temporal expression patterns of these enzymes in the developing olfactory bulb as well as their potential role in neurogenesis where anosmin-1 shows preferential biological activity. The functional role of trypsin-like serine proteases and their early expression have been reported within the olfactory system. Taken together, trypsin-like serine proteases fulfil these criteria and are discussed next.

#### **1.9.1.1 Thrombin**

Dihanich et al. have shown that prothrombin is expressed in both the developing and adult rat brain, with initial low activity in the neonatal rat brain and increasing significantly by adulthood. After birth, prothrombin (mRNA and protein) is expressed in the olfactory bulb, cortex, thalamus and corpus striatum (Dihanich et al., 1991). The proteolytic activity of thrombin is well documented and had been shown to inhibit long-term morphological differentiation in serum-free cultures of several cell types, including spinal cord and brain neurons, astroglial and neuroepithelial cells, effects prevented by prior of co-treatment with the specific thrombin inhibitor, hirudin (Gurwitz and Cunningham, 1988; Grand et al., 1989).

In addition, the role of thrombin is somehow dependent on its cognate receptor characterized as a member of the G protein-coupled receptor family. Consistent with thrombin spatio-temporal expression pattern, the thrombin receptor is also highly expressed throughout the brain including olfactory bulb, hypothalamus and neocortex (Weinstein et al., 1995). This receptor is activated following the cleavage of its NH<sub>2</sub>-terminus arginine-41 residue by bound thrombin, and induces neuronal cell rounding and neurite retraction in various differentiating neuroblastoma N1E-115, NG108-15 and NB2a cells (Jalink and Moolenaar, 1992; Suidan et al., 1992). Thrombin-mediated

cell death has also been reported in spinal motoneurons in culture, which can be mimicked by a thrombin receptor agonist (Turgeon et al., 1998).

#### **1.9.1.2 Plasminogen activator system**

There are two types of plasminogen activators, the urokinase-type (uPA) and the tissue-type (tPA). Both are capable of catalysing the conversion of the inactive zymogen plasminogen to the active protease plasmin, which has trypsin-like broad-spectrum protease activity, and which activates matrix metalloproteinases (MMPs) for degradation of most extracellular proteins (Pittman et al., 1989; Blasi and Carmeliet, 2002). There appears to be general agreement that the primary role of tPA is to generate plasmin for thrombolysis, while it is mainly uPA which generates plasmin in events involving degradation of ECM.

The plasminogen activator (PA) system is incriminated in tissue remodelling, synaptogenesis, and neurite outgrowth *via* its proteolytic activity. Evidence implicating this system in the growth of the nervous system has been obtained from several studies. Initially, it was demonstrated from enzymatic studies, that PA activity is demonstrable in association with the growth cones of sensory neurons and with Schwann cells as well as sympathetic neurons (Krystosek and Seeds, 1981; Krystosek and Seeds, 1984). Later studies showed that the addition of PA or PA inhibitors to cultures of neurons had profound effects on neurite outgrowth and the direction of cell migration (Hawkins and Seeds, 1986; Hawkins and Seeds, 1989).

Differential expression and function of tPA and uPA in the developing CNS has been reported using genetic studies and immunohistochemistry. A retardation of granule cell migration into the cerebellar molecular layer was demonstrated in mice lacking the tPA gene, a phenomenon not observed in wild type mice or the mice lacking uPA gene (Seeds et al., 1999). Furthermore, Hayden and Seeds found differential expression of tPA and uPA during differentiation of mouse dorsal root ganglia cell cultures - tPA expression was restricted to small sensory neurons, whereas uPA was localized predominantly in large sensor neurons (Hayden and Seeds, 1996).

A study by Del Bigio et al provides immunochemical evidence that uPA, its receptor, and its major substrate plasminogen are expressed in postnatal mouse forebrain neurons at a stage when development and refinement of neuronal synaptic connections mostly happen. The authors thus concluded that uPA might function in the processes of synaptogenesis and remodeling rather than in cell migration (Del Bigio et al., 1999). In agreement with this observation, Drapkin et al. reported that implantation of uPA coupled affigel blue beads into the olfactory epithelium of chick embryo at a very early developmental stage (stage 17) did not affect GnRH neuron migration (Drapkin et al., 2002). Of interest is that in mouse as early as E14.5, when olfactory and GnRH neurons have completed their initial migration, uPA is predominantly expressed within the large mitral and related tufted cells lying more superficially in the external plexiform layer of the immature OB (Dent et al., 1993). Therefore, uPA may play an important role in synapse formation and tissue remodelling during olfactory bulb development. In contrast, tPA was expressed within the rostral migratory pathway leading to the developing OB in early embryogenesis, and then located in the olfactory nerve fibre layer (ONL), mitral cell layer (MCL) and granule cell layer (GCL) of OB in adulthood (Thewke and Seeds, 1996).

### **1.9.1.3 Trypsin**

The effect of trypsin on GnRH neuronal development has been investigated in chick embryo by immunohistochemistry and protein coupled bead assays (Drapkin et al., 2002). Trypsin immunoreactivity was present in the vast majority of cells within the olfactory epithelium and throughout the mesenchyme as well as within the olfactory nerve. Furthermore, trypsin coupled beads embedded in the migratory GnRH neuronal complex resulted in a global acceleration of GnRH neuronal migration out of the olfactory epithelium and into the brain. Although these observations implicate an important role of trypsin in GnRH neuronal development, there is hithero no direct evidence to indicate its effect on olfactory bulb morphogenesis.

### **1.9.2 FGF2/FGFR1**



Anosmin-1 and FGFR1 share similar properties both in their actions in OB development and HS binding characteristics. This raises the possibility of a direct interaction between FGFR1 or/and its ligand FGF2 and anosmin-1. Thus, it is pertinent to ask whether anosmin-1 1) participates in FGF2/FGFR1/HS complex formation, 2) directly stimulates FGFR1 as its cognate ligand or 3) indirectly modifies this specific signalling pathway.

FGF2 is a small globular protein with separate binding regions for HS and FGFRs, and is directly involved in receptor dimer formation. It has an internal core region, structurally identified as 12 antiparallel  $\beta$  strands (Zhu et al., 1991; Eriksson et al., 1991). The loop between  $\beta$  strands 10 and 11 contains several basic amino acid residues that form the primary heparin-binding site. The FGFR1 binding region of FGF2 include the  $\beta$ 8- $\beta$ 9 loop, separate from the heparin-binding site (Zhu et al., 1991; Ornitz, 2000; Plotnikov et al., 2000).

FGFR1 is a member of the receptor tyrosine kinase superfamily, containing three immunoglobulin-like (Ig-like) domains and a heparin-binding domain (Murakami et al., 2000). A region of FGFR1 that includes Ig-like domain II and III and the intervening linker domain has been shown to bind the FGF2 ligand, whilst a stretch of 18 conserved residues (K18K) has been demonstrated as a binding site for heparin/HS (Murakami et al., 2000; Wang et al., 2000). These distinct HS binding sites in both FGF2 and FGFR1 support a model in which the heparin/HS could form the bridge between FGF2 and FGFR1.

In terms of the FGF2-FGFR1-HS model, the structural assembly is sufficiently stable in the presence of HS containing as few as hexa or decasaccharide residues, leaving the first Ig-like ectodomain of FGFR1 available for anosmin-1 binding. Furthermore, the binding of anosmin-1 to HS and possibly to FGF2 may help to further stabilize these signalling complex formation. Thus it is unclear what role of additional molecules might have on a preformed FGF2-FGFR1-HS complex. Moreover, it is theoretically possible that anosmin-1 might act as an active ligand

directly stimulating FGFR1 signalling, as occurs when a homologous FnIII domain in NCAM binds to the FGFR1 Ig-like domain inducing FGFR1 activation (phosphorylation) and stimulating neurite outgrowth, albeit with a much lower binding affinity ( $K_d = 9.97 \pm 0.37 \mu\text{M}$ ) (Kiselyov et al., 2003). Finally, it would seem likely that anosmin-1 might modulate the FGF2/FGFR1/HS interaction indirectly, possibly through the modulation on serine protease activity such as uPA since the biological interaction between FGF2/FGFR1 and uPA has been clearly identified (Dell'Era et al., 1999).

### **1.10 Hypothesis**

A hypothesis for the molecular mechanism of anosmin-1 action was therefore developed. Namely, that the N-terminus (specially the WAP domain) of anosmin-1 interacts with a serine protease ligand such as uPA, regulating its protease activity necessary for tissue remodelling and neurogenesis. I further hypothesised that the C-terminal FnIII domains of anosmin-1, by interacting with immobilized cell surface HS or ECM-related HS, directly restrict and specify the site of serine protease activity (Figure 1.11).

### **1.11 Aims of this thesis**

The clinical presentation of KS and known properties of anosmin-1 in cell adhesion and neurogenesis indicated that the molecules implicated in this condition play an important role during embryonic development including neuronal and non-neuronal morphogenesis. However, many questions remain unanswered. First, although HS has been confirmed to interact with anosmin-1, it is still unclear the extent of binding affinity between these two molecules. Second, as serine proteases may constitute candidate interactants for anosmin-1, it is necessary to identify the specific serine protease recognized by N-terminus of anosmin-1. Third, does the anosmin-1/HS/serine protease cooperate in cell processes such as proliferation? Finally, what is the structural characteristics determining anosmin-1 activity?

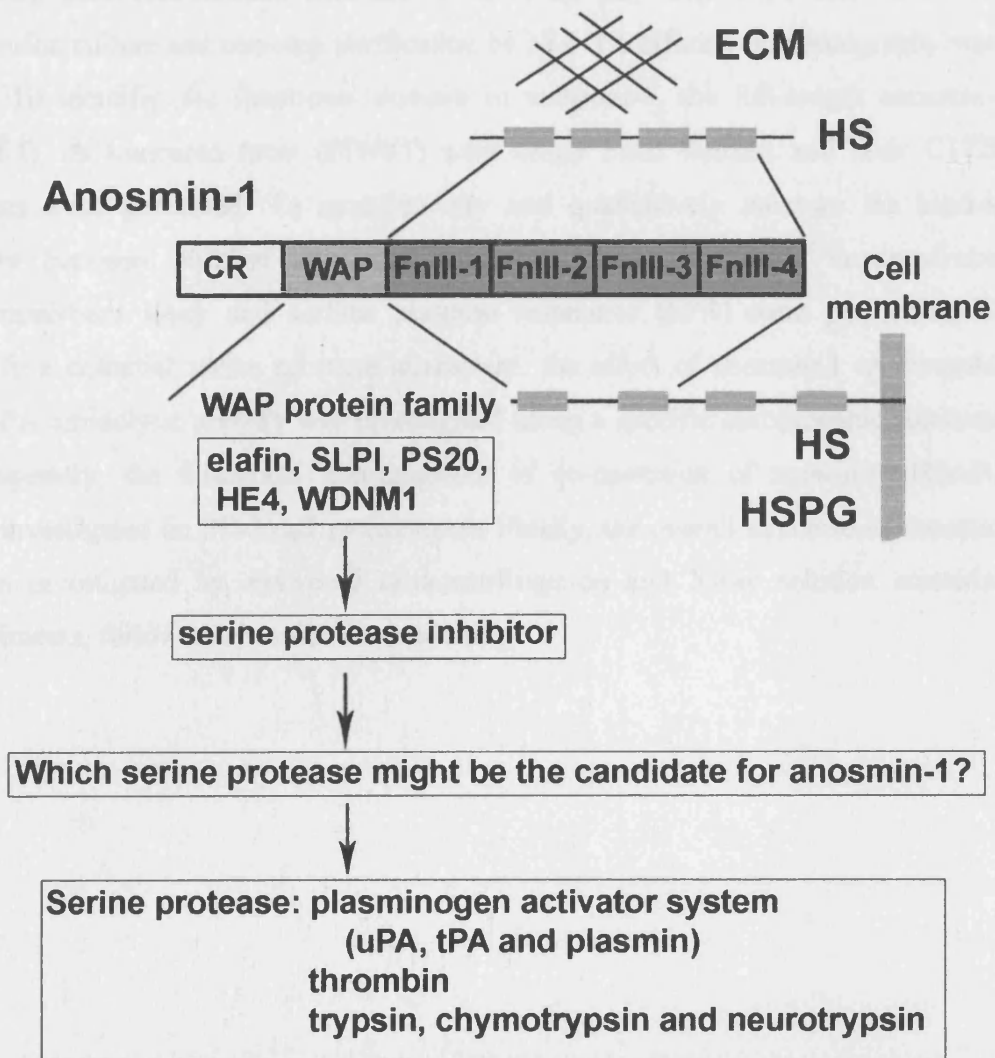


Figure 1.11 A hypothesis of the molecular mechanism of anosmin-1.

In this thesis, a *Drosophila* S2 cell expression system was used to initially generate anosmin-1 expression and to investigate whether HS determines anosmin-1 S2 cell surface binding through interaction with its FnIII domains. To generate sufficient pure recombinant anosmin-1, stable S2 cell lines were established and suspension culture and one-step purification by Ni-NTA affinity chromatography were used. To identify the functional domain in anosmin-1, the full-length anosmin-1 (PIWF4), its truncated form (PIWF1) with single FnIII domain and their C172R mutants were generated. To quantitatively and qualitatively measure the binding affinity between purified anosmin-1 and HS, the solid phase enzyme-linked immunosorbant assay and surface plasmon resonance (SPR) were performed. To identify a potential serine protease interactant, the effect of anosmin-1 on thrombin and uPA amidolytic activity was investigated using a specific chromogenic substrate. Subsequently, the functional consequences of co-operation of anosmin-1/HS/uPA were investigated on PC-3 cell proliferation. Finally, the overall structure of anosmin-1 was investigated by analytical ultracentrifugation and X-ray solution scattering experiments, followed by molecular modelling.

## Chapter 2

### Characterisation of anosmin-1 expressed in *Drosophila* S2 cells

#### 2.1 Introduction

Structural and functional analyses of proteins are only made possible provided a) sufficient quantities (up to milligram levels) can be generated from expression systems b) the protein is of adequate purity. Preliminary attempts in this and other laboratories used coupled systems but failed to generate sufficient anosmin-1 yields of the necessary purity. Hitherto, the only publication detailing a system fulfilling the above criteria is that of Soussi-Yanicostas et al (1996) using CHO cells which generated small recombinant anosmin-1 yields ( $150 \mu\text{g}/10^9$  cells), still inadequate to enable extensive structural and functional studies of this protein.

Proteins generated in bacterial systems are widely used in structural studies including crystallography; however, a major limitation of these systems lies in the fact that proteins cannot be post-translationally modified. Thus glycosylation, which is known to occur in anosmin-1 (Soussi-Yanicostas et al., 1996) cannot occur in such systems. Insect cells appear to overcome such limitations, and have been used as an appropriate substitute, offering a number of advantages over other expression systems. For instance, insect cells can be grown to a high  $2 \times 10^7$  cell/ml density, and continue to proliferate in serum-free medium that facilitate subsequent protein purification. Cells can also be cultured in a suspension phase at room temperature, not requiring  $\text{CO}_2$  and a humidified environment. Furthermore, the generation of stable protein expressing cell lines is generally more rapid, usually within 2-3 weeks. Insect cells confer a further advantage in that they have similar post-translation modification capabilities as mammalian cells. *Drosophila melanogaster* Schneider 2 (S2) cells, have been used to successfully generate biologically active proteins including enzymes, cytokines and viral proteins with generally higher yields (0.4-2.2 mg/litre) (Culp et al., 1991). Moreover recent *in vivo* transgenic *C.elegans* experiments have shown that the human *KAL-1* gene can rescue the phenotype caused by loss of

function of the endogenous *C.elegans Kal-1* orthologue, suggesting close functional similarities between anosmin-1 from two distant species (Rugarli et al., 2002). It therefore seemed highly likely that anosmin-1 generated in insect cells would be capable of retaining the properties of the protein expressed in mammalian cells.

In previous studies from this laboratory, S2 cells were used to transiently express anosmin-1: in this system, however, cleavage of the protein occurred in a *Drosophila* expression medium DES<sup>TM</sup> plus 10% foetal calf serum (Robertson et al., 2001). It had not been established whether anosmin-1 could be expressed in serum-free medium, nor whether cleavage of anosmin-1 in serum culture could be abolished in conditions of serum deprivation. Previous studies had shown that recombinant anosmin-1 generated in COS7 and CHO cells was cell membrane associated. It was unknown whether recombinant anosmin-1 expressed in S2 cell would retain its ability to be anchored to the cell surface and whether this anchorage relied on HS polysaccharide chains from HSPG. The FnIII domains of anosmin-1 have been predicted to interact with HS accounting for cell membrane binding; however the minimum number of such repeats required for cell membrane association had to await the generation of truncated analogues of anosmin-1 with varying numbers of FnIII repeats. The generation of such truncated analogues might also shed light on the role of FnIII domains in both protein expression and secretion efficiency.

## **2.2 Aims**

Five recombinant *KAL-1* cDNA plasmid constructs encoding full length and domain-truncated versions of anosmin-1 were incorporated into an insect expression vector (PMTA/Bip/V5-6His) containing a copper sulphate inducible metallothionein (MT) promoter. The presence of a polyhistidine tag enabled 1) protein detection using an anti-His tag monoclonal antibody 2) subsequent protein purification. The preliminary studies based on the transient transfection aimed to:

(1) investigate anosmin-1 expression and secretory efficiency of transfected S2 cells either in a serum-dependent or in an FnIII domain-specific manner.

- (2) investigate the proteolytic cleavage site in anosmin-1 and whether this phenomenon occurred only in the presence of serum.
- (3) investigate whether recombinant anosmin-1 retained its cell surface binding capability *via* HS using a HS competitive assay.
- (4) estimate potential glycosylation sites within individual domains of the protein.

## 2.3 Materials and methods

### 2.3.1 Construction of expression plasmid:

#### 2.3.1.1 PCR amplification

Five different fragments of human *KAL-1* cDNA were generated based on the N-terminal cysteine-rich and WAP domain backbone, followed by variable numbers of fibronectin III domains. These were named PIW, PIWF1, PIWF2, PIWF3, PIWF4 (Figure 2.1) with primers flanked by *Bam*H1 and XbaI. The following primers were designed to remove the signal sequence from *KAL-1* cDNA :

Forward: CCGGATCCGCGGCCGGCCCCGGCGCGGCTGCT

PIW-rev: CCTCTAGAACCTTTGTACAGAGTCTTGGGTAAGT

PIWF1-rev: CCTCTAGAGGCAGATGGATCTTTGGAAGAACGGAA

PIWF2-rev: CCTCTAGAGGTTGCATGTGTTCGATGTGAAGTGAAG

PIWF3-rev: CCTCTAGACTTAAGAGCAGAGCATGGTGGAGTAGT

PIWF4-rev: CCTCTAGAGTATCTTTCTGGAGAAGGCTTGTAATG

1 ng of PKD1 plasmid DNA (Robertson et al., 2001) containing full length *KAL-1* cDNA was used as template with 50 pmol primers, 200  $\mu$ M dNTPs, 1 $\times$ PCR buffer, 0.5 unit of *Taq* polymerase and water made up to a 50  $\mu$ l final reaction volume. The PCR profile consisted of an initial denaturation at 95°C for 10 min, followed by 30 cycles of 30 sec, 94°C denaturation, 30 sec, 55°C annealing and 50 sec, 72°C extension times, with a final 72°C extension time of 10 min. The PCR products were run on an agarose gel and corresponding fragments were excised and gel purified.

#### 2.3.1.2 Purification of DNA from agarose gel

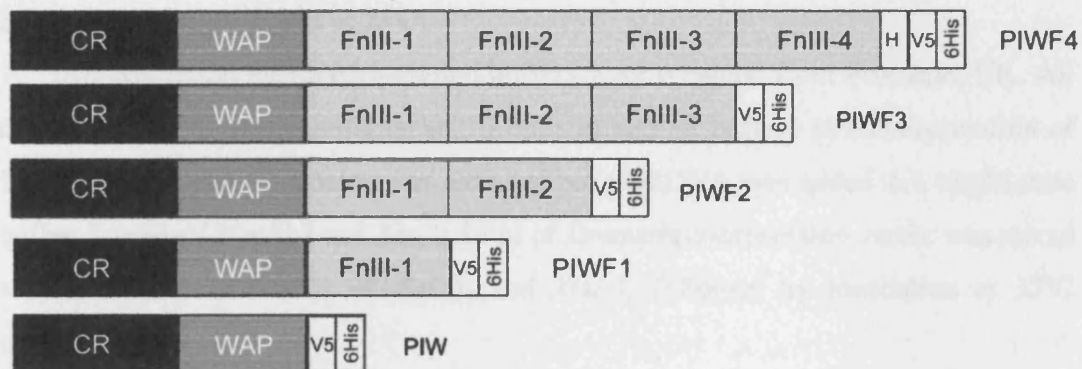


Figure 2.1 Structure of five variants of recombinant anosmin-1. The functional domains represented are; CR, cysteine-rich region; WAP, weakly acidic protein-like domain; FnIII, fibronectin-like type III domain; H, histidine-rich region; V5, the V5 epitope tag derived from simian virus 5; 6His, 6x histidine tag.



The QIAEX II Agarose Gel Extraction kit and protocol (Qiagen) was used to extract PCR products. The gel slice was excised by a sterile scalpel blade, placed into a 1.5 ml tube, weighed and 3 volumes of buffer QX1 added to each 100 mg of gel. 10  $\mu$ l of QIAEX II was added to the tube, which was incubated at 50°C for 10 min by vortexing every 2 min to keep QIAEX II in suspension. The tube was then centrifuged for 30 sec, and the supernatant removed, the pellet washed twice, once with 500  $\mu$ l of buffer QX1 and then PE buffer. The pellet was air dried for 15 min and then resuspended in 20  $\mu$ l distilled H<sub>2</sub>O for 5 min. After centrifugation at 13,000 $\times$ g for 1 min, the DNA was collected into a clean tube.

#### **2.3.1.3 Restriction digest of DNA**

All restriction endonucleases and buffers were obtained from Promega, UK. All enzymes were at a concentration of 10 units/ $\mu$ l and all buffers at a concentration of 10 $\times$  normal working concentration. 20  $\mu$ l of purified DNA was added to 1 $\times$ multi-core buffer, 2 units of *Bam*H I and *Xba* I; 10  $\mu$ l of *Drosophila* expression vector was mixed with 1 $\times$ buffer D, 2 units of *Bgl* II and *Xba* I, followed by incubation at 37°C overnight.

#### **2.3.1.4 DNA ligation**

The digested DNA was purified with the QIAquick PCR Purification kit (Qiagen) to remove the restriction enzymes and digested *Drosophila* vector was run on the gel followed by purification using the above protocol. All DNA ligations were carried out by T4 DNA ligase (Life Technologies) at 1 unit/ $\mu$ l and buffer at 1 $\times$ concentration.

#### **2.3.1.5 Transformation of recombinant DNA into DH5 $\alpha$ competent cells**

A 50  $\mu$ l aliquot of DH5 $\alpha$  cells was thawed on ice and placed into a 1.5 ml tube. 2  $\mu$ l of recombinant DNA was added to the tube and mixed with cells by gently pipetting up and down several times. The tube was placed on ice for 30 min, followed by heat shock at 42°C in a water bath for 45 sec followed by incubation at 37°C for 1 h with addition of 900  $\mu$ l LB medium. 200  $\mu$ l of the 1 in 100 diluted resultant culture

was plated out on LB plates containing ampicillin at 50 µg/ml concentration (LB<sub>amp</sub>) and incubated at 37°C overnight.

#### **2.3.1.6 Recombinant DNA mini preparation**

One colony was picked out from the LB<sub>amp</sub> plate and put into a flask containing 5 ml LB<sub>amp</sub> medium; this was shaken vigorously at 37°C overnight. The Qiagen spin plasmid kit and protocol (Qiagen) were used to purify DNA from the ensuing bacterial culture. 1.5 ml of the bacterial culture was placed into a 1.5 ml tube and centrifuged at 13,000×g for 5 min. The supernatant was removed and the cell pellet resuspended in 250 µl of buffer P1. A 250 µl aliquot of buffer P2 was added to the tube which was then inverted gently 6 times to achieve complete mixing. After 5 min incubation at room temperature, buffer N3 was added to the tube, followed by gentle mixing 6 more times and then centrifugation at 13,000×g for 10 min. The supernatant was loaded onto a QIAprep column. The column was centrifuged at 13,000×g for 1 min and washed with 750 µl PE buffer, followed by 13,000×g centrifugation, the flow through being discarded. The column was centrifuged for an additional 1 min to remove residual wash buffer. The column was then placed in a clean tube and DNA eluted by the addition of 50 µl of EB buffer, incubated at room temperature for 1 min and then centrifuged at 13,000×g for 1 min. The DNA was kept at -20°C.

#### **2.3.1.7 Screening and sequencing of recombinant DNA**

To confirm the identity of the recombinant DNA thereby generated, firstly the restriction enzymes *Bam*H I and *Xba* I were used to digest DNA. The digest was then run on a gel to enable the DNA fragments generation to be compared to the DNA ladder, thereby ensuring the appropriate length of the inserts. Secondly, 30 µg of DNA was sent to MWG-Biotech (Germany) for sequencing.

#### **2.3.1.8 Recombinant DNA maxi preparation**

After confirmation of the correct sequence of recombinant DNA, the Qiagen Endofree plasmid maxi kit and protocol (Qiagen) were used to purify plasmid DNA. A 100 µl volume of LB<sub>amp</sub> media was inoculated with 200 ml of liquid culture, and

then incubated at 37°C overnight. Bacterial cells were harvested by centrifugation at 6,000×g for 15 min at 4°C, and resuspended in 10 ml of cell resuspension buffer and pipetted up and down to separate the cells. 10 ml of cell lysis solution was added to the tube, mixed by inverting 6 times and then allowed to stand for 5 min. 10 ml neutralization solution was added to the tube, mixed 6 times immediately, and the lysate was then poured directly into the barrel of the QIAfilter cartridge followed by 10 min incubation at room temperature. The lysate was filtered through the cartridge into a 50 ml tube and incubated on ice for 30min with addition of 2.5 ml ER buffer. The solution was applied to the buffer QBT equilibrated QIAGEN-tip, and then washed twice with 30 ml QC buffer. DNA was eluted with 15 ml QN buffer and precipitated by adding 10.5 ml isopropanol, mixed and centrifuged at 15,000×g for 30min at 4°C. The DNA pellet was washed with 5 ml of endotoxin-free 70% ethanol, carefully decanting the supernatant and air-drying the pellet for 10 min. The DNA was re-dissolved in 1 ml endotoxin-free TE buffer, transferred to a new 1.5 ml tube and stored at -20°C.

All DNA quantities and qualities were measured in 1:100 dilution by reading the optical density using a spectrophotometer at a wavelength of 260 nm ( $OD_{260}$ ) and 280 nm ( $OD_{280}$ ), and the DNA concentration calculated by the formula:  $[DNA] = (OD_{260} \times 100 \times 50) \mu\text{g/ml}$  and quality estimated by the  $OD_{260}/OD_{280}$  ratio.

### **2.3.2 Transient transfection of S2 cells by calcium phosphate precipitation**

#### **2.3.2.1 Expression in DES<sup>TM</sup> expression medium supplemented with 10% heat-inactivated foetal bovine serum**

S2 cells were seeded at a  $1 \times 10^6$  cells/ml concentration in 5 ml of the DES<sup>TM</sup> expression medium (Gibco BRL) containing 10% heat-inactive serum in 25cm<sup>2</sup> flasks and incubated overnight at 23°C. The calcium phosphate kit (Invitrogen) was used for transfection with 30  $\mu\text{g}$  recombinant DNA. The two transfection solutions were set up as follows: Solution A, 60  $\mu\text{l}$  of 2M CaCl<sub>2</sub>, 30  $\mu\text{g}$  of DNA and water to 500  $\mu\text{l}$  final volume; solution B, 500  $\mu\text{l}$  of 2×HEPES-buffered saline (HBS, pH7.1). DNA was absent in solution A acting as negative control. Solution A was slowly added to

solution B with constant vortexing followed by incubation at room temperature for 40 min. The solution was mixed, added to the cells and incubated at 23°C overnight. The calcium phosphate solution was removed and cells washed three times with Dulbecco's PBS (Gibco BRL); fresh medium was added and cells replated in the same vessel followed by overnight incubation. Expression of the desired protein was induced by addition of 500  $\mu$ M CuSO<sub>4</sub>. On the second post-induction day, the conditioned medium was collected and centrifuged at 1,000 $\times$ g. Cell membrane-attached proteins were extracted by suspending and gently shaking cells in serum-free medium (Gibco BRL) containing additional 350 mM NaCl (1 ml for  $1 \times 10^7$  cells) for 15 minutes at room temperature, the supernatant being collected following centrifuging at 1,000 $\times$ g. The cells were lysed in 1 ml SDS sample buffer and heat-denatured for 10 minutes, and centrifuged at 13,000 $\times$ g at 4°C and supernatant collected.

#### **2.3.2.2 Expression of protein in serum-free medium**

Transfections and other cell manipulations were performed according to the protocol detailed in section 2.3.2.1 except for cell weaning into serum-free medium. After removal from the transfection solution, cells were weaned into 2.5% serum medium, incubated overnight and then washed with PBS twice and replated with 5 ml serum-free medium.

#### **2.3.2.3 HS competition assay**

The method was identical to that employed in section 2.3.2.2; 100  $\mu$ g/ml HS (Sigma, Cat# H7640) was added to the serum-free medium at the same time as the CuSO<sub>4</sub> induction.

#### **2.3.3 Western Blotting**

7  $\mu$ l of molecular weight marker and 10  $\mu$ l of each sample were mixed with sample buffer, denatured at 95°C for 5 min and then loaded onto the Novex Nu-PAGE 4-12% polyacrylamide gel. The gel was run at 180V for 40 min under denaturing conditions using the Novex Xcell II tank and Bis-MES buffer (Invitrogen). Protein

was transferred onto a nitrocellulose membrane (Invitrogen) using the Novex Xcell II blot module and 1×transfer buffer (Invitrogen) with methanol (BDH) and antioxidant (Invitrogen) at 30V for 1.5 h. The blots were blocked with 5% (W/V) fat-free milk in PBS with 0.01% Tween-20 (PBS/T) at 4°C overnight. After washing three times with PBS/T, the membrane was incubated with anti-His antibody (1:1,000, 0.2 µg/ml, Qiagen) in 3% bovine serum albumin (Sigma) in PBS/T for 1 h. All blots were washed 3 ×10min in PBS/T, and then incubated in a 1:10,000 dilution anti-mouse HRP conjugated second antibody (Sigma) in 5%(W/V) fat-free milk in PBS/T for 1h at room temperature. The blots were then washed 3×15 min in PBS/T. The protein bands were detected using the enhanced Chemiluminescence plus kit (ECL+ western detection kit, Amersham, UK). Blots were covered with ECL+reagent (one volume of solution A: 40 volume of solution B) for 5 min at room temperature and placed into an X-ray film cassette. The Kodak BioMax light-2 film (Sigma) was placed onto the blot and developed for 1 min.

## **2.4 Results**

Using a monoclonal anti-His antibody, Western blot analysis of recombinant anosmin-1 from cell lysate, salt extracts (cell surface associated) and conditioned medium (secreted) showed bands of the expected molecular weights, confirming the validity of the S2 cell expression system for recombinant protein generation (Figure 2.2 (a)-(c)).

As expected, more protein was demonstrable within cells, a proportion being secreted from cells in 10% serum medium culture; by contrast, recombinant protein yield was lower under serum-free condition. Of the five expressed recombinant proteins, only PIWF1 has been generated in a large amount, irrespective of whether the culture was performed in the presence or absence of serum. Using constructs encoding increasing numbers of fibronectin type III inserts, lower protein yields were obtained, the lowest yield being obtained with PIWF4 protein. It therefore appeared that increasing numbers of FnIII repeats could modulate the expression efficiency of the integral protein. Part of the explanation may reside in the fact that the longer

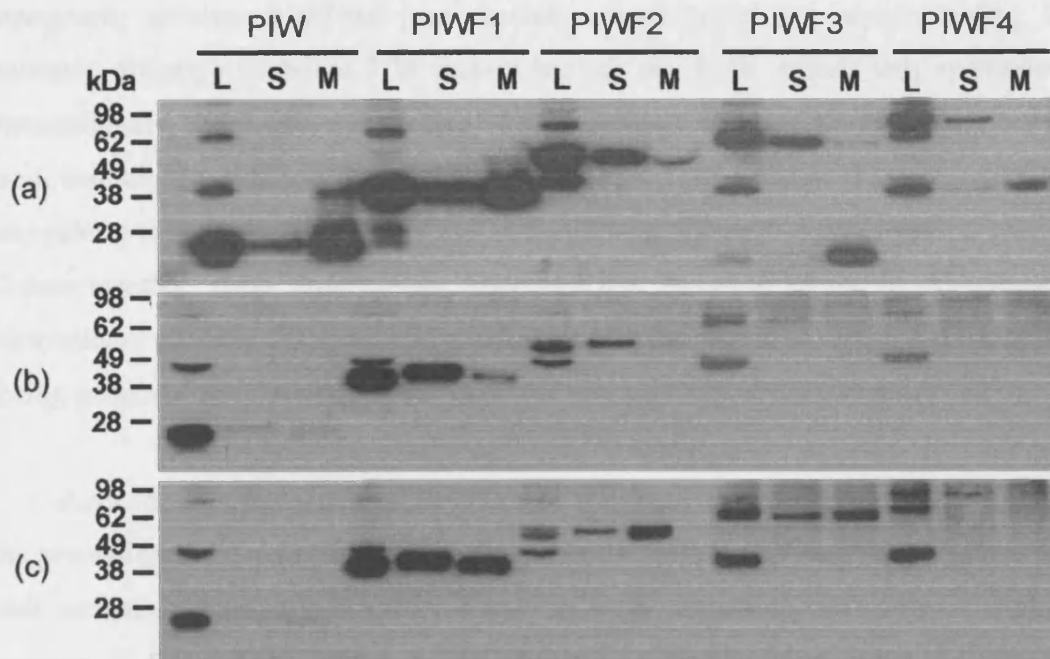


Figure 2.2 Western blot analysis of recombinant anosmin-1 in *Drosophila* S2 cells. (a) Transient expression of recombinant anosmin-1 was induced by 500  $\mu$ M  $\text{CuSO}_4$  in 10% serum containing medium. Recombinant anosmin-1 proteins present in cell lysate (L), salt extract (S) and conditioned medium (M) were identified using an anti-His monoclonal antibody. The molecular weight markers are shown. The generated proteins are attached on the cell surface (S) and secreted into the medium (M). The cleavage is only detected in PIWF3 and PIWF4 with 20 kDa and 45 kDa C-terminal fragments respectively, indicating that the cleavage site is probably either at the end of the 2<sup>nd</sup> fibronectin or the beginning of the 3<sup>rd</sup> fibronectin repeats. Transiently transfected S2 cells in serum free medium culture were induced to express proteins in the absence (b) and presence (c) of 100  $\mu$ g/ml HS. PIW protein was present in large amounts inside cells, with only a little secreted into the medium. Most of PIWF1 and nearly all of the secreted PIWF2, 3, 4 proteins are cell surface attached, which can be dissociated by the addition of exogenous HS. These results indicate that HS anchors recombinant anosmin-1 onto S2 cell surface by interacting with FnIII repeats. Positions of MW markers were as shown.

molecules take more time to go through the full biosynthetic processes, which necessarily involves additional post-translation modification and protein folding. By contrast, although abundant PIW protein lacking any FnIII repeats was synthesized intracellularly, much less was secreted from cells such that the protein in salt extract and conditioned medium generated only a faint band (Figure 2.2 (b) and (c)), suggesting that serum and/or the FnIII modules might be essential for PIW secretion. Taken together, these observations suggested that the FnIII repeat is an important determinant not only for anosmin-1 production but also for its secretion, the best yield being generated by a truncated protein containing a solitary FnIII domain (PIWF1).

Anosmin-1 expressed in S2 cells is also cell-surface associated, in common with its properties when generated in other mammalian cells (CHO and COS-7 cells). The cell surface association of anosmin-1 appears to be determined by the FnIII domain content of the protein. Indeed, when compared to the secreted form, cell surface associated PIW protein generated lower band intensity, whereas increased band intensities were observed for cell-surface associated anosmin-1 which contained increasing numbers of FnIII domain. This result indicates that FnIII domains are necessary for cell surface binding. To investigate whether this phenomenon occurs as a consequence of an interaction with HS, exogenous HS was then used since soluble HS can competitively bind to anosmin-1 leading to the release of anosmin-1 into culture medium. As expected, addition of 100 µg/ml HS to serum-free medium resulted in significant dissociation of cell membrane associated anosmin-1 (Figure 2.2 (c) vs Figure 2.2 (b)). These data suggest that anosmin-1 binds to insect cells through an interaction with the HS polysaccharide chains of HSPG, as previously shown in mammalian cells (Soussi-Yanicostas et al., 1996). In contrast to the longer forms of anosmin-1 (PIWF1, 2, 3, 4), PIW protein without any FnIII domains showed little cell surface association, suggesting that PIW protein had less HS binding affinity. This concurs with the prediction that the N-terminal WAP domain is not involved in HS binding due to its high anionic charge, and evidence from an *in vitro* cell binding assay in which WAP domain shows less avidity for glioblastoma and glioma cells (Bulow et al., 2002). Thus, it can be proposed that anosmin-1 resides on the cell surface through

interaction of its FnIII domain with HS; the more FnIII repeats there are, the less protein becomes detachable from cells.

Cleavage of anosmin-1 was observed under two specific circumstances 1) when both PIWF3 and PIWF4 proteins were expressed and 2) in serum-containing medium. Figure 2.2 (a) show that anosmin-1 was cleavable into small molecular weight fragments of about 20 kDa and 45 kDa corresponding to the C-terminal 3<sup>rd</sup> FnIII and 3<sup>rd</sup> plus 4<sup>th</sup> FnIII domains respectively. This implies that the cleavage site is located at the end of the second fibronectin III and the beginning of the third fibronectin III domain. Notably, no cleavage of PIWF3 and PIWF4 was observed in serum-free medium, regardless of whether HS was added or not. Moreover, proteolysis occurred extracellularly rather than intracellularly since no corresponding cleaved fragments can be detected inside the cells. These observations, in their totality, indicate that cleavage of anosmin-1 is artificially caused by the presence of serum.

The observed bands and the molecular weights of each anosmin-1's variants were estimated as follows: PIW-26 kDa, PIWF1-40 kDa, PIWF2-55 kDa, PIWF3-71 kDa and PIWF4-90 kDa. The deduced molecular weights of the conceptual proteins, based on the amino acid sequence plus vector epitope (4 kDa) are PIW-21 kDa, PIWF1-33 kDa, PIWF2-45 kDa, PIWF3-59 kDa and PIWF4-76 kDa. From the results obtained, it can be speculated that the contribution of glycosylation to the final molecular weight of the full-length anosmin-1 (PIWF4) will be:  $90-76 = 14$  kDa. In addition, the molecular weight of each expressed anosmin-1 was slightly greater than its calculated value, suggesting that glycosylation might be evenly distributed in each distinct domain rather than clustered in limited domains.

## 2.5 Discussion

The present study provides evidence that, in addition to its use as an expression system for recombinant anosmin-1 generation, *Drosophila* S2 cells also provide a model for the investigation of molecular characteristics of anosmin-1, including HS binding properties, cleavage of anosmin-1, as well as glycosylation. However, it



should be noted that, although the protein can be glycosylated in insect cells, the type of sugars and the pattern of glycosylation sites are unlikely to be identical to those in mammalian cells.

Previous studies had demonstrated anosmin-1 binding to cell membrane associated HS in mammalian cells; similar interactions evidently take place in *Drosophila* S2 cells, confirming conservation of anosmin-1 binding to cell surface-bound HS through diverse species. Hitherto, two major families of membrane-bound HSPG have been established: syndecan with its core protein embedded in the lipid bilayer and glypican attached to the cell surface *via* glycosylphosphatidylinositol (GPI)-anchorage. In contrast to mammalian cells which have four members in the syndecan and six in the glypican family, *Drosophila* has only one type of syndecan and two members of the glypican family named *division abnormally delayed (dally)* and *dally-like (dly)* (Forsberg and Kjellen, 2001; Filmus and Selleck, 2001). At present it is unclear which of these two types of HSPG interact with anosmin-1 and the precise sulphate sequence and structure involved in this interaction; it should, however, prove possible to investigate the nature of the HSPG-anosmin-1 interaction using this *Drosophila* cell model. Further studies to distinguish anosmin-1's binding characteristics to either glypican or syndecan might employ specific enzymes and/or metabolic labelling studies. The use of a phosphatidylinositol-specific phospholipase C (PI-PLC) that cleaves the GPI anchor is a commonly employed technique for the identification of protein-GPI anchor associations. Metabolic labelling of cells with tritiated GPI anchor components such as ethanolamine and inositol might further shed light on these relationships (Debierre-Grockiego et al., 2003). By contrast, the syndecan ectodomain can be shed *via* cleavage of the core protein within 15 amino acids near to the plasma membrane. Physiological regulators such as thrombin, plasmin and EGF receptor family members have been shown to accelerate this proteolytic process (Fitzgerald et al., 2000; Holen et al., 2001). Thus, it is possible, using these molecules, to examine the anosmin-1-syndecan interaction. In addition, the use of various heparinase treatments to alter anosmin-1 cell surface binding properties could help identify the crucial HS sequence and structural motifs required for

anosmin-1 recognition, since it is known that heparinase I cleaves the highly-sulphated epitopes, whereas heparinase III cleaves poorly sulphated sites.

There is now considerable evidence that many inactive precursor proteins are rendered active through endopeptidase-induced cleavage; for example, NCAM proteins are all formed as heterodimers by proteolytic cleavage and the activation of vascular endothelial growth factor (VEGF) is *via* uPA-mediated cleavage (Kayyem et al., 1992; Plouet et al., 1997). The present result confirms that anosmin-1 cleavage only occurs by a serum-enzyme mediated reaction since the process did not occur in serum-free medium. Together with the evidence that no cleaved fragment of anosmin-1 was observed in the rat and chicken brain extracts, this suggests that cleavage is most probably unnecessary for anosmin-1's functional activity. However, a full understanding of *in vivo* anosmin-1 cleavage is incomplete, as is the identification of the precise cleavage site. To date, using the insect S2 cell expression system, the sequences K<sup>345</sup>KKRRK<sup>350</sup> and R<sup>422</sup>RR<sup>424</sup> which is located in the FnIII-2 domain and FnIII-2/-3 linker region respectively have been ruled out as candidate cleavage sites (Robertson et al., 2001).

The attachment of oligosaccharides to eukaryotic proteins is the most common post-translational modification process, and includes N- and O-glycosylation which regulate both the structural and functional properties of proteins, such as protein folding and conformation, receptor binding, modulation of enzyme activity, and cellular recognition events (Lis and Sharon, 1993; Apweiler et al., 1999). N-glycosylation occurs only at the specific amino acid sequence, Asn-X-Ser/Thr (where X represents any amino acid except proline), using biosynthetic pathways that are highly conserved. Previous experimental results using tunicamycin to inhibit initial steps of the dolichol N-glycosylation pathway have demonstrated that when expressed in mammalian cells, N-glycosylation contributed up to about 25 kDa for molecular weight of mature anosmin-1 (Soussi-Yanicostas et al., 1996). In contrast to this finding, our result indicates that the oligosaccharide side chains of anosmin-1 are relatively smaller in insect cells. These differences are probably caused by the high

mannose oligosaccharide content of insect cells (Kuroda et al., 1990). The other possibility, such as the lower efficiency of glycosylation in insect cells, cannot be ruled out. Furthermore, the effects of this modification on the structural and functional characteristics of anosmin-1 can be investigated by using specific glycosylation blocking reagents such as tunicamycin to generate unmodified proteins.

## 2.6 Conclusions

Using transient expression experiments, *Drosophila* S2 cells were shown to be effective tools for the generation of recombinant anosmin-1 with a high yield when cultured in serum containing medium. The generated anosmin-1 was glycosylated and retains cell-surface binding characteristics, similar to that produced in mammalian cells. FnIII domains demonstrate multiple actions: first, they determine protein expression and secretion efficiency. Second, they mediate recombinant anosmin-1 attachment to the cell surface through an interaction with HS. Furthermore, cleavage of anosmin-1 is localized to the end of 2<sup>nd</sup> FnIII and the beginning of 3<sup>rd</sup> FnIII domain and is caused by a serum-induced phenomenon.

## Chapter 3

### Expression and Purification of anosmin-1 from stable *Drosophila* S2 cell line

#### 3.1 Introduction

The process of producing recombinant proteins of optimal quality and quantity requires both the generation of a stable cell line, generally using one of the more commonly used selection markers such as neomycin and hygromycin, as well as the use of an appropriate technique for protein purification, which in some cases involves the use of multi-step procedures using the purification strategy of capture, intermediate purification and polishing (CIPP). Depending on the physicochemical properties of the target protein, potential separation and purification techniques include affinity chromatography (biorecognition), ionic exchange chromatography (charge), gel filtration (size) and hydrophobic interaction chromatography (hydrophobicity).

Affinity chromatography separates proteins on the basis of a reversible interaction between a protein and a specific ligand coupled to a chromatographic matrix. Using this principle, the purification of recombinant fusion proteins containing an incorporated tag (glutathione-S-transferase or 6 consecutive histidine residues (6His)) is often straightforward, requiring a single step for purification. Ni-NTA affinity chromatography was used in the present study, to enable purification of recombinant anosmin-1 incorporating a C-terminal 6His tag. Ni-NTA affinity chromatography employs the principle of immobilized-metal affinity chromatography (IMAC), which exploits the binding affinity of imidazole-like histidine chains to the metal ion  $\text{Ni}^{2+}$ . In this method, nitrilotriacetic acid (NTA) is charged with the metal ion  $\text{Ni}^{2+}$  and then coupled to Sepharose CL-6B, thereby generating Ni-NTA agarose. NTA binds tightly to four sites in the nickel ion, leaving two sites free to interact with the 6His-tagged protein. Finally, the bound protein can be eluted off the column by simple competition with high concentration of imidazole.

It was first necessary to establish, validate and then optimise a reliable procedure

for producing anosmin-1, generating the desired yield and purity. The procedure involved establishing a stable S2 cell line with subsequent scale-up of the protein either in static phase or in suspension culture, and the final step of purification and dialysis. Prior to attempting stable transfection with a full-length and mutated anosmin-1 construct, PIWF1, containing the N-terminal WAP and first FnIII domains, was used for initial validation studies, given that it could be generated in abundant quantities as evidenced by the initial transient transfection experiments. There were additional reasons for generating PIWF1. First, it was recognised that the WAP and 1<sup>st</sup> FnIII domains of anosmin-1 were likely to represent key functional motifs (MacColl et al., 2002a). Second, it had already been shown that the FnIII domains (particularly the first one) participated in cell-surface association with immobilized HSPG (shown in Chapter 2). The characteristic WAP four-disulphide core motif shares significant homology with other members of WAP protein family (Heinzel et al., 1986; Wiedow et al., 1990), which are known to act as serine protease inhibitors. The WAP domain has obvious functional importance since clinically, mutations that disrupt the disulphide bridges within this motif result in loss of function of the entire protein. Thus three brothers in a X-KS pedigree share with a cysteine-arginine substitution at site 172 of the WAP domain (C172R) demonstrated the full KS phenotype (Oliveira et al., 2001). This C172R missense mutation was predicted to disrupt the conserved C157-C172 bridge, resulting in a conformational change and loss of biological function. In the present study therefore, I focussed on the C172R WAP mutation to examine the apparently crucial role of the WAP domain of anosmin-1. The production of pure PIWF1, PIWF4 protein and their C172R mutants is thus the main objective of this chapter; their constructs were shown in Figure 3-1.

### **3.2 Aims**

- 1) To explore the establishment of stable cell line for relevant protein expression using PIWF1 transfected S2 cells.
- 2) To scale up recombinant protein production using static and suspension culture.
- 3) To purify recombinant protein using Ni-NTA affinity chromatography.

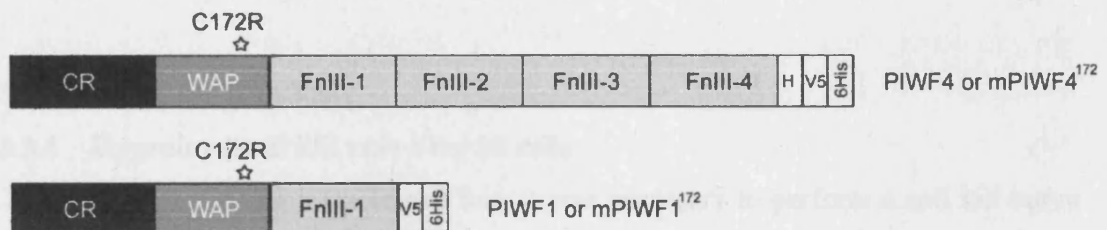


Figure 3.1 Structures of PIWF4, PIWF1 and their C172R mutants. The functional domains represented are; CR, cysteine-rich region; WAP, whey acidic protein-like domain; FnIII, fibronectin-like type III domain; H, histidine-rich region; V5, the V5 epitope tag derived from simian virus 5; 6His, 6×histidine tag. Using site-directed mutagenesis, the cysteine residue (C) at 172 site is replaced with arginine (R) (the mutation obtained in X-KS patients). The missense mutation (C172R) within the WAP domain present in mPIWF4<sup>172</sup> and mPIWF1<sup>172</sup> is indicated by the star.

- 4) To generate stable cell lines for empty vector protein, GFP protein, PIWF4 and the two mutant proteins (mPIWF1<sup>172</sup> and mPIWF4<sup>172</sup>) using an identical protocol to that successfully used to generate PIWF1 protein.
- 5) To generate a polyclonal anti-PIWF1 antibody (AIWF1) in rabbit against purified recombinant PIWF1.
- 6) To confirm the role of HSPG in anosmin-1 association onto S2 cell surface, a HS competitive assay was performed using stable cell lines.

### **3.3 Materials and Methods**

#### **3.3.1 Hygromycin-B kill curve for S2 cells**

Prior to generating a stable cell line, it was necessary to perform a cell kill curve to identify the optimal concentration of appropriate antibiotic for selecting successfully transfected cells; concentrations of antibiotics required for cell selection depend on both cell line and the specific antibiotic. The general principle for selecting stable transformants is to use the lowest concentration of antibiotic leading to 1) the onset of massive cell death after about five days and 2) cell kill of the entire non-resistant population within two weeks. To identify a suitable hygromycin-B concentration for transfected S2 stable cell selection, hygromycin-B at 0, 100, 300, 400, 700, 1,000 µg/ml concentration was used.

S2 cells at  $2 \times 10^6$  cells/ml density were cultured into 25 cm<sup>2</sup> flasks containing 10% serum culture medium with hygromycin-B (Invitrogen) at varying concentrations. Cells were kept growing at 23°C and then total viable cell count established by trypan blue exclusion after 5 and 10 days incubation respectively. 0.1 ml of trypan blue (Sigma) plus 0.1 ml of PBS were mixed and placed in an Eppendorf tube, followed by the addition of 0.1 ml of the cell suspension. Complete mixing was performed to avoid cell aggregation and ensure full cell suspension in solution. A small amount of trypan blue-cell suspension mixture was transferred by capillary action into both chambers of the haemocytometer. Cells were counted in the 1mm centre square and in the four 1 mm corner squares. Non-viable cells stained blue. Computation of cell concentration was as follows: Cells per ml = average cell count per square  $\times 3$  (dilution factor)  $\times 10^4$ .

Cell viability (%) = total viable cells/total cells×100. By the 5<sup>th</sup> day, cells selected by 100 µg/ml hygromycin-B continued to grow at the comparable rate as in the absence of hygromycin-B, whilst in the presence of 300 and 400 µg/ml hygromycin-B concentration, about half of the original S2 cells were killed. By contrast, 700 and 1,000 µg/ml hygromycin-B concentrations were associated with higher selection activity since at these two concentrations, about 70% S2 cells were killed. By the 10<sup>th</sup> day, 70% cells were killed by 300 and 400 µg/ml hygromycin-B, whereas S2 populations were almost completely killed by 700 and 1,000 µg/ml hygromycin-B (Figure 3.2). Therefore, it was estimated that the effective hygromycin-B concentration for selection of stable S2 cell lines lay within the 300-700 µg/ml range; 300 and 700 µg/ml hygromycin-B concentrations were then chosen to investigate optimal selection efficiency generating the best protein yield.

### **3.3.2 Selection of stable PIWF1 transformants with 300, 700µg/ml hygromycin-B**

S2 cells at  $1 \times 10^6$  cells/ml density were seeded in 3 ml medium containing 10% serum into a 25 cm<sup>2</sup> flask and incubated at 23°C overnight. The calcium phosphate kit (Invitrogen) was used to co-transfect with 19 µg recombinant DNA and 1 µg pCoHYGRO selection plasmid (Invitrogen). This selection vector contains the *E.coli* hygromycin-B-phosphotransferase gene under *Drosophila copia* promoter control, conferring resistance to hygromycin-B. The two-transfection solutions were set up as follows: Solution A: 36 µl of 2M CaCl<sub>2</sub>, 30 µg of PIWF1 recombinant DNA, 1 µg pCoHYGRO and sterile water to 300 µl final volume; solution B, 300 µl of 2× HEPES-buffered saline (HBS, pH7.1). Solution A was slowly added, drop by drop, to solution B, with constant vortexing, followed by incubation at room temperature for 40 min. The solution was then mixed, added to cells and incubated at 23°C overnight. After centrifugation, calcium phosphate solution was removed and cells washed three times with Dulbecco's PBS; fresh 10% serum medium was then added, and cells replaced into the same flask and incubated for a further 2 days. Cells were centrifuged and re-suspended in 10% serum containing medium with 300 and 700 µg/ml hygromycin-B respectively, this procedure being repeated every 4 days. At each change of medium, the total number of viable cells was counted to monitor



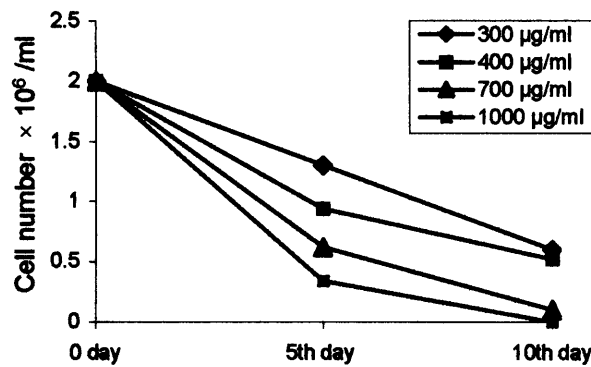
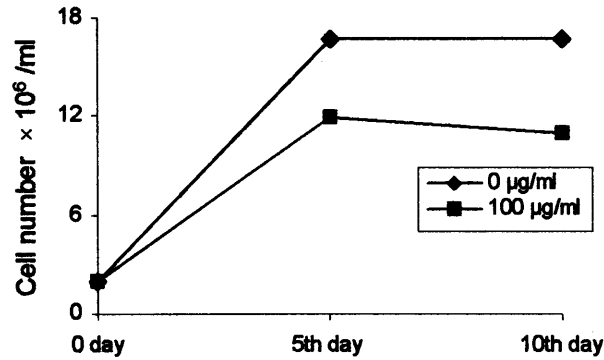


Figure 3.2 Hygromycin-B induced S2 cell kill curve. S2 cells at  $2 \times 10^6$  cells/ml density were cultured in 10% serum containing DES<sup>TM</sup> medium, and co-incubated in the absence or presence of hygromycin-B at the various concentration of 100, 300, 400, 700 and 1000  $\mu\text{g/ml}$ . On the 5<sup>th</sup> and 10<sup>th</sup> day of hygromycin-B selection, cell viability was determined by Trypan blue exclusion and counted by haemocytometer. The cells selected by 100  $\mu\text{g/ml}$  hygromycin-B keep growing at a comparable rate to those without hygromycin-B addition (top graph). About 50% of cells were killed by 300 and 400  $\mu\text{g/ml}$  hygromycin-B, whereas hygromycin-B at or over 700  $\mu\text{g/ml}$  nearly kill all cells by the 10<sup>th</sup> incubation day (bottom graph).

antibiotic selection. Throughout the whole selection process, cell numbers initially dropped by approximately 50% and then rose to over  $1 \times 10^7$  cells/ml, confirming that the resistant S2 cells had been generated. The duration of time for the selection process was generally about 3 weeks. Resistant cells were then split 1:2 into a new flask with addition of fresh selection medium, and incubated for a further 3 days before being split 1:2 again. To confirm PIWF1 protein expression,  $2 \times 10^6$  resistant cells in 2.5 ml 10% serum medium were aliquoted into 6-well plates and copper sulphate added for induction of protein expression. On the 2<sup>nd</sup> post-induction day, proteins were collected for Western blot analysis, according to the protocol described in sections 2.3.2.1 and 2.3.3. Resistant cells with the highest PIWF1 expression were aliquoted and stored in liquid nitrogen, the remainder being used for protein scale up.

### **3.3.3 Scale-up of PIWF1 using stationary flask and spinner flask**

The protein purification process is greatly facilitated if the relevant recombinant protein can be expressed in serum-free medium; in this instance, in order to avoid proteolytic degradation of full length anosmin-1, it was necessary to express the PIWF4 protein in the absence of serum (described in Chapter 2). This necessitated as first step, gradually weaning the cell line expressing PIWF1 into medium devoid of serum.  $1 \times 10^7$  cell/ml stable cells were initially harvested in 10% serum containing medium, then down successively into medium containing 1% serum and finally neat serum-free medium. Stable cells at a final density of  $2 \times 10^6$  cell/ml in 100 ml serum-free medium were then transferred either into a 300 cm<sup>2</sup> stationary flask or into a 250 ml spinner flask for suspension culture. In the latter case, 0.05% (v/v) pluronic F-68 (a surfactant used to protect cells from shearing damage, Sigma) was added to the medium. A constant stirring rate of 100 rpm was used in the spinner flask, with its side arms loose for a quarter (1/4) turn. After overnight incubation, cells were induced to express PIWF1 protein. On the 3<sup>rd</sup> post-induction day, conditioned medium was collected and cell surface associated protein extracted with serum-free medium containing additional 350 mM NaCl.

### **3.3.4 Protein purification by Ni-NTA affinity chromatography**

The salt extract and conditioned medium were loaded into a Vivaspin 20 ml concentrator (Vivascience, 5,000 MWCO membrane) in order to trap PIWF1 protein, while minimising the volume. The loaded concentrator was then centrifuged at 2,500 ×g at 4°C for 50 min. The concentrated solution was transferred into a new tube, and 10×balance buffer (500 mM NaH<sub>2</sub>PO<sub>4</sub>, 50 mM Tris·Cl, 100 mM imidazole, pH 8.0) added. For conditioned medium, this buffer with additional 350 mM NaCl was added and mixed thoroughly. 200 µl 50% Ni-NTA agarose (1 volume Ni-NTA with 1 volume PBS, Qiagen) was then added into each 4 ml mixed solution (1:20), and gently mixed by shaking at 100 rpm at 4°C for 1 hour. The mixture was transferred onto a column with filter on the bottom (Qiagen) and flow-through fraction collected. The column was then washed twice with 1ml wash buffer (50 mM NaH<sub>2</sub>PO<sub>4</sub>, 5 mM Tris·Cl, 300 mM NaCl and 20 mM imidazole, pH 8.0). Protein was eluted 4-6 times with 200 µl elution buffer (50 mM NaH<sub>2</sub>PO<sub>4</sub>, 5 mM Tris·Cl, 300 mM NaCl and 250 mM imidazole, pH 8.0) and analysed by Western blot and silver staining.

### **3.3.5 Silver staining**

10 µl samples and 7 µl of molecular weight markers were loaded onto a Novex Nu-PAGE 4-12% polyacrylamide gel and run at 180V for 40 min. Silver staining kit (Invitrogen) was used for protein detection according to the manufacturer's protocol. The gel was soaked in 100 ml fixing solution containing methanol and acetic acid for 10 min, followed by soaking twice in 100 ml sensitising solution with glutaraldehyde for 1 hour. The gel was then rinsed in 2 × 200 ml changes of ultra pure water for 10 min each, and then soaked in staining solution with silver nitrate and sodium hydroxide for 15 min prior to a further two rinses. The gel was then placed in developing solution until bands reached the desired intensity; staining was then terminated with 5 ml addition of stopper solution and the gel washed twice more with pure water. Water was then decanted and fresh Gel-Dry™ solution (35 ml per gel, Invitrogen) was added. The gels were then placed between two layers of cellophane sheets and assembled into a gel-drying frame for scanning and photography.

### **3.3.6 Quantitative Protein Assay**

The Bio-Rad protein assay (Bio-Rad laboratories, UK) used here is based on the Bradford method. In an acidic solution of Coomassie Brilliant G-250, absorbance shifts from 465 nm to 595 nm upon binding to protein. Bovine plasma albumin was used as protein standard and set up in serial incremental concentrations in PBS to construct a standard curve. PBS only was used as blank. The protein sample was also appropriately diluted with PBS to a final volume of 0.8 ml. 0.2 ml Dye Reagent concentrate was then added to each standard and protein samples and gently inverted several times. After 30 min, the OD<sub>595</sub> was measured and corrected for the reagent blank. OD<sub>595</sub> versus concentration of standards was plotted, enabling sample protein concentration to be read from the standard curve. Final protein concentration = protein concentration obtained from standard curve × dilution factor.

### 3.3.7 Mutagenesis of mPIWF1<sup>172</sup> and mPIWF4<sup>172</sup> incorporating C172R WAP domain mutation.

The QuickChange<sup>™</sup> site-directed mutagenesis kit and protocol (Stratagene) was used with the mutagenic forward primer: GGGTGTGGACACACCCGTCAAGTACCCAAGACTC and reverse primer: GAGTCTTGGGTACTTGACGGGTGTGTCCACACCC containing the mutated codon (C172R) in the middle of the primers. 10-75 ng each of PIWF1 and PIWF4 were used as template with 125 ng of primers, 1 µl of dNTP mix, 2.5 unit of *PfuTurbo* DNA polymerase and water, made up to a final reaction volume of 50 µl. The PCR extension time was calculated according to the recommended formula: 2 minutes/ kb of plasmid length. In the case of PIWF4, the reaction was not initially successful using the calculated time of 11 min. Following investigation, the optimal extension time was determined to be 14 min. The PCR protocol was as follows:

	segment	cycles	temperature	time
mPIWF1 <sup>172</sup>	1	1	95°C	30 sec
	2	12	95°C	30 sec
			55°C	1 min
			68°C	9 min

mPIWF4 <sup>172</sup>	1	1	95°C	5 min
	2	14	95°C	50 sec
			57°C	1 min
			68°C	14 min

Following temperature cycling, the reaction was placed on ice for 2 minutes to cool the reaction to  $\leq 37^{\circ}\text{C}$ . PCR products were then treated with 1  $\mu\text{l}$  of the *Dpn* I endonuclease (10U/ $\mu\text{l}$ ). The *Dpn* I endonuclease is specific for methylated and hemimethylated DNA with the target sequence 5'-GmATC-3' and is used to digest the parental DNA template and to select for mutation-containing synthesized DNA. Each reaction mixture was gently and thoroughly mixed by pipetting the solution up and down several times. The reaction mixture was then spun down and incubated at 37°C for 4 hours to digest parental DNA. 2 $\mu\text{l}$  of *Dpn* I-treated DNA was added to DH5 $\alpha$  competent cells and the protocols outlined in 2.3.1.5-2.3.1.8 sections then followed. All constructs were sequenced to confirm creation of correct mutants. The construct of these two mutants was shown in Figure 3.1.

### 3.3.8 Optimization of expression and purification of recombinant proteins

Similar protocols to those for PIWF1 were used to scale-up PIWF4 and other recombinant proteins, including green fluorescent protein (GFP), PIWF4, mPIWF1<sup>172</sup> and mPIWF4<sup>172</sup>. A stable S2 cell line expressing empty vector protein was also generated for comparison of the protein cell surface association, but not used for protein scale-up. Some modifications were incorporated for certain steps. First, 700  $\mu\text{g}/\text{ml}$  hygromycin-B was used for selection. Second, the suspension culture method was optimised, since larger recombinant protein yields are dependent on this method. The concentration of cell protection reagent -- pluronic F-68 was increased from 0.05% (v/v) to 0.1%, whilst a constant stirring rate was decreased from 100 rpm to 60-70 rpm. Furthermore, the time of incubation was prolonged up to 3 days prior to CuSO<sub>4</sub> induction. Finally, since mutated proteins were expressed at lower efficiency, the ratio of the Ni-NTA to the mixture solution was decreased to 1:40 in order to minimize binding of other non-desirable proteins. All purified samples were analysed by SDS-PAGE and Novex Colloidal Blue stain (Invitrogen). This method is 5 times

more sensitive than traditional Coomassie Blue techniques and easy to use, thus substituting for the previously used silver staining. 2  $\mu$ l samples were loaded for electrophoresis and the gel was shaken in fixing solution (mixture of 40 ml deionised water, 50 ml methonal and 10 ml acetic acid for one gel) for 10 minutes. The gel was then soaked in staining solution containing methonal and stainer A for 10 minutes, followed by the addition of 5 ml stainer B/each gel for a minimum of 3 h shaking.

### **3.3.9 Protein dialysis into PBS**

Purified protein was dialysed against PBS to remove imidazole and salt prior to subsequent functional and structural analyses. Protein samples were injected into a slide-A-lyzer Cassette with a pre-hydrated 10 kDa MWCO membrane (Pierce). Initially, direct dialysis against PBS resulted in significant protein aggregation and precipitation; aggregated protein could however be re-dissolved into the original elution buffer. Thus, different conditions for anosmin-1 protein dialysis were investigated: namely, the effects of PBS pH ranging from 7.0 to 9.0 and the effects of various salt or detergent concentrations. However, none of these conditions were capable of keeping anosmin-1 soluble. Finally, metal ion contamination was considered. Thus metal chelators EDTA together with imidazole were added to the dialysate solution for anosmin-1 dialysis. As expected, this modification abolished anosmin-1 aggregation, confirming that the metal ion was the key determinant of anosmin-1 solubility. There are a number of dialysis steps using different dialysates containing imidazole and EDTA. First, the dialysis was performed against PBS to which was added 160 mM NaCl, 100 mM imidazole and 10 mM EDTA at 4°C for 24 h. Second, protein was dialysed into the buffer to which was added 160 mM NaCl, 20 mM imidazole and 2 mM EDTA, followed by dialysis against PBS with 160 mM NaCl only. Finally, protein was dialysed into pure PBS for functional analysis and into PBS with additional 80 mM NaCl for structural studies. In each procedure the same dialysate was changed 3 times. All dialysed samples were concentrated using a vivascience concentrator with 10 kDa MWCO membrane.

### **3.3.10 Protein storage**

For structure study, the purified and dialysed anosmin-1 was kept at 4°C for short-term storage. For long-term storage, the protein was frozen at -80°C, lyophilized and reduced to dehydrated protein powder. The redissolved anosmin-1 still retained its biological function, indicating that the lyophilization can be used for anosmin-1 storage and maintenance of its stability.

### **3.3.11 HS competitive assay using stable S2 cell lines**

Established PIWF1 and PIWF4 expressing stable S2 cell lines were harvested at  $2 \times 10^6$  cell/ml density into 6-well plates in 2.5 ml serum-free medium. After 24 h incubation, cells were treated with or without 100 µg/ml HS in the presence of 500 µM CuSO<sub>4</sub> for protein expression. Conditioned medium and cell-surface associated proteins were collect for Western blot.

### **3.3.12 Generation of polyclonal antibody against PIWF1 (AIWF1)**

Polyclonal antibodies were raised in rabbit by CN Bioscience (UK). 80 µg/ml of pure PIWF1 was injected with Freund's complete adjuvant for initial immunization and Freund's incomplete adjuvant for the remaining 5×boosts. Pre-immune serum was collected, and following immunization, test bleeds were performed to investigate the sensitivity and specificity of antibodies (AIWF1) generated.

#### **3.3.12.1 Dot-Blot**

1, 0.1, 0.01 µg of PIWF1 protein, diluted in 10-20 µl PBS, were loaded onto a nitrocellulose membrane and allowed to dry at 37°C for 30 minutes. The membrane was cut into slices and placed into 6-well plates prior to incubation with various dilutions of antibody. The samples were incubated in 1 ml 5% fat-free milk in TBS (15 mM Tris, 20 mM NaCl, pH 7.6) for 1 h, and membranes then washed with 4 × 1 ml TBS-0.1% Tween-20, and incubated overnight with the AIWF1 antibodies from the second test serum at the following dilutions: 1:10, 1:100, 1:1,000, 1:10,000, with shaking at 4°C. Pre-immune sera was added without dilution as a negative control. The membrane was washed four times with wash buffer and incubated for two hours with goat anti-rabbit peroxidase antiserum, followed by 3 × wash with TBS/T and a single

wash in 50 mM Tris-HCl pH 7.6. The reaction was developed in DAB 0.025% (50 mM Tris-HCl, pH 7.6) with 0.005% H<sub>2</sub>O<sub>2</sub>, and the reaction terminated in 10 mM EDTA pH 8.0, followed by drying prior to scanning.

### **3.3.12.2 ELISA assay**

1 µg, 0.1 µg and 0.01 µg of PIWF1 protein in 100 µl PBS were coated onto the 96-well Immunlon 4HBX microtitre plate (Thermo LabSystems/ Thermo life science) and incubated at 4°C overnight. Each well was rinsed 3 times with 100 µl wash buffer (50 mM Tris-HCl, 150 mM NaCl, 0.05% Tween-20, pH7.6). 100 µl 1% BSA in PBS-0.1% Tween (PBS/T) was added to cover the remaining protein binding sites during a 1 h incubation at 37°C. Each well was washed with wash buffer and AIWF1 antibody added in dilutions with PBS/T at-- 1:10, 1:100, 1:1,000, 1:10,000, 1:100,000 concentrations, followed by incubation at 37°C for 1 hour. After rinsing each well 3 times, the second anti-rabbit antibody labelled with alkaline phosphatase (1:10,000 dilution with TBS) was added and incubated at 37°C for 1 h. Each well was rinsed thoroughly with wash buffer 4 times and then 100 µl substrate (p-nitrophenyl phosphate, 0.25 mg/ml, Pierce) was added to each well and allowed to react at 37°C for 15 min. Optical density at 405nm was then measured.

### **3.3.12.3 AIWF1 purification**

AIWF1 antibody was purified from serum obtained during the 3<sup>rd</sup> bleed with protein G Sepharose affinity chromatography using a MAB Trap Kit (Amersham Pharmacia). A syringe was filled with distilled water and connected tightly to the column through a Leuer adapter. The twist-off end was removed and the ethanol preservative washed out with 5 ml distilled water at 1 drop/sec. The column was equilibrated with 3 ml binding buffer. The 1:1 binding buffer diluted serum was applied to the column and washed with 10 ml binding buffer. Purified IgG was eluted with 5 ml elution buffer into 200 µl neutralizing buffer pre-loaded tubes for each 1 ml elution solution. The eluates were collected into 1-5 tubes separately. To measure the concentration of purified antibody, 20 µl of eluates were collected and mixed with 980 µl of water and the absorbance read at 280nm. The peak optical density was



observed in the second eluates,  $A_{280} = 0.185$ . The concentration of purified IgG was calculated as follows:  $0.75 \times 0.185 \times 50 = 6.94$  mg/ml. Purity and specificity were assessed by Novex Colloidal Blue stain and Western blot.

#### **3.3.12.4 Western blot**

0.01  $\mu$ g, 0.1  $\mu$ g PIWF1 and 0.1  $\mu$ g, 0.6  $\mu$ g PIWF4 proteins were loaded onto the Nu-PAGE gel for electrophoresis and then transferred to the nitrocellulose membrane. Blotting was carried out with purified AIWF1 antibody or anti-His antibody (positive control) in a 1:1,000 dilution. The secondary anti-rabbit antibody at a 1:10,000 dilution was directed to polyclonal AIWF1 test, whilst anti-mouse secondary antibody directed to the monoclonal anti-His antibody.

### **3.4 Results**

Based on the kill curve of S2 cells (Figure 3.2), a concentration of 300  $\mu$ g/ml hygromycin-B was chosen as starting point and a concentration of 700  $\mu$ g/ml used to compare the selection efficiency. The PIWF1 stable cells selected by 700  $\mu$ g/ml hygromycin-B yielded 5-10 fold more protein (250  $\mu$ g/ml) than that by 300  $\mu$ g/ml hygromycin-B selection. In contrast, 1,000  $\mu$ g/ml hygromycin-B proved too high, being lethal to both transfected and non-transfected cells. These results suggested that the higher concentration of hygromycin-B at 700  $\mu$ g/ml was optimal for selection, possibly because: 1) it generated a relatively pure population of polyclonal stable cells by killing more non-transfected S2 cells and 2) it selected out higher protein-expressing cells with a greater number of copies of recombinant DNA integrated into the host genome. However, compared to PIWF1, the expression of PIWF4 and mutant proteins was much less, about 5 fold lower for PIWF4 and mPIWF1<sup>172</sup> and >10 fold for mPIWF4<sup>172</sup> even with 700  $\mu$ g/ml hygromycin-B selection, the results being consistent with previous observations in the transient transfection experiments.

As shown in Figure 3.3 and 3.4, the purity of PIWF1 from the salt extract was extremely high, as evidenced by the silver staining assay; higher yields were evident with 700  $\mu$ g/ml hygromycin-B selected cells as compared with that with 300  $\mu$ g/ml

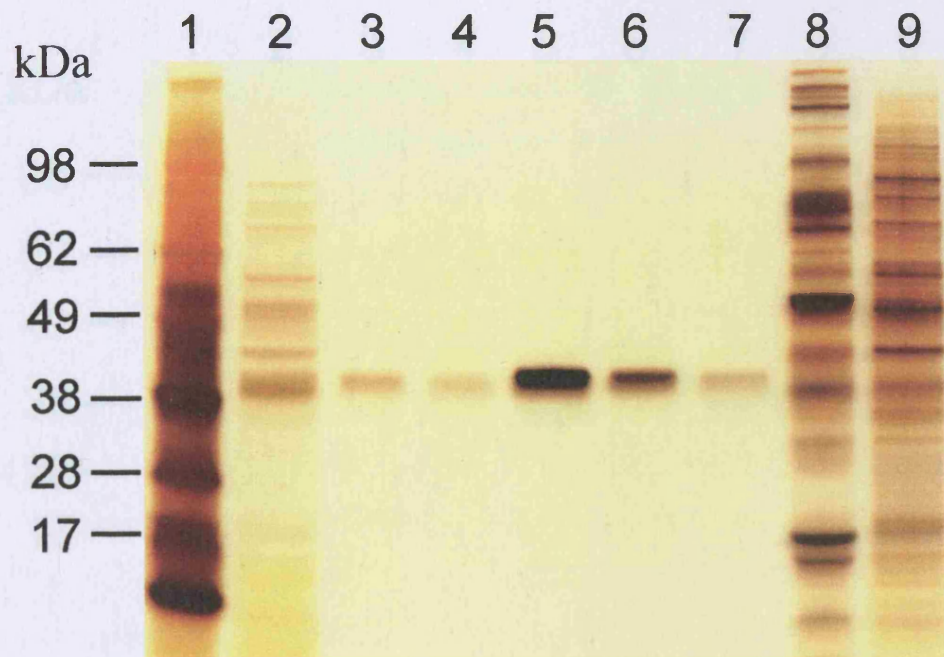


Figure 3.3 Purification of salt extracted PIWF1 generated from 300  $\mu\text{g/ml}$  hygromycin-B selected S2 cells. The stable PIWF1 cells ( $2 \times 10^6$  cell/ml) were harvested in 100 ml serum free medium and the protein expression was induced in static flask. 10  $\mu\text{l}$  of each sample was electrophoresed through SDS/PAGE under non-reducing conditions and stained with silver staining. Lane 1: marker; Lane 2: flow-through pool; Lane 3: 20 mM imidazole wash; Lane 4-7: 250 mM imidazole elution; Lane 8: conditioned medium; Lane 9: 350 mM NaCl extract. The molecular weight is shown.

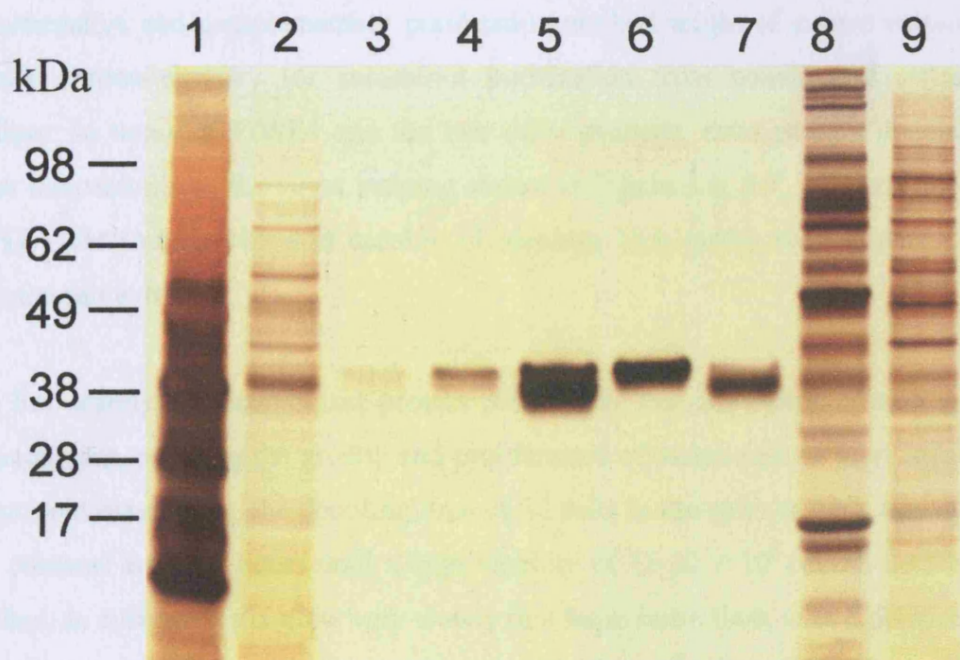


Figure 3.4 Purification of salt extracted PIWF1 generated from 700  $\mu\text{g/ml}$  hygromycin-B selected S2 cells. The PIWF1 stable S2 cells ( $2 \times 10^6$  cell/ml) were harvested in 100 ml serum free medium and the protein expression induced in a static flask. 10  $\mu\text{l}$  of each sample was electrophoresed through SDS/PAGE under non-reducing conditions and stained with silver staining. Lane 1: marker; Lane 2: flow-through pool; Lane 3: 20 mM imidazole wash; Lane 4-7: 250 mM imidazole elution; Lane 8: conditioned medium; Lane 9: 350 mM NaCl extract.

selection. Although devoid of serum in the cultured medium, more protein contaminants were observed when purification was performed directly from conditioned medium (Figure 3.5), possibly due to the presence of free copper ions. These observations reinforce the advantage of one-step purification by Ni-NTA chromatography directly from salt extraction rather than from conditioned medium. An alternative and complementary purification method might of course employ HS affinity chromatography for anosmin-1 purification from conditioned serum-free medium. In terms of PIWF4 and the two other mutants, even present in relatively lower concentrations, the silver staining shown in Figure 3.6, 3.7, 3.8 confirmed that Ni-NTA chromatography was capable of yielding high purity recombinant protein from the salt extract.

For scaling-up recombinant protein production, the suspension culture appears advantageous, enabling the growth and proliferation of insect cells at high density. In the present experiment, the doubling time of S2 cells in the spinner flask was more or less constant at 18-24 hours until a high viability of  $15\text{-}20 \times 10^6$  cell/ml density was reached; in contrast, cells grew very slowly in a large static flask with a division time of 48-72 hours and a tendency to stop growing at  $5 \times 10^6$  cells/ml. Paradoxically, the level of purified protein is opposite; thus, about 20 fold less protein of lesser purity was observed in suspension culture as compared to the stationary flask (Figure 3.9). It is, at first, unclear why cells maintaining a high proliferation rate and population subsequently generate inferior protein yields of lesser purity. The most likely explanation is, however, that continuous shearing stress experienced by cells exposed to harsh stirring, together with the deficiency of cell-membrane protection reagent (pluronic F-68) would cause mechanical damage to rapidly circling cells, leading to the secreted protein detachment from the cell surface. Another possibility is that copper sulphate induction of protein synthesis may be less efficient in cells that have been stirred. As a consequence, minor modifications to the stirring speed and concentration of pluronic F-68, were undertaken, these being the main factors determining mechanical cell damage. As shown in Figure 3.10, the best recombinant protein yield was obtained with a decreased constant stirring rate of 60-70 rpm and by



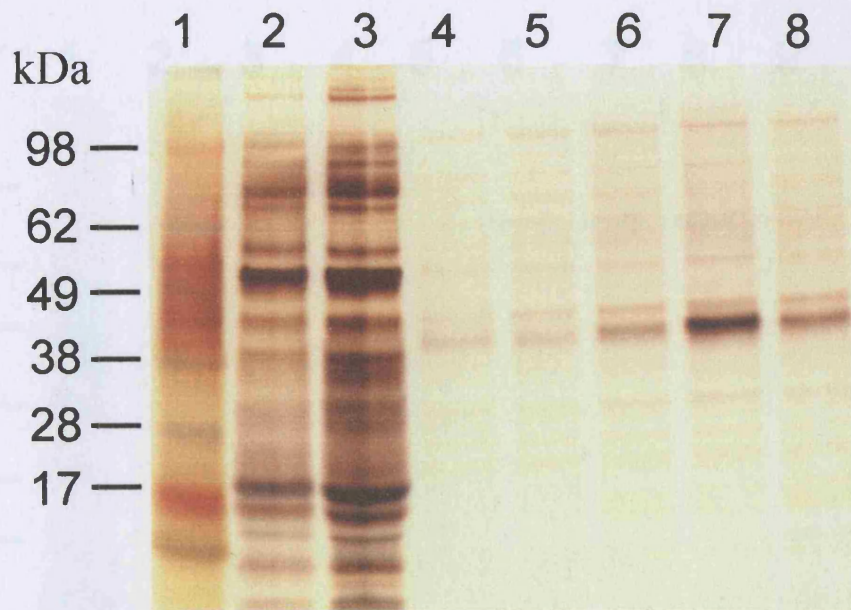


Figure 3.5 Purification of PIWF1 protein from serum-free conditioned medium. The PIWF1 was generated by 700  $\mu\text{g}/\text{ml}$  hygromycin-B selected S2 cells. Lane 1: marker; Lane 2: serum-free conditioned medium; Lane 3: flow-through pool; Lane 4: 20 mM imidazole wash; Lanes 5-8: 250 mM imidazole elution.

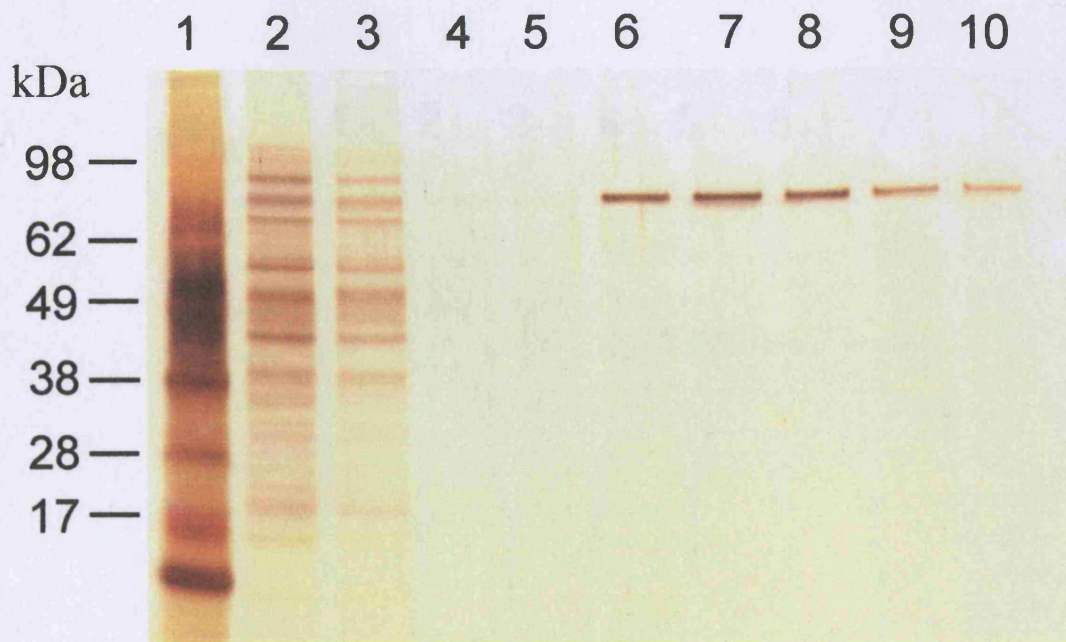
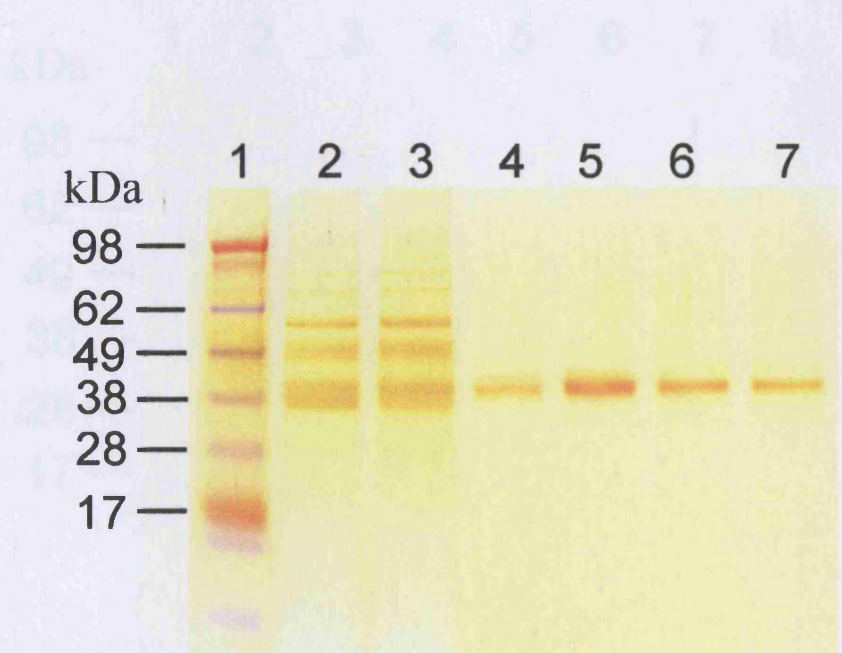


Figure 3.6 Purification of salt extracted PIWF4. Lane 1: marker; Lane 2: 350 mM NaCl extract; Lane 3: flow-through pool; Lane 4: 20 mM imidazole wash; Lanes 5-10: 250 mM imidazole elution.



Figur 3.7 Purification of salt extracted mPIWF1<sup>172</sup>. Lane 1: marker; Lane 2: flow-through pool; Lane 3: 20 mM imidazole wash; Lane 4-7: 250 mM imidazole elution.



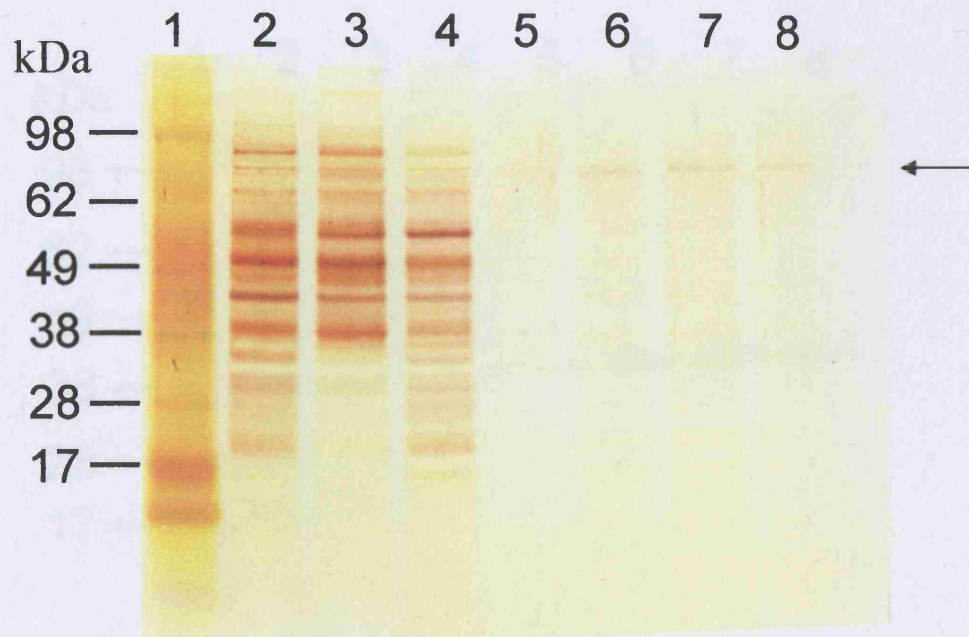


Figure 3.8 Purification of salt extracted mPIWF4<sup>172</sup>. Lane 1: marker; Lane 2: salt extract; Lane 3: flow-through pool; Lane 4: 20 mM imidazole wash; Lanes 5-8: 250 mM imidazole elution. Purified protein is indicated by arrow.



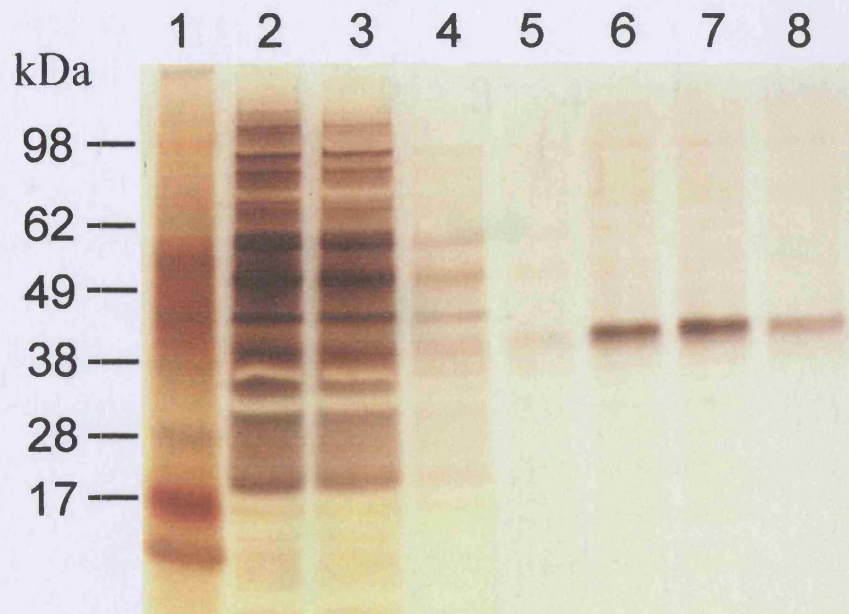


Figure 3.9 Initial investigations on the generation and purification of salt extracted PIWF1 protein using suspension culture. The PIWF1 stable S2 cells ( $2 \times 10^6$  cell/ml) were harvested in 100 ml serum free medium containing 0.05% (v/v) pluronic F-68, and then incubated at a constant stirring rate of 100 rpm. 10  $\mu$ l of each sample was loaded for electrophoresis and silver staining. Lane 1: marker; Lane 2: salt extraction; Lane 3: flow-through pool; Lane 4: 20 mM imidazole wash; Lane 5-8: 250 mM imidazole elution.

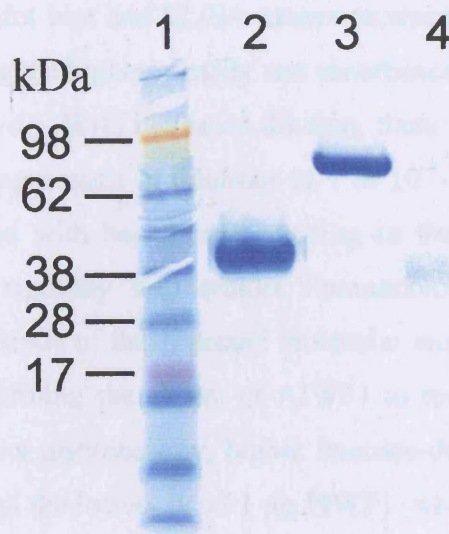


Figure 3.10 Generation and purification of salt extracted PIWF1, PIWF4 protein and GFP using suspension culture to validate the modified protocol. The corresponding protein-expressing stable S2 cells ( $2 \times 10^6$  cell/ml) were cultured in 250 ml serum free medium containing higher concentration of pluronic F-68 to 0.1% (v/v), and incubated at a slower constant stirring rate of 60-70 rpm. 10  $\mu$ l of each sample was loaded for electrophoresis and Novex Colloidal Blue stain. Lane 1: marker; Lane 2: PIWF1; Lane 3: PIWF4; Lane 4: GFP.

increasing pluronic F-68 up to 0.1%, indicating that the importance of restricting cell shearing stress in the suspension culture. This modification proved extremely valuable, resulting in the generation of sufficient pure recombinant protein, for use in subsequent structural analysis.

The successful generation of large amounts of highly purified recombinant PIWF1 protein enabled the generation of a specific anti-anosmin-1 antibody(AIWF1). As expected, the dot blot and ELISA assays produced consistent results (Figure 3.11 and 3.12), showing the highest density and absorbance at 1 in 10 and 1 in 100 antibody dilutions respectively. With increased dilution, there was a corresponding decrease of sensitivity, reaching a nadir at dilutions of 1 in  $10^4$ - $10^5$ . The pre-immune antiserum was not associated with background staining in the dot-blot assay, confirming the specificity of the antibody. Furthermore, immunoblot analysis using 1:1,000 AIWF1 generated single bands of the expected molecular weights for the PIWF1 and PIWF4 respectively, confirming the ability of AIWF1 to recognise both truncated and full-length proteins. Not unexpectedly, higher immuno-detection sensitivity was obtained in 1  $\mu$ g PIWF1 and the lowest in 0.01  $\mu$ g PIWF1, whereas a weak band was observed at higher concentration of 0.6  $\mu$ g PIWF4 (Figure 3.13).

A HS competitive assay using transient transfection (Chapter 2) had previously shown that anosmin-1 was attached to the cell surface by binding to the HS chain of HSPG. To confirm this observation, experiments were also conducted on stable PIWF1 and PIWF4 cell lines, which do not suffer from the disadvantage of requiring multiple-step cell preparation, as well as the variable efficiency of transfection. Exogenous 100  $\mu$ g/ml HS was added at the time when stable cells were induced by  $\text{CuSO}_4$ . Western blot consistently showed a higher intensity band in conditioned medium upon the addition of exogenous HS, demonstrating that 100  $\mu$ g/ml HS could dissociate PIWF1 and PIWF4 from cell surface into medium (Figure 3.14). In order to rule out the possible involvement of the V5 and poly-His tag in cell-surface binding, stable cell lines transfected either with an empty vector or the vector expressing GFP were established. Western blot analysis using anti-His antibody showed that the

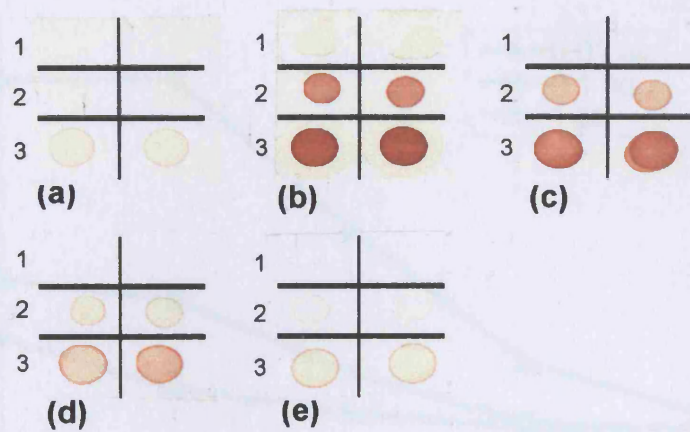


Figure 3.11 Dot blot analysis was performed using the recombinant PIWF1 protein (0.01-1  $\mu\text{g}$ ) as antigen on the nitrocellulose membrane. AIWF1 (1:10-1:10,000 serial dilutions) were used as primary antiserum and preimmune serum serving as negative control. (a) preimmunsera; (b) 1:10 diluted AIWF1 antibody; (c) 1:100 diluted AIWF1; (d) 1:1,000 diluted AIWF1; (e) 1:10,000 diluted AIWF1 antibody. 1. 0.01  $\mu\text{g}$  PIWF1; 2. 0.1  $\mu\text{g}$  PIWF1; 3. 1  $\mu\text{g}$  PIWF1.



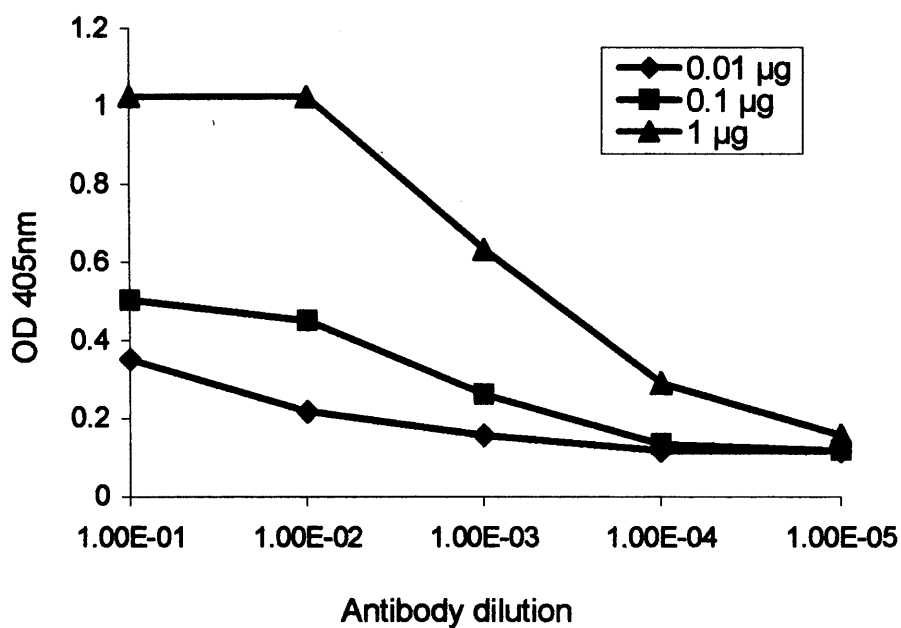


Figure 3.12 AIWF1 antibody analysis by ELISA assay. The microtitre wells were coated with 0.01, 0.1 and 1 µg of PIWF1 respectively. Serial dilutions of AIWF1 antibody (1:10-1:100,000) were added for 1 h incubation at 37°C, followed by incubation with second antibody conjugated with alkaline phosphatase. The optical density was measured at 405nm. 1.00E-01= 1 in 10; 1.00E-02= 1 in 10<sup>2</sup>; 1.00E-03= 1 in 10<sup>3</sup>; 1.00E-04= 1 in 10<sup>4</sup>; 1.00E-05= 1 in 10<sup>5</sup>.

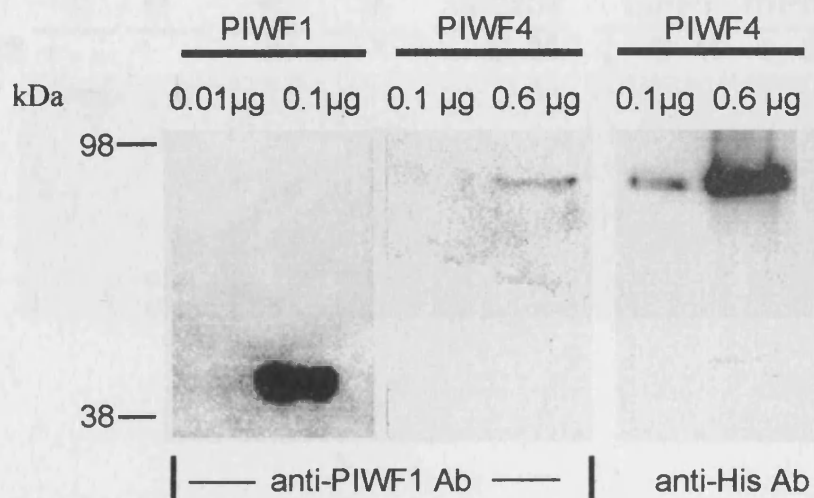


Figure 3.13 AIWF1 antibody analysis by Western blot. 0.01, 0.1 µg PIWF1 and 0.1, 0.6 µg PIWF4 were loaded for SDS-PAGE respectively. The proteins were immunoblotted by 1:1,000 diluted AIWF1 antibody and anti-His antibody as positive control. The corresponding horseradish peroxidase conjugated secondary antibody was used: anti-rabbit secondary antibody for AIWF1 antibody and anti-mouse secondary antibody for anti-His antibody. The molecular weight markers are shown.

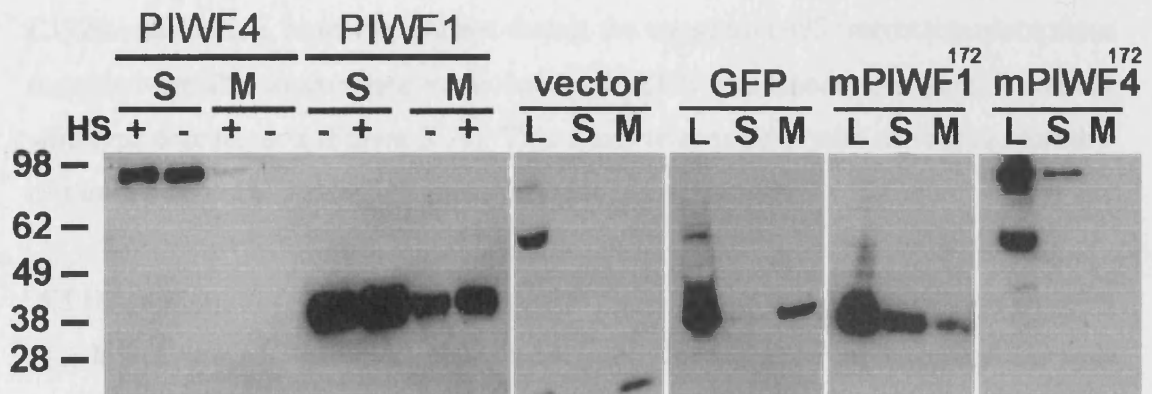


Figure 3.14 Western blot analysis of recombinant anosmin-1, the C172R mutants, empty vector protein and GFP generated by stable S2 cell lines in serum free medium using anti-His antibody. PIWF1 and PIWF4 proteins were analysed in the presence or absence of HS. The proteins in salt extract (S) are cell surface associated, whereas secreted proteins are detected in conditioned medium (M). More recombinant PIWF1 and PIWF4 were dissociated from cell surface by exogenous HS addition, confirming that recombinant anosmin-1 anchors onto the cell by interaction with HS chain of HSPG. The cell surface association patterns of vector, GFP and two C172R mutants (mPIWF1<sup>172</sup> and mPIWF4<sup>172</sup>) using S2 stable cells are also shown. L represents cell lysate.

epitope containing bands were only present in conditioned medium rather than in the salt extract (Figure 3.14), indicating that these epitopes alone are not able to bind to cell surface. To further understand the role of the evolutionarily conserved WAP domain and to study the effects of the C172R substitution, mPIWF1<sup>172</sup> and mPIWF4<sup>172</sup> expression constructs were generated. The expression of mPIWF1<sup>172</sup> and mPIWF4<sup>172</sup> proteins was also confirmed by Western blotting (Figure 3.14). The C172R substitution, however, did not disrupt the anosmin-1-HS interaction since these mutants were able to associate to the cell surface HS in a manner comparable to their wild type counterparts (Figure 3.14). This result is consistent with the conclusion that it is the FnIII, not WAP, which is essential for HS interaction.

### 3.5 Discussion

In the present study, procedures for recombinant anosmin-1 generation have been optimised from initial establishment of a stable cell line to the final steps of dialysis. The main challenges during these processes were the determination of optimal conditions for suspension culture, protein purification and subsequent dialysis. As previously described, spin rate, concentration of pluronic F-68 and even initial cell density had to be taken into account using the spinner flask technique. Although satisfactory protein purity could be obtained using a stationary flask, the inferior cell density generated by this method proved a major limitation when trying to use this method to generate a large protein yield. Furthermore, the present method using Ni-NTA chromatography appeared to offer the best approach for one-step purification of 6His fused proteins when extracted from the cell surface, thereby minimising the protein loss inevitably associated with the more laborious purification procedures. When using CHO cells, for example, to generate and purify anosmin-1, a three step procedure including two affinity chromatographies were required (Soussi-Yanicostas et al., 1996), whereas the single step purification used here with chelated nickel-NTA bound to the 6His-fusion anosmin-1 proved sufficient.

The next biggest challenge proved to be the protein dialysis procedure. Metal ion contamination associated with purification by immobilized metal affinity



chromatography (IMAC) was considered as a key factor for protein aggregation and precipitation during dialysis. Proteins are highly interactive with metal ions by two principle types of interaction; one is based on the carboxy clusters on the protein surface which behave similarly to carboxy chelators such as EDTA and EGTA, the other related to constituent amino acid residues as the imidazolium ring of histidine. Protein-metal binding is 5-60 times stronger than an ion exchange interaction and the metal may also mediate crosslinking, leading to simple dimerization, gross aggregation or even precipitation. It may also alter protein properties, including surface charge and hydrophobicity. Thus, elimination of contaminating metal ions benefits not only the dialysis process but also ensures maintenance of the original protein properties. A two-pronged chemical strategy was therefore adopted. First, the inclusion of 5-50 mM EDTA in the buffers to compete with the carboxy clusters within protein for chelation to metal ions. Second, along with EDTA, inclusion of 5-50 mM of the imidazole containing molecules histidine, or histamine in buffer to compete out the metal ion. In the case of anosmin-1 10 mM EDTA was required during the dialysis process until imidazole gradually reached a nadir level and finally dialysed into PBS. The procedures established here are likely to be useful during dialysis and scavenging of any contaminating metal ion particularly when using IMAC for protein purification.

High efficiency PIWF1 generation was obtained using the above paradigms; however, the relatively poor yield of full-length PIWF4 and mutant proteins require further analysis. Firstly, from a structural point of view, the predicted amino acid sequence of PIWF4 is three times longer than PIWF1, and contains 4 additional N-glycosylation sites when compared to truncated PIWF1 protein. Secondly, PIWF4 contains 4 additional heparan sulphate binding sites, making the full-length protein more tightly cell membrane adherent, leading to a higher salt requirement for protein extraction. Furthermore, when cell membrane HSPG is saturated by secreted recombinant PIWF4, it is possible that protein expression becomes down regulated to maintain a constant balance between protein generation and degradation. An additional possibility is that PIWF4 is somehow internalised and degraded

intracellularly. The fact that PIWF4 was only detected on the cell surface but not in medium supports this possibility. Thus by analogy, newly synthesized Noggin protein has a cellular half-life of approximately 3.6 h and a proportion of cell surface Noggin appears to be internalised and degraded intracellularly (Paine-Saunders et al., 2002). In terms of mutant anosmin-1 generation using the present system, the disruption of the 3-dimensional structure caused by the C172R missense mutation could alter the efficiency of protein folding and secretory efficiency. Therefore, some approaches are worthy of additional consideration. Firstly, transfection of the desired cDNA and hygromycin-B resistant gene using a single construct might enable the generation of a more homogenous stable cell line, akin to the creation of a 'mono-clonal stable cell line'. Secondly, additional exogenous heparin might be added to the serum-free medium to dissociate more anosmin-1 from cell surface thereby reducing potential degradation. Finally, a modified single step IMAC procedure, using iminodiacetic acid (IDA) chelating Sepharose instead of Ni-NTA agarose, has been reported for protein purification from divalent ion containing medium (Lehr et al., 2000), providing an alternative direct approach for anosmin-1 purification from conditioned serum-free medium.

### **3.6 Conclusions**

The present experimental approaches have demonstrated the efficiency, reliability and convenience of using a *Drosophila* S2 cell expression system followed by one-step purification using Ni-NTA affinity chromatography, for successful recombinant anosmin-1 generation. The generation of a stable S2 cell line for recombinant anosmin-1 production was optimal when using a 700 µg/ml hygromycin-B concentration during the selection procedure. Ni-NTA affinity chromatography proved ideal for purification of 6His tagged anosmin-1 from salt extract using a single step. Elimination of metal ion contamination during the dialysis process after IMAC protein purification was mandatory. The greatest protein yield was obtained with PIWF1, while lower yields for PIWF4 and their mutants. The quantity of PIWF1 enabled the generation of a polyclonal antibody against anosmin-1 (AIWF1). Furthermore, a HS competitive assay using PIWF1 and PIWF4 stable cell line

confirmed the dominant role of HSPG in anosmin-1 association onto S2 cell surface. Successful generation of purified recombinant anosmin-1 proved essential for subsequent function and structure analysis.

## Chapter 4

### The binding affinity of anosmin-1 to heparan sulphate

#### 4.1 Introduction

The roles of HS in physiological and pathological processes are determined by HS binding to an extremely broad range of soluble and insoluble molecules (Princivalle and de Agostini, 2002; Sasisekharan et al., 2002). Anosmin-1 appears to be one such interactant, both as a consequence of its predicted amino acid sequence and from previous *in vivo/in vitro* studies. There are five predicted HS-binding sequence motifs identified within or among four FnIII repeats (Robertson et al., 2001), and this has formed the rationale for: 1) The use of a heparin-Sepharose column for anosmin-1 purification; 2) The use of heparin/heparinase to dissociate anosmin-1 protein from transfected CHO cell surfaces (Soussi-Yanicostas et al., 1996). In addition, a HS competitive assay using a transient S2 cell transfection and stable S2 cell line (Chapter 2 and 3) demonstrated that anosmin-1 could also be detached from the transfected S2 cell surface by addition of HS. Furthermore, in an anosmin-1 cell adhesion assay, heparin at a 30  $\mu\text{g/ml}$  concentration, and heparinase (1 unit/ml) were able to inhibit anosmin-1 induced cell adhesion by approximately 50% (Robertson et al., 2001). Perhaps of more relevance, a recent gene locus screen in an anosmin-1 overexpressing transgenic *C.elegans* model has demonstrated that the enzymes required for normal HS synthesis (6-O-sulphotransferase and C5 epimerase) are essential for the anosmin-1 induced phenotype (Bulow et al., 2002). The latter observations represent the first *in vivo* confirmation of HS involvement in the action of anosmin-1.

However, direct binding of anosmin-1 to HS has not previously been systematically investigated. Hitherto, there have been no attempts to quantify the dose-dependency of HS binding to anosmin-1, nor to quantify the affinity of this interaction. The importance of individual fibronectin type III domains in this interaction has not been systematically assessed, nor indeed whether the cysteine-rich N-terminus and WAP domain regulate HS binding affinity through tertiary structure formation.

Although the WAP motif has been predicted not to be directly involved in HS-binding, it is still unknown whether the missense C172R mutation that disrupts the highly conserved disulphide bridge can affect binding affinity to HS indirectly through alteration in tertiary structure of the whole protein.

Conventionally, biomolecular interactions are studied using techniques such as immunoassays (ELISA or RIA), equilibrium dialysis, affinity chromatography and spectroscopy. Chemically similar molecules can be detected by their biospecificity for an immobilized molecule. These biomolecular interactions can also be directly monitored using so-called evanescent field sensors, the most frequently used such technique being surface plasmon resonance (SPR). SPR gives two main advantages over traditional techniques: the binding events are monitored in real-time and it is not necessary to label the interacting biomolecules. Thus, molecules can be studied in their native state to provide results that reflect *in vivo* activity. I therefore used a solid-phase immunosorbant assay and SPR to enable complementary quantitative measurements on anosmin-1-HS interaction.

## **4.2 Aims**

A solid phase immunosorbant assay was used to investigate whether purified anosmin-1 could bind to HS in a dose-dependent manner. SPR was used to measure the kinetic interaction of these two molecules in real-time.

## **4.3 Materials and Methods**

### **4.3.1 Solid phase enzyme-linked immunosorbant assay**

#### **4.3.1.1 Biotinylation of HS**

HS was dissolved in 0.1 M MES pH 5.6 (2-[N-morpholino] ethanesulphonic acid) (Sigma) at 2.5 mg/ml and then added to 2.5 mM EZ-link biotin hydrazine (Pierce) and 0.5 mM EDC [1-Ethyl-3-(3-Dimethylaminopropyl)carbodiimide hydrochloride] (Pierce), and mixed thoroughly by constant shaking at room temperature for 24 hours. The mixture was dialyzed against water to remove unreacted biotin and freeze-dried, re-dissolved in 200  $\mu$ l 0.3 M NaCl.

#### **4.3.1.2 Effects of varying the concentration of biotinylated HS on binding to a fixed concentration of protein**

Immunlon 4HBX plates containing 96-well microtitre wells (Thermo Labsystems/Thermo life science) were coated with 0.1 µg PIWF1, PIWF4, mPIWF1<sup>172</sup> and mPIWF4<sup>172</sup> in 100 µl PBS respectively, and incubated overnight at 4°C. Control wells were coated with 0.1 µg BSA and 2 µg purified rabbit apoE (kindly provided by Prof. Jim Owen). Each well was rinsed with 3×100 µl wash buffer (50 mM Tris, 150 mM NaCl, and 0.05% Tween-20, pH 7.6). The wells were then incubated with 100 µl 1% bovine serum albumin in PBS to block the remaining protein binding sites for 1 h at 37°C. Each well was rinsed with 3×100 µl wash buffer. Biotin-conjugated HS was successively diluted in 1 in 4 with PBS and 100 µl added into each well, followed by incubation at 4°C for 18 h. The wells were then rinsed with 3×100 µl wash buffer, and 100 µl alkaline phosphatase-conjugated avidin (1 µg/ml) added, followed by incubation for 1 h at 37°C. Wells were then rinsed thoroughly with 4×100 µl wash buffer, followed by incubation with 100 µl of 0.25 mg/ml alkaline phosphatase substrate (sigma 104 phosphatase substrate) (Sigma) at 37°C. Absorbance at 405 nm was read at 5, 10, 15, 20 min time intervals.

#### **4.3.1.3 Effects of varying protein concentration on binding to a fixed biotinylated HS**

Microtitre wells were coated with 0.2 nM, 1 nM, 5 nM, 25 nM, 50 nM and 100 nM each of PIWF4, mPIWF4<sup>172</sup>, PIWF1, mPIWF1<sup>172</sup> and BSA and then incubated with 12.5 µg/ml (1 in 200 dilution) biotinylated HS, according to the above method.

#### **4.3.1.4 *In vitro* HS competitive assay**

To confirm the specificity of HS binding to the protein, unlabeled HS at 0, 1, 10, 100 µg/ml concentrations were mixed with 12.5 µg/ml biotinylated HS into the wells coated by 0.1 µg PIWF4 using the same protocol as above.

### **4.3.2 SPR assay**

#### **4.3.2.1 The principle of SPR**

SPR is an optical-electrical phenomenon based on the interaction of light with a metal surface. Under certain conditions, the energy carried by photons of light is transferred to packets of electrons, called plasmons, on a metal's sensor surface. This surface is generally made of gold.

The coupling of light with a metal surface results in the creation of a plasmon, a group of electrons that behave like a single electrical entity. The plasmon, in turn, generates an electrical field that extends about 100 nanometers above and below the metal surface. The interaction between the plasmon's electrical field and the matter within the field determines the resonance wavelength. Any change in the composition of the matter within the range of the plasmon's field causes a change in the wavelength of light that resonates with the plasmon. The magnitude of the change in resonance wavelength, the SPR angle shift, is directly and linearly proportional to the change of the amount of bound macromolecules. Scanning mirror biosensors thus can measure the SPR angle shift in millidegrees as a response unit (RU), to quantify the binding of macromolecules to the sensor surface (Figure 4.1). A change of 120 millidegrees represents a change in surface protein coverage of approximately  $1 \text{ ng/mm}^2$ , or in bulk refractive index of approximately  $10^{-3}$ .

#### **4.3.2.2 The SPR sensor surface and analytical application**

In SPR biosensors, the gold surfaces can be coated with a layer of biomolecules that are capable of binding with a selected analyte target. The binding molecules may be antibodies, DNA probes, enzymes or other reagents that react exclusively with their analyte molecules. However, in general, immobilization of biomolecules directly on the metal surface is not suitable for biosensors because it leads to low coverage of biomolecules with reduced activity and non-specific adsorption. Alternatively, various sensor surface chemistries can provide appropriate chemical properties for stable and defined ligand binding. One approach is to use a streptavidin monolayer immobilized onto a gold film that can be further functionalised with biotinylated biomolecules. The gold surface may also be coated by spreading out liposomes to make hydrophobic character of the surface. Another approach is to form a self-assembled monolayer of

SPR sensors (e.g., Biacore) are used to study binding of a ligand to a receptor. For example, groups of antibodies are immobilized on a surface of a substrate (e.g., glass) and interact with a ligand such as a protein, another antibody or carbohydrate (e.g., a sugar) which is labeled with a fluorescent group such as FITC. Another possibility is to immobilize a ligand of carbohydrate (e.g., a sugar) and interact with an antibody or another protein.

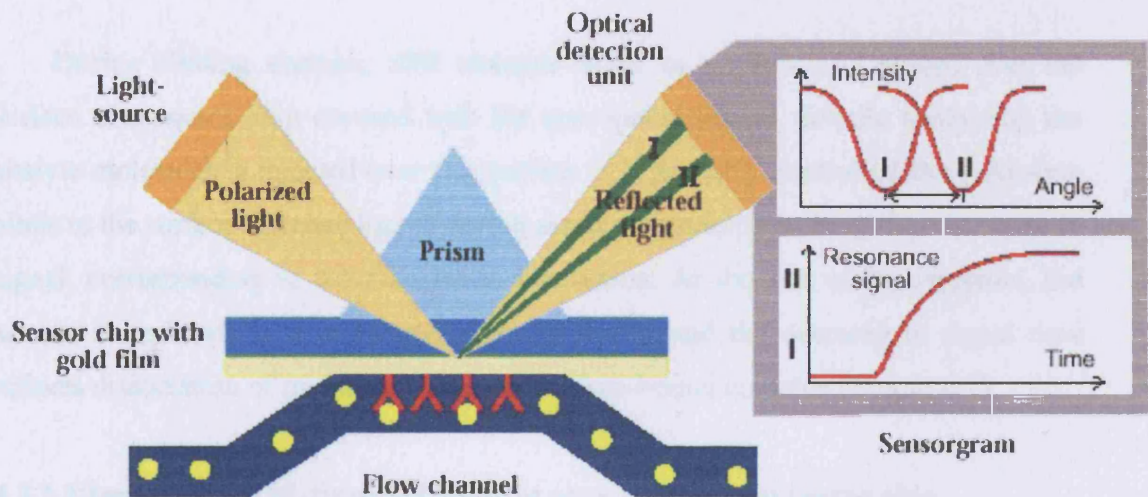


Figure 4.1 The schematic mechanism of SPR. Fixed wavelength light, in a fan-shaped form, is directed at the sensor surface and biomolecular binding events are detected as changes in the particular angle where SPR creates extinction of light. This change is measured continuously to form a sensorgram, which provides a complete record of the progress of association or dissociation of the interactants.



thiol molecules (e.g. 16-thiohexadecanol, alkanethiols) used to enable covalent binding of a dextran layer. The carboxylic groups of dextran can be activated by means of N-hydroxy succinimide (NHS) and ethyl-methyl-diaminopropyl-carbodiimide (EDC), making it possible to couple a ligand with a functional group such as  $-NH_2$ . Another possibility is the immobilization of nitrilotriacetic acid (NTA) onto sensor surface, followed by Ni-chelation to capture polyhistidine tagged ligands.

During binding analysis, SPR changes occur as a solution is passed over the surface of a sensor chip covered with the appropriate ligand. Sample containing the analyte molecules is injected over this surface in a precisely controlled flow. Analyte binds to the surface-attached ligand during sample injection, resulting in an increase in signal, corresponding to the association interaction. At the end of the injection, the sample is replaced by a continuous flow of buffer and the decrease in signal now reflects dissociation of interactant from the surface-bound complex (Figure 4.2).

#### **4.3.2.3 Immobilising biotinylated heparin onto streptavidin sensor chip**

A Biacore 3000 surface plasmon response-based biosensor (BIAcore AB) was then used to measure binding parameters between anosmin-1 (analyte) and immobilized heparin ligand. A streptavidin sensor chip (Biosensor AB, Uppsala, Sweden) was pretreated with 5  $\mu$ l injection of 50 mM NaOH in 1M NaCl to remove non-specifically bound contaminants. 5  $\mu$ l biotinylated heparin (1  $\mu$ g/ml) from porcine intestinal mucosa (CalBiochem, Cat# 375054) in HEPES-buffered saline (10 mM HEPES, 150 mM NaCl, 3.4 mM EDTA, pH 7.4, containing 0.005%(v/v) P-20) was injected at a flow rate of 5  $\mu$ l/min, giving low levels of immobilized ligand (200 resonance units) to minimize mass transfer effects. Three flow cells were coupled and one flow cell contained a blank sensor chip to serve as a reference surface. The coupling was monitored by injection of purified rabbit apoE at 0.5 and 1  $\mu$ M since apoE has been shown to be a heparin-binding molecule; 2% BSA was run as a negative control and 2 M NaCl was injected to remove bound apoE.

#### **4.3.2.4 SPR kinetic measurement of the heparin interaction with anosmin-1**

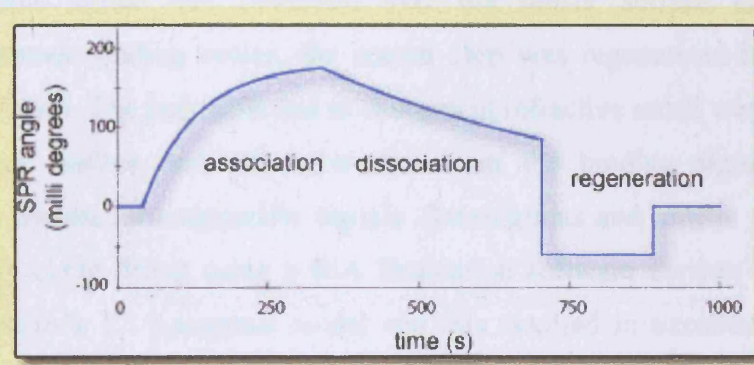


Figure 4.2 Typical SPR-plot of the specific interaction of biomolecules to a single spot of the biochip surface. After equilibration with the buffer the sample is injected. A binding of the biomolecule to the surface is the result (association phase). After removing the sample, the bound biomolecule will dissociate slowly (dissociation phase). The sensor chip can be regenerated by injection of a solution to get rid of the specific interaction (regeneration phase). The biochip can be reused for a new binding event, in the case the non-specific interaction is still relatively low (the baseline should be stable).

Purified wild type and mutated anosmin-1, typically at six different concentrations (15  $\mu$ l, in HEPES-buffered saline), were injected at a flow rate of 5  $\mu$ l/min to ensure recovery of data prior to curve fitting: 25, 37.5, 50, 75, 100, 200 nM for truncated anosmin-1 (PIWF1 and mPIWF1<sup>172</sup>) and 12.5, 25, 37.5, 50, 75, 100 nM for full-length anosmin-1 (PIWF4 and mPIWF4<sup>172</sup>). Each experiment was performed from the lowest to the highest concentration, followed by injection in the reverse order. This procedure was designed to confirm the specificity of the molecular interaction and the complete recovery of binding property of ligand on the sensor surface. The same buffer was circulated over the sensor surface to facilitate dissociation. Between binding cycles, the coated chip was regenerated by a 10  $\mu$ l injection of 2 M NaCl. The bulk shift due to changes in refractive index was measured using a reference surface and was subtracted from the binding signal at each concentration to correct for nonspecific signals. Sensorgrams and kinetic parameters were analysed by curve fitting using a BIA Evaluation software version 3.0. Curve fitting conformed to a 1:1 Langmuir model and this resulted in excellent fits with random small residuals.

#### 4.4 Results

The sensitivity and specificity of the solid phase enzyme-linked immunosorbant assay was initially evaluated using increasing concentrations of HS coupled to the 0.1  $\mu$ g protein-coated plates. ApoE and bovine serum albumin (BSA) were used as positive and negative controls respectively. As shown in Figure 4.3 (a), HS did not bind to BSA-coated wells, whereas apoE binding to biotinylated HS was increased dramatically with the addition of > 3.1  $\mu$ g/ml biotinylated HS. Subsequently, the HS interaction with immobilized fixed concentrations of anosmin-1 (at 0.1  $\mu$ g) was investigated. HS binding to all tested anosmin-1 variants was observed in a concentration-dependent manner; higher affinity binding was evident for full-length PIWF4 and PIWF4<sup>172</sup> (Figure 4.3 (b)). Binding sensitivity was high as a minimum tested HS concentration < 0.2  $\mu$ g/ml resulted in the detectable HS/anosmin-1 binding. To further confirm the specificity of HS/anosmin-1 interaction, the unlabeled HS was co-cultured with biotinylated HS since it can competitively attenuate labelled

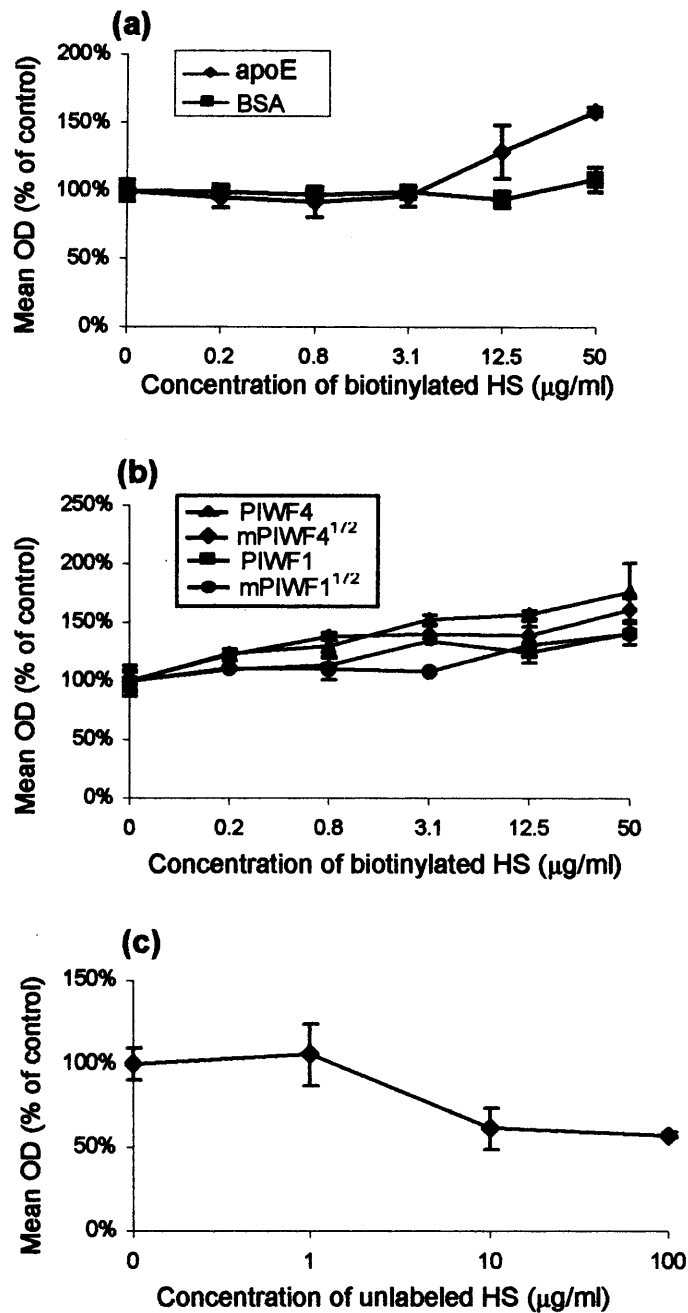


Figure 4.3 Investigation of immunosorbent method for protein-HS binding affinity assay. 0.1  $\mu\text{g}$  apoE and BSA (a) and 0.1  $\mu\text{g}$  wild-type, mutated PIWF1 and PIWF4 (b) were coated respectively onto microtiter wells. Soluble biotinylated HS at increasing concentrations were added and incubated at 4°C. Alkaline phosphatase-conjugated avidin and an alkaline phosphatase substrate were added, and the plates were incubated at 37°C. Absorbance was measured at 405nm. (c) Competitive inhibition assay using unlabeled biotinylated HS binding to 0.1  $\mu\text{g}$  PIWF4. 0, 1, 10, 100  $\mu\text{g/ml}$  HS without biotin-conjugate were co-incubated with a constant concentration of biotinylated HS (12.5  $\mu\text{g/ml}$ ) onto 0.1  $\mu\text{g}$  PIWF4 coated microtiter wells.

HS/anosmin-1 binding. Different concentrations of unlabeled HS were mixed with 12.5 µg/ml labelled HS and then added onto 0.1 µg PIWF4 coated wells. As expected, 10-100 µg/ml non-biotin labelled HS resulted in an about 50% attenuation of the HS-PIWF4 interaction (Figure 4.3 (c)). Taken together, these results confirm the sensitivity and specificity of the immunosorbant assay in anosmin-1-HS interaction, validating this model for subsequent quantitative analysis.

Increasing concentrations of purified anosmin-1 were then coated onto microtitre wells, followed by the addition of a constant concentration of biotinylated HS (12.5 µg/ml) as soluble component. As shown in Figure 4.4, significant binding to BSA coated wells was not observed. However, HS bound effectively in a dose-dependent manner to the wells coated with all the anosmin-1 in the 5 nM to 100 nM concentration range. These data suggested high affinity binding of anosmin-1 to HS. Both wild type (PIWF4) and mutated (mPIWF4<sup>172</sup>) full-length anosmin-1 exhibited higher HS binding affinity than their truncated counterparts, an observation consistent with previous experimental results. Therefore increasing numbers of FnIII domains lead to greater HS binding.

The kinetic measurements of the binding affinity between anosmin-1's variants and heparin were then carried out using SPR technology, which enables ligand/analyte interaction measurements in real-time. Representative sensorgrams for binding of truncated and full-length proteins to the immobilized heparin are shown in Figure 4.5. The initial rising portion of the binding curve represents association of injected proteins with immobilized heparin, the final portion of the curve corresponding to dissociation of bound proteins from the sensor chip surface. The relatively steep association phase with shallow dissociation phase in all four recombinant anosmin-1 indicated their high heparin-binding affinity. The dissociation constant ( $K_d$ ) was calculated as the ratio of the rate of dissociation constant ( $k_{off}$ ) to the rate of association constant ( $k_{on}$ ) (Table 4.1).  $K_d$  values were all less than 10 nM, indicating high heparin-binding affinity for the full range of proteins tested. The truncated PIWF1 protein, containing a single 1<sup>st</sup> FnIII domain, had a lower binding affinity ( $K_d$ , 4.31±0.99 nM)

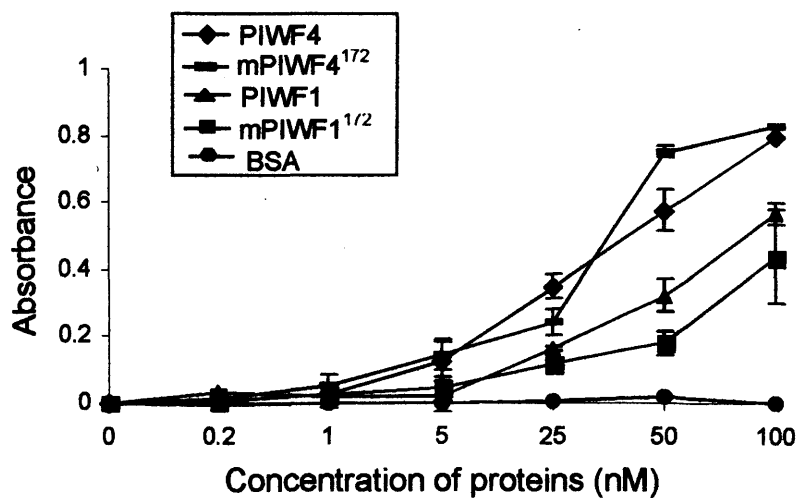


Figure 4.4 Immunosorbant assay analysis of anosmin-1-HS binding. Immobilized proteins at the indicated concentrations were coated onto microtiter wells and incubated with soluble 12.5  $\mu\text{g/ml}$  biotinylated HS. Alkaline phosphatase-conjugated avidin and an alkaline phosphatase substrate were added and absorbance was measured at 405 nm.



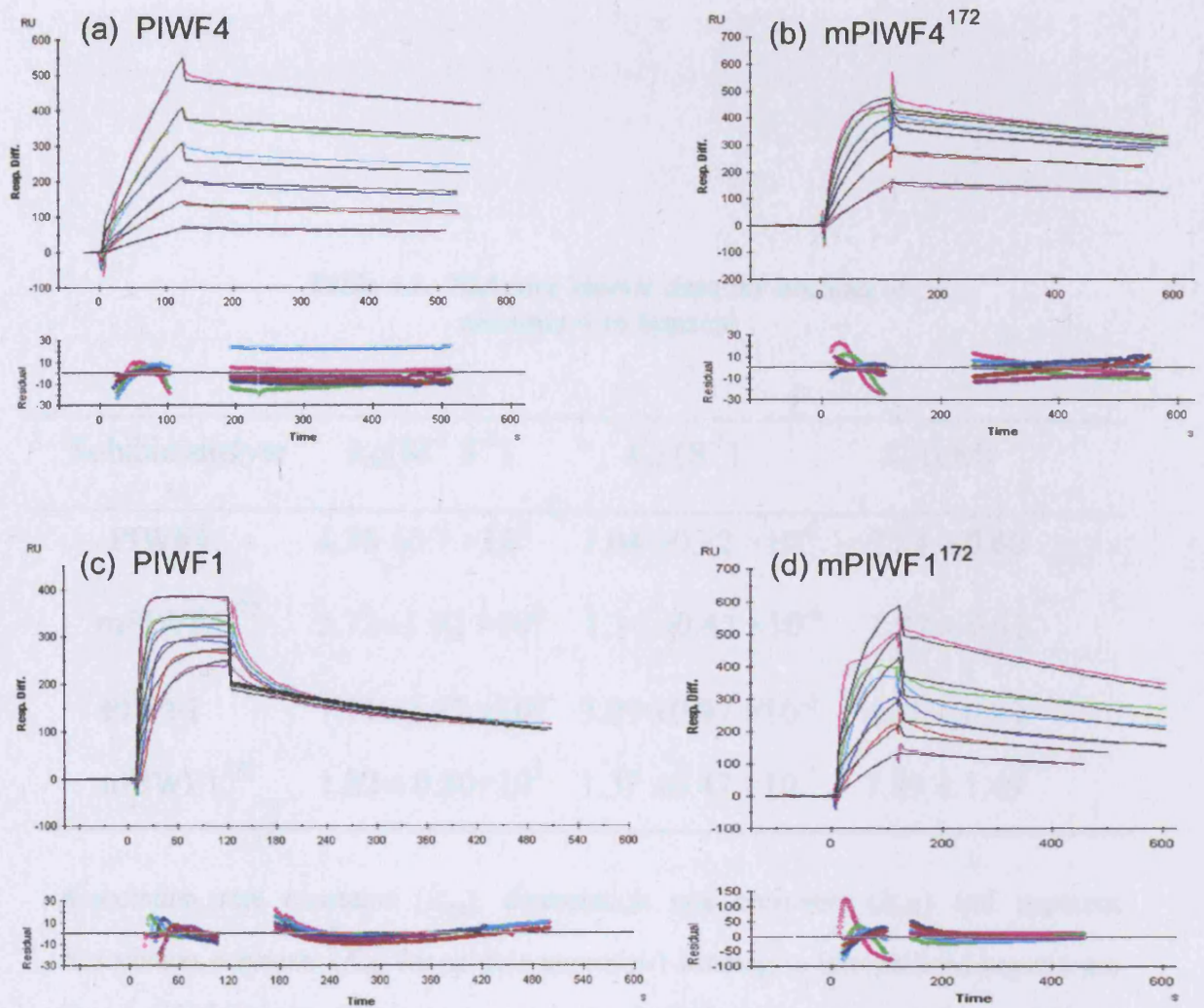


Figure 4.5 BIAcore analysis of anosmin-1 interaction with heparin. Representative sensorgrams are shown for the interaction of immobilized heparin with soluble PIWF4 (a), mPIWF4<sup>172</sup> (b), PIWF1 (c) and mPIWF1<sup>172</sup> (d). Six different concentrations of analyte were used for these analyses: 25, 37.5, 50, 75, 100, 200 nM for PIWF1 and mPIWF1<sup>172</sup>, 12.5, 25, 37.5, 50, 75, 100 nM for PIWF4 and mPIWF4<sup>172</sup> (color lines, upper panel) The top sensorgram line in each graph represents the highest concentration of proteins, and the bottom line the lowest concentration. Residual plot showed the difference between measured and calculated responses (bottom panel in (a) - (d)). The artifact fragment in association curve was removed from PIWF4 sensorgram.

**Table 4.1. BIAcore kinetic data for binding of anosmin-1 to heparin**

Soluble analyte	$k_{\text{on}}(\text{M}^{-1} \text{S}^{-1})$	$k_{\text{off}}(\text{S}^{-1})$	$K_{\text{d}}(\text{nM})$
PIWF4	$4.36 \pm 0.7 \times 10^5$	$1.04 \pm 0.12 \times 10^{-3}$	$2.51 \pm 0.60$
mPIWF4 <sup>172</sup>	$5.72 \pm 1.92 \times 10^5$	$1.14 \pm 0.47 \times 10^{-3}$	$1.97 \pm 0.42$
PIWF1	$7.71 \pm 3.57 \times 10^5$	$3.09 \pm 0.97 \times 10^{-3}$	$4.31 \pm 0.99$
mPIWF1 <sup>172</sup>	$1.82 \pm 0.80 \times 10^5$	$1.37 \pm 0.47 \times 10^{-3}$	$7.89 \pm 1.49$

Association rate constants ( $k_{\text{on}}$ ), dissociation rate constants ( $k_{\text{off}}$ ) and apparent dissociation constants ( $K_{\text{d}}$ ) for soluble anosmin-1 binding to immobilized heparin are shown. Values are shown as mean  $\pm$  standard deviation derived from triplicate measurements.



than full-length protein ( $K_d$ ,  $2.51 \pm 0.6$  nM). These results appear to be consistent with the previous data obtained by immunoabsorbant assay. The WAP mutation increased the PIWF1  $K_d$  value, with less impact on full length PIWF4; thus the C172R substitution has an effect only on the heparin binding kinetics of truncated protein.

#### 4.5 Discussion

The affinity and specificity of HS-protein binding are determined by its polysaccharide sequence, the 2-O, 3-O and 6-O monosaccharide sulphated residues, and the peptide sequence of protein ligand (Esko and Lindahl, 2001; Merry and Wilson, 2002). More than 100 proteins are known to interact with HS *via* three specific mechanisms: 1) ionic interaction based on the XBBXBX and XBBBXXBX (where B represents basic residues, including lysine, arginine and histidine, X represents a hydrophobic residue) consensus sequences, 2) hydrophobic interaction and 3) hydrogen bond formation. In lipoprotein metabolism for example, HS plays a crucial role in complex formation of apoE and lipoprotein *via* certain polysaccharide residues of IdoA(2-OSO<sub>3</sub>)-GlcNS(6-OSO<sub>3</sub>). The N-sulpho groups on the GlcN residues of HS and O-sulpho groups contribute to high binding affinity (Libeu et al., 2001). Furthermore, the consecutive alignment of basic amino acid in apoE containing Arg-142, Lys-143, Arg-145, Lys-146, and Arg-147 has been shown to be necessary for its high HS-binding. The Lys-146 participates in an ionic interaction with the heparin fragment, whereas Lys-143 is implicated in hydrogen bond formation.

In a previous study, all anosmin-1 analogues could be dissociated from S2 cell surface by the serum-free medium containing additional 350 mM NaCl (Chapter 2 and 3); moreover 2 M NaCl also eluted bound anosmin-1 from an immobilized heparin sensor chip surface, indicating that charged residues are crucially involved in the anosmin-1-HS interaction. The large positively charged surfaces of the FnIII domains are likely to participate in an ionic interaction with the negatively charged HS, whereas the WAP domain is unlikely to be involved due to its higher acidic residue components leading to a large negative charged surface. This prediction was confirmed both in a cell-based measurement using a S2 cell HS competition assay

(Chapter 2 and 3) and in a solid-phase analysis using an immunosorbant assay and surface plasmon resonance techniques (Figure 4.4 and Table 4.1). The protein with greater numbers of FnIII repeats exerts higher cell-surface association *via* HSPG interaction and great HS-binding affinity, whereas the WAP domain mutant does not alter the HS-binding characteristics shared by PIWF4 and mPIWF4<sup>172</sup>.

Dose-dependent, high nanomolar affinity binding was demonstrated between anosmin-1 and HS. The PIWF1-HS binding affinity is only slightly lower than the binding affinity of the full-length PIWF4 ( $4.31 \pm 0.99$  nM and  $2.51 \pm 0.60$  nM respectively), indicating that the 1<sup>st</sup> FnIII domain constitutes the main HS binding module. These results are consistent with previous studies by Soussi-Yanicostas *et al.* who previously reported that a synthetic 32 amino acid peptide derived from the 1<sup>st</sup> FnIII domain induced heparin associated cell adhesion (Soussi-Yanicostas *et al.*, 1998), and by Bulow *et al* who observed that the introduction of a missense mutation (corresponding to the human N267K substitution) in the 1<sup>st</sup> FnIII of the *C. elegans* Kal-1 abolished heparin-dependent cell binding and axon branching activity (Bulow *et al.*, 2002). In addition, our data show that a structural alteration in the WAP domain interferes with the FnIII domain-HS interaction when incorporated in a truncated (PIWF1) but not full length (PIWF4) anosmin-1, suggesting that the structural alteration of the WAP domain probably influences the charged residue distribution in the 1<sup>st</sup> FnIII domain, especially when not followed by additional FnIII repeats. Thus, the impact of a disrupted WAP domain on the anosmin-1-HS interaction is dependent on the number of FNIII repeats present, with less interference associated with increasing FNIII repeats. One explanation for this observation could be that if the WAP and 1<sup>st</sup> FnIII domains form a stereochemically compacted structure, whereas an elongated conformation is assumed by the full-length protein. To further unravel these observations will require further studies using experimentally based molecular modeling coupled with higher resolution structural analysis.

The specific polysaccharide sequences and the extent of monosaccharide sulphation of HS required for anosmin-1 binding remains to be elucidated. Two HS-

binding sites have been identified in fibronectin: the N-terminus HEPI with weak affinity of a dissociation constant between  $10^{-6}$  to  $10^{-5}$  M, and the C-terminal HEPII with a higher  $10^{-8}$  to  $10^{-7}$  M affinity constant. The HEPII site is located in the FnIII repeats of fibronectin, the homologous domain present in anosmin-1. Thus, its high HS-binding affinity is consistent with the kinetic  $K_d$  value (2 nM) shown in anosmin-1's FnIII domain. The sequence of HS for HEPII site was identified as the GlcA-GlcNSO<sub>3</sub>-[IdoA(±2S)-GlcNSO<sub>3</sub>]<sub>5,6</sub>-IdoA-GlcNAc (Walker and Gallagher, 1996). This may also provide a useful clue for identifying the specific HS component for anosmin-1 binding.

The present results provide the first biochemical evidence that anosmin-1 binds to HS in a dose-dependent manner with high nanomolar binding affinity, suggesting that the interaction between these two macromolecules is likely to be functionally relevant. The main action of HS on protein function is thought to be mediated through modulation of free protein ligand concentration, modulation of cell-cell/cell-ECM adhesion, and the regulation of ligand dimerization and the possible stabilization of ligand-receptor complexes. A detailed mechanism of HS involvement in anosmin-1 function can be proposed based on the known interaction of HS with other proteins. Firstly, given the high binding affinity of HS to anosmin-1, one can speculate that HS modulates the gradient concentration of anosmin-1 by regulating the diffusion from either cell surface or extracellular matrix; a similar mechanism has been proposed in the Noggin and BMP system in which HS retains BMP on the cell surface and establishes an activity gradient (Paine-Saunders et al., 2002). Secondly, the interaction with HS perhaps induces a structural rearrangement of anosmin-1 and subsequently stabilises complex formation between the WAP domain and a putative extracellular serine protease, resulting in the increase of protease inhibitory activity. The role of HS in the anticoagulation system reinforces this prediction. Upon binding to the specific HS pentasaccharide sequence on the surface of endothelial cells, anti-thrombin III subsequently forms an inhibitory protein-protein complex by inducing a conformational change, leading to 1000-fold increase of inhibitory activity on serine protease Xa and IIa (Shriver et al., 2000a; Shriver et al., 2000b). Furthermore, in a

molecular model of apoE, the shallow groove on the apoE molecular surface can be widened by the interaction with 2-O-sulphation of IdoA5 in HS (Libeu et al., 2001). This observation raises the possibility that HS may induce a conformational alteration in anosmin-1. Finally, anosmin-1 might interact with an unknown receptor (perhaps FGFR1) through HS, followed by ligand and receptor dimerization as occurs with the FGF2-FGFR-HS system. HS facilitates specific binding of FGF2 to FGFR and serves as a platform for FGF2, FGFR oligomerization and dimerization, followed by transphosphorylation of specific tyrosine residues which lead to cell proliferation and migration. The absence of HS reduces FGF2-induced cell proliferation significantly due to loss of contact between two FGF2 molecules and FGFR (Kwan et al., 2001). It therefore can be proposed that anosmin-1 may 1) stabilize FGFR1/FGF2/HS complex formation, 2) recruit FGF2/HS to their high-affinity receptor and 3) even determine HS specificity for cell-specific intracellular response to extracellular FGF2/FGFR1 signal.

#### **4.6 Conclusions**

Consistent with cell-based HS competitive assay (Chapter 2 and 3), an immunosorbant assay and SPR analysis have shown the interaction between anosmin-1 and HS: 1) their binding is in a dose-dependent manner, 2) quantification of kinetic interaction was at 2 nM ( $K_d$ ). In addition, the FnIII repeats, particularly the first one, has been identified as a dominant HS binding site.

In addition to the HS/FnIII domain interaction, prior to this study the identity of ligands interacting with the N-terminal CR and WAP domains was still unknown. Members of the serine protease family might represent putative candidates. The identification of a serine protease interactant, together with the investigation on their functional interaction with the anosmin-1/HS complex is addressed in the next chapter.

## Chapter 5

### **Interaction between anosmin-1, HS and urokinase-type plasminogen activator in prostate carcinoma PC-3 cell proliferation**

#### **5.1 Introduction**

The interaction between the FnIII domains of anosmin-1 and HS was previously shown to occur at nanomolar affinity with  $K_d$  values  $< 10$  nM. An outstanding question remains the identity of potential ligands that might interact with anosmin-1's N-terminal CR and WAP domains as well as the functional relevance of such interactants.

The WAP domain of anosmin-1 has been hypothesized to function as a serine protease inhibitor based on its homology with other WAP family members. Thus elafin and SLPI are well-defined serine protease inhibitors whose substrates are elastase, chymotrypsin and trypsin respectively. A highly variable V region and a conserved methionine residue in the P<sub>1</sub>' position have been identified as the active binding centre for complex formation with elafin and chymotrypsin (Grutter et al., 1988; Tsunemi et al., 1996). Based on these data, it was hypothesized that anosmin-1 might regulate cell processes *via* the interaction of its WAP domain with an as yet unidentified serine protease. In this respect, it is pertinent that several trypsin-like serine proteases are expressed in the developing OB including the urokinase plasminogen activator (uPA), tissue plasminogen activator (tPA) and thrombin (Dihanich et al., 1991; Dent et al., 1993). Of these, in the olfactory bulb, uPA expression is predominantly within the large mitral and related tufted cells lying more superficially in the external plexiform layer as early as E14.5, a time at which the HS proteoglycan N-syndecan, is expressed by migrating olfactory and GnRH neurons (Dent et al., 1993). Early expression of uPA has also been observed in the spinal cord, central neurons (by embryonic day 12.5) and epithelial cells of the kidney (Sumi et al., 1992), where anosmin-1 might also be biologically active. uPA has been reported to influence tissue remodelling, synaptogenesis, neurite outgrowth and cell proliferation

(Hantai et al., 1989). A proteolytic cascade involving uPA may underpin its potential role in tissue remodelling and angiogenesis through the primary degradation of ECM and secondarily through the activation of transforming growth factor- $\beta$  or basic FGF release from extracellular matrix (Pepper, 2001). In addition, uPA expression has been reported to correlate with synapse elimination in developing skeletal muscle (Hantai et al., 1989). A critical role of uPA in mediating neural synaptic plasticity has also been supported by evidence from transgenic mice overexpressing uPA, which resulted in reduction in spatial olfactory capability as well as taste-aversion (Meiri et al., 1994). The molecular mechanism by which uPA exerts its biological function appears to be either through the pericellular conversion of the zymogen plasminogen to plasmin, which in turn catalyses the activation of the pro-matrix metalloproteinases (MMPs), or *via* a proteolysis-independent mechanism whereby secreted uPA binds with its high affinity cell surface receptor (uPAR) and other classical signalling receptors to activate related signalling pathways (Pittman et al., 1989; Blasi and Carmeliet, 2002). uPA was thus considered a putative serine protease candidate ligand for the N-terminus of anosmin-1.

uPA is secreted as an inactive single-chain protein (known as pro-uPA or sc-uPA) activated into a two-chain uPA molecule following a single proteolytic event. The overall folding topology of the uPA and pro-uPA molecules can be divided into three functionally independent regions: an amino-terminal epidermal growth factor (EGF)-like domain, a kringle domain and a carboxy-terminal catalytic domain (known as low-molecular-weight uPA). The first two domains comprise the amino-terminal A-chain fragment (ATF). The receptor (uPAR)-binding module resides in the growth factor domain, in residues 21-32 (Appella et al., 1987). In addition, both the kringle and proteolytic domains are recognised by the I domain of the  $\alpha_M$  subunit within integrin  $\alpha_M\beta_2$ , which is distinct from the uPAR binding site. The trimolecular complex of uPA, uPAR and integrin, in which uPA binds to both receptors, appears to occur on the cell surface and mediate its unique functional properties including cell adhesion and migration (Pluskota et al., 2003).

uPAR is a three-domain (D1, D2 and D3) GPI-anchored protein with high affinity for uPA, pro-uPA and the ATF (Ploug and Ellis, 1994). Binding of uPA to cell-surface-located uPAR leads to activation of cell signalling. A common finding in uPA signalling resulting in chemotaxis, is the activation of intracellular tyrosine kinases (Src, Hck, FAK) and serine/threonine kinases such as ERK/MAPK. uPA also causes membrane translocation of Raf, Src and Fak, and of the Rho family GTPase Rac, and nuclear localization of ERK/MAPK1/2 (Nguyen et al., 2000; Degryse et al., 2001; Kjoller and Hall, 2001). The functional importance of these interactions has been shown in studies of uPA/uPAR dependent cell proliferation and cytoskeletal reorganization. uPAR-dependent tumour growth involved both integrin and ERK/MAPK signalling, as high levels of uPAR activated the ERK/MAPK1/2 pathway and suppressed growth-inhibiting p38 MAPK (Aguirre Ghiso et al., 1999). Furthermore, treatment of cells with uPA causes uPAR- and integrin-dependent cell-shape changes and cytoskeletal reorganization with membrane ruffling, formation of actin rings and lamellipodia, and localization of integrins, uPAR and Src to the lamellipodia (Degryse et al., 1999). uPA is, however, able to stimulate vascular smooth muscle growth in the absence of uPAR *in vivo* (Carmeliet et al., 1998).

Therefore, I hypothesized that the molecular mechanism for the biological function of anosmin-1 might be *via* an interplay between two cross-talk molecules--HS and uPA. I further hypothesized that the N-terminal anosmin-1 (WAP domain) might modulate the catalytic activity of uPA and its signalling pathway, whereas HS, the FnIII domain ligand, might determine cell surface localisation of the anosmin-1/uPA complex. To test these hypotheses, it was first necessary to determine whether anosmin-1 could regulate uPA catalytic activity *in vitro*. Secondly, a human PC-3 prostatic carcinoma cell line was thus employed as a model to investigate the functional relevance of an anosmin-1/HS/uPA interaction. I tentatively chose the PC-3 cell line based on a number of characteristics: first, PC-3 cell growth can be inhibited by a novel member of the WAP protein family, PS20, which shares a 30% amino acid similarity with the WAP domain of anosmin-1 (Larsen et al., 1998). Second, the role of uPA/uPAR in tumorigenesis has been well established, processes known to be

modulated by HS. Finally, PC-3 cells have been shown to produce HS either onto the cell surface or into the cultured medium (Kosir and Quinn, 1995), and to express high-level uPA and uPAR (Lyon et al., 1995; Forbes et al., 2004).

## **5.2 Aims**

- (1) To investigate the effect of anosmin-1 on uPA and thrombin amidolytic activity using specific chromogenic substrates.
- (2) To investigate the functional consequence of an anosmin-1/uPA/HS interaction; actions of anosmin-1 on the PC-3 cell proliferation were examined in the presence and absence of exogenous HS, heparinase III and anti-uPA antibody.
- (3) To further characterize WAP domain function; WAP mutated proteins (mPIWF1<sup>172</sup>, PIWF4<sup>172</sup>) were investigated in the presence and absence of exogenous HS.
- (4) To identify whether anosmin-1 was either cell membrane associated or inside cells: immunocytochemistry was used with purified AIWF1 antibody.
- (5) To identify complex formation between anosmin-1 and uPA, co-immunoprecipitation was performed in PC-3 cell lysate and their direct binding was investigated by SPR.

## **5.3 Materials and Methods**

### **5.3.1 uPA and thrombin amidolytic activity assay**

uPA and thrombin activities were quantified in PBS containing 20 mM Tris·HCl, using the specific chromogenic substrate S2366 (Glu-Pro-Arg-pNA·HCl, pNA: p-Nitroaniline hydrochloride) (Enzyme Reach Laboratories) for thrombin and S2444 (Glu-Gly-Arg-pNA·HCl) (Chromogenix) for uPA. Cleavage of synthetic chromogenic substrate releases pNA (S2366 or S2444 → Peptide + pNA), which can be quantified by measuring an increase in absorbance at 405 nm. For the thrombin assay, the hirudin (NOVARTIS), a specific thrombin inhibitor, was first used to validate the system and to determine the optimal enzyme concentration. Hirudin in serial 1 in 2 dilutions (from 0.007 µg/ml to 1 µg/ml) was mixed with 0.8 nM thrombin and then loaded onto 96-well plate for 2 min incubation at 37°C. The reaction was initiated by addition of



substrate S2366 (0.42 mg/ml), and the absorbance was recorded every 1 min on a microtiter plate reader. For the preliminary uPA activity assay, 1 nM uPA was used and the hydrolysis reaction measured every 1 h. Triplicates of 50  $\mu$ l of anosmin-1 at varying concentrations were pre-incubated with 50  $\mu$ l of 0.8 nM thrombin and 1 nM human high molecular weight uPA (American Diagnostic Inc) in the absence and presence of 10  $\mu$ g/ml HS at 25°C for 2min or 15min incubation respectively. 50  $\mu$ l specific substrates were then added to start the reaction at 37°C and substrate hydrolysis was measured at 405 nm every 1 min for thrombin and every 1 h for uPA. Residue amidolytic activity of proteases was calculated as the ratio between the initial reaction velocity with anosmin-1 treatment and that of a control group without anosmin-1. To confirm the specificity of anosmin-1 on uPA amidolytic activity, a negative control was set up. First, purified GFP was used to replace anosmin-1 for the uPA interaction. Second, purified anosmin-1 was incubated with chromogenic substrate without addition of uPA.

### **5.3.2 Proliferation assays**

#### **5.3.2.1 Anosmin-1 on PC-3 cell proliferation**

PC-3 cells were seeded in a 100  $\mu$ l volume in 96-well flat bottom microtitre plates (Nunc, NY, USA) at  $5.0 \times 10^4$  cells/ml density in Coon's modified Ham's F12 medium (Sigma) containing 7% FBS, 100 U penicillin/ml, 100  $\mu$ g streptomycin/ml and 2 mM glutamine, and were allowed to adhere overnight. On the following day, the medium was removed and replaced with serum-free medium. After a 24 h period of serum starvation, cells were treated with set anosmin-1 concentrations in replicates of 5 (purified and freeze-dried recombinant anosmin-1 was dissolved in serum-free medium). Cells were cultured for 2 days at 37°C, with 5% CO<sub>2</sub> humidified incubation. At the end of the incubation period, cell proliferation was measured by the Cell Titer 96 AQueous non-radioactive cell proliferation assay using tetrazolium compounds (Promega, Southampton, UK) which measures the activity of the mitochondrial enzyme, succinyl dehydrogenase, expressed only in living cells (Mosmann, 1983). 20  $\mu$ l of the MTS/PMS solution was added directly to the each well and incubated for 1.5 h. Absorbance of optic density (OD) was measured at 492 nm using an ELISA plate

reader (Anthos ht III). Each experiment was performed several times ( $n > 2$ ). The culture without any treatment was used as negative control. Effects of different treatments were measured as percentage of absorbance compared to control group set to 100%. To prove that this assay directly correlates with cell proliferation, actual cell counting was also performed. After treatment with 10 nM PIWF1, PIWF4 and GFP proteins, cells were washed twice with PBS and trypsinized with 1×Trypsin EDTA. Trypsinized cells were thoroughly resuspended in PBS to avoid cell aggregation and checked under the microscope to ensure collection of all the cells. Intact cells, determined by trypan blue exclusion, were counted by hemocytometer as described in section 3.3.1.

#### **5.3.2.2 Function-blocking experiment**

Purified polyclonal anti-anosmin-1 (AIWF1) antibody and anti-uPA antibody at a 50 µg/ml concentration were added respectively into PC-3 cell culture with PIWF1 treatment. Non-specific rabbit antiserum (Santa Cruz Biotechnology) was used as negative control.

#### **5.3.2.3 Effect of HS on anosmin-1 function using exogenous HS and heparinase III**

After serum starvation, cells were incubated with anosmin-1 in the presence of 100 µg/ml HS or 2.5 units/ml heparinase III; in an additional experiment, an increased 500 µg/ml HS concentration was used for PIWF4 and 5 units/ml heparinase III for PIWF1. Furthermore, to investigate whether HS regulates anosmin-1 function in a dose-dependent manner, HS at concentrations of 1, 5, 10, 25, 50, 100, 250, 500 µg/ml were co-incubated with 10 nM truncated and full-length proteins and their mutants respectively.

#### **5.3.3 Immunocytochemistry**

*In vitro* immunofluorescence technique using specific antibodies against anosmin-1 (AIWF1) was used to localise recombinant anosmin-1 in PC-3 cells.

#### **5.3.3.1 Fluorescence labelling of cell surface associated anosmin-1**

After 48 hours incubation with 10 nM and 100 nM PIWF1 in serum-free medium, cells were rinsed several times in PBS and incubated in 0.5% blocking reagent (BSA in PBS) for 30 minutes. 1:1000 AIWF1 antibody was used for overnight incubation at 4°C. After several rinses in PBS, extra-cellular protein-antibody complex was immunodetected using an anti-rabbit Texas Red fluorescent secondary antibody (Jackson, PA, USA). Cells were then fixed in a chamber slide with 2% paraformaldehyde and 2% glutaraldehyde in PBS. A PIWF1/HS binding interference assay was carried out by immunofluorescent labelling of cells treated by co-culturing 100 µg/ml exogenous HS with 10 nM and 100 nM PIWF1 respectively. Controls consisted of replacing primary antibody with rabbit pre-immune sera for 100 nM PIWF1 treated cells. Control cells revealed no cross-reactivity between the first and second labelling procedures.

#### **5.3.3.2 Fluorescence labelling of intracellular anosmin-1**

For intracellular protein detection, cells were rinsed in PBS+0.1% Triton X-100 and fixed in a chamber slide with 2% paraformaldehyde, 2% glutaraldehyde in PBS. Subsequently, cells were incubated in 0.5% blocking reagent in PBS/T for 30 minutes. The same conditions were used for antibody incubation. Cells were mounted in glycerol and immunophenotyped by confocal microscopy (Bio-Rad Radiance 2100).

#### **5.3.4 Immunoprecipitation**

After 48 hour incubation in serum free medium,  $6 \times 10^6$  PC-3 cells were scraped and lysed in 0.5 ml lysis buffer (50 mM Tris-HCl, 350 mM NaCl, 1% Triton X-100, 1% NP-40, 1 mM EDTA, 1 mM EGTA, pH 7.4, protease inhibitor cocktail (Boehringer Mannheim), 0.02% NaN<sub>3</sub>) at 4°C for 30 min. The cell lysate was spun at 10,000 ×g for 15 min and supernatant harvested. Protein A beads (Amersham Pharmacia, UK) were washed 3 times with lysis buffer for the next cell lysate pre-clearing and immunoprecipitation. For cell lysate pre-clearing, 200 µl protein A beads was mixed into 2 ml cell lysate and incubated on ice for 1 h. After spinning at 10,000 ×g for 10 min, supernatant was collected. 0.5 ml of cleared cell lysate was then

incubated with 1  $\mu$ g PIWF1 at 4°C for 2 h before immunoprecipitation with 5  $\mu$ g of polyclonal or monoclonal anti-uPA antibody (American Diagnostica Inc) and anti-anosmin-1 antibody (AIWF1). The mixed solution was then incubated at 4°C overnight and 50  $\mu$ l pre-cleared protein A beads added for 1 h incubation at 4°C. The protein A beads were collected by centrifugation at 10,000 g for 30 sec, followed by 4 washes with lysis buffer. 50  $\mu$ l of 1  $\times$  Laemmli sample buffer was added to the bead pellet, followed by vortexing and heating to 90°C for 10 min. The supernatant containing the precipitated proteins was collected by centrifugation at 10,000  $\times$ g for 5 min, and then separated by SDS-PAGE and probed with anti-uPA and anti-His antibodies respectively.

### **5.3.5 SPR kinetic measurement of the uPA interaction with anosmin-1**

For the measurement of anosmin-1-uPA binding, uPA at 20  $\mu$ g/ml in 10 mM sodium acetate buffer, pH 5.0, was covalently immobilized by amine coupling to a CM5 - certified grade sensor chip (Biosensor AB, Uppsala, Sweden) preactivated with N-hydroxysuccinimide (NHS)/1-ethyl-3-[3-dimethylaminopropyl] carbodiimide hydrochloride (EDC). Coupling was achieved by injection of uPA at a flow rate of 5  $\mu$ l/min for 6 min, resulting in a coupling yield of 5,000 resonance units. Unreacted groups were blocked with 1 M ethanolamine, pH 8.5. A flow cell without protein coupling but with same treatment of activation and blocking served as a control. Binding was measured at a flow rate of 5  $\mu$ l/min using different concentrations of PIWF1 and PIWF4 dissolved in HEPES-buffered saline, followed by dissociation for 10 minutes. Sensor chips were regenerated at the end of each run by injection of 0.1 M acetic acid containing 0.5 M NaCl.

## **5.4 Results**

### **5.4.1 Anosmin-1 increases uPA amidolytic activity, but does not alter thrombin activity**

To investigate whether the N-terminal WAP domain of anosmin-1 has serine protease inhibitory activity, the effect of anosmin-1 was tested on two serine proteases, uPA and thrombin. First, the enzymatic activity of 0.8 nM thrombin on the

chromogenic substrate S2366 was measured spectrophotometrically every 1 min. Absorbance increased linearly over the time range of 4 min (Figure 5.1 (a)), whereas hirudin, a specific thrombin inhibitor exhibited a dose-dependent inhibition on thrombin amidolytic activity, complete inhibition being observed at over 0.25  $\mu\text{g/ml}$  hirudin concentration (Figure 5.1 (b)). These results confirmed the reliability of this system for the study of anosmin-1-thrombin interaction. As shown in Figure 5.1 (c) and (d), thrombin activity was not altered by increasing concentration of PIWF1 and PIWF4 treatments regardless of the presence or absence of HS, indicating that anosmin-1 did not interact with thrombin *in vitro*.

uPA enzymatic activity was then analyzed using the chromogenic S2444 substrate; 1 nM uPA treatment resulted in a linear increase of absorbance measured every 1 h (Figure 5.2 (a)), enabling subsequent analysis of the anosmin-1-uPA interaction. In the absence of uPA, no discernible stimulation of amidolytic activity was demonstrable in purified PIWF1 treatment; furthermore, purified recombinant GFP caused a negligible effect on uPA activity (Figure 5.2 (b)). However, as compared with thrombin, *in vitro* amidolytic activity of uPA was significantly enhanced by addition of all anosmin-1 analogues at concentrations of 10 nM and above. Up to 300% enhancement of activity was induced by both wild type and WAP mutated full-length anosmin-1, PIWF4 and mPIWF4<sup>172</sup> (Figure 5.2 (c) and (d)). The truncated PIWF1, however, showed only 100% maximum enhancement, about 60% less than full-length proteins (Figure 5.2 (e)). These results demonstrate that the wild type and WAP mutated full-length anosmin-1 variants behave similarly in induction of uPA activity. Thus the C172R substitution *per se* does not cause significant impairment on this particular function of anosmin-1. Alternatively, disruption of a single disulfide bond may not be enough to significantly block the interaction between anosmin-1 and uPA. However, loss of the other three FnIII domains as in the PIWF1 seems to cause reduction of anosmin-1's effect in this assay. Notably, the truncated WAP mutant mPIWF1<sup>172</sup> exhibited a higher magnitude of activation compared to full-length proteins (Figure 5.2 (f)). The reason why the truncated WAP mutant further enhances uPA activation is not clear.

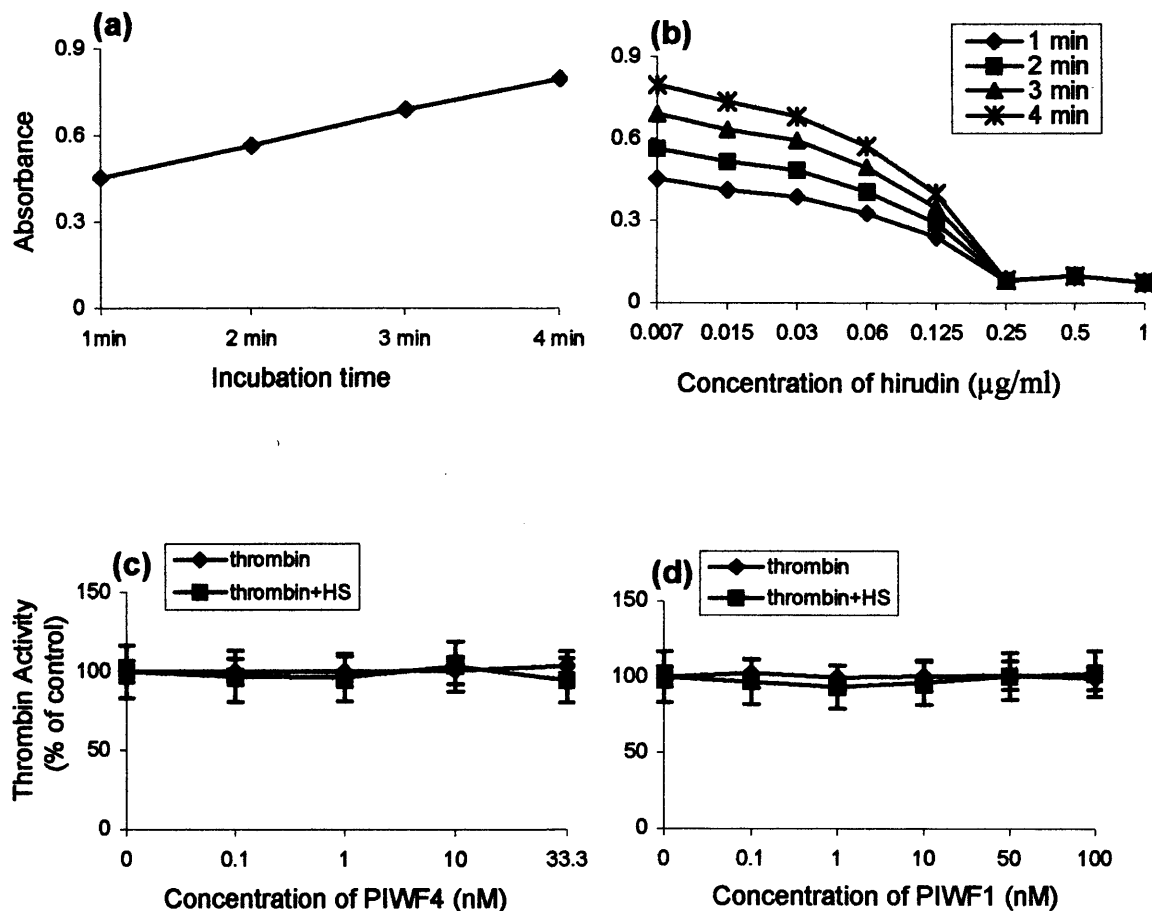


Figure 5.1 Effect of anosmin-1 on thrombin amidolytic activity. (a) Thrombin amidolytic activity was firstly assessed. 0.8 nM thrombin in PBS containing 20 mM Tris-HCl was loaded onto microtiter wells, followed by addition of specific substrate S2366 (0.42 mg/ml). The absorbance was recorded every 1 min at 405 nm. (b) Hirudin (a specific thrombin inhibitor) in a serial of dilution was co-incubated with 0.8 nM thrombin. The absorbance was measured every 1 min. Triplicates of PIWF4 (c) and PIWF1 (d) at the indicated concentrations were pre-incubated with 0.8 nM thrombin in the absence and presence of 10  $\mu\text{g/ml}$  HS. Residual amidolytic activity of thrombin was calculated as the ratio between the initial reaction velocity with anosmin-1 treatment and that of a control group without anosmin-1.

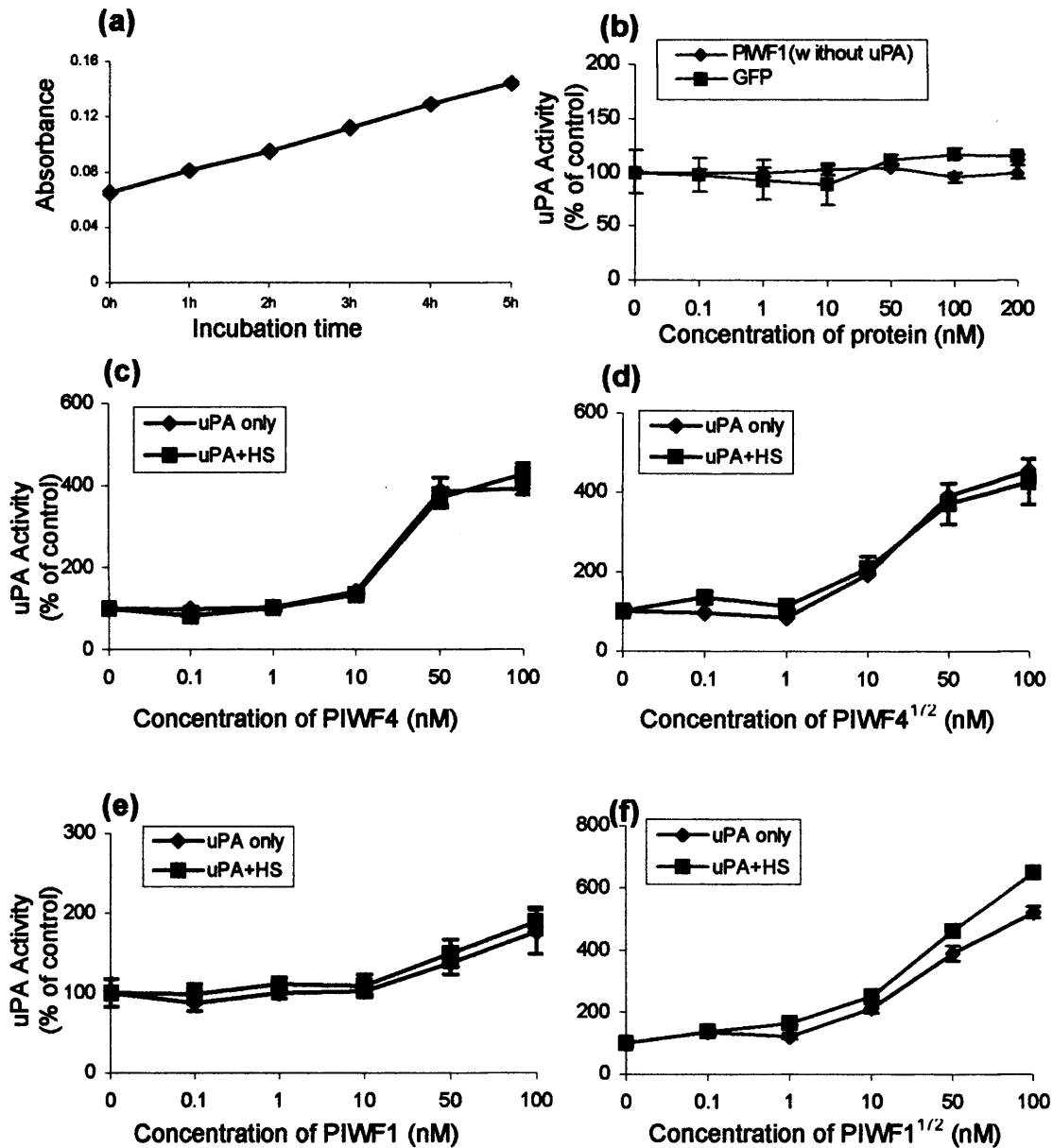


Figure 5.2 Effect of anosmin-1 on uPA amidolytic activity. (a) uPA amidolytic activity was first assessed using 1 nM uPA in PBS containing 20 mM Tris-HCl and the specific substrate S2444 (0.42 mg/ml). The absorbance was recorded every 1 h at 405 nm. (b) Negative control analysis of amidolytic activity. Purified PIWF1 was incubated with S2444 substrate without uPA addition, and GFP at the indicated concentrations was incubated with 1 nM uPA and substrate S2444. The absorbance was recorded every 1 h. Triplicates of PIWF4 (c), mPIWF4<sup>1/2</sup> (d), PIWF1 (e) and mPIWF1<sup>1/2</sup> (f) were pre-incubated with 1 nM uPA in the absence and presence of 10  $\mu$ g/ml HS. Residual amidolytic activity of uPA was calculated as the ratio between the initial reaction velocity with anosmin-1 treatment and that of a control group without anosmin-1.

HS is known to modulate the proteolytic activity of serine proteases through interaction with its inhibitors; binding of HS to antithrombin III increase its inhibitory activity on thrombin by 1,000 fold in the coagulation cascade (Shriver et al., 2000a). The effects of HS on anosmin-1 induced uPA amidolytic activity were then investigated. When anosmin-1 was co-incubated with 10  $\mu\text{g/ml}$  HS, the catalytic activity was unchanged except that a slight increase was observed with mPIWF1<sup>172</sup>; thus anosmin-1 induced enhancement of uPA activity is independent of HS in this assay (Figure 5.2). Taken together, although the finding that anosmin-1 enhances uPA activity rather than inhibits is contradictory to the initial expectation and previous suggestions of the role of the conserved WAP domain as a serine protease inhibitor, these data provide the first evidence identifying uPA as a putative anosmin-1 interactant whose activity is regulated by anosmin-1.

#### **5.4.2 Effects of anosmin-1 on promoting PC-3 cell proliferation are HS dependent**

The effects of PIWF1 and PIWF4 on PC-3 cell proliferation were assessed using the non-radioactive tetrazolium cell proliferation assay, which measures total viable cell number. PC-3 cells incubated for 48 h in serum free-defined medium without recombinant protein supplementation (control cells) were arbitrarily designated as 100% growth. Figure 5.3 (a) shows that, at all tested concentration from 1 nM to 100 nM, PIWF4 significantly increases PC-3 cell proliferation by 20%. Compared with PIWF4, PIWF1 stimulated PC-3 cell replication in a dose-dependent manner with a statistically significant 20-30% increase, whilst this activity was not observed at higher (100nM) concentrations (Figure 5.3 (b)). Peak activity was observed following 10 nM PIWF1 and PIWF4 treatments. These observations were confirmed by direct cell counting, in which total viable cell number was significantly increased by 10 nM PIWF4 and PIWF1 treatments, whereas purified GFP had no effect (Figure 5.3 (c)). To demonstrate the functional specificity of anosmin-1, purified polyclonal AIWF1 antibody was incubated with the PC-3 cells in the presence of PIWF1 and this abolished the stimulant activity of PIWF1 on cell growth (Figure 5.3 (b)). The quantitatively similar cell proliferative responses to PIWF1 and PIWF4 indicate that



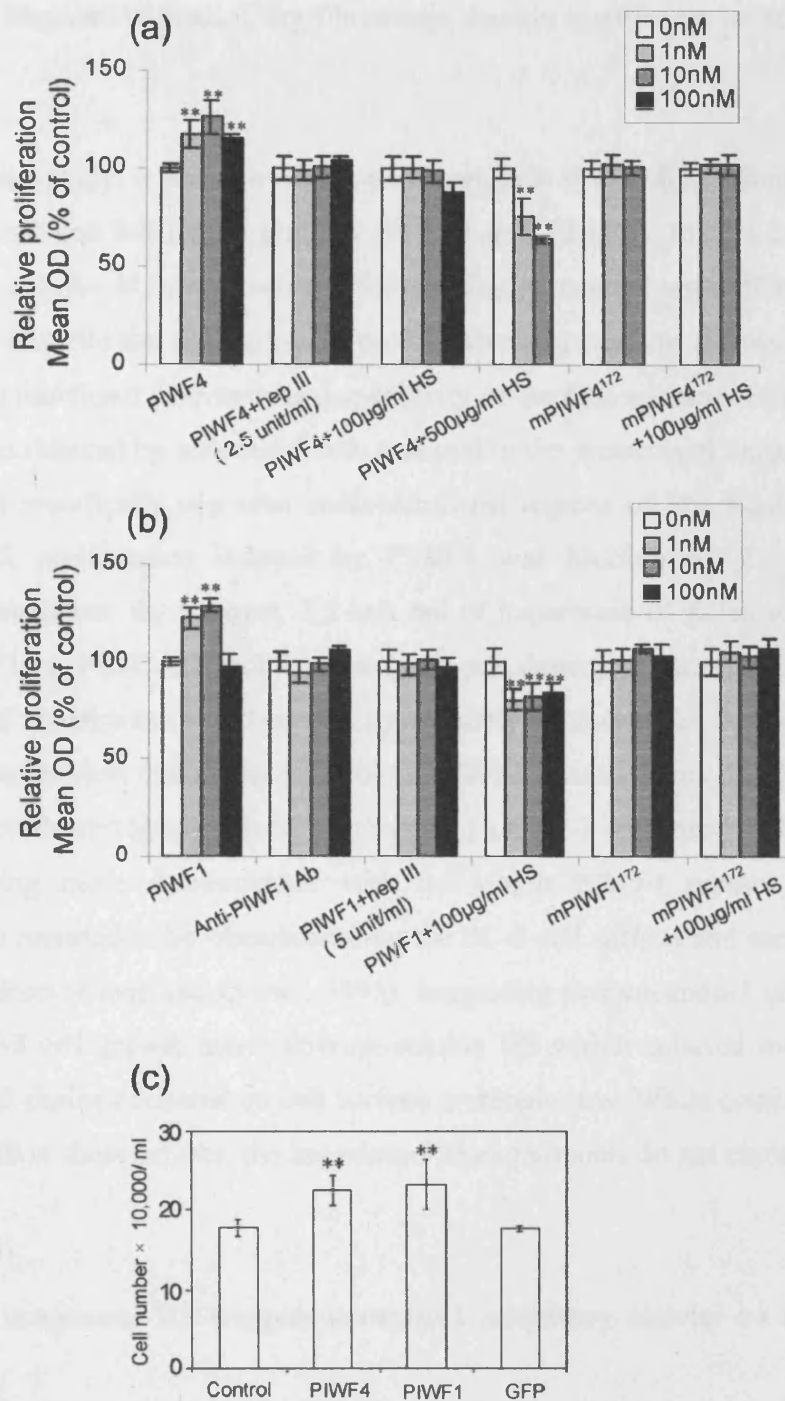


Figure 5.3 Effect of anosmin-1 on PC-3 cell proliferation. PC-3 cell proliferation was determined by MTT assay with PIWF4 and mPIWF4<sup>172</sup> (a), PIWF1 and mPIWF1<sup>172</sup> (b) respectively in the absence or presence of heparinase III (hep. III), exogenous HS and anti-PIWF1 antibody. Culture without addition of anosmin-1 was used as control. The graph shows the percentage change in optical density (OD) compared to control cultures. (c) Following 10 nM anosmin-1 or GFP treatment, cell viability was determined by Trypan blue exclusion and counted by haemocytometer. Student's T-test (2-tailed) was used to analyze the difference between treatment and control; \*\* P<0.01. Each value represents the mean ± S.D (n=5).

the N-terminal fragment with a solitary fibronectin domain is sufficient for stimulating cell division.

In a previous study, it was shown that a difference in HS binding affinity existed between truncated and full-length proteins (PIWF1 and PIWF4), PIWF1 having the lowest affinity and the highest binding affinity being associated with PIWF4; these properties may underlie the differences in proliferative responses to the two proteins. To examine the functional relevance and specificity of the HS/ anosmin-1 interaction, cell proliferation induced by anosmin-1 was assessed in the presence of heparinase III, an enzyme that specifically degrades under-sulphated regions of HS. Figure 5.3 (a) shows that cell proliferation induced by PIWF4 was blocked by 2.5 unit /ml heparinase III treatment. By contrast, 2.5 unit /ml of heparinase III failed to alter the effect of PIWF1 on PC-3 cell proliferation (data not shown), whereas doubling the concentration of heparinase III to 5 unit/ml significantly abolished this function - i.e. a higher concentration than that necessary to block PIWF4 action (Figure 5.3 (b)). These data confirm that the mitogenic effects of anosmin-1 on PC-3 cells are HS dependent, the effects being more demonstrable with full-length PIWF4 protein. HS has previously been reported to be immobilised on the PC-3 cell surface and secreted into the culture medium (Kosir and Quinn., 1995), suggesting that anosmin-1 effected its actions on PC-3 cell growth either through soluble HS within cultured medium, or immobilized HS chains anchored on cell surface proteoglycans. While confirming the specificity of HS in these actions, the heparinase III experiments do not clarify the site of action of HS.

#### **5.4.3 Soluble exogenous HS triggers anosmin-1 inhibitory activity on PC-3 cell growth**

If cell-surface associated HS mediates anosmin-1 function, excess exogenous HS in the culture medium should be able to neutralise anosmin-1 activity by competitively detaching anosmin-1 from the cell surface. As expected, 100 µg/ml HS attenuated PIWF4 induced cell proliferation, whereas 500 µg/ml HS began to elicit an anti-proliferative effect of PIWF4, observed initially at 1 nM and more evident at 10 nM

with a 20–40% decrease (Figure 5.3 (a)). By contrast, in the presence of 100 µg/ml HS, a 20% decrease was observed following PIWF1 treatment at all tested concentrations (Figure 5.3 (b)). This result indicated that the reversal of cell proliferation by PIWF1 requires less exogenous HS, consistent with the anosmin-1–HS binding characteristics. The higher binding affinity of PIWF4 to HS leads to a need for greater exogenous HS concentration in order to detach protein from cell surface, thereby abolishing PIWF4 induced proliferation. It is noteworthy that an inhibitory activity of anosmin-1 is evident on the addition of higher exogenous HS concentrations. These results demonstrate that anosmin-1 promotes PC-3 cell growth through cell surface HS and also raises the possibility that anosmin-1 possesses biphasic biological functions, with proliferative activity when binding on the cell surface and with inhibitory effect in the presence of more soluble HS.

#### **5.4.4 Recombinant anosmin-1 is associated with PC-3 cell surface *via* HS binding**

The fact that anosmin-1 might stimulate PC-3 cell proliferation *via* cell surface HS and the previous results that anosmin-1 was S2 cell-surface associated *via* an HS interaction lead to the question as to whether anosmin-1 was also localised to the PC-3 cell surface through HS binding. PC-3 cells were incubated with 10 nM and 100 nM PIWF1 in the presence and absence of HS respectively, followed by the immunofluorescence staining with AIWF1 antibody. In membrane labelling analysis (without Triton X-100 induced membrane permeability), recombinant PIWF1 was shown to bind to the cell surface in a dose-dependent manner with no labelling being observed in the negative control groups with pre-immune serum, thereby directly confirming the cell-surface associated localization of recombinant anosmin-1 (Figure 5.4). Notably, the staining of PIWF1 is punctuated rather than evenly spread out on the cell surface, suggesting that anosmin-1 may be involved in complex formation in the certain localisation. PIWF1 labelling was significantly decreased by 100 µg/ml exogenous HS, further indicating anosmin-1 attachment to cell-surface associated HS (Figure 5.4). Further analyses were performed to investigate if anosmin-1 could be internalised following attachment to cells, prior to possible protein degradation. Following cell permeabilisation thereby disrupting the cell membrane (the procedure

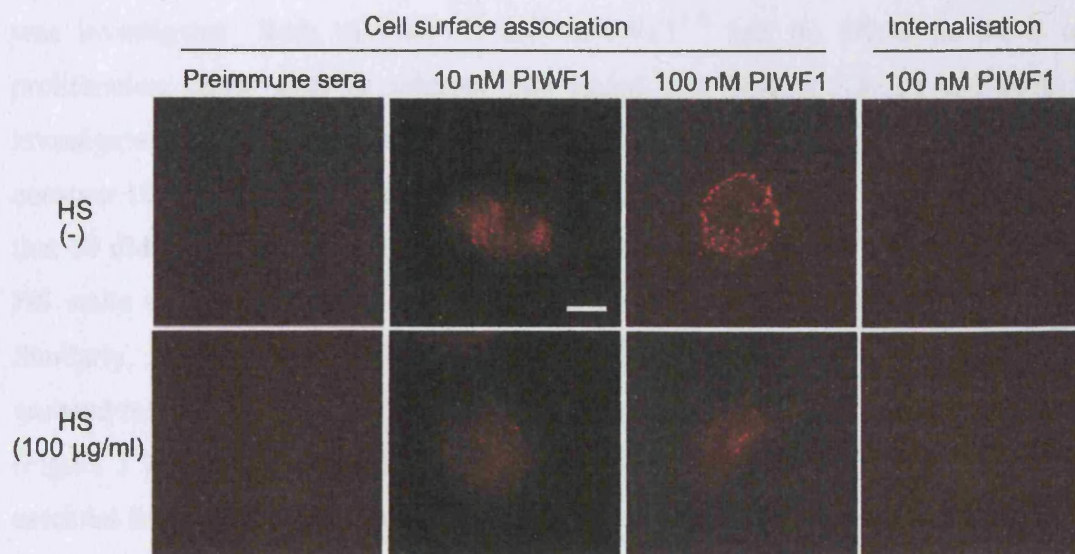


Figure 5.4 Immunofluorescence analysis of PIWF1 dissociation from PC-3 cell and internalisation following addition of exogenous HS. Following incubation with 10 nM and 100 nM PIWF1, with or without addition of exogenous 100 µg/ml HS, PC-3 cell surface protein was detected using AIWF1 antibody and Texas Red conjugated secondary antibody. The preimmune serum was used to replace AIWF1 as negative control for 100 nM PIWF1 treated cells. The permeabilisation operation to disrupt cell membrane allows antibody enter cells for anosmin-1 internalisation assay. The bar scale represents 5 µm.

allows antibody to enter cells), no PIWF1 staining signal could be detected inside cells, suggesting that anosmin-1 was unlikely to be internalised (Figure 5.4).

#### **5.4.5 WAP mutated anosmin-1 blocks cell proliferative activity**

To identify the potential roles of the N-terminal WAP domain in anosmin-1 function, the effects of a loss of function mutant of the WAP domain on cell growth was investigated. Both mPIWF4<sup>172</sup> and mPIWF1<sup>172</sup> had no effect on PC-3 cell proliferation either with or without 100 µg/ml HS (Figure 5.3 (a) and (b)). To investigate this phenomenon further, the effects of increasing HS concentrations with constant 10 nM wild type and mutated anosmin-1 were studied. Figure 5.5 (a) shows that 10 nM PIWF4 decreased cell proliferation in the presence of 250 and 500 µg/ml HS while the corresponding mutated protein exerted no effect on cell proliferation. Similarly, 10 nM PIWF1 inhibited cell growth in a HS dose-dependent manner, while mutated mPIWF1<sup>172</sup> showed the opposite effect in the presence of over 50 µg/ml HS (Figure 5.5 (b)). Thus, based on these findings, it appears that the WAP domain is essential for anosmin-1 action.

#### **5.4.6 Anosmin-1 induces PC-3 cell proliferation through interaction with uPA**

I next questioned whether uPA is directly involved in anosmin-1-induced PC-3 cell proliferation. Since our results showed that proliferative activity induced by PIWF4 was retained by its truncated version, I opted to firstly use PIWF1 in the subsequent studies of uPA/anosmin-1 interaction since it had a higher yield of recombinant protein production. Addition of anti-human uPA antibody along with 10 nM PIWF1 resulted in total abolition of PIWF1-induced PC-3 cell proliferation, while non-specific rabbit anti-sera did not show this effect (Figure 5.6 (a)); thus uPA seems to be required for anosmin-1 induced mitogenesis. To further investigate the physical association between anosmin-1 and uPA, a co-immunoprecipitation assay was performed using total cell lysates in the presence and absence of PIWF1. As shown in Figure 5.6 (b), both monoclonal and polyclonal anti-uPA antibody co-precipitated PIWF1 and uPA as detected by Western blotting with anti-His (for PIWF1) or anti-uPA antibody. Anti-PIWF1 immunoprecipitation also generated the corresponding

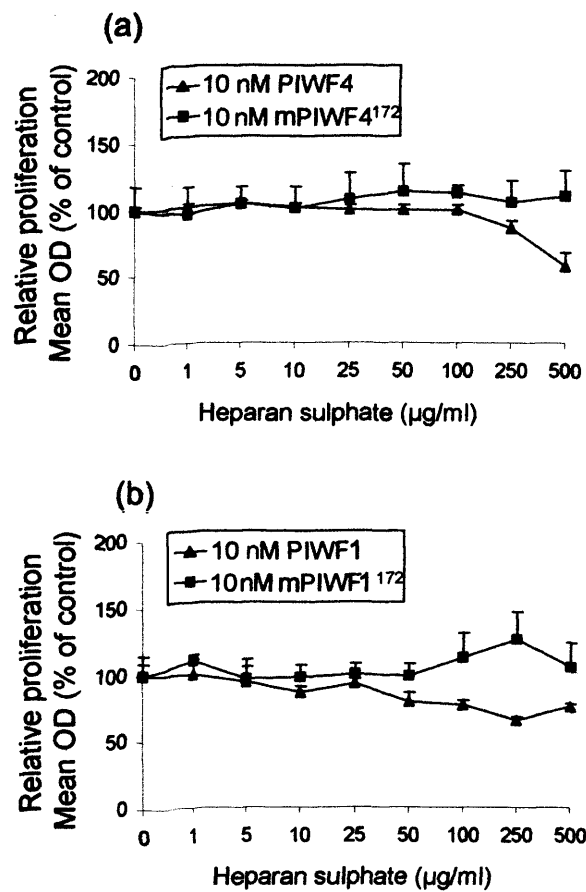


Figure 5.5 Growth suppression effect of anosmin-1 in PC-3 cells. PC-3 cells were treated with 10 nM PIWF4 and mPIWF4<sup>172</sup> (a), PIWF1 and mPIWF1<sup>172</sup> (b) in the presence of increasing concentrations of HS. Cell proliferation was measured by percentage change in O.D. compared to control.

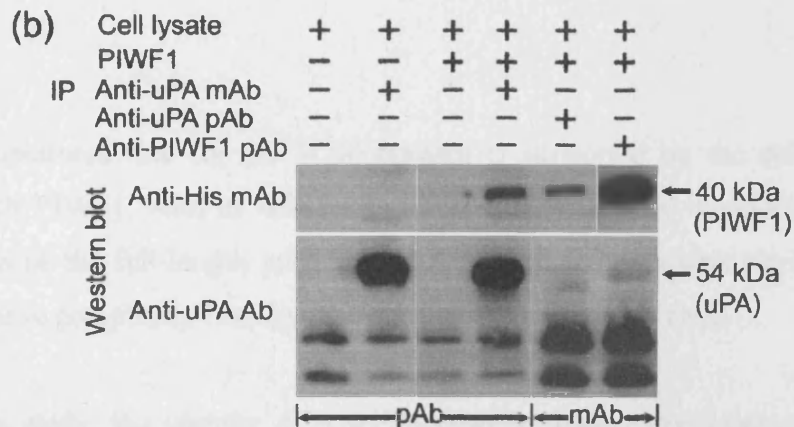
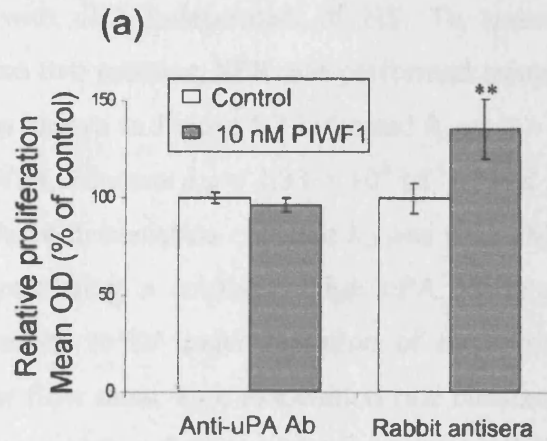


Figure 5.6 Involvement of uPA in anosmin-1 induced PC-3 cell proliferation. (a) Proliferation of PC-3 cells treated with 10 nM PIWF1 in presence of anti-uPA antibody or non-specific rabbit anti-sera. (b) PC-3 cell lysate were incubated with PIWF1 and immunoprecipitated with the corresponding antibodies. The immunoprecipitated complex was analysed by SDS-PAGE and Western blot using anti-His or anti-uPA antibody. Although polyclonal and monoclonal anti-uPA antibody (pAb and mAb) can pick up different forms of uPA, both of them visualise HMW uPA as indicated. Bands corresponding to PIWF1 and uPA are shown.



uPA and PIWF1 bands. These reciprocal immunoprecipitations clearly demonstrate a complex formation between these two proteins, an effect absent in negative controls. Since uPA has also been previously reported to have high HS binding affinity (Herndon et al., 1999; Pucci et al., 2001), I sought to investigate whether anosmin-1 can directly interact with uPA independent of HS. To assess the direct binding properties between these two proteins, SPR was performed using uPA coupled sensor chips. The sensorgrams shown in Figure 5.7 indicated  $k_{\text{on}} = 2 \times 10^5 \text{ M}^{-1}\text{S}^{-1}$  and  $k_{\text{off}} = 1.38 \times 10^{-3} \text{ S}^{-1}$  for PIWF4, whereas  $k_{\text{on}} = 1.33 \times 10^4 \text{ M}^{-1}\text{S}^{-1}$  and  $k_{\text{off}} = 4.36 \times 10^{-3} \text{ S}^{-1}$  for PIWF1. The calculated dissociation constant  $K_d$  was 6.91 nM for PIWF4 and 328 nM for PIWF1, demonstrating a relatively high uPA binding affinity. The mass transport limitation leading to an underestimation of the intrinsic kinetics can be associated with the low flow rates, high association rate constants and high levels of immobilized ligand. Since higher flow rate data are not available, the possibility of mass transport due to a high association rate of PIWF1 with uPA should be considered.

## 5.5 Discussion

A crucial functional role for the WAP domain is supported by the cell-based evidence in which PIWF1, with its solitary FnIII domain, can fully recapitulate the biological actions of the full-length protein, and yet WAP mutants with similar HS binding affinity have completely lost their mitogenic activity in PC-3 cells.

Prior to this study, the identity of a serine protease ligand that interacts with anosmin-1 was unknown. Our data show that anosmin-1 augments uPA amidolytic activity *in vitro* and participates in a direct protein-protein interaction with uPA, indicating that the serine protease uPA represents a potential molecular target for anosmin-1 action. Although the C172R mutation did not abolish anosmin-1's effect on *in vitro* uPA activity, one cannot exclude the possibility of the WAP domain representing an active uPA binding site. A single C157-C172 disulfide-bond disruption may only affect the WAP domain structural scaffold, but not be sufficient to interrupt the sequence necessary for interaction with uPA. Indeed, previous homology



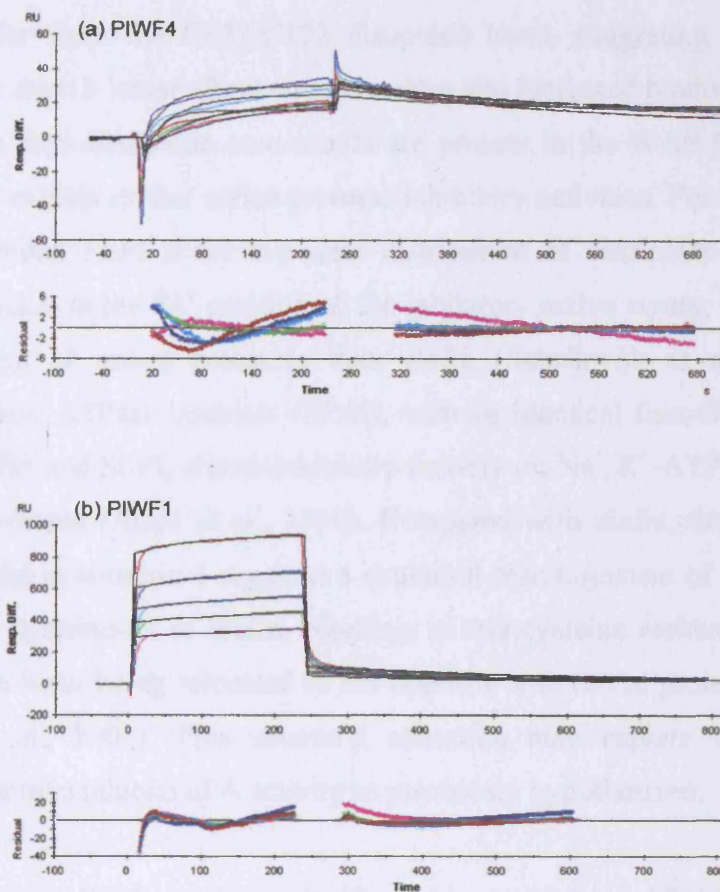


Figure 5.7 BIAcore analysis of anosmin-1 binding to uPA. Representative sensorgrams are shown for the interaction of immobilized uPA with soluble PIWF4 (a) and PIWF1 (b). Five different concentrations of analyte were used for these analyses: 50, 100, 175, 250, 375 nM for PIWF4, 250, 375, 500, 750, 1000 nM for PIWF1 (color lines, upper panel). This allowed global fitting to the 1:1 binding model (black lines, upper panel). The top sensorgram line in each graph represents the highest concentration of proteins, and the bottom line the lowest concentration. Residual plot showed the difference between measured and calculated responses (bottom panel in (a) and (b)).

modelling has shown that the predicted scissile peptide bond resides in the opposite loop surface far from the C157-C172 disulphide bond, suggesting that this bond disruption may exert a lesser effect on the reactive site for ligand binding. On the other hand, although four-disulphide core motifs are present in the WAP family proteins, they do not all exhibit similar serine protease inhibitory activities. For example, elafin and the C-terminal SLPI share the same distribution of disulphide bridges and a methionine residue in the P1' position of the inhibitory active centre; SLPI inhibits a far wider range of serine proteases than elafin (Schalkwijk et al., 1999). The sodium/potassium ATPase inhibitor (SPAI), with an identical four-disulphide bonds location to elafin and SLPI, shows inhibitory activity on Na<sup>+</sup>,K<sup>+</sup>-ATPases but not on other serine protease (Araki et al., 1990). Compared with elafin, the WAP domain homology model in anosmin-1 suggests a structural rearrangement of cysteine-147 in relation to the cysteine-83 of elafin, resulting in this cysteine residue and predicted scissile peptide bond being relocated to the opposite side of the protein surface loop (Robertson et al., 2001). This structural alteration may explain why anosmin-1 increases rather than inhibits uPA activity as previously hypothesized.

In addition to WAP proteins, specific serine proteinase inhibitors belonging to the structural class of serpins (serine protease inhibitors) also show differential specificity and activity on trypsin-like serine protease. Members of this serpin family include plasminogen inhibitor 1 and 2 (PAI-1, -2), anti-plasmin, anti-thrombin III (AT III), protease nexin-1 (PN-1) and neuroserpin; their inhibitory specificity and activity critically depend on their amino acid composition at the reactive centre (Sherman et al., 1992; Osterwalder et al., 1998). Although an arginine residue at the P1 position is highly conserved in these serpin family members, the P1' position is mostly occupied by a methionine residue, other reactive positions being more promiscuous. For instance, neuroserpin specifically binds to tPA, uPA and plasmin and inhibits their amidolytic activity, but have no effects on thrombin; the putative reactive site P1-P1' (Arg<sup>362</sup> and Met<sup>363</sup>) was proved to interact with all target proteases (Osterwalder et al., 1998). In contrast, PN-1 with arginine and serine at P1-P1' site is directed against thrombin (Liu et al., 1994). Based on these observations, one would expect that

anosmin-1 must carry arginine as a crucial residue for trypsin-like serine protease binding. In the anosmin-1 WAP domain, there are five arginine residues (at 136, 140, 144-146 position respectively), very close to the predicted active site of glycine-142-phenylalanine-143, further suggesting that these regions may act as a putative binding site for uPA. Further demonstration of the WAP domain role in uPA catalytic activity will depend on the generation of a mutant that deletes this region or even the entire WAP domain.

Functional HS/uPA co-operation was revealed by anosmin-1's mitogenic activity on PC-3 cells, where a biphasic HS dependent action was demonstrated. Specifically, 1) stimulation of cell proliferation *via* a cell-surface HS associated mechanism, 2) inhibitory effect on cell proliferation when exogenous HS was added. These conclusions were based on the following experimental results: (1) heparinase III and addition of increasing doses of HS decreased or abolished anosmin-1 induced stimulation of cell proliferation, whereas significant inhibition was achieved with higher concentrations of HS. (2) immunofluorescence analysis provided direct evidence that anosmin-1 was cell surface associated *via* HS. (3) an anti-uPA antibody blocked anosmin-1 activity and uPA-anosmin-1 complex formation as confirmed by co-immunoprecipitation. These data are the first to demonstrate that anosmin-1 can modulate cell proliferation *via* an HS-dependent and uPA related mechanism.

Central questions remain as to how: 1) the HS/uPA/anosmin-1 complex mediates a biphasic effect on PC-3 cell proliferation and 2) which domain of anosmin-1 mediates these biphasic activities. It is notable that the N-terminal truncated protein comprising the WAP and 1<sup>st</sup> fibronectin type III demonstrates similar biological activities to its full-length counterpart, with the exception that it has a lower HS requirement. These data are consistent with the notion that the major functional part of anosmin-1 is located at WAP and 1<sup>st</sup> fibronectin type III repeat (MacColl et al., 2002a). Since the FnIII domain is a major HS binding site, and given its HS dependent effect on cell proliferation, anosmin-1's mitogenic activity appears to depend upon the FnIII domains (especially the first one) *via* attachment to cell-surface associated HS.

The WAP domain, on the other hand, is also functionally important for integral anosmin-1 action, although it remains unclear whether the WAP domain binds directly to uPA.

It is known that cell surface HS chains act as receptor or co-receptor to regulate binding protein signalling by diverse mechanisms: converting ligands from inactive to active forms through conformational changes, promoting ligand and receptor dimerization inducing signal transduction and stabilising the active ligand-receptor complexes through ternary complex formation (Kwan et al., 2001). The best example is the significant role of HS in FGF2 activation through FGFR signalling. PC-3 cells have been shown to generate endogenous HSPG on the cell surface (Jarrard et al., 1994; Kosir and Quinn, 1995). Therefore, with respect to anosmin-1, through FnIII domain binding, HS could serve at least three functions: (1) acting as co-receptor or stabilisation platform determining ligand distribution, (2) concentrating N-terminus (CR and WAP domain) in a location-specific manner in preparation for uPA binding, (3) acting as modulator, inducing conformational alterations of the anosmin-1 N-terminus, thereby exposing its ligand specific binding site. Thus, the effect of anosmin-1 on PC-3 cell proliferation appears dependent on the uPA receptor and uPA related proteolysis. Anosmin-1 may act as a transporter and bridge to facilitate a uPA/uPAR interaction thereby stimulating the uPAR signalling transduction pathway for cell proliferation. Moreover, an increase in uPA proteolytic activity may lead to activation of a number of growth factors such as the insulin-like growth factor, basic fibroblast growth factor, and transforming growth factor- $\beta$  (Jarrard et al., 1994), all of which have been shown to be expressed in PC-3 cells (Angelloz-Nicoud and Binoux, 1995). Disruption of the normal WAP domain structure may attenuate wild-type anosmin-1 interaction with the uPA/uAPR complex and proteolytic activation of the growth factors.

On the other hand, the attenuation of stimulation and even inhibitory effect of anosmin-1 on PC-3 cell proliferation was observed in the presence of exogenous HS. This observation might be explained in terms of the HS structure, its specific form

(soluble or immobilized) and uPA related proteolysis. In the best-studied FGF2 signalling loops, HS have been demonstrated as either inhibitors or potentiators according to their diverse specific sequences and structures (Liu et al., 2002a). Heparinase III-treated HS fragments from B16BL6 melanoma cell surfaces inhibit tumour cell proliferation *in vivo* and *in vitro* by preventing activation of the FGF2 mediated signalling pathway, principally the MAP kinase pathway, whereas heparinase I derived HS fragments exert the opposing effects. Furthermore, specific form of HS also demonstrate diverse activities; cell-bound heparin stimulates FGF2-receptor binding whereas soluble heparin exhibits the opposite effect, both correlating with changes in FGF2-induced tyrosine kinase activity and cell proliferation (Fannon et al., 2000). Importantly, HS with certain 5 dimeric repeats of GlcN(3-OSO<sub>3</sub>)(6-OSO<sub>3</sub>)-IdoA(2-OSO<sub>3</sub>) has been shown as an adaptor molecule to confer specificity on uPA/uPAR binding (Pucci et al., 2001). Therefore, it can be proposed that an alteration in the sequence and structural arrangement of HS binding to signalling molecules such as uPA/uPAR might be regulated by anosmin-1, leading to up or down regulation of binding affinity and specificity between mitogenic molecules and their cognate receptors. In addition, it has been reported that cell surface uPAR can be cleaved by uPA (Hoyer-Hansen et al., 1997). One might then expect that elevated uPA activity induced by anosmin-1 could down-regulate uPAR related proliferation by proteolytic cleavage on uPAR. Finally, it should be noted that the proteolytic products of mitogenic signalling-related molecules caused by serine proteases have biphasic effects on cell proliferation. For example, the two fragments of IGFBP-3 generated after cleavage by uPA and plasmin, corresponding to 160 and 95 residues of IGFBP-3, possess dual effects on PC-3 cell proliferation, in which the large fragment stimulates cell growth and the smaller one shows the opposing activity (Angelloz-Nicoud et al., 1998).

The identification of HS and uPA as “cross-talk” partners for anosmin-1 provide novel potential insights into the molecular basis of the neuronal and non-neuronal manifestation of X-KS. In the developing OB, early expression of anosmin-1 and uPA is detected (Dent et al., 1993), whereas conditional disruption of the HS-

polymerization enzyme *Ext-1* in embryonic mouse brain results in absence of major commissural tracts and OB (Inatani et al., 2003). In human kidney, uPA expression is mainly detected in tubular epithelial cells in the deep cortex and the outer medulla (Xu et al., 1996). Furthermore, uPA can induce Madin-Darby canine kidney (MDCK) epithelial cells to form branching tubules in fibrin gel (Pepper et al., 1992). These observations suggest that uPA increases extracellular proteolysis, required for epithelial morphogenesis in kidney. The immunohistochemical study on X-KS patients with disrupted anosmin-1 has revealed the appearances of dysplastic tubules and cysts (Deeb et al., 2001). The dysfunction of glypican-3 results in decreased proliferation of medullary collecting duct cells and medullary degeneration (Grisaru and Rosenblum, 2001). Thus, any interruption of the interaction among these three molecules (anosmin-1, uPA and HS) may lead to the olfactory as well as the renal developmental defects seen in X-KS patients.

In conclusion, I postulate that uPA-induced activation of the plasmin cascade system on the cell surface causes proteolytic degradation of ECM components enabling cell-cell and cell-ECM adhesion and release of activated growth factors, thereby facilitating cell migration, tissue remodeling, angiogenesis and neuronal synaptogenesis. Anosmin-1 may modulate these processes by increasing uPA catalytic activity, whereas the role of HS may be to concentrate and restrict uPA/anosmin-1 distribution on the cell surface (Figure 5.8). HS may further help and stabilize anosmin-1 and uPA complex formation through binding to both of these two molecules as seen with antithrombin/thrombin and FGF/FGFR. It is likely that uncontrolled uPA activity is potentially harmful; the developmental stage specific and tissue specific activation of uPA requires a careful balance between proteolysis and anti-proteolytic actions regulated by several known activators (plasmin) and inhibitors (plasminogen activator inhibitor 1,2, antiplasmin, neuroserpin). Our results clearly identify anosmin-1's role as a novel activator of uPA; anosmin-1/HS/uPA may therefore mediate different functions in a tissue and developmental stage specific way leading to different phenotypic outcomes, such as tubulogenesis during kidney epithelial tissue morphogenesis or cell differentiation in neuronal development.

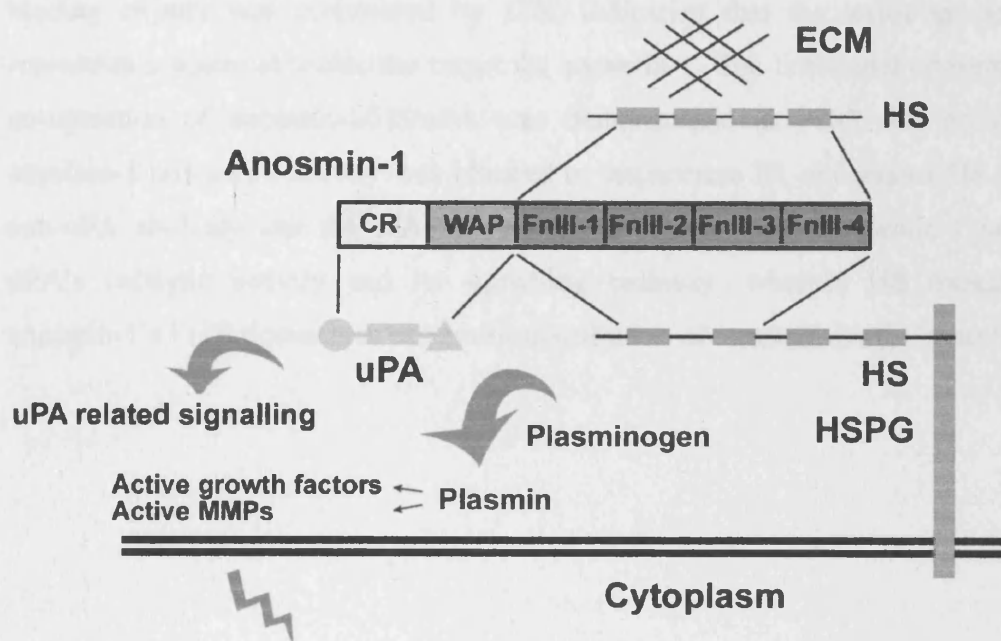


Figure 5.8 Hypothesis of molecular mechanism of anosmin-1 action. HS side chains of HSPG anchor anosmin-1 to the cell surface *via* binding to FnIII domains, thus facilitating N-terminal anosmin-1-uPA interaction. HS may further help and stabilize anosmin-1 and uPA complex formation through binding to both of these two molecules as seen with antithrombin/thrombin and FGF/FGFR. Increased uPA proteolytic activity induces plasmin/MMPs mediated ECM degradation releasing a number of growth factors involved in cell proliferation, migration and tissue remodeling. Different functional domains of uPA are schematically represented: growth-factor-like domain (circle); kringle domain (rectangle); catalytic domain (triangle).

## 5.6 Conclusions

Prior to the present study, the identity of serine protease ligands for anosmin-1 was unknown. Our data showed that anosmin-1 could increase uPA amidolytic activity *in vitro*, but has no effect on thrombin, and that co-immunoprecipitation has demonstrated anosmin-1/uPA complex formation in PC-3 cell lysates and their high binding affinity was determined by SPR, indicating that the serine protease uPA represents a potential molecular target for anosmin-1. The functional consequence of co-operation of anosmin-1/HS/uPA was demonstrated in PC-3 cell proliferation; anosmin-1 mitogenic activity was blocked by heparinase III, exogenous HS addition, anti-uPA antibody and the WAP mutant. I thus propose that anosmin-1 modulates uPA's catalytic activity and its signalling pathway, whereas HS interacts with anosmin-1's FnIII domains to determine distribution of anosmin-1/uPA complex.



## Chapter 6

### Structure analysis of anosmin-1 by analytical ultracentrifugation and X-ray scattering

#### 6.1 Introduction

The elucidation of the structural conformation of a molecule can assist in the understanding of its biological functions; by establishing the overall 3-dimensional structural parameters, it may identify surface-exposed residues and reveal ligand-binding sites in the presence or absence of ligand. Although the biological activity of anosmin-1 has been extensively studied in a variety of *in vivo* and *in vitro* paradigms, prior to the present study, no attempt at an experimentally based structural determination had been undertaken in the past decade, limiting our ability to understand its structure-function relationship. Homology molecular modelling of individual WAP and FnIII domains has been established by our group previously; thus, the availability of the atomic structure of the homologous protein elafin enabled the three-dimensional visualization of the WAP domain of anosmin-1. In these studies, it was also possible to model the fibronectin type III repeat of anosmin-1 on the known fibronectin seven-stranded  $\beta$ -sheet sandwich structure with its ABE-GFCC' configuration (Robertson et al., 2001). However, the assembly of multidomain arrays of CR, WAP and FnIII domains, either in a compacted or extended fashion, remained unknown.

On present evidence, a fully elongated conformation can be proposed for full-length anosmin-1. First, it was established that disruption of the WAP domain exerted an impact only on the HS binding affinity ( $K_d$ ) value of PIWF1, which lacks three C-terminal FnIII domains, whereas the same disrupted WAP domain did not alter HS binding affinity when part of a full-length anosmin-1 molecule. These data suggested that the effects of a structural alteration in the WAP domain might influence the charge distribution in the first FnIII domain, but only when not followed by additional FnIII repeats. This model would be given greater credence if it could be demonstrated that full-length PIWF4 had an elongated structure. In addition, full-length anosmin-1

induced enhancement on uPA amidolytic activity was affected neither by the addition of HS nor the presence of a WAP mutation, suggesting that a compacted multidomain conformation was unlikely. An extended structure of multidomain FnIII domains has been revealed both in fibronectin and tenascin using electron microscopy (Engel et al., 1981; Erickson et al., 1981). High-resolution structures of a fragment of neuroglian (*Drosophila* homology of L1) containing two FnIII repeats and a fragment of fibronectin containing four such repeats also showed an extended configuration (Huber et al., 1994; Leahy et al., 1996). To investigate whether the conformation of anosmin-1 is in an extended configuration, structural studies were performed including X-ray solution scattering and analytical ultracentrifugation, both of which are discussed in the following sections.

## **6.2 Methods for protein structural analysis**

The structures of proteins are commonly determined using spectroscopic or diffraction methods complemented by other techniques. Spectroscopy is the study of the diffraction of electromagnetic radiation with matter, excluding chemical effects. The diffraction of neutrons and electrons by matter is commonly included in a discussion of spectroscopy because, like electromagnetic radiation, they can be described by wave functions. X-ray crystallography involves the diffraction of X-rays by a crystallized molecule, whereas the effect of an applied magnetic field on nuclei that possess a magnetic moment or spin is determined in NMR spectroscopy. Both methods complement each other and currently provide protein structure at atomic resolution.

Other spectroscopic and non-spectroscopic low-resolution techniques that provide information on the overall dimensions of a molecule include small-angle solution X-ray scattering, analytical ultracentrifugation and electron microscopy. Small-angle solution X-ray scattering is used to study gross structural parameters of macromolecules in solution to a resolution of 2 to 4 nm. Information on the gross structure of a protein molecule can also be obtained from hydrodynamic analyses. The basis of ultracentrifugation experiments is that, for a solution subjected to a centrifugal

force, the movement of the macromolecule is dependent on the mass ( $M_r$ ) and shape. Electron microscopy can visualize the whole macromolecule down to a resolution of around 2 nm, although the images are studied in a vacuum and after staining, both of which may cause structural artifacts.

X-ray solution scattering and analytical ultracentrifugation are versatile and powerful techniques for characterizing the solution-state behaviour of macromolecules. The structural arrangement of domains or subunits in multidomain or oligomeric proteins in dilute solutions can be determined by X-ray study in near-physiological conditions (Perkins, 1988). X-rays visualize the macromolecule in a high positive solute-solvent contrast and provides structural parameters at low resolution. It is complementary to analytical ultracentrifugation, which provides more limited information on macromolecular elongation from sedimentation coefficients.

Traditional solution scattering is seen as an enabling method that provides the first gross macromolecular structural information on a newly purified protein. From the data collection, one can obtain scattering curves  $I(Q)$  and their analysis can yield the overall radius of gyration  $R_G$ , the radius of gyration of the cross-section  $R_{XS}$ . The distance distribution function  $P(r)$  will provide structural information in real space. These will yield a set of dimension for the macromolecule. Thus the molecular modelling of scattering curves will verify the correct interpretation of scattering data and enable visualization of the structure. The known multidomain protein volume and the known atomic structure of small domains or subunits from crystallography and NMR can be applied in modelling to generate a model of the full macromolecule as well as enabling the calculation of a scattering curve to determine whether it is compatible with the experimental data. It can also be refined by complementary information from sedimentation coefficients derived from analytical ultracentrifugation.

Analytical ultracentrifugation methods are capable of rigorously determining sample purity, characterizing assembly and disassembly mechanisms of biomolecular complexes, determining subunit stoichiometries, detecting and characterizing

macromolecular conformational changes, and measuring equilibrium constants and thermodynamic parameters for self- and hetero-associating systems (Schuster and Toedt, 1996; Hensley, 1996; Laue and Stafford, III, 1999). Two types of experiments in analytical ultracentrifugation can be performed, to generate 1) the sedimentation velocity and 2) the sedimentation equilibrium. Sedimentation velocity is a hydrodynamic technique and is sensitive to the mass and shape of the macromolecular species. In a sedimentation velocity experiment, a moving boundary is formed on application of a strong centrifugal field and a series of scans are recorded at regular intervals to determine the rate of movement and broadening of the boundary as a function of time. In contrast, sedimentation equilibrium is a thermodynamic technique that is sensitive to the mass but not the shape of the macromolecular species. This experiment is performed at lower speeds than sedimentation velocity experiment and measures the equilibrium concentration distribution of macromolecules that eventually form when sedimentation is balanced by diffusion. The sedimentation velocity and equilibrium measurements provide complementary information, and it is often useful to apply both techniques to a given problem.

### **6.3 X-ray solution scattering**

#### **6.3.1 X-ray scattering theory**

Small angle X-ray methods examine the scattered waves produced from the diffraction of an incident beam by protein molecules in solution. It is a diffraction technique that can be used to study the overall structure of proteins. An X-ray scattering experiment is performed by irradiating a sample with a highly collimated beam of monochromatic X-rays, and measuring the intensity of scattering  $I$  as a function of  $Q$ , where  $Q$  corresponds to the scattering angle  $2\theta$ , from which the scattering curve  $I(Q)$  is obtained (Figure 6.1). Scattering is due to interaction of X-rays with electrons in the sample: upon irradiation, each electron oscillates and emits electromagnetic waves of the same wavelength  $\lambda$  in all direction, but phase-shifted by  $\pi$  with respect to the incident X-ray beam. This type of scattering is known as coherent scattering. The intensity of scattering by an electron is proportional to the X-ray scattering length  $f$  of the electron, which has a value of 2.81 fm. For an atom, the X-

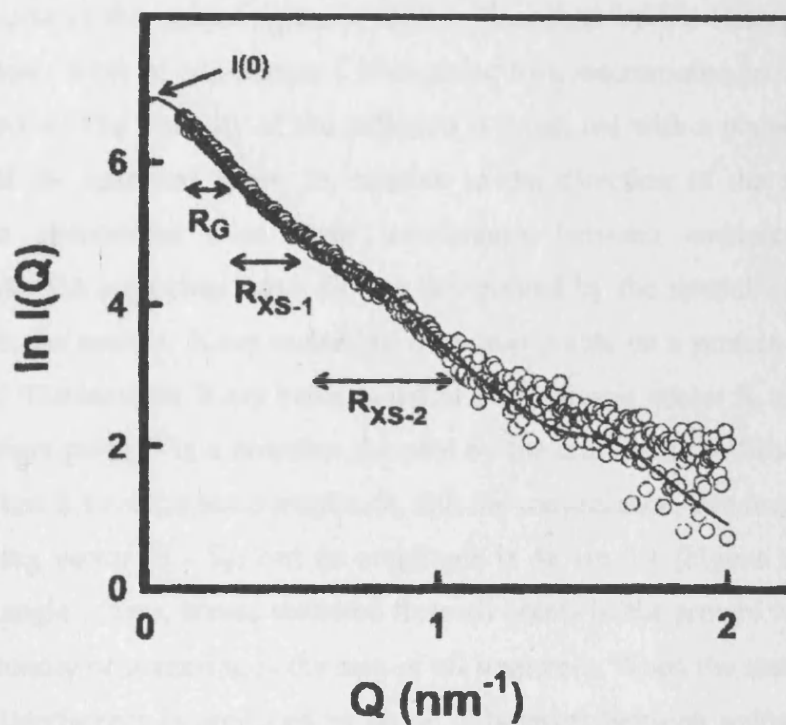


Figure 6.1 General features of a solution scattering curve  $\ln I(Q)$  measured over a  $Q$  range, exemplified using an antibody molecule. At low  $Q$  range ( $\ln I(Q)$  vs.  $Q^2$  at low  $Q$  value,  $0.1-0.5 \text{ nm}^{-1}$ ) Guinier plot results in the overall radius of gyration  $R_G$  and the intensity  $I(0)$  at zero scattering angle. At larger  $Q$  ( $\ln [I(Q)Q]$  vs.  $Q^2$ ,  $Q$  within  $0.3-1.0 \text{ nm}^{-1}$ ) the cross-sectional  $R_G$  ( $R_{XS}$ ) can be calculated. For “T-shaped” protein structures such as the immunoglobulins, the cross-sectional plot exhibits two linear regions, a steeper innermost one and a flatter outermost one (Pilz et al., 1975) and in this type of analysis the two regions are referred to as  $R_{XS-1}$  and  $R_{XS-2}$  respectively.

ray scattering length is the atomic number (the number of electrons it contains) multiplied by the scattering length of an electron.

### 6.3.1.1 The Debye equation

The form of the scattering curve  $I(Q)$  is described by the Debye equation. An incident planar wave of wavelength  $\lambda$  is scattered by a macromolecule in the form of a spherical wave. The intensity of the radiation is measured with a planar detector as a function of the scattered angle  $2\theta$ , relative to the direction of the incident wave. Diffraction phenomena arise from interference between scattered waves and consequently the scattering curve  $I(Q)$  is determined by the spatial arrangements of electrons in the protein. X-ray scattering from two points on a protein is depicted on Figure 6.2. The incident X-ray beam is defined by the unit vector  $S_0$  and is scattered from an origin point  $O$  in a direction denoted by the unit vector  $S$ . Since scattering is elastic,  $S_0$  and  $S$  have the same amplitude, and for convenience, this is set as  $2\pi/\lambda$ .  $Q$  is the scattering vector ( $S - S_0$ ) and its amplitude is  $4\pi \sin \theta/\lambda$  (Figure 6.2). When the scattering angle is zero, waves scattered from all points in the protein will be in phase and the intensity of scattering is the sum of all scatterers. When the scattering angle is non-zero, interference is produced by phase differences between scattering points. In Figure 6.2, the incident X-ray beam is scattered by a second point  $P$ , and the path difference between waves scattered by points  $O$  and  $P$  is  $AO + OB$ . This path difference corresponds to a phase difference of  $2\pi(AO + BO)/\lambda$ . If the vector between  $O$  and  $P$  is  $r$ , then  $AO = -rS_0$  and  $OB = rS$  and the phase difference is  $r(S - S_0)$ , or more simply  $rQ$ . The phase difference  $rQ$  between each individual scatterer in a macromolecule determines its scattering curve  $I(Q)$ , and this relationship is contained within the Debye equation:

$$\overline{F^2(Q)} = \sum_p \sum_q f_p f_q \frac{\sin(rQ)}{rQ} \quad \text{Eq. 6.1}$$

$F^2(Q)$  is the square of the structure factor  $F(Q)$  of the macromolecule,  $F(Q)$  is a regulation of the scattering curve  $I(Q)$  to the intensity of scattering by one electron at

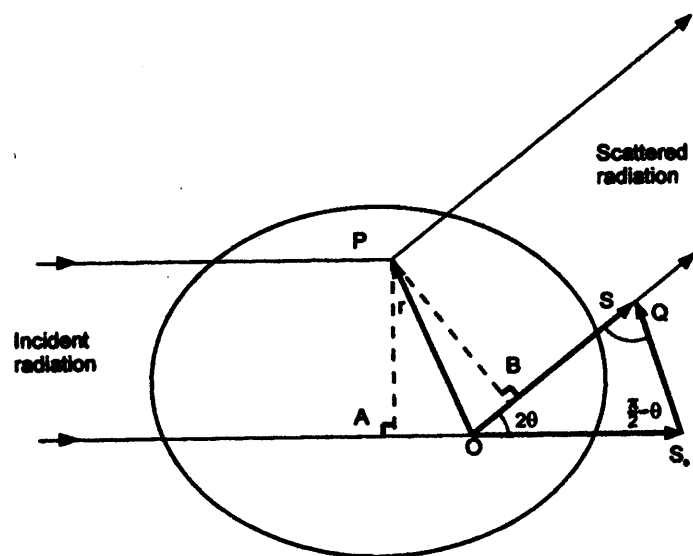


Figure 6.2 Schematic representation of X-ray scattering from two points in a protein molecule. Diffraction is by two points O and P separated by a distance  $r$  within a single particle in a solution scattering experiment. A and B correspond to the perpendiculars to the incident and scattered beams. The unit vectors  $S_0$  and  $S$  define the incident and scattered radiation, and  $Q$  defines the scattering vector ( $S - S_0$ ). (Adapted from Perkins, 1998).

zero scattering angle  $Ie[I(Q) = Ie F^2(Q)]$ , and the summations are performed over all points  $p$  and  $q$ , where  $f_p$  and  $f_q$  are the respective X-ray atomic scattering lengths. The Debye equation gives the average of  $F^2(Q)$  for all possible orientations of the molecule, and this would therefore require that scattering is spherically symmetrical about the incident beam. It can be seen that the Debye equation is only dependent on the magnitude of  $Q$ . For this to be true in a scattering experiment, the scattering sample would have to consist of a monodisperse solution of identical molecules that occupy all orientations equally, and act as independent scattering entities. A limitation of the Debye equation is that it describes particles in *vacuo* and it therefore needs to be modified in order to consider aqueous protein solutions.

### 6.3.1.2 Two-phase model of solution scattering

The simplest consideration of an aqueous protein solution is as a two-phase system of solute and solvent. The Debye equation is modified to consider the contrast  $\Delta\rho$  between the scattering density of the macromolecule *in vacuo*  $\rho_v$  and the scattering density of the solvent  $\rho_s$ , where  $\Delta\rho = \rho_v - \rho_s$ . The Debye equation can also be revised according to the resolution limits of the solution scattering experiment. In an X-ray solution scattering experiment, data are typically collected to a maximum usable  $Q$  of approximately  $2.0 \text{ nm}^{-1}$ . The maximum  $Q$  value can be used to calculate the structural resolution of scattering, i.e. the smallest distance  $d$  measured in the experiment. Bragg's Law ( $\lambda = 2d\sin\theta$ ) is used for this calculation. A  $Q$  value of  $2.0 \text{ nm}^{-1}$  corresponds to a structural resolution of around 3 nm. At this resolution, a few large volume elements  $dv_p$  of scattering density  $\rho(r_p)$  can be used to replace individual X-ray atomic scattering lengths  $f_p$  in the Debye equation ( $f_p = \rho(r_p)dv_p = \rho(r_p)d^3r_p$ ). Thus the intensity of scattering is:

$$\overline{F^2(Q)} = \int_V \int_V (\rho(r_p) - \rho_s)(\rho(r_q) - \rho_s) \frac{\sin(rQ)}{rQ} d^3r_p d^3r_q \quad \text{Eq.6.2}$$

where the integration is taken over the macromolecular volume  $V$ .



## **6.3.2. Experimental X-ray solution scattering**

### **6.3.2.1. Sample preparation**

X-ray solution scattering experiments were designed according to the two-phase model of solution scattering. The first requirement was for a pure, monodisperse solution of protein at a concentration that was high enough for its scattering curve to be measured. The tendency of protein samples to aggregate necessitated that each sample was subjected to gel filtration to remove non-specific aggregates, then reconcentrated as shortly before data collection as possible. The choice of buffer was also important. In X-ray scattering experiments, the closer the buffer density is to that of pure water, the higher the sample transmission becomes, and hence better counting statistics can be obtained. Phosphate buffered saline (PBS; 12 mM phosphate, 140 mM NaCl, pH 7.4) was used for X-ray scattering experiments. To ensure appropriate accurate corrections were made for solvent scattering, the protein sample was dialysed against its buffer, and the scattering of the buffer was subtracted from the scattering of the protein solution. Ideally, a sample of volume 0.5 ml and concentrated to 10 mg/ml should be used for X-ray experiments.

### **6.3.2.2 X-ray scattering at ESRF Grenoble**

X-ray scattering experiments were performed at the European Synchrotron Radiation facility (ESRF) at Grenoble, France. Synchrotron radiation is emitted from electrons that are accelerated while moving at speeds close to the speed of light. Several stages are involved in the production of synchrotron X-rays. Electrons are produced by a hot cathode source and then accelerated to almost the speed of light in a linear accelerator (Linac). The energy of the electrons leaving the Linac is increased in a booster synchrotron from 200 to 600 million electron volts (MeV). In the storage ring, the electrons are forced by 64 bending magnets and 320 quadrupoles to follow a circular orbit with 844.4 m circumference. As the electrons are deflected by the magnetic field, they emit 'white' X-rays of all wavelengths down tangential beamlines where experimental stations are set up to use the X-ray beam for dedicated experiments. The beam current at the start of its 'life time' in single bunch mode is

typically at 40 mA, but the current continually decreases as electrons are lost. The electrons are usually kept in orbit for up to 8 hours before the beam has to be regenerated. Small angle X-ray solution scattering experiments were performed on Station ID02 in single bunch mode in order to reduce the incident flux on the sample. A Si-111 channel-cut monochromator is used to monochromate the X-ray beam to a wavelength of 0.1 nm. The X-ray beam is then focused by a toroidal mirror. This monochromatisation method produces an X-ray beam that has negligible wavelength spread. Experiments were performed with beam currents within 200 mA and a ring energy of 6.0 GeV.

Samples were placed in a specially designed Perspex cell with 10 to 20  $\mu\text{m}$  thick ruby mica window. The ruby mica windows were held in place with Teflon plugs, and the windows were regularly changed during data collection sessions. The sample cell had a 1 mm path length, a surface area of 2 mm (vertical) by 8 mm (horizontal) and holds a maximum volume of 25  $\mu\text{l}$ . The sample cell was positioned in the X-ray beam by a brass sample holder which was maintained at 15°C using a water bath. The scattering intensities of the sample were measured using a FRELON CCD camera coupled with the Thomson X-ray intensifier (TH49-427) lens. This detector has an active area of  $1024 \times 1024$  pixels with a dynamic range of 14 bit and high count rate capability of 14-35 frames/sec, enabling millisecond range time-resolved experiments (Narayanan et al., 2001). The sample is aligned by scanning across the beam to monitor the transmitted intensity profile. This allows to position the sample with an accuracy of 10  $\mu\text{m}$ . For each data collection session the X-ray diffraction pattern of the powder silver behenate [ $\text{CH}_3(\text{CH}_2)_{20}\text{COOAg}$ ] was measured for calibrating the  $Q$  range based on a diffraction spacing of 5.84 nm (Huang et al., 1993). The distance between the detector and the sample was set so that intensities were measured from a minimum  $Q$  value of 0.07-0.09  $\text{nm}^{-1}$  to a maximum  $Q$  value of 2.0-2.2  $\text{nm}^{-1}$ . X-rays produce free radicals that can be destructive to proteins, causing them to aggregate quickly on exposure. To check for this possibility, the scattering intensity of each sample was measured for 0.5-1.0 second in 10 equal time frames, and the time frames were inspected for radiation-damage effects. The protein samples were measured in

alteration with their respective buffers in order to minimize buffer subtraction errors as the incident beam decreased in intensity. The product of incident flux and the sample transmission was measured using calibrated silicon p-i-n photodiodes embedded in the beamstop.

### **6.3.2.3 Reduction of ESRF scattering data**

ESRF scattering data were reduced to obtain scattering curves  $I(Q)$ . The data reduction routines include the correction of detector artifacts such as dark current, image distortion and spatial inhomogeneities, as well as normalization of intensities to incident photon flux and sample transmission. The online data reduction was automatically applied after exposure using the SPEC acquisition program and several important correction steps (Figure 6.3). The raw data image and the dark data image were saved to disk and a dark image was subtracted from the raw image as the first correction step. The spatial distortion of the image was then corrected using a set of spline functions to describe the distortion and generated an undistorted virtual image. In the third step, the flat field correction was performed through the division of the spatially corrected intensity pattern by the quantum efficiency of the detector (flat field). Finally, the normalization converted the raw data to absolute scattering intensity as the ratio between the numbers of scattering photons per spherical angle and the number of incident photons during exposure. A Lupolen sample was used as a standard scatterer to calibrate the absolute scattering intensities. The silver behenate diffraction pattern used for calculating the  $Q$  value of the detector consists of 13 well defined peaks (Figure 6.4). The spacing between successive peaks corresponds to a diffraction spacing  $d$  of 5.84 nm, and this enabled the  $Q$  values of the detector to be calculated ( $Q = 2\pi/d$ ) for combining with the intensities. The combination of the resulting intensity data files with the  $Q$  axis file produce scattering curve files.

### **6.3.3 Analysis of reduced scattering curves $I(Q)$**

#### **6.3.3.1 Guinier analyses**

At low  $Q$  values, the Debye equation is reduced to a Gaussian curve, and this

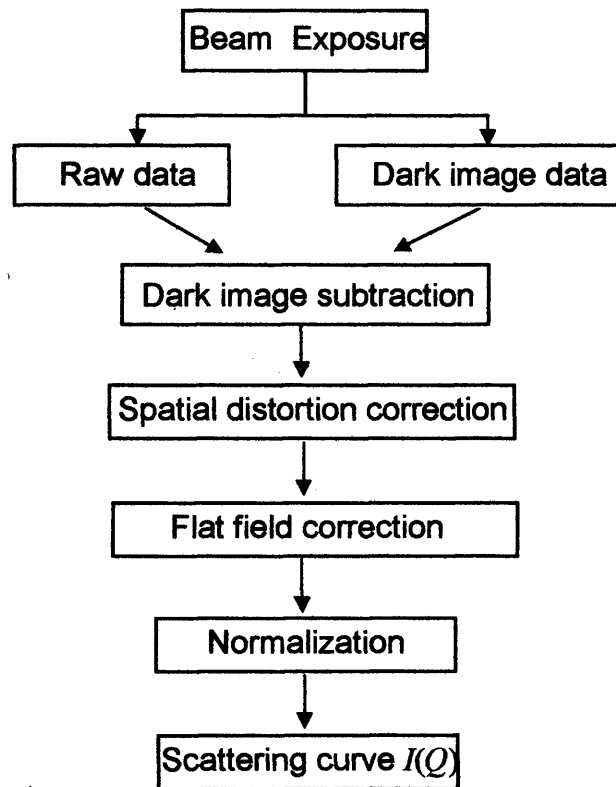


Figure 6.3 Flow diagram of the reduction procedure for ESRF X-ray scattering data.

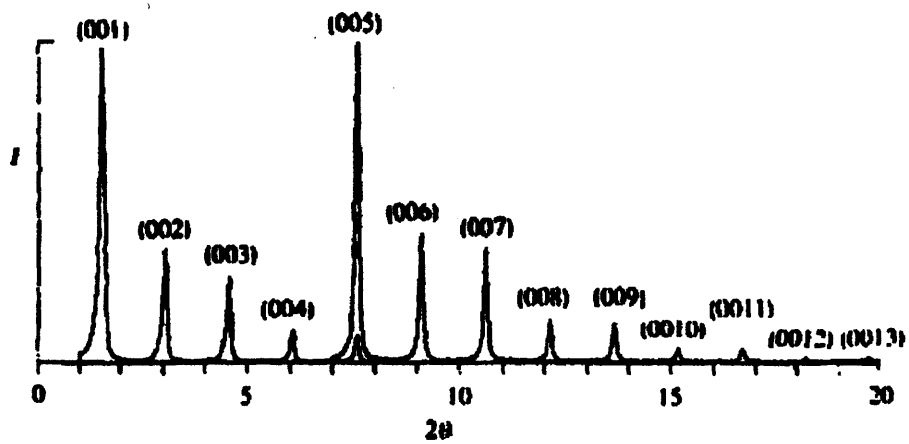


Figure 6.4 The X-ray diffraction pattern of silver behenate. A total of 13 well defined peaks at  $2\theta \leq 20^\circ$  are plotted. The peak separation is  $2\pi/5.84 \text{ nm}^{-1}$ . (Taken from Huang et al, 1993).

becomes the Guinier approximation. In this, the  $R_G$  is the radius of gyration and is defined as the root-mean-square distance of all scattering centres in the macromolecule from its centre of gravity

$$\ln I(Q) = \ln I(0) - \frac{R_G^2 Q^2}{3} \quad \text{Eq 6.3}$$

and  $I(0)$  is the intensity at zero scattering angle (Figure 6.1). This expression is valid in a  $Q \cdot R_G$  range up to 0.7-1.3 depending on the macromolecular shape.  $R_G$  and  $I(0)$  are determined from an experimental scattering curve by plotting  $\ln I(Q)$  against  $Q^2$  to give a straight line of slope  $-R_G^2/3$  and intercept  $\ln I(0)$ .  $R_G$  is a measure of elongation if the internal inhomogeneity is negligible, and a useful application of  $R_G$  is in the calculation of the anisotropy ratio of a macromolecule. The anisotropy is  $R_G/R_0$ , where  $R_0$  is the  $R_G$  of the sphere of volume equal to that of the macromolecule. For typical globular proteins, the anisotropy ratio is approximately 1.28 (Perkins, 1988). The intensity at zero scattering angle  $I(0)$  is proportional to  $M_r^2$ , i.e.  $I(0)/C$  is proportional to  $M_r$ ; where  $C$  = protein concentration.

Guinier plots were performed using the FORTRAN program SCTPL7 (J.T. Eaton & S.J. Perkins, unpublished software). The  $Q$  range selected for line-fitting returned a maximum  $Q \cdot R_G$  of approximately 1.5. Nonspecific aggregated proteins were identified by steeply curved Guinier plots at low  $Q$  values and were discarded.

### 6.3.3.2 Cross-sectional radius of gyration

If the protein has an elongated structure, Guinier-type analyses of the scattering curve at larger  $Q$  will give the mean radius of gyration of the cross-section  $R_{xs}$  and the mean cross-sectional intensity at zero scattering angle  $[I(Q)Q]_{Q \rightarrow 0}$  (Hjelm, 1985):

$$\ln[I(Q)Q] = [I(Q)Q]_{Q \rightarrow 0} - \frac{R_{xs}^2 Q^2}{2} \quad \text{Eq. 6.4}$$

$R_{xs}$  and  $[I(Q)Q]_{Q \rightarrow 0}$  are determined from an experimental scattering curve by plotting  $[I(Q)Q]$  against  $Q^2$  to give a straight line of slope  $-R_{xs}^2/2$  and intercept  $[I(Q)Q]_{Q \rightarrow 0}$ .

Generally, elongated proteins have a single  $R_{XS}$  value, and this was the case for anosmin-1 (Figure 6.1).

Cross-sectional plots were performed using SCTPL7. The  $Q$  range selected for line-fitting went from a minimum  $Q$  value which was greater than the largest  $Q$  values used in the Guinier  $R_G$  fits to a maximum  $Q \cdot R_{XS}$  of 1.5.

### 6.3.3.3 Estimation of macromolecular dimensions

Assuming a protein is shaped like an elongated elliptical cylinder, the  $R_G$  and  $R_{XS}$  values can be combined to determine its length  $L$  (Glatter O and Kratky O, 1982):

$$L = \sqrt{12(R_G^2 - R_{XS}^2)} \quad \text{Eq 6.5}$$

Alternatively,  $L$  is given by (Perkins et al, 1986):

$$L = \frac{\pi I(0)}{[I(Q)Q]_{Q \rightarrow 0}} \quad \text{Eq 6.6}$$

The consistency of these two calculations of  $L$  is a useful control of a correct cross-sectional analysis for a rod-like particle.

### 6.3.3.4 Real space distance distribution function

The scattering curve  $I(Q)$  represents the macromolecular structure in reciprocal space. The experimental  $I(Q)$  curve can be converted into real space by a Fourier transform over  $Q = 0 \leq Q \leq \infty$  :

$$P(r) = \frac{1}{2\pi^2} \int_0^\infty I(Q) Q r \sin(Qr) dQ \quad \text{Eq 6.7}$$

$P(r)$  is the distance distribution function and corresponds to the number of distance between any two volume elements within the macromolecule weighted by the product of their respective scattering densities. The maximum in  $P(r)$  is the most frequently occurring intramolecular distance.  $P(r)$  offers an alternative calculation of  $R_G$ .

$$R_G^2 = \frac{\int_0^\infty P(r)r^2 dr}{2 \int_0^\infty P(r) dr}$$

Eq 6.8

In practice,  $P(r)$  calculations result in termination errors because the experimental  $I(Q)$  curve cannot be measured at zero angle or at very large  $Q$ , and in addition high signal to noise ratios are associated with measurements at large  $Q$ . Mathematical procedures are needed to minimize these termination errors by the fitting of the experimental curve to B-splines, which are then transformed. This was performed using the GNOM program which is relatively automated and easy to use (Semenyuk and Svergun, 1991; Svergun, 1992).  $D_{\max}$  is the maximum macromolecular dimension, and therefore corresponds to the length  $L$ . In GNOM, the  $P(r)$  curve was selected according to several criteria: (1)  $P(r)$  should exhibit positive values; (2) the  $R_G$  from GNOM and Guinier analyses should agree; (3)  $P(r)$  should be zero when  $r$  is zero; (4)  $P(r)$  should be stable and reproducible for different experimental  $I(Q)$  curves when  $D_{\max}$  is varied over a reasonable range. The length  $L$  was determined from  $P(r)$  when this became zero at large  $r$ , however errors in  $L$  can be significant as a result of the low intensity of  $P(r)$  in this region.

## 6.4 Analytical ultracentrifugation

### 6.4.1 Sedimentation velocity experiments

One of the two major types of analytical ultracentrifugation experiment is the sedimentation velocity experiment. Movement of the solute away from the air-solvent interface (i.e. the meniscus) in sedimentation velocity experiment leads to formation of a solute concentration gradient, called the boundary. Because it is a concentration gradient, the boundary sediments and diffuses with time, leading to 'boundary spreading' over the course of the experiment. After a sufficient centrifugal force is applied, the boundary forms and subsequently moves toward the bottom of the cell at a rate proportional to the sedimentation coefficients of the components in the sample



(Figure 6.5). The rate of sedimentation in a centrifugal field is described by the Svedberg equation:

$$S_{20,w}^0 = v/\omega^2 r = M(1 - \bar{v}\rho)/Nf \quad \text{Eq 6.9}$$

$S_{20,w}^0$  is the sedimentation coefficient,  $v$  is the velocity of the molecule ( $v = dr/dt$ ),  $\omega^2 r$  is the strength of the centrifugal field ( $\omega$  is  $2\pi \cdot \text{rpm}/60$  and  $r$  is the radial distance from the centre of rotation),  $M$  is the molecular mass,  $f$  is the frictional coefficient (which is directly related to macromolecular shape and size),  $\rho$  is the density of the solvent,  $N$  is Avogadro's number ( $6.023 \times 10^{23}$ ), and  $\bar{v}$  is the partial specific volume of the solute ( $M$  and  $\bar{v}$  can be calculated from the molecular composition using SLUV) (Perkins, 1986).

The sedimentation coefficient of a glycoprotein is useful as this is a shape parameter that leads to the calculation of its frictional coefficient  $f$  that can then be compared with  $f$  calculated for a molecular model. The frictional coefficient can also be used to calculate the frictional ratio  $f/f_0$  of the glycoprotein.  $f_0$  is the frictional coefficient of the sphere with the same volume as the glycoprotein, which is given by Stokes law:

$$f_0 = 6\pi\eta r_s \quad \text{Eq 6.10}$$

where  $\eta$  is the viscosity of the solvent, which is assumed to be  $0.001002 \text{ N s m}^{-2}$  for aqueous protein solutions and  $r_s$  is the radius of the sphere. The frictional ratio is a measure of the elongation of the glycoprotein, and it is analogous to the use of the solution scattering anisotropy ratio  $R_G/R_0$ . The only quantity that needs to be measured is the sedimentation coefficient, re-expressed as:

$$S_{20,w}^0 dt = \frac{1}{\omega^2} \frac{dr}{r} \quad \text{Eq 6.11}$$

Integration over the distance travelled by the particle from  $r_0$  ( $t=0$ ) to  $r$  ( $t=t$ ) gives:

$$S_{20,w}^0 = \frac{1}{t\omega^2} \ln \frac{r}{r_0} \quad \text{Eq 6.12}$$

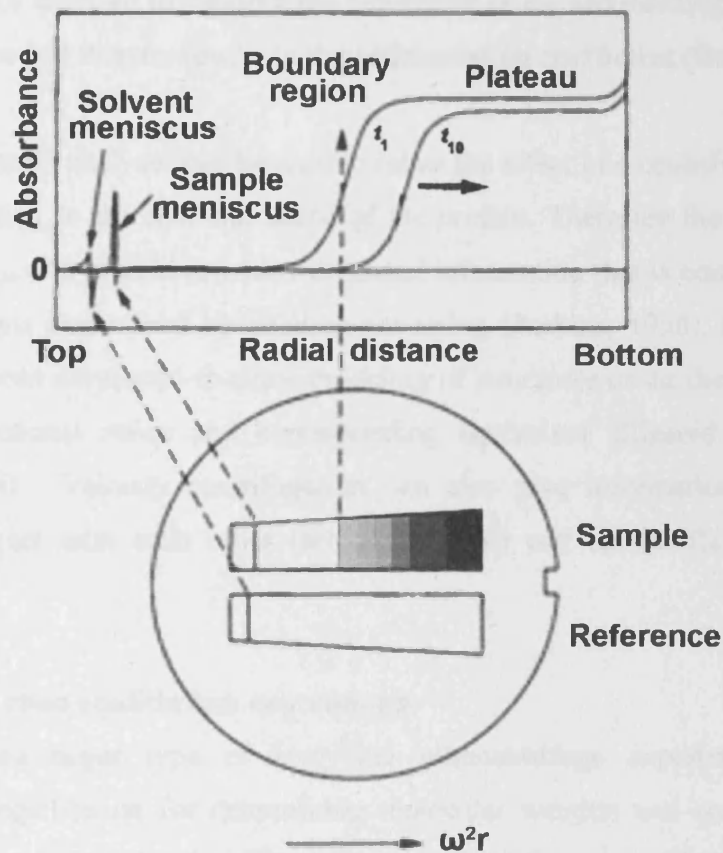


Figure 6.5 Sedimentation velocity cell design and data collection. The sample is placed in one sector (sample), and an aliquot of the solvent in the other sector (reference). The samples are centrifuged at high rotational velocity, generating a boundary that moves toward the bottom of the cell. As the boundary progresses down the cell, the concentration in the plateau region decreases from radial dilution and the boundary broadens from diffusion. The position of the boundary is indicated. A set of 10 scans ( $t_1$  represents the first scan, and  $t_{10}$  - the 10<sup>th</sup> scan) is collected at set time intervals using the absorbance optical system.  $\omega^2 r$  is the strength of the centrifugal field, and is also indicated above.

Because  $\omega$  is known,  $S_{20,w}^0$  is calculable (Chang, 1981). Suitable optical means such as refractive-index measurements using classical Schlieren optics or scanning absorption optics are used to measure the movement of the sedimenting boundary as a function of time and thereby results in the sedimentation coefficient (Harding, 1994).

Hydrodynamic analyses can be used to relate the effect of a centrifugal force on a protein in solution to the size and shape of the protein. Therefore the sedimentation coefficient  $S_{20,w}^0$  of a protein provides structural information that is complementary to  $R_g$  measurements determined by solution scattering (Perkins, 1998). Hydrodynamic theories have been developed to allow modeling of structures using the sedimentation coefficient, frictional ratios and corresponding equivalent ellipsoid of revolution (Harding, 1994). Velocity centrifugation can also give information on how the molecules interact with each other (self-association) and on the flexibility of the molecule.

#### 6.4.2 Sedimentation equilibrium experiments

The second major type of analytical ultracentrifuge experiments involves sedimentation equilibrium for determining molecular weights and consequently the oligomeric state of biomolecules. When the centrifugal force is sufficiently small, the process of diffusion significantly opposes the process of sedimentation, and an equilibrium concentration distribution of macromolecules can eventually be obtained. In diffusion, solute molecules move from a higher concentration to a lower one, while sedimentation reverses this process (Figure 6.6). When an equilibrium is established, no net flow occurs. For an ideal non-interacting single component system, the equilibrium distribution obtained is an exponential function of the buoyant mass of the macromolecule,  $M(1 - \bar{v}\rho)$ , as described by the equation:

$$\ln C(r)/C_0 = M(1 - \bar{v}\rho) \omega^2 (r^2 - r_0^2) / 2RT \quad \text{Eq 6.13}$$

$C(r)$  is the sample concentration at radial position  $r$ ,  $C_0$  is the sample concentration at a reference radial distance  $r_0$ , and  $R$  and  $T$  represent the gas constant and absolute

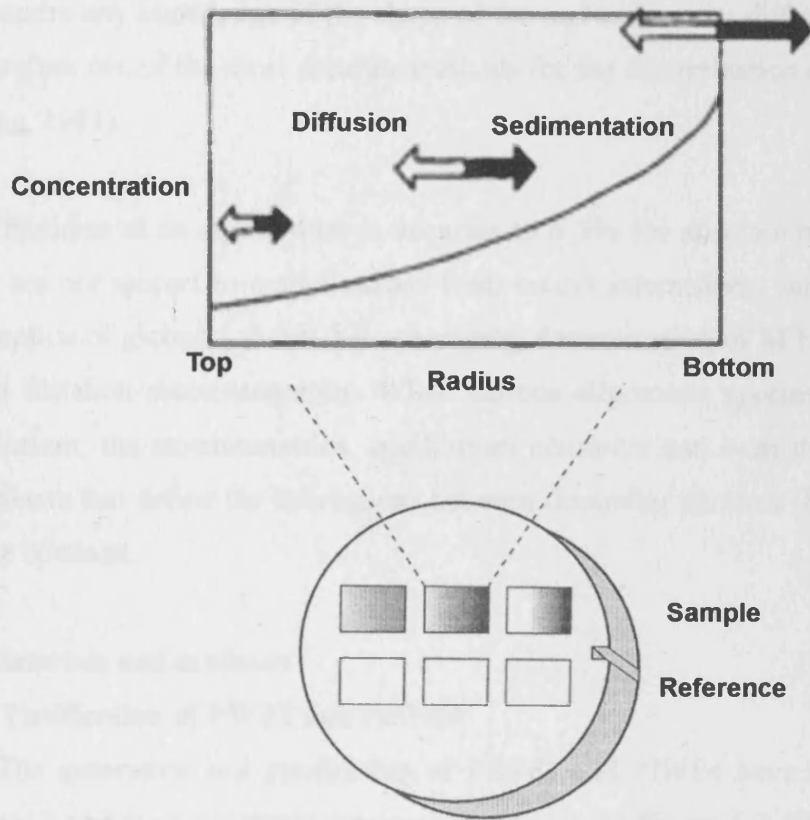


Figure 6.6 Schematic representation of sedimentation equilibrium. A six-channel sedimentation equilibrium cell is illustrated. Three sample-reference pairs are loaded into the cell. The samples are subject to centrifugation at moderate rotational velocity. The flow of solute due to sedimentation (black arrows) increases with radial distance. This process is balanced at equilibrium by the reverse flow from diffusion (open arrows), which increases with concentration gradient.

temperature, respectively. As with sedimentation velocity ultracentrifugation, optical techniques measure the protein concentrations  $C(r)$  and  $C_0$  at  $r$  and  $r_0$ . If  $\bar{v}$ ,  $\rho$ , and  $\omega$  are known,  $M$  can be calculated. Unlike velocity ultracentrifugation, the technique does not require any knowledge of the shape of the molecule or its diffusion coefficient. It is therefore one of the most accurate methods for the determination of molecular mass (Chang, 1981).

Sedimentation equilibrium is accurate to  $\pm 3\%$  for absolute molecular weights. They are not subject to complications from matrix interactions, sample dilution, and assumption of globular shape that accompany determination of  $M$  by techniques such as gel filtration chromatography. When various oligomeric species are in reversible equilibrium, the stoichiometries, equilibrium constants and even the thermodynamic parameters that define the interactions between dissimilar partners (hetero-association) can be obtained.

## **6.5 Materials and methods**

### **6.5.1 Purification of PWF1 and PIWF4**

The generation and purification of PIWF1 and PIWF4 have been described in Chapter 3 and their schematic structures are shown in Figure 6.7. The eluted fractions containing the highest concentration of the desired protein were harvested and dialysed into phosphate-buffered saline (total 220 mM NaCl), followed by concentrating to 0.5 ml using a 5,000 Da cut-off concentrator (Pierce).

### **6.5.2 X-ray scattering data acquisition at ESRF**

X-ray scattering data was measured in three independent sessions at the ESRF, Grenoble, France, at the solution scattering cameras on Station ID02. Experiments were performed with beam currents in a range between 9 and 12 mA for PIWF1 and 26 to 41 mA for PIWF4 with a ring energy of 6.0 GeV in single bunch mode to reduce radiation damage. PIWF1 between 0.6 and 1.2 mg/ml and PIWF4 between 0.2 and 0.4 mg/ml were measured at 15°C in 10 time frames with checks for radiation damage in Perspex cells, contained within mica windows of thickness 25  $\mu\text{m}$ . Data reduction

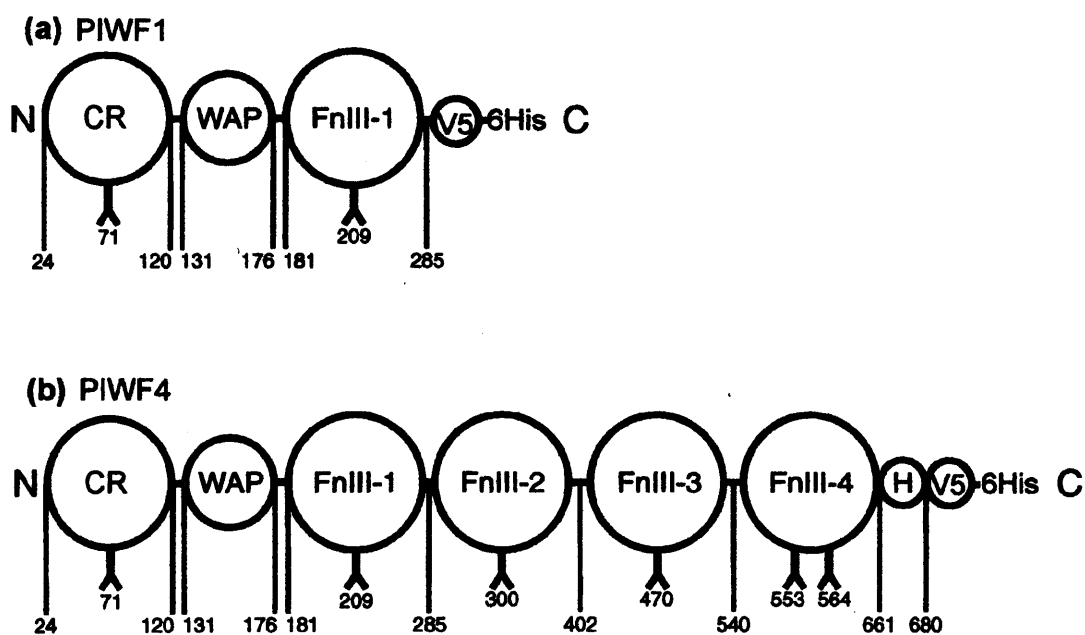


Figure 6.7 Domain structure of recombinant anosmin-1. Each domain in the truncated analogue PIWF1 (a) and the mature protein PIWF4 (b) is represented by a circle, followed by V5 and 6His epitope at its C-terminus. Residue numbering indicates the size of each domain. The location of six putative N-glycosylation sites is indicated by numbered Y symbols. The signal peptide is not shown but contributes residues 1-23. CR, cysteine-rich region; H, histidine-rich region; V5, the V5 epitope tag derived from simian virus 5; 6His, 6×histidine tag.

included the use of the Lupolen sample for the calibration of detector intensities, and a silver behenate salt standard for the calibration of the  $Q$  range.

### 6.5.3 Analysis of reduced X-ray data

In a given solute-solvent contrast, the radius of gyration  $R_G$  is a measure of structural elongation if the internal inhomogeneity of scattering densities has no effect. Guinier analyses at low  $Q$  give the  $R_G$  and the forward scattering at zero angle  $I(0)$  (Eq 6.3). This expression is valid in a  $Q \cdot R_G$  range up to 0.7 for extended rod-like particles, and is approximate in a  $Q \cdot R_G$  range up to 1.5 for more spherical particles in which it slightly underestimates the true  $R_G$  value. The relative  $I(0)$  values for samples measured in the same buffer during a data session gives the relative molecular mass  $M_r$  of the proteins when referenced against a suitable standard. If the structure is elongated, the mean radius of gyration of the cross-sectional intensity at zero angle  $(I(Q) \cdot Q)_{Q \rightarrow 0}$  is obtained from Eq 6.4. The  $R_G$  and  $R_{XS}$  analysis lead to the triaxial dimensions of the macromolecule and give the length of a protein if shaped like an elongated elliptical cylinder (Eq 6.5). Indirect transformation of the scattering data  $I(Q)$  in reciprocal space into real space to give the distance distribution function  $P(r)$  was performed using GNOM. This offers an alternative calculation of the  $R_G$  and  $I(0)$  that is based on the full scattering curve, and gives a model-independent maximum dimension of the macromolecule  $L$ .

### 6.5.4 Analytical ultracentrifugation data acquisition and analysis

Analytical ultracentrifugation was performed on a Beckman XL-I instrument in which the protein concentration distribution within the cell was monitored using its absorbance monitored at a single wavelength set between 280 nm and 295 nm, and its refractive index was measured by interferometry. Sedimentation equilibrium experiments were performed for PIWF1 at three concentrations between 0.24 mg/ml to 0.8 mg/ml in PBS + 80 mM NaCl and for PIWF4 at three concentrations between 0.12 mg/ml to 0.4 mg/ml in PBS + 80 mM NaCl. Data were acquired over 45 hours using six-sector cells in an AnTi 50 rotor with column heights of 12 mm at rotor speeds of 11,000 rpm, 14,000 rpm, 17,000 rpm and 20,000 rpm until equilibrium had been

reached at each speed, as shown by the perfect overlay of runs measured at five hour intervals. The molecular mass ( $M$ ) was analyzed on the basis of a single species using Beckman software provided as an add-on to Origin Version 4.1 (Microcal Inc), for which the partial specific volume  $\bar{v}$  for PIWF1 and PIWF4 were calculated to be 0.720 ml/g and 0.723 ml/g, respectively, from their sequences (Perkins, 1986a).

Sedimentation velocity data were acquired over 16 hours at rotor speeds of 35,000 rpm and 42,000 rpm in two-sector cells in an AnTi 50 rotor with solution column heights of 12 mm. The PIWF1 concentration was 0.8 mg/ml, and that for PIWF4 was 0.4 mg/ml, both being in PBS + 80 mM NaCl. For the  $g(s^*)$  analysis, successive absorbance and interference scans were recorded at eight minute intervals. In time derivative analysis, the five pairs of concentration scans within 10 scans were subtracted from each other and averaged to eliminate systematic errors arising from baseline distortions. The extrapolation of individual subtractions to the start time gives the  $g(s^*)$  function, which was computed using the DCDT+ program, from which the sedimentation and diffusion coefficients were determined from the peak position and width, respectively. The fits were determined in conditions when the maximum permissible measurable molecular mass was over 16 times the expected value, meaning that time broadening effects were negligible.

## 6.6 Experimental results and discussion

The preparations of PIWF1 and PIWF4 proteins for scattering and ultracentrifugation studies resulted in single bands in silver staining, indicating their high purity. X-ray scattering experiments were performed on PIWF1 and PIWF4. In Guinier analyses to determine the overall shape of the proteins from the radius of gyration  $R_G$  (a measure of elongation), the fits in Guinier plots were linear in an appropriate  $Q \cdot R_G$  range up to 1.2 for PIWF1 and PIWF4 (Figure 6.8 (a) and (b)), where  $Q = 4\pi \sin \theta/\lambda$  ( $2\theta$  = scattering angle;  $\lambda$  = wavelength). With PIWF1, the ten successive time-frames obtained during each X-ray data acquisition for each sample were unchanged, and therefore showed that no radiation damage effects had occurred. Radiation damage on PIWF4 was observed with successive sessions; however, the



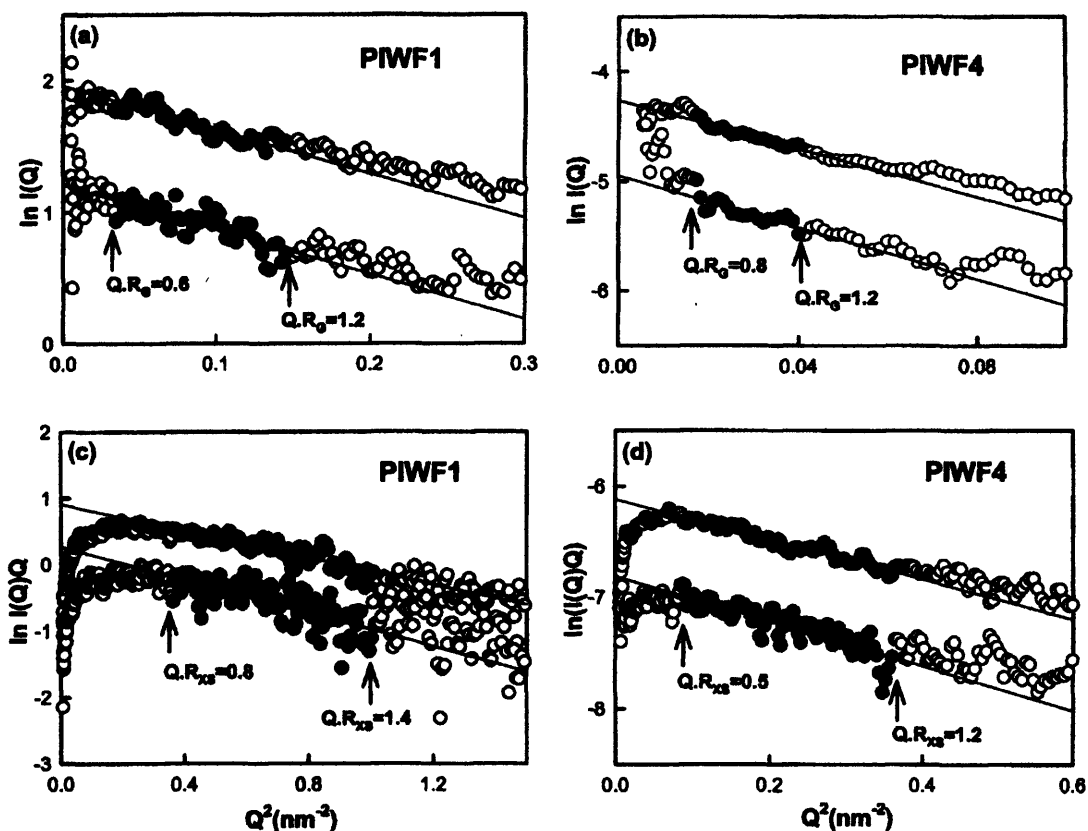


Figure 6.8 Guinier  $R_G$  and  $R_{XS}$  analyses of PIWF1 and PIWF4. The Guinier plots are displaced arbitrarily on the intensity axis for reason of clarity. The  $I(Q)$  data used to obtain  $R_G$  and  $R_{XS}$  values are denoted by filled circles in the  $Q \cdot R_G$  and  $Q \cdot R_{XS}$  enclosed by arrows depicted on the curves. (a) X-ray  $R_G$  fits using a  $Q$  range of 0.19-0.38  $\text{nm}^{-1}$  for PIWF1 at a concentration of 0.68 mg/ml (upper graph) and 0.34 mg/ml. (b) X-ray  $R_G$  fits using a  $Q$  range of 0.1-0.2  $\text{nm}^{-1}$  for PIWF4 at a concentration of 0.4 mg/ml (upper graph) and 0.2 mg/ml. (c) X-ray Guinier  $Q \cdot R_{XS}$  fits using a  $Q$  range of 0.6-1.0  $\text{nm}^{-1}$  for PIWF1. (d) X-ray Guinier  $Q \cdot R_{XS}$  fits using a  $Q$  range of 0.3-0.6  $\text{nm}^{-1}$  for PIWF4.

first time-frame for each diluted sample was consistently measured, and thus only the first acquisition time frames were analyzed. The mean final X-ray  $R_G$  of PIWF1 was  $3.09 \pm 0.21$  nm, and that for the X-ray  $R_G$  of PIWF4 was  $7.78 \pm 0.97$  nm.

In cross-sectional Guinier analyses to determine the shorter axes of the two proteins from the cross-sectional radius of gyration  $R_{xs}$ , a single linear fit range at  $Q$  values higher than those used for the Guinier  $R_G$  plots above was identified for both PIWF1 and PIWF4 (Figure 6.8 (c) and (d)). These  $Q$  range results in mean cross-sectional radii of gyration  $R_{xs}$  of  $1.49 \pm 0.13$  nm for PIWF1 and  $1.88 \pm 0.07$  nm for PIWF4. The similarity of  $R_{xs}$  value shared by these two proteins suggested that it monitors the interdomain orientations between adjacent N-terminus CR, WAP domain and FnIII domains. It can therefore be inferred that this interdomain orientation is similar between these two proteins. If the solution structures of PIWF1 and PIWF4 are approximates as an elongated elliptical cylinder, the length of the cylinder  $L$  was then calculated. The  $R_G$  and  $R_{xs}$  values resulted in a length of  $9.6 \pm 0.7$  nm for PIWF1 and an equivalent length estimate of  $26.1 \pm 3.5$  nm for PIWF4.

The indirect transformation of the scattering curve  $I(0)$  (measured in reciprocal space) into real space gives the distance distribution function  $P(r)$ . This represents the summation of all the distances  $r$  between every pair of atoms within the protein. The  $R_G$ ,  $I(0)$  and  $L$  values that are calculated from the  $P(r)$  curve are now based on the full scattering curve in the  $Q$  range between  $0.013 \text{ nm}^{-1}$  and  $2.2 \text{ nm}^{-1}$ , and give another determination of  $L$  that is now independent of shape assumptions. The  $R_G$  values calculated from the  $P(r)$  were in good agreement with the Guinier values. The most frequently occurring distance for PIWF1 is  $r = 2.5$  nm from the maximum  $M$  in the  $P(r)$  curve, and its length  $L$  was determined to be  $11 \pm 1$  nm at the point when  $P(r)$  becomes zero at large  $r$  (Figure 6.9 (a)). The  $P(r)$  curve gives the maximum  $M$  at an  $r$  value of 4 nm and length  $L$  of  $24 \pm 1$  nm for PIWF4 (Figure 6.9 (b)).

Analytical ultracentrifugation provided an independent monitor of the solution scattering results. Molecular masses were determined using equilibrium experiments

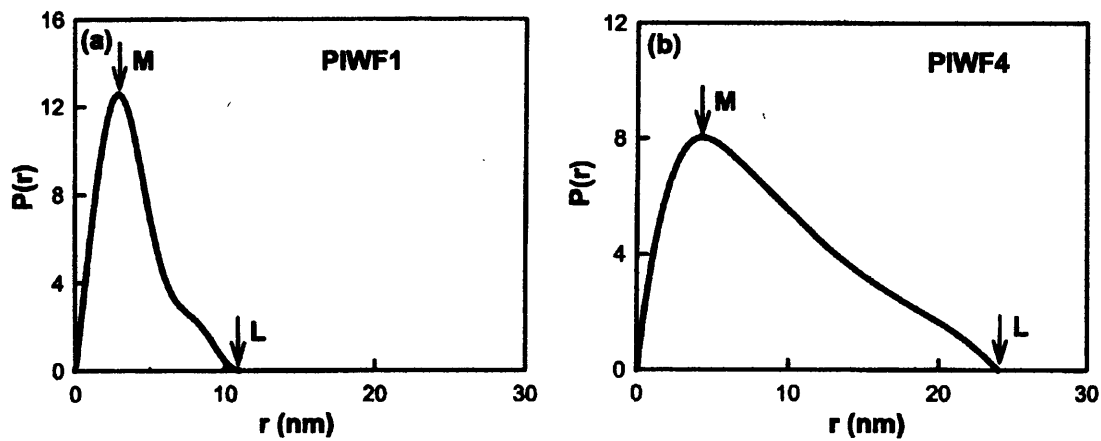


Figure 6.9 Distance distribution functions  $P(r)$  for PIWF1 (a) and PIWF4 (b). The maximum of the  $P(r)$  curve is denoted by M, the most frequently occurring distance within PIWF1 and PIWF4. The maximum dimensions of PIWF1 and PIWF4 are denoted respectively by L, which is taken to be where the  $P(r)$  curve intersects  $P(r) = 0$ .

(Materials and Methods). Curve fits assumed the presence of a single species, and this resulted in excellent fits with random small residuals (Figure 6.10 and 6.11).

The sedimentation coefficient  $S_{20,w}^0$  from sedimentation velocity experiments monitors macromolecular elongation and complements the  $R_G$  determination. Typical time-derivative analysis using the  $g(s^*)$  method to analyse pairs of sedimentation boundaries resulted in  $S_{20,w}^0$  values of 2.46 S (absorbance) and 2.32 S (interference) for PIWF1 (Figure 6.10 (a) and (b)), 3.31 S (absorbance) and 3.26 S (interference) for PIWF4 from the peak centres in Figure 6.10 (c) and (d). In the final analyses, the mean  $S_{20,w}^0$  values was determined to be  $2.40 \pm 0.13$  S from a total of 15 determinations for PIWF1, and  $3.27 \pm 0.77$  S from a total of 18 determinations for PIWF4.

Molecular masses were determined using sedimentation equilibrium experiments (Materials and Methods). Curve fits assumed the presence of a single species, and this resulted in excellent fits with random small residuals (Figure 6.11 (a)-(d)). Based on curve fits for rotor speeds of 17,000 rpm, 20,000 rpm and 25,000 rpm, the molecular masses of PIWF1 were similar at  $38,000 \pm 700$  Da for interference and  $38,000 \pm 1,200$  Da for absorbance (Figure 6.11 (a) and (b)). A systematic decrease in the molecular mass of PIWF4 was observed with increasing rotor speed. A rotor speed of 14,000 rpm gave PIWF4 molecular mass values of  $90,000 \pm 1400$  Da and 17,000 rpm for  $77100 \pm 500$  Da respectively, and the representative curve fits were shown in Figure 6.11 (c). Consistent with the predicted molecular mass, the slow rotor speed of 11,000rpm gave  $94,500 \pm 8,300$  Da for more diluted PIWF4 (Figure 6.11 (d)). These experiments confirmed that anosmin-1 is a monomer, but the decrease in molecular weight is consistent with some polydispersity, which is attributed to variable carbohydrate contents at the six glycosylation sites in anosmin-1 (Figure 6.7).

The length of 11 nm for PIWF1 and 24 nm for PIWF4 gave a difference of 13 nm which corresponds to the total length of the C-terminal three FnIII domains. In fibronectin the dimensions of individual FnIII domains have been measured by crystallography, resulting in an average length of about 3.5 nm. The presence of these

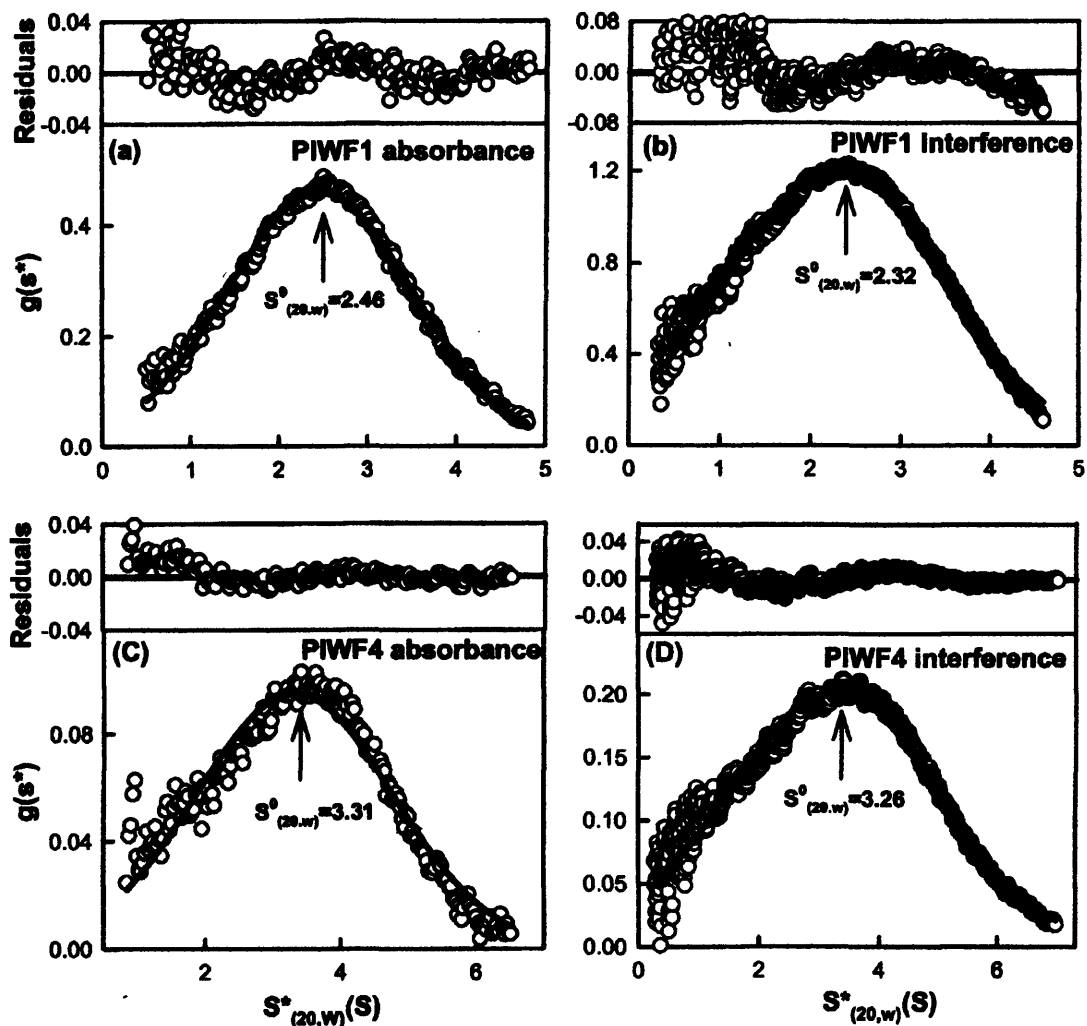


Figure 6.10 Sedimentation velocity fit of the  $g(s^*)$  distribution for PIWF1 and PIWF4. Ten scans recorded at eight minute intervals were recorded using absorbance (a, c) and interference (b, d) optics at 280 nm and a rotor speed of 35,000 rpm for PIWF1 (a, b) at 1.12 mg/ml and PIWF4 (c, d) at 0.32 mg/ml. Analysis gave  $s^0_{(20,w)}$  values of 2.46 S (a) and 2.32 S (b) for PIWF1 and 3.31 (c), 3.26 S (d) for PIWF4 respectively, as arrowed.

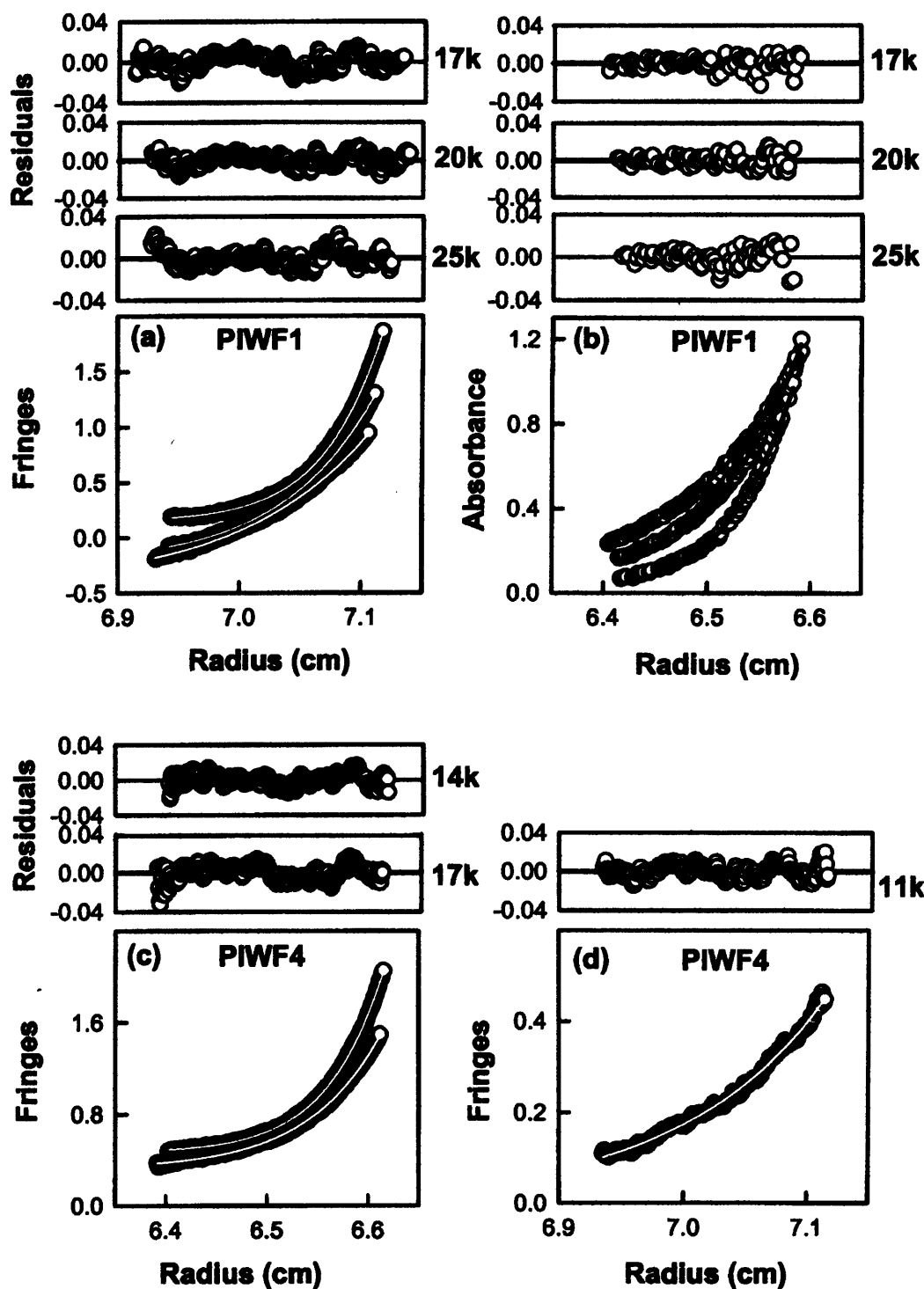


Figure 6.11 Sedimentation equilibrium fit for PIWF1 and PIWF4. Best-fit curves for PIWF1 at rotor speeds of 17,000 rpm, 20,000 rpm and 25,000 rpm using interference (a) and absorbance optics (b). Best-fit curves for PIWF4 at rotor speeds of 14,000 rpm, 17,000 rpm (c) and 11,000 rpm (d) using interference optics. The residuals of the curve fits are shown in the upper panels respectively.

three FnIII domains would measure ~10.5 nm in total length if arranged head to tail, compatible to the 13 nm obtained in the present X-ray scattering experimental results. This result is consistent with the expectation for the elongated conformation of the C-terminal FnIII domains in anosmin-1.

Although hydrodynamic analysis is less straightforward for evaluating the shape of a protein molecule, it is still considered as a complementary method for X-ray scattering and electron microscopy analysis. The most useful hydrodynamic parameter is  $S_{\max}/S$ , where  $S_{\max}/S$  is the maximum possible sedimentation coefficient for a protein of the given mass, corresponding to a sphere of the minimum diameter to contain the given mass of protein, with no water of hydration. The ratio  $S_{\max}/S$  is the same as  $f/f_{\min}$ , where  $f$  is the actual frictional ration of the hydrated protein, and  $f_{\min}$  is the friction coefficient of the unhydrated protein (Schurmann et al., 2001). The theoretical value of  $S_{\max}$  can be calculated by the equation:  $S_{\max} = 0.00361 \times M^{2/3}$  Svedberg unit. Some typical numerical values for protein from 10,000 to 1,000,000 Da are sphere (Protein structure, Harold P. Erickson, Jan. 2003, <http://www.cellbio.duke.edu/Faculty/Erickson>):

Protein Mr (kDa)	10	25	50	100	200	500	1,000
$S_{\max}$	1.68	3.1	4.9	7.8	12.3	22.7	36.1

The guideline for estimation of protein overall structures is

1. No protein has  $S_{\max}/S$  smaller than 1.15-1.2.
2. Globular proteins has  $S_{\max}/S$  between 1.25-1.4
3. Moderately elongated proteins is in the range of 1.6-1.9
4. Highly elongated protein is in the range of 2.0-3.0.
5. Very long, thread-like molecules can have  $S_{\max}/S$  in the range of 3.0-4.0.

PIWF1 is 38 kDa, and has a measured sedimentation coefficient of 2.4 S, whereas PIWF4 with 90 kDa has a 3.27 S. The predicted  $S_{\max}$  for a 38 kDa protein is 4.03 S and for 90 kDa is 7.22 S.  $S_{\max}/S$  can be calculated as 1.68 for PIWF1 and 2.21 for PIWF4. These results suggest a moderately elongated conformation for PIWF1 and a higher elongation for PIWF4. This result is consistent with the observation derived

from the X-ray scattering data that the C-terminal three FnIII domains in anosmin-1 should be fully extended.

### 6.7 Homology modelling of anosmin-1 domains

There are six domains to be modelled (Figure 6.7 (b)). Their sequences and the linkers are defined in Figure 6.12. Homology models of the WAP and four fibronectin domains in PIWF1 and PIWF4 were generated previously in our laboratory by Dr A. Robertson using InsightII and its packages (Biosym/San Diego) on Silicon Graphics O2 workstations as previously described (Robertson et al., 2001). Briefly, the FnIII domains were modelled using the known structures of *Drosophila* neuroglian (PDB: 1CFB), human fibronectin (PDBs: 1FNF, 1TTG, 1TTF and 1FNA), human tissue factor (PDBs 2HFT, 1BOY and 1DAN), tenascin (PDB: 1TEN), erythropoietin (PDB: 1EBP), human growth hormone (PDB: 3HHR), and murine granulocyte colony-stimulating factor (PDB: 1GCF). The WAP domain was based on the crystal and NMR structures of the closely homologous WAP domain from elafin (PDB codes: 1FLE, 1REL and 2REL).

The sixth domain is the N-terminal 107 residues of both PIWF1 and PIWF4 that comprised the CR which is attached to the WAP domain by a short linker (Figure 6.12). Its structure was unknown, and database searches were performed in collaboration with Dr. J.T.Eaton. A psi-BLAST search of the CR sequence against a non-redundant database of protein sequences identified the subtilisin-like proprotein convertase (gi: 7435770) as a homolog sharing 28% sequence identity and 38% similarity with an 80 residue section of the CR where seven of the ten CR cystines were conserved. This convertase in turn shared 38% sequence identity and 45% similarity over the same region with rat epidermal growth factor receptor (EGFR, gi: 24987353, PDB: 1N8Y), whose structure has been determined by X-ray crystallography. Consequently, the CR was aligned with EGFR. No significant alignment was found using the program BLAST. However, alignment with the program lalign, performed using the less stringent gap opening penalty of -10 (default = -14) produced the alignment shown in



(a) Sequence of PIWF1 for modelling

```

          30      40      50      60      70
-|-----+-----|-----+-----|-----+-----|-----+
CR      AAGPGAAAARRLDESLSAGSVQRARCASRCLSLQITRISAFFQHFN
          80      90      100     110     120
-----|-----+-----|-----+-----|-----+-----|-----+
      NGLVWCQNHKQCSKCLEPCKESGDLRKHQCQSFCEPLFPKKSYECLTSC
          130
-----|-----+
Linker 1 EFLKYILLVK
          140     150     160     170
-----|-----+-----|-----+-----|-----+
WAP domain      QGDCPAPEKASGFAAACVESCEVDNECSGVKKCCSNGCGH
-----|-----
      TCQVPK
          180
-----+-----|-----
Linker 2      TLYKGVPLKPR
          190     200     210     220
-----+-----|-----+-----|-----+
FnIII-1      KELRFTELQSGQLEVKWSSKFNISIEPVIYVQ
          230     240     250     260     270
-----|-----+-----|-----+-----|-----+
      RRWNYGIHPSEDDATHWQTVAQTTDERVQLTDIRPSRWYQFRVAAVNVHG
          280
-----|-----+-----
      TRGFTAPSKHFRSS
          285
          |-----
Linker 3      KDPSA
V5-epitope      GKPIP NPLLGLDSTRTG
6-His tag      HHHHHH
```

**(b) Sequence of PIWF4 for modelling**

The CR + WAP domain + FnIII-1 are the same as in PIWF1 shown in (a).

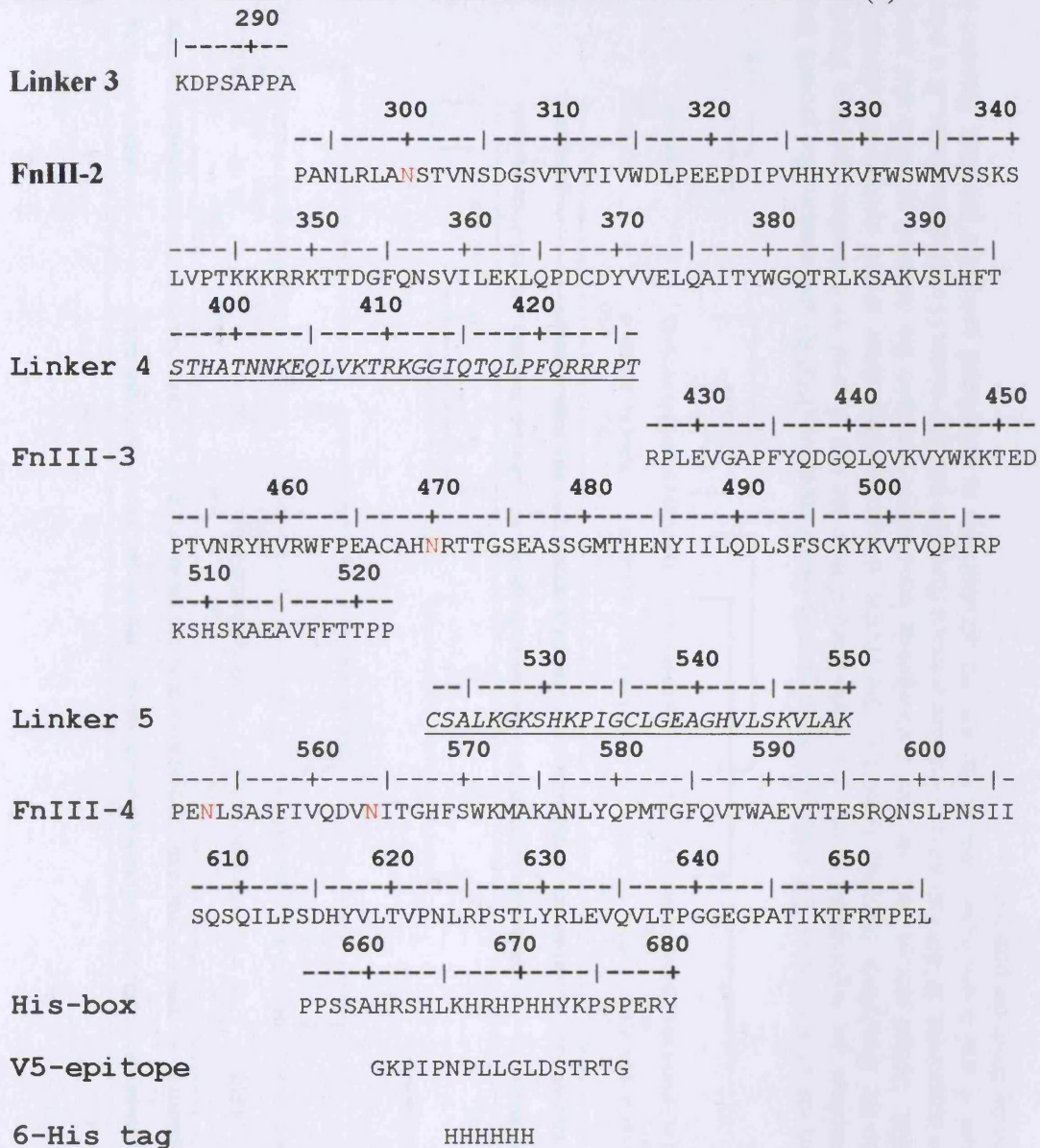
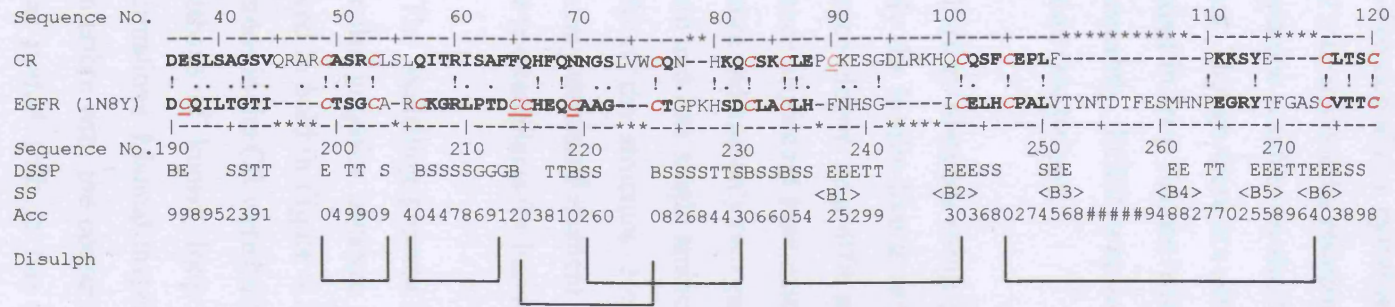


Figure 6.12 The amino acid sequence and residue numbering of the individual domains of recombinant anosmin-1. The sequences of PIWF1 (a) and PIWF4 (b) for modelling are shown. The linker peptides are indicated by underlining. The six glycosylation sites are marked in red.



Epidermal Growth Factor Receptor



Insulin-like Growth Factor Receptor

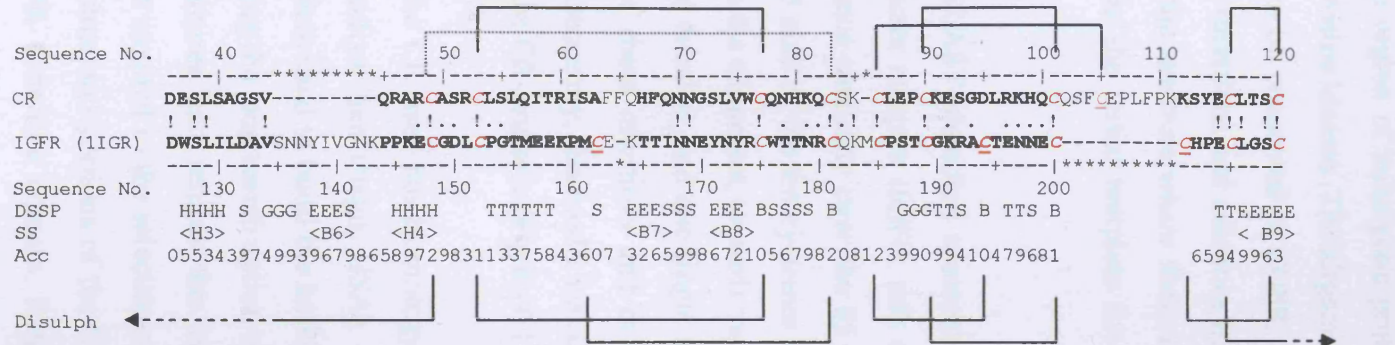


Figure 6.13 Sequence alignments of anosmin-1 CR with epidermal growth factor receptor (EGFR) and insulin-like growth factor receptor (IGFR). Cysteine residues are highlighted in red, and underlined if they are not aligned with another cysteine. Brackets below the alignment indicate the disulphide bonding pattern of the crystal structure, while those above indicate the disulphide bonding pattern for the model. Dotted arrows indicate that a disulphide bond exists between the denoted cysteine and another cysteine that is not part of the alignment. DSSP secondary structure is taken from the pdb file where H is an alpha-helix, E is a beta-strand, B is a beta-ladder, and T and S are loops. Acc is the solvent accessibility as calculated using the program Naccess and hashes represent residues missing from the pdb file.

Figure 6.13, with 25.8% residue identity and 45.8% residue similarity over the 85 residues of the CR sequence used in the alignment. This segment of EGFR constitutes a furin-like domain, a cysteine-rich region of eukaryotic proteins which is involved in signal transduction by receptor tyrosine kinases. The alignment also showed nine of the ten cysteine residues in the CR to be conserved in EGFR, including three disulphide bridges. Though there are several insertions and deletions in the alignment, these were all found in loop regions within the structure where these are readily accommodated. Consequently, EGFR was used as the initial template for the modelling of the CR structure (see below).

Further searches using psi-BLAST identified a second homologue for the CR, namely the insulin-like growth factor receptor (IGFR, pdb code: 1IGR), with 22.4% sequence identity and 40% sequence similarity over the 85 residues of the CR. This sequence alignment now matched nine of the ten cysteines in the CR with the IGFR structure and had only two gaps in the alignment, towards the beginning and end of the domain and one single amino acid deletion, and one single amino acid insertion in the middle of the structure. None of these insertions and deletions occurred inside a secondary structural element. Consequently, this model was considered to be the better of the two templates for building the CR structure (Figure 6.13).

The modelling process for the CR used the Homology module of the InsightII molecular graphics package (Accelrys, San Diego, USA). The conserved residues (marked in bold in Figure 6.13) were used to build the backbone of the CR structure. Insertions in the CR were built using the loop search option of Homology, which scans a database of known loop structures and returns the ten most favourable loop conformations. Manual inspection resulted in the selection of loop regions which did not interfere with the conserved structural portions of the CR, and which followed a similar spatial path to the EGFR furin-like domain. Residues either side of the deletions in the CR structure were manually repositioned and energy minimised by the lego-loop option of the molecular visualisation and building package O (Jones et al., 1991).

Of the five disulphide bridges present in the IGFR structure, two are conserved in the CR (Cys 53-Cys77, Cys90-Cys101), and another two can be generated by minor rearrangement of the loops in the structure (Cys87-Cys105, Cys116-Cys120). A fifth disulphide bond (Cys49-Cys83) (marked with a dotted line in Figure 6.13) could be generated, but this would require gross conformational changes in the N-terminal part of the CR. As a result, these residues were left as free cysteines. Both the CR and IGFR structures are highly similar (Figure 6.14). It was concluded that the pattern of Cys disulphide bridges in the CR is well understood, using the IGFR structure, especially in the lower half of the structure as shown in Figure 6.14.

Oligosaccharide chains were added to the six glycosylation sites on the FnIII N-linked glycosylation sites and the CR as required (N<sup>71</sup>, N<sup>209</sup>, N<sup>300</sup>, N<sup>470</sup>, N<sup>553</sup> and N<sup>564</sup>) (Figure 6.12). The oligosaccharide structure was taken from the Fc fragment of human IgG1 KOL (1FC1) and extended using the BIOPOLYMER package into a bi-antennary complex-type structure Asn-GlcNAc-GlcNAc-Man-(Man-GlcNAc-Gal-NeuNAc)<sub>2</sub>, and oriented to point away from the domain surface to which it was attached.

### **6.8 Construction of the full models for PIWF1 and PIWF4**

The CR, WAP and FnIII-1 domains are separated from one another by linkers of varying lengths (Figure 6.12). These linker peptides were modelled in the BIOPOLYMER package of InsightII with extended conformations. The peptides were then subjected to a maximum of 300 cycles of steepest descent and Polak-Ribiere conjugate gradient minimisation at a temperature of 773K using the DISCOVER\_3 package with default convergence values. This was followed by a 5000 fs molecular dynamics simulation, and a further  $1.5 \times 10^6$  fs simulation saving the linker structure every 100fs. This generated libraries of 1,000 peptide conformations that will in future be used to generate several thousand models of intact PIWF1 and PIWF4 by joining the peptide linkers with the separate domain homology models for a thorough analysis of

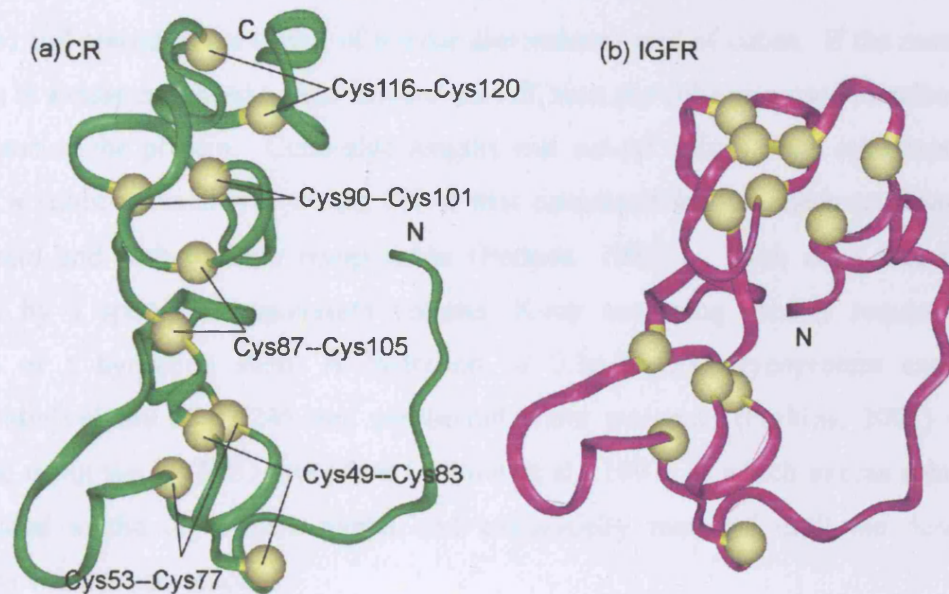


Figure 6.14 Structural comparison of the CR domain of anosmin-1 and IGFR. Ribbon representations show the comparison of the homology model for the anosmin-1 CR (a) with that of IGFR cysteine rich region (b). The  $\alpha$ -carbon atoms of cysteine residues are represented by yellow spheres and the disulphide bridges are also indicated. N: N-terminus; C: C-terminus.

the structure of these proteins. For the purpose of this thesis, only a preliminary analysis of the overall structures of PIWF1 and PIWF4 has been made and these are set out below.

### **6.8.1 Debye scattering curve modelling of PIWF1 and PIWF4**

In order to calculate theoretical scattering curves, Debye sphere models were constructed from the protein models. For each construct, an extended model was generated and placed in the centre of a three dimensional grid of cubes. If the number of atoms in a cube exceeded a user-defined cut-off, then the cube was used to calculate the volume of the protein. Cube side lengths and cut-off values were optimised to produce a volume which was within 1% of that calculated for the construct from its amino acid and carbohydrate composition (Perkins, 1986b). Each cube was then replaced by a sphere of equivalent volume. X-ray scattering models require the addition of a hydration shell. A hydration of 0.3g H<sub>2</sub>O/g glycoprotein and an electrostatic volume of 0.0245 nm<sup>3</sup> per bound water molecule (Perkins, 2001) was modelled using the HYPRO procedure (Ashton et al., 1997) in which excess spheres were added to the dry sphere model and sequentially removed until the desired hydration volume was reached.

The X-ray scattering curves for PIWF1 and PIWF4 were calculated assuming a uniform scattering density for the spheres, using the Debye equation adapted for spheres (Perkins and Weiss, 1983). The X-ray scattering curves were calculated from the hydrated models assuming no wavelength spread or beam divergence as these are considered minimal for synchrotron X-ray radiation. The  $R_G$  and  $R_{XS}$  values of the models were calculated in the same  $Q$  range as the experimental Guinier fits, and the assumption of a  $\pm$  5-10% deviation from the experimental values  $R_G$  and  $R_{XS}$  was assumed to constitute an accurate model. Additionally, the models were assessed using a goodness-of-fit  $R$ -factor defined by analogy with protein crystallography and based on the experimental curves in the  $Q$  range extending to 2.0 nm<sup>-1</sup> (denoted  $R_{(2.0)}$ ) such that:



$$R_{(2.0)} = 100 * \sum_{Q=0}^{Q=2.0} \frac{|\ln I(Q)_E - \ln I(Q)_M|}{\ln I(Q)_E}$$

where  $\ln I(Q)$  is the natural logarithm of the intensity,  $I$ , at scattering angle,  $Q$ , and the subscripts E and M refer to the experimental and model data respectively. From this it can be seen that the lower the value of  $R_{(2.0)}$ , the better the model data fits the experimental data.  $R$ -factors in the range 1.2 – 8.7 % represent good fits (Perkins et al., 1998).

### 6.8.2 PIWF1 and PIWF4 models

The approximate maximal lengths of each domain are as follows: CR, ~4.8 nm; WAP domain, ~4.3 nm, and each FnIII domain ~4.2 nm. Because the  $P(r)$  curves of the PIWF1 and PIWF4 showed maximal molecular lengths of 11 nm and 24 nm respectively (Figure 6.9), it can already be deduced from the difference of 13 nm between them that the C-terminal three FnIII domains of predicted length 12.6 nm lie in an extended conformation. The sum of the lengths of the CR, WAP and the first FnIII domain gives ~13.3 nm, which is comparable with the experimental length of 11 nm for PIWF1 if this is extended. Hence it was assumed that the two structures for PIWF1 and PIWF4 would be relatively elongated.

To assess the domain structure of PIWF1 and PIWF4, the domains of PIWF1 were aligned in InsightII to produce a number of linear models from which theoretical X-ray scattering curves were generated. Table 6.1 shows the comparison of the  $R_G$  and  $R_{XS}$  values of the models with the experimentally derived values from X-ray solution scattering, and the associated  $R$ -factors. While the  $R_G$  values for both the extended and compact models of PIWF1 are close to those experimentally derived, the  $R_{XS}$  value for the extended form is less than half that required, while the  $R_{XS}$  value for the compact form is within 10% of the experimental value. These results suggest that the compact model for PIWF1 is a fairer representation of the protein in solution than is the elongated form used. In contrast, the values derived for an extended model of



PIWF4 are better than those generated using a compact N-terminus (Figure 6.15). This is unexpected as it would be presumed that both PIWF1 and PIWF4 could possess similar domain structures. There is no difference in the calculated  $R_{XS}$  values, and the compacted PIWF4 molecule generates an  $R$ -factor that is only slightly worse than that of the elongated form. The  $R_G$  value of the compacted form of PIWF4 is 66% of that derived from experimental measurement, whereas the extended model has an  $R_G$  value which is 80% of the target value. Though there are not enough data at present to definitively state that the elongated form is the correct model of PIWF4, it is certainly the best model until a more complete analysis of the modelling is carried out. The quality of both the PIWF1 and PIWF4 models can be seen in the  $\ln I(Q) \text{ v } Q$  curve fits below (Figure 6.16). The significance of these models is discussed in Chapter 7.

Table 6.1 Summary of the results of modelling PIWF1 and PIWF4 in compact and extended conformations

Model	$R_G$ Range	$R_G$ Experiment	$R_G$ Model	$R_{xs}$ Range	$R_{xs}$ Experiment	$R_{xs}$ Model	Rfactor
PIWF1- extended	0.19-0.38	3.09+/- 0.21	3.54+/- 0.01	0.6-1.0	1.49+/-0.13	0.67+/-0.01	13.9
PIWF1 compact	0.19-0.38	3.09+/- 0.21	3.21+/-0.04	0.6-1.0	1.49+/-0.13	1.35+/-0.00	6.0
PIWF4- extended	0.1-0.2	7.78+/-0.97	6.16+/-0.02	0.3-0.6	1.88+/-0.77	1.33+/-0.01	11.4
PIWF4 compact	0.1-0.2	7.78+/-0.97	5.13+/-0.01	0.3-0.6	1.88+/-0.77	1.33+/-0.00	13.6

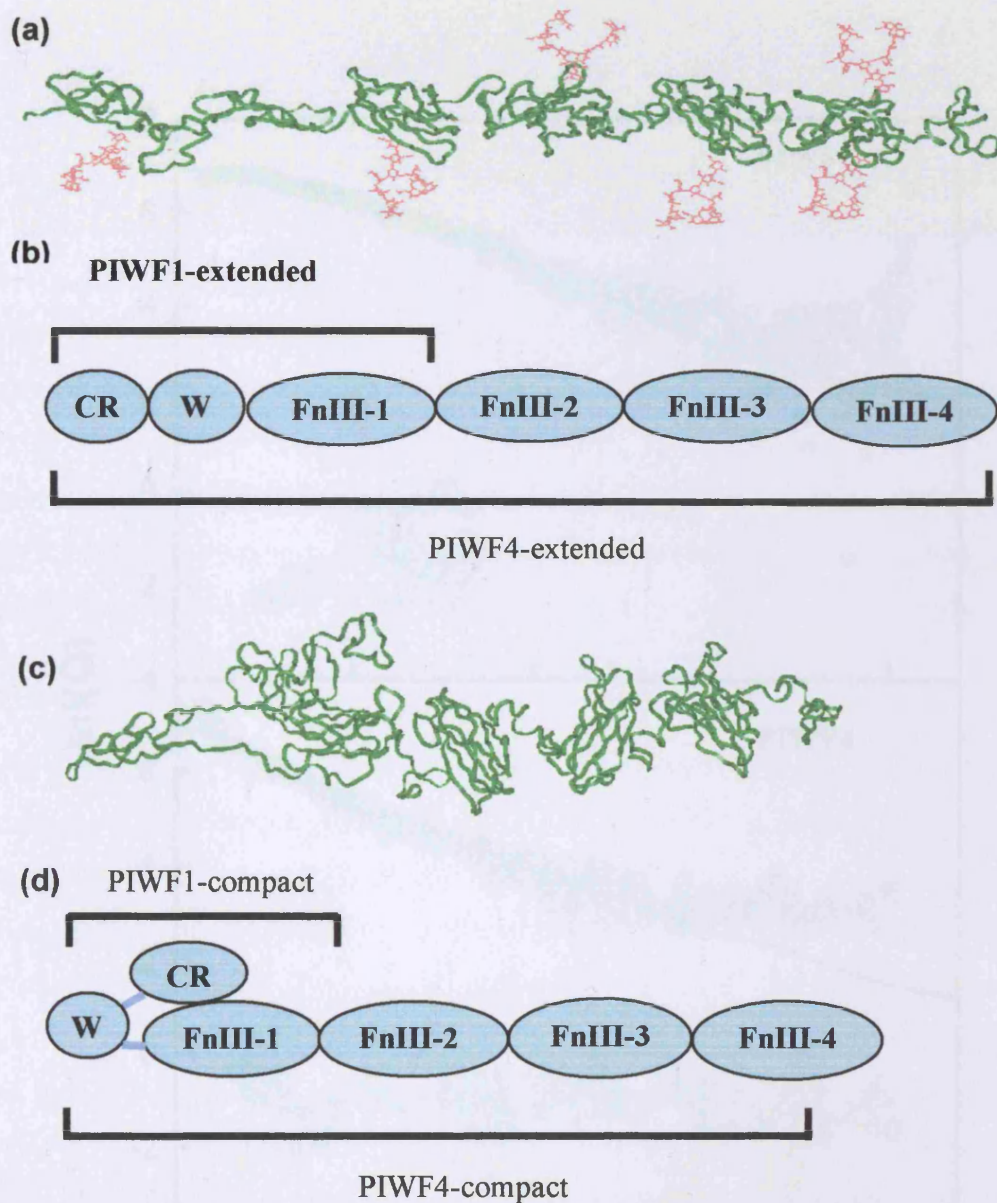


Figure 6.15 Representations of extended and compact forms of the PIWF4 construct. (a) Ribbon diagram of the extended conformation of PIWF4 used in modeling. The polypeptide backbone is illustrated in green, while the glycosylation are represented in red. (b) Cartoon representation of (a) showing where the model has been cleaved to generate the comparably extended PIWF1 model. (c) As (a), for the compacted model. For the purposes of clarity, the sugar groups have been omitted. The CR and FnIII-1 glycosylations run perpendicular to the plane of the page. (d) As (b), but illustrating that the CR is folded onto the FnIII-1 domain and the WAP domain is to the outside of the structure.

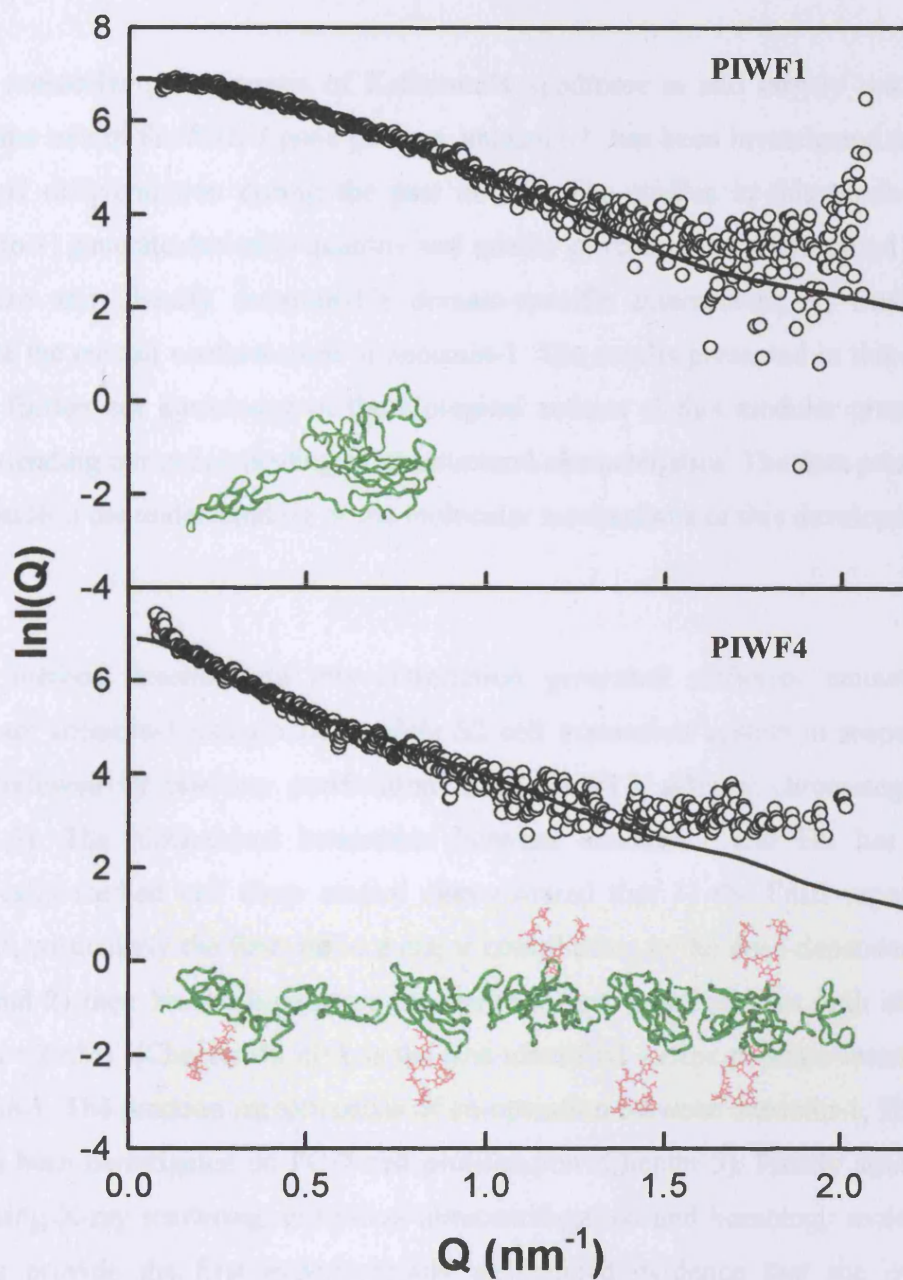


Figure 6.16  $\ln I(Q) \text{ v } Q$  curve fits for the compact model of PIWF1 (top) and PIWF4 (bottom). Experimental data is represented by circles while the theoretical curve is a solid line. Ribbon diagram representations of each of the models used to generate the scattering curves are shown in inset.

## Chapter 7

### Conclusions and future studies

The molecular pathogenesis of Kallmann's syndrome is still largely unknown although the role of the *KAL-1* gene product, anosmin-1, has been investigated mainly in neuronal differentiation during the past decade. The studies in this thesis were designed to 1) generate desirable quantity and quality of recombinant anosmin-1; 2) to characterize and identify anosmin-1's domain-specific interactants; 3) finally to investigate the overall conformation of anosmin-1. The results presented in this thesis will help further our knowledge of the biological actions of this modular protein as well as extending our understanding of its structural characteristics. The data presented will also extend the understanding of the molecular mechanisms of this developmental disease.

The method described in this dissertation generated sufficient amounts of recombinant anosmin-1 using a *Drosophila* S2 cell expression system in suspension culture, followed by one-step purification using Ni-NTA affinity chromatography (Chapter 3). The biochemical interaction between anosmin-1 and HS has been systematically studied and these studies demonstrated that 1) the FnIII repeats of anosmin-1, particularly the first, make a major contribution to the dose-dependent HS binding and 2) their kinetic interaction measured in real-time indicates high affinity ( $K_d$  value = 2 nM) (Chapter 4). uPA is the first identified serine protease interactant of anosmin-1. The function repercussions of co-operation between anosmin-1, HS and uPA have been investigated on PC-3 cell proliferation (Chapter 5). Finally structural studies using X-ray scattering, analytical ultracentrifugation and homology molecular modelling provide the first experimentally determined evidence that the overall conformation of anosmin-1 is an elongated structure (Chapter 6).

#### 7.1 The questions raised from this study

The studies described in this thesis have spawned new and important scientific questions that will need to be addressed in future studies. Thus, what is the structural



specificity of the HS sequence motif involved in anosmin-1 binding and function? As described previously, the modified sulphated pattern at the 6-O site of HS monosaccharide residue has been identified as a determining structural requirement for anosmin-1 induced neurite outgrowth and axonal branching as demonstrated in transgenic *C.elegans* model (Bulow et al., 2002). However, in these and previous studies, there were no data to show whether lack of 6-O sulphation in HS might affect the affinity of HS to anosmin-1. The heparin and HS used in the present study were composed of more than 80 fully sulphated saccharide residues, and have not enabled us to shed further light on this question. In order to do so, it will be necessary to generate specific HS fragments with distinct structural composition, and investigate their specific anosmin-1 binding characteristics.

What are the dominant amino acid residues within the FnIII domains that participate in the HS interaction? Hitherto, a total of three missense mutations have been identified within the FnIII domains: N267K in the 1<sup>st</sup> FnIII domain, E514K and F517L in 3<sup>rd</sup> FnIII domain, suggesting that the basic amino acid components around these regions are highly likely to represent the main HS binding sites. Of these important missense mutations, the N267K seems to be more important since it has been established that the 1<sup>st</sup> FnIII domain is mainly responsible for HS binding. During these studies, I attempted to generate full-length mutated anosmin-1 with the N267K substitution, but the protein yield was too poor to allow further studies. Thus the generation of individual FnIII domains incorporating the individual missense mutation might be an alternative approach.

What is the molecular mechanism of anosmin-1 regulation of uPA activity during cell processes either *via* modulation of uPA catalytic activity or through the uPAR related signaling pathway? I have generated a hypothesis based on the effect of anosmin-1/HS/uPA interplay on PC-3 cell proliferation (Figure 5.8). Anosmin-1, with its cell surface association *via* FnIII domain-HS interactions, may come in contact with uPA *via* its N-terminus including the WAP domain, causing uPA receptor (uPAR) activation and/or induction of uPA mediated proteolysis. Studies have shown

a role of uPA and uPAR during cell proliferation *in vitro*, and in human malignant tumours, uPAR overexpression is often observed (Blasi and Carmeliet, 2002). Enhancement of uPA proteolytic activity can lead to activation of a number of growth factors such as insulin-like growth factor, FGF2 and transforming growth factor- $\beta$  (Angelloz-Nicoud and Binoux, 1995; Rosini et al., 2002). It is not known, however, whether this mitogenic activity is dependent on the uPA mediated proteolysis or uPA binding to uPAR. Furthermore, the active domain in anosmin-1 (either WAP or CR domain) for uPA interaction still requires further clarification.

What are the structural implications in anosmin-1's biological function? The preliminary homology modelling results showing PIWF1 and PIWF4 possess different N-terminal structural conformation may give explanations about the different biochemical characteristics between these two recombinant proteins. It is known that the FnIII domains are involved in binding HS. The main binding domain is FnIII-1, which is present in both PIWF1 and PIWF4. The reduced affinity of PIWF1 for HS can be explained by the absence of three FnIII domains. However, this does not explain why the C172R mutation in the WAP domain reduces the affinity of PIWF1 for HS but does not affect the binding affinity of PIWF4. This difference may be explained by noting that in PIWF1 the WAP domain is in closer proximity to the FnIII-1 domain than it is in PIWF4. Structural changes in the WAP domain, introduced by removing a cysteine residue involved in a disulphide bond, may more strongly affect the overall conformation of the PIWF1 construct than it does the PIWF4 construct. The misfolding of the WAP domain in PIWF1 may cause it to elongate. Thus, it is possible that either the CR or WAP domain may facilitate HS binding to FnIII-1 in PIWF1. In contrast, because the structure of PIWF4 is already extended, disrupting the conformation of the WAP domain has no effect on its binding to HS.

uPA amidolytic activity *in vitro* is not significantly affected by the C172R mutation in PIWF4; both wild-type and mutant PIWF4 increased uPA activity by three-fold in this assay. However, PIWF1 produces a one-fold increase whereas the

mPIWF1<sup>172</sup> has the same effect as the full-length PIWF4. If the WAP domain interacts with trypsin-like serine proteases, the WAP domain partially unfolded as a result of the C172R mutation may cause the serine protease binding site to be fully exposed, thus restoring wild-type activity. This suggests that although the WAP domain has to some extent unfolded, the parts of its structure required for interaction with serine proteases remains intact.

Certainly, further understanding of the coordinate atomic structure of anosmin-1 and three-dimensional visualization of the complex formed by anosmin-1/ligands will require studies using homology modeling, crystallography and NMR.

## **7.2 Future studies**

The availability of a diverse group of structurally modified HS is likely to shed important new insights on the interaction between HS and anosmin-1. The libraries of size-defined saccharides in mass quantities have been recently generated by partial degradation of HS from tissue sources. In addition, the chemical synthesis of defined HS and heparin saccharides can serve as the alternative approach to provide such molecules. First, biosensor interaction kinetics can be carried out by immobilizing HS saccharides containing defined HS size and sulphation patterns onto the sensor chip surface, followed by running the purified recombinant anosmin-1. Second, the role of specific saccharide sequences in mediating anosmin-1's biological function can be identified through study of signal-transduction kinetics and neuron differentiation studies following co-treatment of defined HS and anosmin-1. Finally, homology modelling and crystallography can provide structural visualization and atomic elucidation of complex formation among anosmin-1, uPA and HS. The direct interaction of anosmin-1 with uPA, FGF2 or FGFR1 can be investigated in a domain-specific manner using the SPR studies by coupling either anosmin-1 or other macromolecules respectively onto the sensor chip surface. FNC-B4 cells have been identified as an excellent model system to investigate anosmin-1's role during GnRH1 olfactory neuroblast differentiation. Thus, FNC-B4 cells may be used productively in enabling further studies on the mechanisms of anosmin-1/uPA interaction. One



approach might be to use a method such as Boyden chamber assay or protein coupled beads embedded in fibrin gel to investigate the effect of anosmin-1 on GnRH neuron migration. Also it can provide a good model for analysis of whether uPA proteolysis is involved in neuronal differentiation and migration. *In vivo* studies such as implanting anosmin-1 coupled beads into the olfactory system of chicken embryo may further provide insights into the effects of anosmin-1 function on tissue morphogenesis and neuronal differentiation.

## **Publications:**

### **Papers:**

**Hu Y, Tanriverdi F, MacColl GS, Bouloux PM.** Kallmann's syndrome: Molecular Pathogenesis. *Int J Biochem Cell Biol.* 2003 ;35:1157-62.

**Hu Y, González-Martínez D, Kim S and Bouloux PM.** Cross talk of anosmin-1, the protein implicated in X-linked Kallmann's syndrome, with heparan sulphate and urokinase-type plasminogen activator. *Biochemical Journal.* 2004; 384:495-505.

**Bouloux PM, Hu Y, MacColl G.** Recent advances in the pathogenesis of Kallmann's syndrome. *Prog Brain Res.* 2002; 141:79-83.

**Gonzalez-Martinez D, Hu Y, Bouloux PMG.** "Ontogeny of GnRH and Olfactory Neuronal Systems in Man: Novel Insights from the Investigation of Inherited forms of Kallmann's Syndrome". *Frontiers in Neuroendocrinology.* 2004; 25:108-130.

### **Abstracts and posters:**

**Hu Y, Bouloux PMG, MacColl, G.S.** Expression and purification of histidine-tagged anosmin-1 by *Drosophila* S2 cells and Ni-NTA agarose chromatography. *British Endocrine Societies 21<sup>st</sup> Joint Meeting.* P184 (2002).

**Hu Y, Gonzalez-Martinez D, Tanriverdi F, MacColl GS and Bouloux PMG.** Heparan sulphate modulates anosmin-1 induced PC-3 cell proliferation. *The 85th Annual Meeting of The Endocrine Society (ENDO 2003, Philadelphia).*

**Hu Y, Gonzalez-Martinez D and Bouloux PMG.** Functional interactions between anosmin-1, heparan sulphate and urokinase-type plasminogen activator and the pathogenesis of X-Linked Kallmann's Syndrome. *23rd Joint Meeting of the British Endocrine Societies, Brighton, 22-24 March 2004.*

**González-Martínez D, Hu Y, Guimond S, Kim S and Bouloux PMG.** KAL-1 and KAL-2 ontogeny and *in vitro* function in human GnRH-1 developing system. *23rd Joint Meeting of the British Endocrine Societies, Brighton, 22-24 March 2004.* Novartis Award for the best abstract.

**González-Martínez D, Hu Y, Guimond S, Kim S and Bouloux PMG.** Anosmin-1, an extracellular matrix protein modulates neurite outgrowth of human embryonic GnRH-1 neurons *via* stimulation of a fibroblast growth factor receptor 1 pathway. *Pfizer and British Endocrine Societies Award at the 23rd Joint Meeting of the British Endocrine Societies, Brighton, 22-24 March 2004.*

## Reference

- Aguirre Ghiso, J.A., Kovalski, K., and Ossowski, L. (1999). Tumor dormancy induced by downregulation of urokinase receptor in human carcinoma involves integrin and MAPK signaling. *J. Cell Biol.* *147*, 89-104.
- Akiyama, S.K. (1996). Integrins in cell adhesion and signaling. *Hum. Cell* *9*, 181-186.
- Angelloz-Nicoud, P. and Binoux, M. (1995). Autocrine regulation of cell proliferation by the insulin-like growth factor (IGF) and IGF binding protein-3 protease system in a human prostate carcinoma cell line (PC-3). *Endocrinology* *136*, 5485-5492.
- Angelloz-Nicoud, P., Lalou, C., and Binoux, M. (1998). Prostate carcinoma (PC-3) cell proliferation is stimulated by the 22-25-kDa proteolytic fragment (1-160) and inhibited by the 16-kDa fragment (1-95) of recombinant human insulin-like growth factor binding protein-3. *Growth Horm. IGF. Res.* *8*, 71-75.
- Aoyagi, A., Nishikawa, K., Saito, H., and Abe, K. (1994). Characterization of basic fibroblast growth factor-mediated acceleration of axonal branching in cultured rat hippocampal neurons. *Brain Res.* *661*, 117-126.
- Appella, E., Robinson, E.A., Ullrich, S.J., Stoppelli, M.P., Corti, A., Cassani, G., and Blasi, F. (1987). The receptor-binding sequence of urokinase. A biological function for the growth-factor module of proteases. *J. Biol. Chem.* *262*, 4437-4440.
- Apweiler, R., Hermjakob, H., and Sharon, N. (1999). On the frequency of protein glycosylation, as deduced from analysis of the SWISS-PROT database. *Biochim. Biophys. Acta* *1473*, 4-8.
- Arai, T., Parker, A., Busby, W., Jr., and Clemmons, D.R. (1994). Heparin, heparan sulfate, and dermatan sulfate regulate formation of the insulin-like growth factor-I and insulin-like growth factor-binding protein complexes. *J. Biol. Chem.* *269*, 20388-20393.
- Araki, K., Kuwada, M., Ito, O., Kuroki, J., and Tachibana, S. (1990). Four disulfide bonds' allocation of Na<sup>+</sup>, K<sup>(+)</sup>-ATPase inhibitor (SPAI). *Biochem. Biophys. Res. Commun.* *172*, 42-46.
- Ashikari, S., Habuchi, H., and Kimata, K. (1995). Characterization of heparan sulfate oligosaccharides that bind to hepatocyte growth factor. *J. Biol. Chem.* *270*, 29586-29593.
- Ashton, A.W., Boehm, M.K., Gallimore, J.R., Pepys, M.B., and Perkins, S.J. (1997). Pentameric and decameric structures in solution of serum amyloid P component by X-ray and neutron scattering and molecular modelling analyses. *J. Mol. Biol.* *272*, 408-422.

- Baeg,G.H., Lin,X., Khare,N., Baumgartner,S., and Perrimon,N. (2001). Heparan sulfate proteoglycans are critical for the organization of the extracellular distribution of Wingless. *Development* 128, 87-94.
- Bass,M.D. and Humphries,M.J. (2002). Cytoplasmic interactions of syndecan-4 orchestrate adhesion receptor and growth factor receptor signalling. *Biochem. J.* 368, 1-15.
- Bazin,H.G., Marques,M.A., Owens,A.P., III, Linhardt,R.J., and Crutcher,K.A. (2002). Inhibition of apolipoprotein E-related neurotoxicity by glycosaminoglycans and their oligosaccharides. *Biochemistry* 41, 8203-8211.
- Bellaiche,Y., The,I., and Perrimon,N. (1998). Tout-velu is a Drosophila homologue of the putative tumour suppressor EXT-1 and is needed for Hh diffusion. *Nature* 394, 85-88.
- Bernfield,M., Gotte,M., Park,P.W., Reizes,O., Fitzgerald,M.L., Lincecum,J., and Zako,M. (1999). Functions of cell surface heparan sulfate proteoglycans. *Annu. Rev. Biochem.* 68, 729-777.
- Bernfield,M., Kokenyesi,R., Kato,M., Hinkes,M.T., Spring,J., Gallo,R.L., and Lose,E.J. (1992). Biology of the syndecans: a family of transmembrane heparan sulfate proteoglycans. *Annu. Rev. Cell Biol.* 8, 365-393.
- Berryman,D.E. and Bensadoun,A. (1995). Heparan sulfate proteoglycans are primarily responsible for the maintenance of enzyme activity, binding, and degradation of lipoprotein lipase in Chinese hamster ovary cells. *J. Biol. Chem.* 270, 24525-24531.
- Blasi,F. and Carmeliet,P. (2002). uPAR: a versatile signalling orchestrator. *Nat. Rev. Mol. Cell Biol.* 3, 932-943.
- Bourin,M.C. and Lindahl,U. (1993). Glycosaminoglycans and the regulation of blood coagulation. *Biochem. J.* 289 (Pt 2), 313-330.
- Brunjes,P.C. and Frazier,L.L. (1986). Maturation and plasticity in the olfactory system of vertebrates. *Brain Res.* 396, 1-45.
- Brunner,G., Reibold,K., Meissauer,A., Schirmacher,V., and Erkell,L.J. (1998). Sulfated glycosaminoglycans enhance tumor cell invasion in vitro by stimulating plasminogen activation. *Exp. Cell Res.* 239, 301-310.
- Bulfone,A., Wang,F., Hevner,R., Anderson,S., Cutforth,T., Chen,S., Meneses,J., Pedersen,R., Axel,R., and Rubenstein,J.L. (1998). An olfactory sensory map develops in the absence of normal projection neurons or GABAergic interneurons. *Neuron* 21, 1273-1282.

Bullock,S.L., Fletcher,J.M., Beddington,R.S., and Wilson,V.A. (1998). Renal agenesis in mice homozygous for a gene trap mutation in the gene encoding heparan sulfate 2-sulfotransferase. *Genes Dev.* *12*, 1894-1906.

Bulow,H.E., Berry,K.L., Topper,L.H., Peles,E., and Hobert,O. (2002). Heparan sulfate proteoglycan-dependent induction of axon branching and axon misrouting by the Kallmann syndrome gene *kal-1*. *Proc. Natl. Acad. Sci. U. S. A* *99*, 6346-6351.

Bulow,H.E. and Hobert,O. (2004). Differential sulfations and epimerization define heparan sulfate specificity in nervous system development. *Neuron* *41*, 723-736.

Burrige,K., Turner,C.E., and Romer,L.H. (1992). Tyrosine phosphorylation of paxillin and pp125FAK accompanies cell adhesion to extracellular matrix: a role in cytoskeletal assembly. *J. Cell Biol.* *119*, 893-903.

Calof,A.L. and Lander,A.D. (1991). Relationship between neuronal migration and cell-substratum adhesion: laminin and merosin promote olfactory neuronal migration but are anti-adhesive. *J. Cell Biol.* *115*, 779-794.

Carmeliet,P., Moons,L., Dewerchin,M., Rosenberg,S., Herbert,J.M., Lupu,F., and Collen,D. (1998). Receptor-independent role of urokinase-type plasminogen activator in pericellular plasmin and matrix metalloproteinase proteolysis during vascular wound healing in mice. *J. Cell Biol.* *140*, 233-245.

Chang,R. (1981). *Physical Chemistry with Application to Biological Systems*. Second Edition. Macmillan New York p. 49-63, 512-519.

Conrad,B., Kriebel,J., and Hetzel,W.D. (1978). Hereditary bimanual synkinesis combined with hypogonadotropic hypogonadism and anosmia in four brothers. *J. Neurol.* *218*, 263-274.

Crandall,J.E., Dibble,C., Butler,D., Pays,L., Ahmad,N., Kostek,C., Puschel,A.W., and Schwarting,G.A. (2000). Patterning of olfactory sensory connections is mediated by extracellular matrix proteins in the nerve layer of the olfactory bulb. *J. Neurobiol.* *45*, 195-206.

Crossley,P.H. and Martin,G.R. (1995). The mouse *Fgf8* gene encodes a family of polypeptides and is expressed in regions that direct outgrowth and patterning in the developing embryo. *Development* *121*, 439-451.

Culp,J.S., Johansen,H., Hellmig,B., Beck,J., Matthews,T.J., Delers,A., and Rosenberg,M. (1991). Regulated expression allows high level production and secretion of HIV-1 gp120 envelope glycoprotein in *Drosophila* Schneider cells. *Biotechnology (N. Y.)* *9*, 173-177.

de Castro,F., Hu,L., Drabkin,H., Sotelo,C., and Chedotal,A. (1999). Chemoattraction and chemorepulsion of olfactory bulb axons by different secreted semaphorins. *J. Neurosci.* *19*, 4428-4436.

Dear, T.N. and Kefford, R.F. (1991). The WDNM1 gene product is a novel member of the 'four-disulphide core' family of proteins. *Biochem. Biophys. Res. Commun.* *176*, 247-254.

Debierre-Grockiego, F., Desaint, C., Fuentes, V., Poussin, M., Socie, G., Azzouz, N., Schwarz, R.T., Prin, L., and Gouilleux-Gruart, V. (2003). Evidence for glycosylphosphatidylinositol (GPI)-anchored eosinophil-derived neurotoxin (EDN) on human granulocytes. *FEBS Lett.* *537*, 111-116.

Deeb, A., Robertson, A., MacColl, G., Bouloux, P.M., Gibson, M., Winyard, P.J., Woolf, A.S., Moghal, N.E., and Cheetham, T.D. (2001). Multicystic dysplastic kidney and Kallmann's syndrome: a new association? *Nephrol. Dial. Transplant.* *16*, 1170-1175.

Degryse, B., Orlando, S., Resnati, M., Rabbani, S.A., and Blasi, F. (2001). Urokinase/urokinase receptor and vitronectin/alpha(v)beta(3) integrin induce chemotaxis and cytoskeleton reorganization through different signaling pathways. *Oncogene* *20*, 2032-2043.

Degryse, B., Resnati, M., Rabbani, S.A., Villa, A., Fazioli, F., and Blasi, F. (1999). Src-dependence and pertussis-toxin sensitivity of urokinase receptor-dependent chemotaxis and cytoskeleton reorganization in rat smooth muscle cells. *Blood* *94*, 649-662.

Deiner, M.S. and Sretavan, D.W. (1999). Altered midline axon pathways and ectopic neurons in the developing hypothalamus of netrin-1- and DCC-deficient mice. *J. Neurosci.* *19*, 9900-9912.

Del Bigio, M.R., Hosain, S., and Altumbabic, M. (1999). Localization of urokinase-type plasminogen activator, its receptor, and inhibitors in mouse forebrain during postnatal development. *Int. J. Dev. Neurosci.* *17*, 387-399.

Dell'Era, P., Mohammadi, M., and Presta, M. (1999). Different tyrosine autophosphorylation requirements in fibroblast growth factor receptor-1 mediate urokinase-type plasminogen activator induction and mitogenesis. *Mol. Biol. Cell* *10*, 23-33.

Dent, M.A., Sumi, Y., Morris, R.J., and Seeley, P.J. (1993). Urokinase-type plasminogen activator expression by neurons and oligodendrocytes during process outgrowth in developing rat brain. *Eur. J. Neurosci.* *5*, 633-647.

Dihanich, M., Kaser, M., Reinhard, E., Cunningham, D., and Monard, D. (1991). Prothrombin mRNA is expressed by cells of the nervous system. *Neuron* *6*, 575-581.

Dodd, J. and Jessell, T.M. (1988). Axon guidance and the patterning of neuronal projections in vertebrates. *Science* *242*, 692-699.

Dode,C., Levilliers,J., Dupont,J.M., De Paepe,A., Le Du,N., Soussi-Yanicostas,N., Coimbra,R.S., Delmaghani,S., Compain-Nouaille,S., Baverel,F., Pecheux,C., Le Tessier,D., Cruaud,C., Delpech,M., Speleman,F., Vermeulen,S., Amalfitano,A., Bachelot,Y., Bouchard,P., Cabrol,S., Carel,J.C., Delemarre-Van De Waal,H., Goulet-Salmon,B., Kottler,M.L., Richard,O., Sanchez-Franco,F., Saura,R., Young,J., Petit,C., and Hardelin,J.P. (2003). Loss-of-function mutations in FGFR1 cause autosomal dominant Kallmann syndrome. *Nat. Genet.* 33:463-5

Dono,R., Texido,G., Dussel,R., Ehmke,H., and Zeller,R. (1998). Impaired cerebral cortex development and blood pressure regulation in FGF-2-deficient mice. *EMBO J.* 17, 4213-4225.

Dow,K.E., Mirski,S.E., Roder,J.C., and Riopelle,R.J. (1988). Neuronal proteoglycans: biosynthesis and functional interaction with neurons in vitro. *J. Neurosci.* 8, 3278-3289.

Drapkin,P.T., Monard,D., and Silverman,A.J. (2002). The role of serine proteases and serine protease inhibitors in the migration of gonadotropin-releasing hormone neurons. *BMC. Dev. Biol.* 2, 1.

Duke,V., Quinton,R., Gordon,I., Bouloux,P.M., and Woolf,A.S. (1998). Proteinuria, hypertension and chronic renal failure in X-linked Kallmann's syndrome, a defined genetic cause of solitary functioning kidney. *Nephrol. Dial. Transplant.* 13, 1998-2003.

Engel,J., Odermatt,E., Engel,A., Madri,J.A., Furthmayr,H., Rohde,H., and Timpl,R. (1981). Shapes, domain organizations and flexibility of laminin and fibronectin, two multifunctional proteins of the extracellular matrix. *J. Mol. Biol.* 150, 97-120.

Erickson,H.P., Carrell,N., and McDonagh,J. (1981). Fibronectin molecule visualized in electron microscopy: a long, thin, flexible strand. *J. Cell Biol.* 91, 673-678.

Eriksson,A.E., Cousens,L.S., Weaver,L.H., and Matthews,B.W. (1991). Three-dimensional structure of human basic fibroblast growth factor. *Proc. Natl. Acad. Sci. U. S. A* 88, 3441-3445.

Esko,J.D. and Lindahl,U. (2001). Molecular diversity of heparan sulfate. *J. Clin. Invest* 108, 169-173.

Ethell,I.M., Hagihara,K., Miura,Y., Irie,F., and Yamaguchi,Y. (2000). Synbindin, A novel syndecan-2-binding protein in neuronal dendritic spines. *J. Cell Biol.* 151, 53-68.

Ethell,I.M., Irie,F., Kalo,M.S., Couchman,J.R., Pasquale,E.B., and Yamaguchi,Y. (2001). EphB/syndecan-2 signaling in dendritic spine morphogenesis. *Neuron* 31, 1001-1013.

- Fannon, M., Forsten, K.E., and Nugent, M.A. (2000). Potentiation and inhibition of bFGF binding by heparin: a model for regulation of cellular response. *Biochemistry* 39, 1434-1445.
- Feyzi, E., Lustig, F., Fager, G., Spillmann, D., Lindahl, U., and Salmivirta, M. (1997a). Characterization of heparin and heparan sulfate domains binding to the long splice variant of platelet-derived growth factor A chain. *J. Biol. Chem.* 272, 5518-5524.
- Feyzi, E., Lustig, F., Fager, G., Spillmann, D., Lindahl, U., and Salmivirta, M. (1997b). Characterization of heparin and heparan sulfate domains binding to the long splice variant of platelet-derived growth factor A chain. *J. Biol. Chem.* 272, 5518-5524.
- Filmus, J. (2001). Glypicans in growth control and cancer. *Glycobiology* 11, 19R-23R.
- Filmus, J. and Selleck, S.B. (2001). Glypicans: proteoglycans with a surprise. *J. Clin. Invest* 108, 497-501.
- Fitzgerald, M.L., Wang, Z., Park, P.W., Murphy, G., and Bernfield, M. (2000). Shedding of syndecan-1 and -4 ectodomains is regulated by multiple signaling pathways and mediated by a TIMP-3-sensitive metalloproteinase. *J. Cell Biol.* 148, 811-824.
- Forbes, K., Gillette, K., Kelley, L.A., and Sehgal, I. (2004). Increased levels of urokinase plasminogen activator receptor in prostate cancer cells derived from repeated metastasis. *World J. Urol.* 22, 67-71.
- Ford-Perriss, M., Guimond, S.E., Greferath, U., Kita, M., Grobe, K., Habuchi, H., Kimata, K., Esko, J.D., Murphy, M., and Turnbull, J.E. (2002). Variant heparan sulfates synthesized in developing mouse brain differentially regulate FGF signaling. *Glycobiology* 12, 721-727.
- Forsberg, E. and Kjellen, L. (2001). Heparan sulfate: lessons from knockout mice. *J. Clin. Invest* 108, 175-180.
- Forsberg, E., Pejler, G., Ringvall, M., Lunderius, C., Tomasini-Johansson, B., Kusche-Gullberg, M., Eriksson, I., Ledin, J., Hellman, L., and Kjellen, L. (1999). Abnormal mast cells in mice deficient in a heparin-synthesizing enzyme. *Nature* 400, 773-776.
- Franco, B., Guioli, S., Pragliola, A., Incerti, B., Bardoni, B., Tonlorenzi, R., Carozzo, R., Maestrini, E., Pieretti, M., Taillon-Miller, P., et al. (1991). A gene deleted in Kallmann's syndrome shares homology with neural cell adhesion and axonal path-finding molecules. *Nature* 353, 529-536.
- Gao, Y., Li, M., Chen, W., and Simons, M. (2000). Synectin, syndecan-4 cytoplasmic domain binding PDZ protein, inhibits cell migration. *J. Cell Physiol* 184, 373-379.
- Georgopoulos, N.A., Pralong, F.P., Seidman, C.E., Seidman, J.G., Crowley, W.F., Jr., and Vallejo, M. (1997). Genetic heterogeneity evidenced by low incidence of KAL-1 gene



mutations in sporadic cases of gonadotropin-releasing hormone deficiency. *J. Clin. Endocrinol. Metab* 82, 213-217.

Glatter O and Kratky O (1982). Editors of Small-angle X-ray scattering. Academic Press, New York.

Goldman,S.A. and Luskin,M.B. (1998). Strategies utilized by migrating neurons of the postnatal vertebrate forebrain. *Trends Neurosci.* 21, 107-114.

Gong,Q. and Shipley,M.T. (1996). Expression of extracellular matrix molecules and cell surface molecules in the olfactory nerve pathway during early development. *J. Comp Neurol.* 366, 1-14.

Grand,R.J., Grabham,P.W., Gallimore,M.J., and Gallimore,P.H. (1989). Modulation of morphological differentiation of human neuroepithelial cells by serine proteases: independence from blood coagulation. *EMBO J.* 8, 2209-2215.

Grisaru,S. and Rosenblum,N.D. (2001). Glypicans and the biology of renal malformations. *Pediatr. Nephrol.* 16, 302-306.

Grutter,M.G., Fendrich,G., Huber,R., and Bode,W. (1988). The 2.5 Å X-ray crystal structure of the acid-stable proteinase inhibitor from human mucous secretions analysed in its complex with bovine alpha-chymotrypsin. *EMBO J.* 7, 345-351.

Guimond,S., Maccarana,M., Olwin,B.B., Lindahl,U., and Rapraeger,A.C. (1993). Activating and inhibitory heparin sequences for FGF-2 (basic FGF). Distinct requirements for FGF-1, FGF-2, and FGF-4. *J. Biol. Chem.* 268, 23906-23914.

Guimond,S.E. and Turnbull,J.E. (1999). Fibroblast growth factor receptor signalling is dictated by specific heparan sulphate saccharides. *Curr. Biol.* 9, 1343-1346.

Gulisano,M., Broccoli,V., Pardini,C., and Boncinelli,E. (1996). *Emx1* and *Emx2* show different patterns of expression during proliferation and differentiation of the developing cerebral cortex in the mouse. *Eur. J. Neurosci.* 8, 1037-1050.

Gurwitz,D. and Cunningham,D.D. (1988). Thrombin modulates and reverses neuroblastoma neurite outgrowth. *Proc. Natl. Acad. Sci. U. S. A* 85, 3440-3444.

Halfter,W., Dong,S., Schurer,B., and Cole,G.J. (1998). Collagen XVIII is a basement membrane heparan sulfate proteoglycan. *J. Biol. Chem.* 273, 25404-25412.

Hantai,D., Rao,J.S., Kahler,C., and Festoff,B.W. (1989). Decrease in plasminogen activator correlates with synapse elimination during neonatal development of mouse skeletal muscle. *Proc. Natl. Acad. Sci. U. S. A* 86, 362-366.

Hardelin,J.P., Julliard,A.K., Moniot,B., Soussi-Yanicostas,N., Verney,C., Schwanzel-Fukuda,M., Ayer-Le Lievre,C., and Petit,C. (1999). Anosmin-1 is a regionally restricted component of basement membranes and interstitial matrices during

organogenesis: implications for the developmental anomalies of X chromosome-linked Kallmann syndrome. *Dev. Dyn.* 215, 26-44.

Hardelin,J.P., Levilliers,J., Blanchard,S., Carel,J.C., Leutenegger,M., Pinard-Bertelto,J.P., Bouloux,P., and Petit,C. (1993). Heterogeneity in the mutations responsible for X chromosome-linked Kallmann syndrome. *Hum. Mol. Genet.* 2, 373-377.

Harding,S.E. (1994). Determination of Macromolecular Homogeneity, Shape, and Interactions Using Sedimentation Velocity Analytical Ultracentrifugation. IN Jones,C., Mulloy, B., and Thomas, A.S.(eds) *Methods in Molecular Biology*, Vol. 22:Microscopy, Optical Spectroscopy, and Macroscopic Techniques. Human Press Inc. Totowa,N. J pp 61-73.

Hawkins,R.L. and Seeds,N.W. (1986). Effect of proteases and their inhibitors on neurite outgrowth from neonatal mouse sensory ganglia in culture. *Brain Res.* 398, 63-70.

Hawkins,R.L. and Seeds,N.W. (1989). Protease inhibitors influence the direction of neurite outgrowth. *Brain Res. Dev. Brain Res.* 45, 203-209.

Hayden,S.M. and Seeds,N.W. (1996). Modulated expression of plasminogen activator system components in cultured cells from dissociated mouse dorsal root ganglia. *J. Neurosci.* 16, 2307-2317.

Hebert,J.M., Lin,M., Partanen,J., Rossant,J., and McConnell,S.K. (2003). FGF signaling through FGFR1 is required for olfactory bulb morphogenesis. *Development* 130, 1101-1111.

Heinzel,R., Appelhans,H., Gassen,G., Seemuller,U., Machleidt,W., Fritz,H., and Steffens,G. (1986). Molecular cloning and expression of cDNA for human antileukoprotease from cervix uterus. *Eur. J. Biochem.* 160, 61-67.

Hensley,P. (1996). Defining the structure and stability of macromolecular assemblies in solution: the re-emergence of analytical ultracentrifugation as a practical tool. *Structure.* 4, 367-373.

Herndon,M.E., Stipp,C.S., and Lander,A.D. (1999). Interactions of neural glycosaminoglycans and proteoglycans with protein ligands: assessment of selectivity, heterogeneity and the participation of core proteins in binding. *Glycobiology* 9, 143-155.

Hileman,R.E., Fromm,J.R., Weiler,J.M., and Linhardt,R.J. (1998). Glycosaminoglycan-protein interactions: definition of consensus sites in glycosaminoglycan binding proteins. *Bioessays* 20, 156-167.

Hjelm,R.P. (1985). The small-angle approximation of X-ray and neutron scatter from rigid rods of non-uniform cross section and finite length. *J. Appl. Cryst* 18, 452-460.

- Holen,I, Drury,N.L., Hargreaves,P.G., and Croucher,P.I. (2001). Evidence of a role for a non-matrix-type metalloproteinase activity in the shedding of syndecan-1 from human myeloma cells. *Br. J. Haematol.* *114*, 414-421.
- Hoyer-Hansen,G., Ploug,M., Behrendt,N., Ronne,E., and Dano,K. (1997). Cell-surface acceleration of urokinase-catalyzed receptor cleavage. *Eur. J. Biochem.* *243*, 21-26.
- Hu,H. (1999). Chemorepulsion of neuronal migration by Slit2 in the developing mammalian forebrain. *Neuron* *23*, 703-711.
- Hu,H. (2001). Cell-surface heparan sulfate is involved in the repulsive guidance activities of Slit2 protein. *Nat. Neurosci.* *4*, 695-701.
- Huang TC, Toraya H, Blanton TN, and Wu Y (1993). X-ray powder diffraction analysis of silver behenate, a possible low-angle diffraction standard. *J. Appl. Cryst* *26*, 180-184.
- Huber,A.H., Wang,Y.M., Bieber,A.J., and Bjorkman,P.J. (1994). Crystal structure of tandem type III fibronectin domains from *Drosophila* neuroglian at 2.0 Å. *Neuron* *12*, 717-731.
- Hynes,M., Porter,J.A., Chiang,C., Chang,D., Tessier-Lavigne,M., Beachy,P.A., and Rosenthal,A. (1995). Induction of midbrain dopaminergic neurons by Sonic hedgehog. *Neuron* *15*, 35-44.
- Inatani,M., Irie,F., Plump,A.S., Tessier-Lavigne,M., and Yamaguchi,Y. (2003). Mammalian brain morphogenesis and midline axon guidance require heparan sulfate. *Science* *302*, 1044-1046.
- Iozzo,R.V. (1998). Matrix proteoglycans: from molecular design to cellular function. *Annu. Rev. Biochem.* *67*, 609-652.
- Jaakkola,P., Kontusaari,S., Kauppi,T., Maata,A., and Jalkanen,M. (1998). Wound reepithelialization activates a growth factor-responsive enhancer in migrating keratinocytes. *FASEB J.* *12*, 959-969.
- Jackson,R.L., Busch,S.J., and Cardin,A.D. (1991). Glycosaminoglycans: molecular properties, protein interactions, and role in physiological processes. *Physiol Rev.* *71*, 481-539.
- Jalink,K. and Moolenaar,W.H. (1992). Thrombin receptor activation causes rapid neural cell rounding and neurite retraction independent of classic second messengers. *J. Cell Biol.* *118*, 411-419.
- Jarrard,D.F., Blitz,B.F., Smith,R.C., Patai,B.L., and Rukstalis,D.B. (1994). Effect of epidermal growth factor on prostate cancer cell line PC3 growth and invasion. *Prostate* *24*, 46-53.

Jayson,G.C., Lyon,M., Paraskeva,C., Turnbull,J.E., Deakin,J.A., and Gallagher,J.T. (1998). Heparan sulfate undergoes specific structural changes during the progression from human colon adenoma to carcinoma in vitro. *J. Biol. Chem.* 273, 51-57.

Jones,J.R. and Kemmann,E. (1976). Olfacto-genital dysplasia in the female. *Obstet. Gynecol. Annu.* 5, 443-466.

Jones,T.A., Zou,J.Y., Cowan,S.W., and Kjeldgaard (1991). Improved methods for building protein models in electron density maps and the location of errors in these models. *Acta Crystallogr. A* 47 ( Pt 2), 110-119.

Jung,K.M., Cotman,S.L., Halfter,W., and Cole,G.J. (2003). The heparan sulfate proteoglycan agrin modulates neurite outgrowth mediated by FGF-2. *J. Neurobiol.* 55, 261-277.

Kallmann, F. J. Schoenfeld W. A. Barrere S. E. The genetic aspects of primary eunuchoidism. *Am.J.Ment.Deficiency* XLVIII , 203-236. 1944.

Kayyem,J.F., Roman,J.M., de la Rosa,E.J., Schwarz,U., and Dreyer,W.J. (1992). Bravo/Nr-CAM is closely related to the cell adhesion molecules L1 and Ng-CAM and has a similar heterodimer structure. *J. Cell Biol.* 118, 1259-1270.

Kiselyov,V.V., Skladchikova,G., Hinsby,A.M., Jensen,P.H., Kulahin,N., Soroka,V., Pedersen,N., Tsetlin,V., Poulsen,F.M., Berezin,V., and Bock,E. (2003). Structural basis for a direct interaction between FGFR1 and NCAM and evidence for a regulatory role of ATP. *Structure. (Camb. )* 11, 691-701.

Kjellen,L. and Lindahl,U. (1991). Proteoglycans: structures and interactions. *Annu. Rev. Biochem.* 60, 443-475.

Kjoller,L. and Hall,A. (2001). Rac mediates cytoskeletal rearrangements and increased cell motility induced by urokinase-type plasminogen activator receptor binding to vitronectin. *J. Cell Biol.* 152, 1145-1157.

Klint,P. and Claesson-Welsh,L. (1999). Signal transduction by fibroblast growth factor receptors. *Front Biosci.* 4, D165-D177.

Kosir,M.A. and Quinn,C.C. (1995). Sorting of heparan sulfate proteoglycan into matrix compartments of prostate adenocarcinoma cells. *J. Surg. Res.* 58, 46-52.

Kramer,P.R. and Wray,S. (2000). Novel gene expressed in nasal region influences outgrowth of olfactory axons and migration of luteinizing hormone-releasing hormone (LHRH) neurons. *Genes Dev.* 14, 1824-1834.

Krams,M., Quinton,R., Ashburner,J., Friston,K.J., Frackowiak,R.S., Bouloux,P.M., and Passingham,R.E. (1999). Kallmann's syndrome: mirror movements associated with bilateral corticospinal tract hypertrophy. *Neurology* 52, 816-822.

- Krams,M., Quinton,R., Mayston,M.J., Harrison,L.M., Dolan,R.J., Bouloux,P.M., Stephens,J.A., Frackowiak,R.S., and Passingham,R.E. (1997). Mirror movements in X-linked Kallmann's syndrome. II. A PET study. *Brain* 120 (Pt 7), 1217-1228.
- Kristensen,C., Wiberg,F.C., and Andersen,A.S. (1999). Specificity of insulin and insulin-like growth factor I receptors investigated using chimeric mini-receptors. Role of C-terminal of receptor alpha subunit. *J. Biol. Chem.* 274, 37351-37356.
- Krystosek,A. and Seeds,N.W. (1981). Plasminogen activator release at the neuronal growth cone. *Science* 213, 1532-1534.
- Krystosek,A. and Seeds,N.W. (1984). Peripheral neurons and Schwann cells secrete plasminogen activator. *J. Cell Biol.* 98, 773-776.
- Kuroda,K., Geyer,H., Geyer,R., Doerfler,W., and Klenk,H.D. (1990). The oligosaccharides of influenza virus hemagglutinin expressed in insect cells by a baculovirus vector. *Virology* 174, 418-429.
- Kwan,C.P., Venkataraman,G., Shriver,Z., Raman,R., Liu,D., Qi,Y., Varticovski,L., and Sasisekharan,R. (2001). Probing fibroblast growth factor dimerization and role of heparin-like glycosaminoglycans in modulating dimerization and signaling. *J. Biol. Chem.* 276, 23421-23429.
- Lander,A.D. (1989). Understanding the molecules of neural cell contacts: emerging patterns of structure and function. *Trends Neurosci.* 12, 189-195.
- Larsen,M., Ressler,S.J., Lu,B., Gerdes,M.J., McBride,L., Dang,T.D., and Rowley,D.R. (1998). Molecular cloning and expression of ps20 growth inhibitor. A novel WAP-type "four-disulfide core" domain protein expressed in smooth muscle. *J. Biol. Chem.* 273, 4574-4584.
- Laue,T.M. and Stafford,W.F., III (1999). Modern applications of analytical ultracentrifugation. *Annu. Rev. Biophys. Biomol. Struct.* 28, 75-100.
- Leahy,D.J., Aukhil,I., and Erickson,H.P. (1996). 2.0 A crystal structure of a four-domain segment of human fibronectin encompassing the RGD loop and synergy region. *Cell* 84, 155-164.
- Legouis,R., Hardelin,J.P., Levilliers,J., Claverie,J.M., Compain,S., Wunderle,V., Millasseau,P., Le Paslier,D., Cohen,D., Caterina,D., et al. (1991). The candidate gene for the X-linked Kallmann syndrome encodes a protein related to adhesion molecules. *Cell* 67, 423-435.
- Lehr,R.V., Elefante,L.C., Kikly,K.K., O'Brien,S.P., and Kirkpatrick,R.B. (2000). A modified metal-ion affinity chromatography procedure for the purification of histidine-tagged recombinant proteins expressed in *Drosophila* S2 cells. *Protein Expr. Purif.* 19, 362-368.

- Li,H.S., Chen,J.H., Wu,W., Fagaly,T., Zhou,L., Yuan,W., Dupuis,S., Jiang,Z.H., Nash,W., Gick,C., Ornitz,D.M., Wu,J.Y., and Rao,Y. (1999). Vertebrate slit, a secreted ligand for the transmembrane protein roundabout, is a repellent for olfactory bulb axons. *Cell* 96, 807-818.
- Libeu,C.P., Lund-Katz,S., Phillips,M.C., Wehrli,S., Hernaiz,M.J., Capila,I., Linhardt,R.J., Raffai,R.L., Newhouse,Y.M., Zhou,F., and Weisgraber,K.H. (2001). New insights into the heparan sulfate proteoglycan-binding activity of apolipoprotein E. *J. Biol. Chem.* 276, 39138-39144.
- Lindahl,U., Thunberg,L., Backstrom,G., Riesenfeld,J., Nordling,K., and Bjork,I. (1984). Extension and structural variability of the antithrombin-binding sequence in heparin. *J. Biol. Chem.* 259, 12368-12376.
- Lis,H. and Sharon,N. (1993). Protein glycosylation. Structural and functional aspects. *Eur. J. Biochem.* 218, 1-27.
- Liu,D., Shriver,Z., Qi,Y., Venkataraman,G., and Sasisekharan,R. (2002a). Dynamic regulation of tumor growth and metastasis by heparan sulfate glycosaminoglycans. *Semin. Thromb. Hemost.* 28, 67-78.
- Liu,D., Shriver,Z., Venkataraman,G., El Shabrawi,Y., and Sasisekharan,R. (2002b). Tumor cell surface heparan sulfate as cryptic promoters or inhibitors of tumor growth and metastasis. *Proc. Natl. Acad. Sci. U. S. A* 99, 568-573.
- Liu,Y., Fields,R.D., Festoff,B.W., and Nelson,P.G. (1994). Proteolytic action of thrombin is required for electrical activity-dependent synapse reduction. *Proc. Natl. Acad. Sci. U. S. A* 91, 10300-10304.
- Lortat-Jacob,H., Turnbull,J.E., and Grimaud,J.A. (1995). Molecular organization of the interferon gamma-binding domain in heparan sulphate. *Biochem. J.* 310 ( Pt 2), 497-505.
- Lyon,M. and Gallagher,J.T. (1994). Hepatocyte growth factor/scatter factor: a heparan sulphate-binding pleiotropic growth factor. *Biochem. Soc. Trans.* 22, 365-370.
- Lyon,M., Rushton,G., and Gallagher,J.T. (1997). The interaction of the transforming growth factor-betas with heparin/heparan sulfate is isoform-specific. *J. Biol. Chem.* 272, 18000-18006.
- Lyon,P.B., See,W.A., Xu,Y., and Cohen,M.B. (1995). Diversity and modulation of plasminogen activator activity in human prostate carcinoma cell lines. *Prostate* 27, 179-186.
- MacColl,G., Bouloux,P., and Quinton,R. (2002a). Kallmann syndrome: adhesion, afferents, and anosmia. *Neuron* 34, 675-678.

MacColl,G., Quinton,R., and Bouloux,P.M. (2002b). GnRH neuronal development: insights into hypogonadotrophic hypogonadism. *Trends Endocrinol. Metab* 13, 112-118.

Maestre de San Juan (1856). Teratología:falta total de los nervios olfatorios con anosmia en un individuo en quien existía una atrofia congénita de los testículos y miembro viril. *El siglo medico*, Madrid 211.

Mahanthappa,N.K., Cooper,D.N., Barondes,S.H., and Schwarting,G.A. (1994). Rat olfactory neurons can utilize the endogenous lectin, L-14, in a novel adhesion mechanism. *Development* 120, 1373-1384.

Maya-Nunez,G., Cuevas-Covarrubias,S., Zenteno,J.C., Ulloa-Aguirre,A., Kofman-Alfaro,S., and Mendez,J.P. (1998a). Contiguous gene syndrome due to deletion of the first three exons of the Kallmann gene and complete deletion of the steroid sulphatase gene. *Clin. Endocrinol. (Oxf)* 48, 713-718.

Maya-Nunez,G., Zenteno,J.C., Ulloa-Aguirre,A., Kofman-Alfaro,S., and Mendez,J.P. (1998b). A recurrent missense mutation in the KAL gene in patients with X-linked Kallmann's syndrome. *J. Clin. Endocrinol. Metab* 83, 1650-1653.

Mayston,M.J., Harrison,L.M., Quinton,R., Stephens,J.A., Krams,M., and Bouloux,P.M. (1997). Mirror movements in X-linked Kallmann's syndrome. I. A neurophysiological study. *Brain* 120 (Pt 7), 1199-1216.

McMahon,A.P. and Bradley,A. (1990). The Wnt-1 (int-1) proto-oncogene is required for development of a large region of the mouse brain. *Cell* 62, 1073-1085.

Meiri,N., Masos,T., Rosenblum,K., Miskin,R., and Dudai,Y. (1994). Overexpression of urokinase-type plasminogen activator in transgenic mice is correlated with impaired learning. *Proc. Natl. Acad. Sci. U. S. A* 91, 3196-3200.

Merry,C.L. and Wilson,V.A. (2002). Role of heparan sulfate-2-O-sulfotransferase in the mouse. *Biochim. Biophys. Acta* 1573, 319-327.

Meyers,E.N., Lewandoski,M., and Martin,G.R. (1998). An Fgf8 mutant allelic series generated by Cre- and Flp-mediated recombination. *Nat. Genet.* 18, 136-141.

Mochizuki,Y., Tsuda,S., Kanetake,H., and Kanda,S. (2002). Negative regulation of urokinase-type plasminogen activator production through FGF-2-mediated activation of phosphoinositide 3-kinase. *Oncogene* 21, 7027-7033.

Molina,L., Marino-Buslje,C., Quinn,D.R., and Siddle,K. (2000). Structural domains of the insulin receptor and IGF receptor required for dimerisation and ligand binding. *FEBS Lett.* 467, 226-230.

Moos,M., Tacke,R., Scherer,H., Teplow,D., Fruh,K., and Schachner,M. (1988). Neural adhesion molecule L1 as a member of the immunoglobulin superfamily with binding domains similar to fibronectin. *Nature* 334, 701-703.

Murakami,S., Seki,T., Rutishauser,U., and Arai,Y. (1998). LHRH neurons migrate into the trigeminal nerve when the developing olfactory nerve fibers are physically interrupted in chick embryos. *Gen. Comp Endocrinol.* 112, 312-321.

Murakami,S., Seki,T., Rutishauser,U., and Arai,Y. (2000). Enzymatic removal of polysialic acid from neural cell adhesion molecule perturbs the migration route of luteinizing hormone-releasing hormone neurons in the developing chick forebrain. *J. Comp Neurol.* 420, 171-181.

Murase,S. and Horwitz,A.F. (2002). Deleted in colorectal carcinoma and differentially expressed integrins mediate the directional migration of neural precursors in the rostral migratory stream. *J. Neurosci.* 22, 3568-3579.

Murphy-Ullrich,J.E., Westrick,L.G., Esko,J.D., and Mosher,D.F. (1988). Altered metabolism of thrombospondin by Chinese hamster ovary cells defective in glycosaminoglycan synthesis. *J. Biol. Chem.* 263, 6400-6406.

Najjam,S., Mulloy,B., Theze,J., Gordon,M., Gibbs,R., and Rider,C.C. (1998). Further characterization of the binding of human recombinant interleukin 2 to heparin and identification of putative binding sites. *Glycobiology* 8, 509-516.

Nakashiba,T., Ikeda,T., Nishimura,S., Tashiro,K., Honjo,T., Culotti,J.G., and Itohara,S. (2000). Netrin-G1: a novel glycosyl phosphatidylinositol-linked mammalian netrin that is functionally divergent from classical netrins. *J. Neurosci.* 20, 6540-6550.

Narayanan T, Diat O, and Bosecke P (2001). SAXS and USAXS on the high brilliance beamline at the ESRF. *Nuclear Instruments and Methods in Physics Research A* 467-468, 1005-1009.

Nguyen Ba-Charvet,K.T., Brose,K., Marillat,V., Kidd,T., Goodman,C.S., Tessier-Lavigne,M., Sotelo,C., and Chedotal,A. (1999). Slit2-Mediated chemorepulsion and collapse of developing forebrain axons. *Neuron* 22, 463-473.

Nguyen,D.H., Webb,D.J., Catling,A.D., Song,Q., Dhakephalkar,A., Weber,M.J., Ravichandran,K.S., and Gonias,S.L. (2000). Urokinase-type plasminogen activator stimulates the Ras/Extracellular signal-regulated kinase (ERK) signaling pathway and MCF-7 cell migration by a mechanism that requires focal adhesion kinase, Src, and Shc. Rapid dissociation of GRB2/Sps-Shc complex is associated with the transient phosphorylation of ERK in urokinase-treated cells. *J. Biol. Chem.* 275, 19382-19388.

Norgren,R.B., Jr. and Brackenbury,R. (1993). Cell adhesion molecules and the migration of LHRH neurons during development. *Dev. Biol.* 160, 377-387.



Nurcombe,V., Smart,C.E., Chipperfield,H., Cool,S.M., Boilly,B., and Hondermarck,H. (2000). The proliferative and migratory activities of breast cancer cells can be differentially regulated by heparan sulfates. *J. Biol. Chem.* 275, 30009-30018.

Nyhus,J.K. and Denburg,J.L. (1998). The in vivo regulation of pioneer axon growth by FGF-2 and heparan sulfate proteoglycans in cultured embryos of the cockroach. *Mol. Cell Neurosci.* 11, 305-323.

Oh,E.S., Woods,A., Lim,S.T., Theibert,A.W., and Couchman,J.R. (1998). Syndecan-4 proteoglycan cytoplasmic domain and phosphatidylinositol 4,5-bisphosphate coordinately regulate protein kinase C activity. *J. Biol. Chem.* 273, 10624-10629.

Oliveira,L.M., Seminara,S.B., Beranova,M., Hayes,F.J., Valkenburgh,S.B., Schipani,E., Costa,E.M., Latronico,A.C., Crowley,W.F., Jr., and Vallejo,M. (2001). The importance of autosomal genes in Kallmann syndrome: genotype-phenotype correlations and neuroendocrine characteristics. *J. Clin. Endocrinol. Metab* 86, 1532-1538.

Ornitz,D.M. (2000). FGFs, heparan sulfate and FGFRs: complex interactions essential for development. *Bioessays* 22, 108-112.

Ornitz,D.M., Xu,J., Colvin,J.S., McEwen,D.G., MacArthur,C.A., Coulier,F., Gao,G., and Goldfarb,M. (1996). Receptor specificity of the fibroblast growth factor family. *J. Biol. Chem.* 271, 15292-15297.

Osterwalder,T., Cinelli,P., Baici,A., Pennella,A., Krueger,S.R., Schrimpf,S.P., Meins,M., and Sonderegger,P. (1998). The axonally secreted serine proteinase inhibitor, neuroserpin, inhibits plasminogen activators and plasmin but not thrombin. *J. Biol. Chem.* 273, 2312-2321.

Padro,T., Mesters,R.M., Dankbar,B., Hintelmann,H., Bieker,R., Kiehl,M., Berdel,W.E., and Kienast,J. (2002). The catalytic domain of endogenous urokinase-type plasminogen activator is required for the mitogenic activity of platelet-derived and basic fibroblast growth factors in human vascular smooth muscle cells. *J. Cell Sci.* 115, 1961-1971.

Paine-Saunders,S., Viviano,B.L., Economides,A.N., and Saunders,S. (2002). Heparan sulfate proteoglycans retain Noggin at the cell surface: a potential mechanism for shaping bone morphogenetic protein gradients. *J. Biol. Chem.* 277, 2089-2096.

Parthasarathy,N., Goldberg,I.J., Sivaram,P., Mulloy,B., Flory,D.M., and Wagner,W.D. (1994). Oligosaccharide sequences of endothelial cell surface heparan sulfate proteoglycan with affinity for lipoprotein lipase. *J. Biol. Chem.* 269, 22391-22396.

Parthasarathy,N., Gotow,L.F., Bottoms,J.D., Kute,T.E., Wagner,W.D., and Mulloy,B. (1998). Oligosaccharide sequence of human breast cancer cell heparan sulfate with high affinity for laminin. *J. Biol. Chem.* *273*, 21111-21114.

Pepper,M.S. (2001). Role of the matrix metalloproteinase and plasminogen activator-plasmin systems in angiogenesis. *Arterioscler. Thromb. Vasc. Biol.* *21*, 1104-1117.

Pepper,M.S., Matsumoto,K., Nakamura,T., Orci,L., and Montesano,R. (1992). Hepatocyte growth factor increases urokinase-type plasminogen activator (u-PA) and u-PA receptor expression in Madin-Darby canine kidney epithelial cells. *J. Biol. Chem.* *267*, 20493-20496.

Perkins,S.J. (1998). X-ray and neutron solution scattering. In: *Modern physical methods in biochemistry, part B*. Editors A. Neuberger, and L. L. van Deenen. Elsevier science publishers B. V. pp 143-265.

Perkins,S.J. (1986). Protein volumes and hydration effects. The calculations of partial specific volumes, neutron scattering matchpoints and 280-nm absorption coefficients for proteins and glycoproteins from amino acid sequences. *Eur. J. Biochem.* *157*, 169-180.

Perkins,S.J. (1988). Structural studies of proteins by high-flux X-ray and neutron solution scattering. *Biochem. J.* *254*, 313-327.

Perkins,S.J. (2001). X-ray and neutron scattering analyses of hydration shells: a molecular interpretation based on sequence predictions and modelling fits. *Biophys. Chem.* *93*, 129-139.

Perkins,S.J., Ashton,A.W., Boehm,M.K., and Chamberlain,D. (1998). Molecular structures from low angle X-ray and neutron scattering studies. *Int. J. Biol. Macromol.* *22*, 1-16.

Perkins,S.J. and Weiss,H. (1983). Low-resolution structural studies of mitochondrial ubiquinol:cytochrome c reductase in detergent solutions by neutron scattering. *J. Mol. Biol.* *168*, 847-866.

Perrimon,N. and Bernfield,M. (2000). Specificities of heparan sulphate proteoglycans in developmental processes. *Nature* *404*, 725-728.

Pitteloud,N., Hayes,F.J., Boepple,P.A., DeCruz,S., Seminara,S.B., MacLaughlin,D.T., and Crowley,W.F., Jr. (2002). The role of prior pubertal development, biochemical markers of testicular maturation, and genetics in elucidating the phenotypic heterogeneity of idiopathic hypogonadotropic hypogonadism. *J. Clin. Endocrinol. Metab* *87*, 152-160.

Pittman,R.N., Ivins,J.K., and Buettner,H.M. (1989). Neuronal plasminogen activators: cell surface binding sites and involvement in neurite outgrowth. *J. Neurosci.* *9*, 4269-4286.

Plotnikov,A.N., Hubbard,S.R., Schlessinger,J., and Mohammadi,M. (2000). Crystal structures of two FGF-FGFR complexes reveal the determinants of ligand-receptor specificity. *Cell* *101*, 413-424.

Plouet,J., Moro,F., Bertagnolli,S., Coldeboeuf,N., Mazarguil,H., Clamens,S., and Bayard,F. (1997). Extracellular cleavage of the vascular endothelial growth factor 189-amino acid form by urokinase is required for its mitogenic effect. *J. Biol. Chem.* *272*, 13390-13396.

Ploug,M. and Ellis,V. (1994). Structure-function relationships in the receptor for urokinase-type plasminogen activator. Comparison to other members of the Ly-6 family and snake venom alpha-neurotoxins. *FEBS Lett.* *349*, 163-168.

Pluskota,E., Soloviev,D.A., and Plow,E.F. (2003). Convergence of the adhesive and fibrinolytic systems: recognition of urokinase by integrin alpha Mbeta 2 as well as by the urokinase receptor regulates cell adhesion and migration. *Blood* *101*, 1582-1590.

Powell,A.K., Fernig,D.G., and Turnbull,J.E. (2002). Fibroblast growth factor receptors 1 and 2 interact differently with heparin/heparan sulfate. Implications for dynamic assembly of a ternary signaling complex. *J. Biol. Chem.* *277*, 28554-28563.

Princivalle,M. and de Agostini,A. (2002). Developmental roles of heparan sulfate proteoglycans: a comparative review in *Drosophila*, mouse and human. *Int. J. Dev. Biol.* *46*, 267-278.

Pucci,M., Fibbi,G., Magnelli,L., and Del Rosso,M. (2001). Regulation of urokinase/urokinase receptor interaction by heparin-like glycosaminoglycans. *J. Biol. Chem.* *276*, 4756-4765.

Quinton,R., Beirne,P., Bouloux,P.M., Stanhope,R.G., and Conway,G.S. (2001). Routine neuroimaging in classical isolated gonadotrophin deficiency is of limited clinical value. *Clin. Endocrinol. (Oxf)* *54*, 127-129.

Quinton,R., Duke,V.M., de Zoysa,P.A., Platts,A.D., Valentine,A., Kendall,B., Pickman,S., Kirk,J.M., Besser,G.M., Jacobs,H.S., and Bouloux,P.M. (1996). The neuroradiology of Kallmann's syndrome: a genotypic and phenotypic analysis. *J. Clin. Endocrinol. Metab* *81*, 3010-3017.

Quinton,R., Hasan,W., Grant,W., Thrasivoulou,C., Quiney,R.E., Besser,G.M., and Bouloux,P.M. (1997). Gonadotropin-releasing hormone immunoreactivity in the nasal epithelia of adults with Kallmann's syndrome and isolated hypogonadotropic hypogonadism and in the early midtrimester human fetus. *J. Clin. Endocrinol. Metab* *82*, 309-314.

Rahmoune,H., Chen,H.L., Gallagher,J.T., Rudland,P.S., and Fernig,D.G. (1998). Interaction of heparan sulfate from mammary cells with acidic fibroblast growth factor

(FGF) and basic FGF. Regulation of the activity of basic FGF by high and low affinity binding sites in heparan sulfate. *J. Biol. Chem.* 273, 7303-7310.

Rapraeger, A.C. (1993). The coordinated regulation of heparan sulfate, syndecans and cell behavior. *Curr. Opin. Cell Biol.* 5, 844-853.

Ringvall, M., Ledin, J., Holmborn, K., van Kuppevelt, T., Ellin, F., Eriksson, I., Olofsson, A.M., Kjellen, L., and Forsberg, E. (2000). Defective heparan sulfate biosynthesis and neonatal lethality in mice lacking N-deacetylase/N-sulfotransferase-1. *J. Biol. Chem.* 275, 25926-25930.

Robertson, A., MacColl, G.S., Nash, J.A., Boehm, M.K., Perkins, S.J., and Bouloux, P.M. (2001). Molecular modelling and experimental studies of mutation and cell-adhesion sites in the fibronectin type III and whey acidic protein domains of human anosmin-1. *Biochem. J.* 357, 647-659.

Rodier, J.M., Valles, A.M., Denoyelle, M., Thiery, J.P., and Boyer, B. (1995). pp60c-src is a positive regulator of growth factor-induced cell scattering in a rat bladder carcinoma cell line. *J. Cell Biol.* 131, 761-773.

Ronnekleiv, O.K. and Resko, J.A. (1990). Ontogeny of gonadotropin-releasing hormone-containing neurons in early fetal development of rhesus macaques. *Endocrinology* 126, 498-511.

Rosini, P., Bonaccorsi, L., Baldi, E., Chiasserini, C., Forti, G., De Chiara, G., Lucibello, M., Mongiat, M., Iozzo, R.V., Garaci, E., Cozzolino, F., and Torcia, M.G. (2002). Androgen receptor expression induces FGF2, FGF-binding protein production, and FGF2 release in prostate carcinoma cells: role of FGF2 in growth, survival, and androgen receptor down-modulation. *Prostate* 53, 310-321.

Rugarli, E.I., Di Schiavi, E., Hilliard, M.A., Arbucci, S., Ghezzi, C., Faccioli, A., Coppola, G., Ballabio, A., and Bazzicalupo, P. (2002). The Kallmann syndrome gene homolog in *C. elegans* is involved in epidermal morphogenesis and neurite branching. *Development* 129, 1283-1294.

Rugarli, E.I., Ghezzi, C., Valsecchi, V., and Ballabio, A. (1996). The Kallmann syndrome gene product expressed in COS cells is cleaved on the cell surface to yield a diffusible component. *Hum. Mol. Genet.* 5, 1109-1115.

Ruppert, R., Hoffmann, E., and Sebald, W. (1996). Human bone morphogenetic protein 2 contains a heparin-binding site which modifies its biological activity. *Eur. J. Biochem.* 237, 295-302.

Sanderson, R.D. (2001). Heparan sulfate proteoglycans in invasion and metastasis. *Semin. Cell Dev. Biol.* 12, 89-98.

Saoncella, S., Echtermeyer, F., Denhez, F., Nowlen, J.K., Mosher, D.F., Robinson, S.D., Hynes, R.O., and Goetinck, P.F. (1999). Syndecan-4 signals cooperatively with

integrins in a Rho-dependent manner in the assembly of focal adhesions and actin stress fibers. *Proc. Natl. Acad. Sci. U. S. A* **96**, 2805-2810.

Sasisekharan,R., Shriver,Z., Venkataraman,G., and Narayanasami,U. (2002). Roles of heparan-sulphate glycosaminoglycans in cancer. *Nat. Rev. Cancer* **2**, 521-528.

Sato,N., Katsumata,N., Kagami,M., Hasegawa,T., Hori,N., Kawakita,S., Minowada,S., Shimotsuka,A., Shishiba,Y., Yokozawa,M., Yasuda,T., Nagasaki,K., Hasegawa,D., Hasegawa,Y., Tachibana,K., Naiki,Y., Horikawa,R., Tanaka,T., and Ogata,T. (2004). Clinical assessment and mutation analysis of Kallmann syndrome 1 (KAL1) and fibroblast growth factor receptor 1 (FGFR1, or KAL2) in five families and 18 sporadic patients. *J. Clin. Endocrinol. Metab* **89**, 1079-1088.

Schalkwijk,J., Wiedow,O., and Hirose,S. (1999). The trappin gene family: proteins defined by an N-terminal transglutaminase substrate domain and a C-terminal four-disulphide core. *Biochem. J.* **340** (Pt 3), 569-577.

Schally,A.V., Arimura,A., Kastin,A.J., Matsuo,H., Baba,Y., Redding,T.W., Nair,R.M., Debeljuk,L., and White,W.F. (1971). Gonadotropin-releasing hormone: one polypeptide regulates secretion of luteinizing and follicle-stimulating hormones. *Science* **173**, 1036-1038.

Schlaepfer,D.D. and Hunter,T. (1998). Integrin signalling and tyrosine phosphorylation: just the FAKs? *Trends Cell Biol.* **8**, 151-157.

Schurmann,G., Haspel,J., Grumet,M., and Erickson,H.P. (2001). Cell adhesion molecule L1 in folded (horseshoe) and extended conformations. *Mol. Biol. Cell* **12**, 1765-1773.

Schuster,T.M. and Toedt,J.M. (1996). New revolutions in the evolution of analytical ultracentrifugation. *Curr. Opin. Struct. Biol.* **6**, 650-658.

Schwanzel-Fukuda,M., Crossin,K.L., Pfaff,D.W., Bouloux,P.M., Hardelin,J.P., and Petit,C. (1996). Migration of luteinizing hormone-releasing hormone (LHRH) neurons in early human embryos. *J. Comp Neurol.* **366**, 547-557.

Schwanzel-Fukuda,M. and Pfaff,D.W. (1989). Origin of luteinizing hormone-releasing hormone neurons. *Nature* **338**, 161-164.

Schwarting,G.A. and Crandall,J.E. (1991). Subsets of olfactory and vomeronasal sensory epithelial cells and axons revealed by monoclonal antibodies to carbohydrate antigens. *Brain Res.* **547**, 239-248.

Schwarting,G.A., Kostek,C., Ahmad,N., Dibble,C., Pays,L., and Puschel,A.W. (2000). Semaphorin 3A is required for guidance of olfactory axons in mice. *J. Neurosci.* **20**, 7691-7697.

Schwartz,M.A., Schaller,M.D., and Ginsberg,M.H. (1995). Integrins: emerging paradigms of signal transduction. *Annu. Rev. Cell Dev. Biol.* *11*, 549-599.

Seeds,N.W., Basham,M.E., and Haffke,S.P. (1999). Neuronal migration is retarded in mice lacking the tissue plasminogen activator gene. *Proc. Natl. Acad. Sci. U. S. A* *96*, 14118-14123.

Sehgal,A., Patil,N., and Chao,M. (1988). A constitutive promoter directs expression of the nerve growth factor receptor gene. *Mol. Cell Biol.* *8*, 3160-3167.

Selleck,S.B. (2000). Proteoglycans and pattern formation: sugar biochemistry meets developmental genetics. *Trends Genet.* *16*, 206-212.

Semenyuk AV and Svergun DI (1991). GNOM-a program package for small-angle scattering data-processing. *J. Appl. Cryst* *24*, 537-540.

Serafini,T. (1999). Finding a partner in a crowd: neuronal diversity and synaptogenesis. *Cell* *98*, 133-136.

Sherman,P.M., Lawrence,D.A., Yang,A.Y., Vandenberg,E.T., Paielli,D., Olson,S.T., Shore,J.D., and Ginsburg,D. (1992). Saturation mutagenesis of the plasminogen activator inhibitor-1 reactive center. *J. Biol. Chem.* *267*, 7588-7595.

Shriver,Z., Raman,R., Venkataraman,G., Drummond,K., Turnbull,J., Toida,T., Linhardt,R., Biemann,K., and Sasisekharan,R. (2000a). Sequencing of 3-O sulfate containing heparin decasaccharides with a partial antithrombin III binding site. *Proc. Natl. Acad. Sci. U. S. A* *97*, 10359-10364.

Shriver,Z., Sundaram,M., Venkataraman,G., Fareed,J., Linhardt,R., Biemann,K., and Sasisekharan,R. (2000b). Cleavage of the antithrombin III binding site in heparin by heparinases and its implication in the generation of low molecular weight heparin. *Proc. Natl. Acad. Sci. U. S. A* *97*, 10365-10370.

Shu,T., Valentino,K.M., Seaman,C., Cooper,H.M., and Richards,L.J. (2000). Expression of the netrin-1 receptor, deleted in colorectal cancer (DCC), is largely confined to projecting neurons in the developing forebrain. *J. Comp Neurol.* *416*, 201-212.

Smith,C.E. and Johnson,D.A. (1985). Human bronchial leucocyte proteinase inhibitor. Rapid isolation and kinetic analysis with human leucocyte proteinases. *Biochem. J.* *225*, 463-472.

Soderlund,D., Canto,P., and Mendez,J.P. (2002). Identification of three novel mutations in the KAL1 gene in patients with Kallmann syndrome. *J. Clin. Endocrinol. Metab* *87*, 2589-2592.

Soussi-Yanicostas,N., de Castro,F., Julliard,A.K., Perfettini,I., Chedotal,A., and Petit,C. (2002). Anosmin-1, defective in the X-linked form of Kallmann syndrome,

promotes axonal branch formation from olfactory bulb output neurons. *Cell* 109, 217-228.

Soussi-Yanicostas,N., Faivre-Sarrailh,C., Hardelin,J.P., Levilliers,J., Rougon,G., and Petit,C. (1998). Anosmin-1 underlying the X chromosome-linked Kallmann syndrome is an adhesion molecule that can modulate neurite growth in a cell-type specific manner. *J. Cell Sci.* 111 ( Pt 19), 2953-2965.

Soussi-Yanicostas,N., Hardelin,J.P., Arroyo-Jimenez,M.M., Ardouin,O., Legouis,R., Levilliers,J., Traincard,F., Betton,J.M., Cabanie,L., and Petit,C. (1996). Initial characterization of anosmin-1, a putative extracellular matrix protein synthesized by definite neuronal cell populations in the central nervous system. *J. Cell Sci.* 109 ( Pt 7), 1749-1757.

Spillmann,D., Witt,D., and Lindahl,U. (1998). Defining the interleukin-8-binding domain of heparan sulfate. *J. Biol. Chem.* 273, 15487-15493.

St John,J.A. and Key,B. (2001). EphB2 and two of its ligands have dynamic protein expression patterns in the developing olfactory system. *Brain Res. Dev. Brain Res.* 126, 43-56.

Strigini,M. and Cohen,S.M. (1997). A Hedgehog activity gradient contributes to AP axial patterning of the Drosophila wing. *Development* 124, 4697-4705.

Stringer,S.E. and Gallagher,J.T. (1997). Specific binding of the chemokine platelet factor 4 to heparan sulfate. *J. Biol. Chem.* 272, 20508-20514.

Suidan,H.S., Stone,S.R., Hemmings,B.A., and Monard,D. (1992). Thrombin causes neurite retraction in neuronal cells through activation of cell surface receptors. *Neuron* 8, 363-375.

Svergun,D.I. (1992). Determination of the regularization parameter in indirect transform methods using perceptual criteria. *J. Appl. Cryst.* 25, 495-503.

Takada,T., Katagiri,T., Ifuku,M., Morimura,N., Kobayashi,M., Hasegawa,K., Ogamo,A., and Kamijo,R. (2003). Sulfated polysaccharides enhance the biological activities of bone morphogenetic proteins. *J. Biol. Chem.* 278, 43229-43235.

Thewke,D.P. and Seeds,N.W. (1996). Expression of hepatocyte growth factor/scatter factor, its receptor, c-met, and tissue-type plasminogen activator during development of the murine olfactory system. *J. Neurosci.* 16, 6933-6944.

Thompson,K. and Rabinovitch,M. (1996). Exogenous leukocyte and endogenous elastases can mediate mitogenic activity in pulmonary artery smooth muscle cells by release of extracellular-matrix bound basic fibroblast growth factor. *J. Cell Physiol* 166, 495-505.

Thompson,L.D., Pantoliano,M.W., and Springer,B.A. (1994). Energetic characterization of the basic fibroblast growth factor-heparin interaction: identification of the heparin binding domain. *Biochemistry* 33, 3831-3840.

Thompson,M.A. and Ziff,E.B. (1989). Structure of the gene encoding peripherin, an NGF-regulated neuronal-specific type III intermediate filament protein. *Neuron* 2, 1043-1053.

Toba,Y., Horie,M., Sango,K., Tokashiki,A., Matsui,F., Oohira,A., and Kawano,H. (2002). Expression and immunohistochemical localization of heparan sulphate proteoglycan N-syndecan in the migratory pathway from the rat olfactory placode. *Eur. J. Neurosci.* 15, 1461-1473.

Treloar,H.B., Nurcombe,V., and Key,B. (1996). Expression of extracellular matrix molecules in the embryonic rat olfactory pathway. *J. Neurobiol.* 31, 41-55.

Tsunemi,M., Matsuura,Y., Sakakibara,S., and Katsube,Y. (1996). Crystal structure of an elastase-specific inhibitor elafin complexed with porcine pancreatic elastase determined at 1.9 Å resolution. *Biochemistry* 35, 11570-11576.

Tumova,S., Woods,A., and Couchman,J.R. (2000). Heparan sulfate chains from glypican and syndecans bind the Hep II domain of fibronectin similarly despite minor structural differences. *J. Biol. Chem.* 275, 9410-9417.

Turgeon,V.L. and Houenou,L.J. (1997). The role of thrombin-like (serine) proteases in the development, plasticity and pathology of the nervous system. *Brain Res. Brain Res. Rev.* 25, 85-95.

Turgeon,V.L., Lloyd,E.D., Wang,S., Festoff,B.W., and Houenou,L.J. (1998). Thrombin perturbs neurite outgrowth and induces apoptotic cell death in enriched chick spinal motoneuron cultures through caspase activation. *J. Neurosci.* 18, 6882-6891.

Turnbull,J., Powell,A., and Guimond,S. (2001). Heparan sulfate: decoding a dynamic multifunctional cell regulator. *Trends Cell Biol.* 11, 75-82.

Vermeulen,S., Messiaen,L., Scheir,P., De Bie,S., Speleman,F., and De Paepe,A. (2002). Kallmann syndrome in a patient with congenital spherocytosis and an interstitial 8p11.2 deletion. *Am. J. Med. Genet.* 108, 315-318.

Vlodavsky,I., Miao,H.Q., Medalion,B., Danagher,P., and Ron,D. (1996). Involvement of heparan sulfate and related molecules in sequestration and growth promoting activity of fibroblast growth factor. *Cancer Metastasis Rev.* 15, 177-186.

Walker,A. and Gallagher,J.T. (1996). Structural domains of heparan sulphate for specific recognition of the C-terminal heparin-binding domain of human plasma fibronectin (HEPII). *Biochem. J.* 317 (Pt 3), 871-877.



- Walther,C. and Gruss,P. (1991). Pax-6, a murine paired box gene, is expressed in the developing CNS. *Development* *113*, 1435-1449.
- Walz,A., McFarlane,S., Brickman,Y.G., Nurcombe,V., Bartlett,P.F., and Holt,C.E. (1997). Essential role of heparan sulfates in axon navigation and targeting in the developing visual system. *Development* *124* , 2421-2430.
- Wang,F., Nemes,A., Mendelsohn,M., and Axel,R. (1998). Odorant receptors govern the formation of a precise topographic map. *Cell* *93*, 47-60.
- Wang,Q., McEwen,D.G., and Ornitz,D.M. (2000). Subcellular and developmental expression of alternatively spliced forms of fibroblast growth factor 14. *Mech. Dev.* *90*, 283-287.
- Wegenke,J.D., Uehling,D.T., Wear,J.B., Jr., Gordon,E.S., Bargman,J.G., Deacon,J.S., Herrmann,J.P., and Opitz,J.M. (1975). Familial Kallmann syndrome with unilateral renal aplasia. *Clin. Genet.* *7*, 368-381.
- Weinstein,J.R., Gold,S.J., Cunningham,D.D., and Gall,C.M. (1995). Cellular localization of thrombin receptor mRNA in rat brain: expression by mesencephalic dopaminergic neurons and codistribution with prothrombin mRNA. *J. Neurosci.* *15*, 2906-2919.
- Whitesides,J.G., III and LaMantia,A.S. (1996). Differential adhesion and the initial assembly of the mammalian olfactory nerve. *J. Comp Neurol.* *373*, 240-254.
- Wiedow,O., Schroder,J.M., Gregory,H., Young,J.A., and Christophers,E. (1990). Elafin: an elastase-specific inhibitor of human skin. Purification, characterization, and complete amino acid sequence. *J. Biol. Chem.* *265*, 14791-14795.
- Wiesmann,C. and de Vos,A.M. (1999). Putting two and two together: crystal structure of the FGF-receptor complex. *Structure. Fold. Des* *7*, R251-R255.
- Wight,T.N., Kinsella,M.G., and Qwarnstrom,E.E. (1992). The role of proteoglycans in cell adhesion, migration and proliferation. *Curr. Opin. Cell Biol.* *4*, 793-801.
- Woolf,A.S. (2001). The life of the human kidney before birth: its secrets unfold. *Pediatr. Res.* *49*, 8-10.
- Wray,S. (2002). Molecular mechanisms for migration of placodally derived GnRH neurons. *Chem. Senses* *27*, 569-572.
- Xu,Y., Hagege,J., Mougnot,B., Sraer,J.D., Ronne,E., and Rondeau,E. (1996). Different expression of the plasminogen activation system in renal thrombotic microangiopathy and the normal human kidney. *Kidney Int.* *50*, 2011-2019.
- Yan,G., Fukabori,Y., McBride,G., Nikolaropolous,S., and McKeehan,W.L. (1993). Exon switching and activation of stromal and embryonic fibroblast growth factor

(FGF)-FGF receptor genes in prostate epithelial cells accompany stromal independence and malignancy. *Mol. Cell Biol.* *13*, 4513-4522.

Ying, Q.L., Kemme, M., and Simon, S.R. (1994). Functions of the N-terminal domain of secretory leukoprotease inhibitor. *Biochemistry* *33*, 5445-5450.

Ying, Q.L. and Simon, S.R. (1993). Kinetics of the inhibition of human leukocyte elastase by elafin, a 6-kilodalton elastase-specific inhibitor from human skin. *Biochemistry* *32*, 1866-1874.

Yoshida, M., Suda, Y., Matsuo, I., Miyamoto, N., Takeda, N., Kuratani, S., and Aizawa, S. (1997). *Emx1* and *Emx2* functions in development of dorsal telencephalon. *Development* *124*, 101-111.

Yoshida, S. and Shiosaka, S. (1999). Plasticity-related serine proteases in the brain (review). *Int. J. Mol. Med.* *3*, 405-409.

Yoshihara, Y., Kawasaki, M., Tamada, A., Fujita, H., Hayashi, H., Kagamiyama, H., and Mori, K. (1997). OCAM: A new member of the neural cell adhesion molecule family related to zone-to-zone projection of olfactory and vomeronasal axons. *J. Neurosci.* *17*, 5830-5842.

Zhu, X., Komiya, H., Chirino, A., Faham, S., Fox, G.M., Arakawa, T., Hsu, B.T., and Rees, D.C. (1991). Three-dimensional structures of acidic and basic fibroblast growth factors. *Science* *251*, 90-93.